

# Capacity of Steel and Concrete Containment Vessels With Corrosion Damage

Sandia National Laboratories

Office of Nuclear Regulatory Research  
U.S. Nuclear Regulatory Commission  
Washington, DC 20555-0001



## AVAILABILITY OF REFERENCE MATERIALS IN NRC PUBLICATIONS

### NRC Reference Material

As of November 1999, you may electronically access NUREG-series publications and other NRC records at NRC's Public Electronic Reading Room at [www.nrc.gov/NRC/ADAMS/index.html](http://www.nrc.gov/NRC/ADAMS/index.html).

Publicly released records include, to name a few, NUREG-series publications; *Federal Register* notices; applicant, licensee, and vendor documents and correspondence; NRC correspondence and internal memoranda; bulletins and information notices; inspection and investigative reports; licensee event reports; and Commission papers and their attachments.

NRC publications in the NUREG series, NRC regulations, and *Title 10, Energy*, in the Code of *Federal Regulations* may also be purchased from one of these two sources.

1. The Superintendent of Documents  
U.S. Government Printing Office  
Mail Stop SSOP  
Washington, DC 20402-0001  
Internet: [bookstore.gpo.gov](http://bookstore.gpo.gov)  
Telephone: 202-512-1800  
Fax: 202-512-2250
2. The National Technical Information Service  
Springfield, VA 22161-0002  
[www.ntis.gov](http://www.ntis.gov)  
1-800-553-6847 or, locally, 703-605-6000

A single copy of each NRC draft report for comment is available free, to the extent of supply, upon written request as follows:

Address: Office of the Chief Information Officer,  
Reproduction and Distribution  
Services Section  
U.S. Nuclear Regulatory Commission  
Washington, DC 20555-0001  
E-mail: [DISTRIBUTION@nrc.gov](mailto:DISTRIBUTION@nrc.gov)  
Facsimile: 301-415-2289

Some publications in the NUREG series that are posted at NRC's Web site address [www.nrc.gov/NRC/NUREGS/indexnum.html](http://www.nrc.gov/NRC/NUREGS/indexnum.html) are updated periodically and may differ from the last printed version. Although references to material found on a Web site bear the date the material was accessed, the material available on the date cited may subsequently be removed from the site.

### Non-NRC Reference Material

Documents available from public and special technical libraries include all open literature items, such as books, journal articles, and transactions, *Federal Register* notices, Federal and State legislation, and congressional reports. Such documents as theses, dissertations, foreign reports and translations, and non-NRC conference proceedings may be purchased from their sponsoring organization.

Copies of industry codes and standards used in a substantive manner in the NRC regulatory process are maintained at—

The NRC Technical Library  
Two White Flint North  
11545 Rockville Pike  
Rockville, MD 20852-2738

These standards are available in the library for reference use by the public. Codes and standards are usually copyrighted and may be purchased from the originating organization or, if they are American National Standards, from—

American National Standards Institute  
11 West 42<sup>nd</sup> Street  
New York, NY 10036-8002  
[www.ansi.org](http://www.ansi.org)  
212-642-4900

Legally binding regulatory requirements are stated only in laws; NRC regulations; licenses, including technical specifications; or orders, not in NUREG-series publications. The views expressed in contractor-prepared publications in this series are not necessarily those of the NRC.

The NUREG series comprises (1) technical and administrative reports and books prepared by the staff (NUREG-XXXX) or agency contractors (NUREG/CR-XXXX), (2) proceedings of conferences (NUREG/CP-XXXX), (3) reports resulting from international agreements (NUREG/IA-XXXX), (4) brochures (NUREG/BR-XXXX), and (5) compilations of legal decisions and orders of the Commission and Atomic and Safety Licensing Boards and of Directors' decisions under Section 2.206 of NRC's regulations (NUREG-0750).

**DISCLAIMER:** This report was prepared as an account of work sponsored by an agency of the U.S. Government. Neither the U.S. Government nor any agency thereof, nor any employee, makes any warranty, expressed or implied, or assumes any legal liability or responsibility for any third party's use, or the results of such use, of any information, apparatus, product, or process disclosed in this publication, or represents that its use by such third party would not infringe privately owned rights.

NUREG/CR-6706  
SAND2000-1735

---

---

# Capacity of Steel and Concrete Containment Vessels With Corrosion Damage

---

---

Manuscript Completed: January 2001

Date Published: February 2001

Prepared by

J.L. Cherry, J.A. Smith

Sandia National Laboratories  
Albuquerque, NM 87185-0744

H.L. Graves III, NRC Project Manager

**Division of Engineering Technology  
Office of Nuclear Regulatory Research  
U.S. Nuclear Regulatory Commission  
Washington, DC 20555-0001  
NRC Job Code J6042**



---

For sale by the Superintendent of Documents, U.S. Government Printing Office  
Internet: bookstore.gpo.gov Phone: (202) 512-1800 Fax: (202) 512-2250  
Mail: Stop SSOP, Washington, DC 20402-0001

ISBN 0-16-050738-3

## ABSTRACT

Corrosion damage has been found in a number of nuclear power plant containment structures, and this could degrade the pressure capacity of the vessel. This has prompted concerns regarding the capacity of corroded containments to withstand accident loadings. For the low-carbon, low-strength steels used in containments, the effect of corrosion on material properties is discussed in this report, and a basis for using finite element analyses to calculate the capacity of a vessel with corrosion damage is developed. The pressure capacity was calculated for two typical steel containment vessels with no corrosion damage: a PWR Ice Condenser containment and a BWR Mark I containment. The pressure capacity was also calculated for two typical concrete containment vessels

with no corrosion damage: a PWR reinforced concrete sub-atmospheric containment and a PWR prestressed concrete containment vessel. Multiple analyses were then performed with the location of corrosion and the amount of corrosion varied in each analysis. A "lower bound", "best estimate", and "upper bound" failure level was predicted for each case. These limits were established by: determining the amount of variability that exists in material properties of typical containments, estimating the amount of uncertainty associated with the level of modeling detail and modeling assumptions, and estimating the stress concentration effect caused by a rough, uneven, corroded surface.

# CONTENTS

ABSTRACT .....	iii
CONTENTS .....	v
LIST OF FIGURES .....	vii
LIST OF TABLES .....	x
1 INTRODUCTION .....	1-1
2 BASIS FOR PREDICTING CAPACITY OF CORRODED CONTAINMENTS USING FINITE ELEMENT ANALYSIS .....	2-1
2.1 Scaled Model Tests and Analyses of Uncorroded Containments and Pressure Vessels .....	2-2
2.2 Lessons Learned from Corroded Pipeline Research .....	2-6
2.3 Material Properties and Aging Issues .....	2-7
2.3.1 Types of Degradation. ....	2-7
2.3.2 Damage Mechanisms for Low-Carbon Steel. ....	2-8
2.3.3 Fracture toughness. ....	2-9
2.3.3.1 Crack growth rate. ....	2-9
2.3.3.2 Critical crack length. ....	2-10
2.3.3.3 Corrosion pits and fracture. ....	2-10
2.3.3.4 Fracture summary. ....	2-11
2.3.4 Fatigue and Corrosion Fatigue. ....	2-11
2.3.5 Welded Properties. ....	2-12
2.3.5.1 Tests on welded specimens. ....	2-13
2.3.5.2 Welds in steel containments and liners. ....	2-15
2.4 Corroded Coupon Tests .....	2-16
2.4.1 Uniform Corrosion. ....	2-16
2.4.2 "Pitted" Coupon Tests. ....	2-20
3 OBSERVED CORROSION DAMAGE .....	3-1
4 FINITE ELEMENT MODELING .....	4-1
4.1 Modeling Considerations .....	4-1
4.2 Failure Criteria of Steel .....	4-3
4.2.1 Failure criteria used in previous analyses. ....	4-3
4.2.2 Failure criteria in the literature. ....	4-5
4.2.3 Fracture Mechanics Versus Effective Plastic Strain. ....	4-5
4.3 Steel Failure Criteria Used in this Project .....	4-6
4.3.1 f1 (stress triaxiality) factor .....	4-8
4.3.2 f2 (model sophistication) factor. ....	4-9
4.3.3 f3 (material variability) factor. ....	4-9
4.3.4 f4 (corrosion variability) factor. ....	4-9
4.3.5 Application. ....	4-10

4.4	Concrete Material Model.....	4-10
5	ANALYSIS OF TYPICAL PWR ICE CONDENSER CONTAINMENT.....	5-1
5.1	Geometry.....	5-2
5.2	Finite Element Model.....	5-2
5.3	Material Properties.....	5-4
5.4	Loads.....	5-5
5.5	Analysis Results.....	5-5
6	ANALYSES OF TYPICAL BWR MARK I CONTAINMENT.....	6-1
6.1	Geometry.....	6-1
6.2	Finite Element Models.....	6-4
6.3	Material Properties.....	6-7
6.4	Loads.....	6-8
6.5	Analysis Results.....	6-8
7	ANALYSES OF TYPICAL REINFORCED CONCRETE CONTAINMENT.....	7-1
7.1	Material Properties.....	7-1
7.2	Corrosion/Degradation.....	7-2
7.3	Loading.....	7-2
7.4	Failure Criteria.....	7-2
7.5	FEA Models.....	7-3
7.5.1	Axisymmetric.....	7-4
7.5.2	3-dimensional submodel.....	7-4
7.5.3	2-dimensional submodels.....	7-5
7.6	Finite Element Results.....	7-6
7.7	Discussion.....	7-9
7.8	Conclusions.....	7-11
8	ANALYSES OF TYPICAL PRESTRESSED CONCRETE CONTAINMENT.....	8-1
8.1	Material Properties.....	8-2
8.2	Corrosion/Degradation.....	8-2
8.3	Loading.....	8-3
8.4	Failure Criteria.....	8-3
8.5	FEA Models.....	8-4
8.5.1	Axisymmetric.....	8-5
8.5.2	3-dimensional submodel.....	8-6
8.5.3	2-dimensional submodels.....	8-6
8.6	Finite Element Results.....	8-7
8.7	Discussion.....	8-11
8.8	Conclusions.....	8-12
9	SUMMARY AND CONCLUSIONS.....	9-1

9.1	Basis For Predicting Capacity of Corroded Containments Using Finite Element Analyses .....	9-1
9.1.1	Scaled Model Tests and Analyses of Uncorroded Containments. ....	9-1
9.1.2	Material Properties and Aging Issues. ....	9-1
9.1.3	Lessons Learned From Corroded Pipeline Research. ....	9-2
9.1.4	Corroded Coupon Tests. ....	9-2
9.2	Finite Element Modeling .....	9-2
9.2.1	Modeling Corrosion.....	9-2
9.2.2	Failure Criteria for Steel Shell and Liner of Concrete Containment. ....	9-3
9.2.3	Actual Containment Behavior versus Analytical Predictions. ....	9-3
9.2.4	Analyses of Typical Steel Containments. ....	9-4
9.2.5	Analyses of Typical Concrete Containments. ....	9-5
9.3	Simplified Analogy.....	9-5
9.3.1	Steel Containments. ....	9-5
9.3.2	Liners in Concrete Containments.....	9-7
9.4	Repairs of Steel Containments or Liners of Concrete Containments .....	9-8
10	REFERENCES.....	10-1

## LIST OF FIGURES

2.1	Corrosion damage modes .....	2-9
2.2	Welded test specimens for 1:6 scale concrete containment liner.....	2-14
2.3	ASTM dogbone shaped coupons used in tensile tests .....	2-16
2.4	Thickness measurement points .....	2-17
2.5	Photographs of coupons 2A and 2E with 5% corrosion .....	2-17
2.6	A516 Gr. 70 steel stress-strain curve – 5% corrosion.....	2-18
2.7	Photographs of coupons 1C and 1D with 10% corrosion .....	2-18
2.8	A516 Gr. 70 steel stress-strain curve – 10% corrosion.....	2-18
2.9	Photographs of coupons 3A and 3C with 20% corrosion .....	2-19
2.10	A516 Gr. 70 steel stress-strain curve – 20% corrosion.....	2-19
2.11	Stress vs. elongation for coupons with “pits” .....	2-21
5.1	“Typical” PWR ice condenser containment .....	5-2
5.2	Observed damage to steel shell near basemat.....	5-2
5.3	Observed damage near upper and lower floor .....	5-3
5.4	Finite element model .....	5-3
5.5	Submodel of upper floor region.....	5-4
5.6	Finite element model shell thickness and stringer and stiffener locations .....	5-4
5.7	A516 Grade 60 temperature dependence.....	5-5
5.8	Saturated steam temperature-pressure relationship.....	5-5

5.9 Largest equivalent plastic membrane strains in ice basket region .....	5-6
5.10 Largest Equivalent Plastic Membrane Strains in Upper Floor Region. ....	5-6
5.11 Typical Equivalent Plastic Surface (Bending) Strains in Basemat Region.....	5-7
5.12 Typical equivalent plastic strains in basemat region that has 50% corrosion .....	5-7
5.13 Von mises membrane stress (MPa) in global model with no corrosion, displacements magnified by a factor of 5 .....	5-10
5.14 Equivalent plastic membrane strain in global model with no corrosion, displacements magnified by a factor of 5 .....	5-12
5.15 Von mises membrane stress (MPa) in ice basket region with no corrosion, displacements magnified by a factor of 5 .....	5-14
5.16 Equivalent plastic membrane strain in ice basket region with no corrosion, displacements magnified by a factor of 5 .....	5-15
5.17 Von mises membrane stress (MPa) in local model of upper floor region with 50% corrosion, displacements magnified by a factor of 5 .....	5-16
5.18 Equivalent plastic membrane strain in local model of upper floor region with 50% corrosion, displacements magnified by a factor of 5 .....	5-17
6.1 “Typical” BWR Mark I containment.....	6-2
6.2 Observed damage in sand pocket region .....	6-3
6.3 Finite element model around sphere-to-cylinder knuckle region.....	6-5
6.4 Finite element model around sand-pocket region .....	6-5
6.5 Model of suppression pool .....	6-5
6.6 Drywell shell model thickness .....	6-7
6.7 Suppression pool shell thickness .....	6-7
6.8 A516 Grade 70 temperature dependence.....	6-8
6.9 Largest equivalent plastic membrane strains at waterline in suppression pool.....	6-9
6.10 Typical equivalent plastic membrane strains in knuckle region .....	6-9
6.11 Typical equivalent plastic surface (bending) strains in sand pocket region.....	6-10
6.12 Typical equivalent plastic strains in sand pocket region that has 50% corrosion .....	6-10
6.13 Von mises membrane stress (MPa) in suppression pool model with 50% corrosion, displacements magnified by a factor of 5.....	6-13
6.14 Equivalent plastic membran strain in suppression pool model with 50% corrosion, displacements magnified by a factor of 5.....	6-14
6.15 Von mises membrane stress (MPa) in drywell with 50% corrosion in knuckle region, displacements magnified by a factor of 5.....	6-15
6.16 Equivalent plastic membrane strain (MPa) in drywell with 50% corrosion in knuckle region, displacements magnified by a factor of 5 .....	6-16
6.17 Von mises membrane stress (MPa) in knuckle region with 50% corrosion, displacements magnified by a factor of 5.....	6-17
6.18 Equivalent plastic membrane strain (MPa) in knuckle region with 50% corrosion, displacements magnified by a factor of 5.....	6-17
6.19 Von mises membrane stress (MPa) in sand pocket region with 50% corrosion, displacements magnified by a factor of 5.....	6-18

6.20 Equivalent plastic membrane strain in sand pocket region with 50% corrosion, displacements magnified by a factor of 5.....	6-18
7.1 A516 Grade 60 true stress versus true strain .....	7-2
7.2 Temperature-pressure relationship .....	7-2
7.3 Schematic of typical reinforced concrete containment .....	7-4
7.4 Typical reinforcing layout .....	7-4
7.5 Axisymmetric finite element mesh .....	7-4
7.6 3D hatch finite element model.....	7-5
7.7 Load displacement relationship for studs .....	7-5
7.8 Liner mid-height 2D sub-model.....	7-6
7.9 Liner base mat 2D sub-model.....	7-6
7.10 Reinforcing and liner stresses for axisymmetric model .....	7-7
7.11 Displaced mesh of axisymmetric model .....	7-8
7.12 Plastic strains in liner of axisymmetric model .....	7-8
7.13 Plastic strains versus pressure for the base mat sub-model.....	7-8
7.14 Plastic strains versus pressure for the mid-height liner sub-model .....	7-8
7.15 Plastic strain versus pressure for the 50% degradation cases .....	7-9
7.16 Plastic strain in liner near the base mat of the containment .....	7-9
7.17 Plastic strain in liner at mid-height of the containment.....	7-9
7.18 Stud force for typical stud in 50% corrosion liner model.....	7-10
8.1 Liner material stress-strain curves .....	8-2
8.2 Temperature pressure relationship.....	8-3
8.3 Schematic of prestressed containment .....	8-4
8.4 Schematic of typical prestressing tendon and reinforcing bar layout.....	8-4
8.5 Continuous liner anchorage layout .....	8-5
8.6 Axisymmetric finite element mesh .....	8-5
8.7 Hatch three dimensional model .....	8-6
8.8 Load displacement relationship for continuous anchors .....	8-6
8.9 Schematic of the liner mid-height model .....	8-7
8.10 Schematic of liner basemat model .....	8-7
8.11 Schematic of the hatch liner sub-model.....	8-7
8.12 Displaced shape of axisymmetric model (5X).....	8-10
8.13 Plastic strain in axisymmetric model .....	8-10
8.14 Plastic strain versus pressure for hatch liner sub-model .....	8-10
8.15 Plastic strain versus pressure for the liner mid-height sub-model.....	8-10
8.16 Plastic strain versus pressure for the liner basemat sub-model .....	8-10
8.17 Hatch liner sub-model plastic strains.....	8-11
8.18 Liner mid-height sub-model plastic strains.....	8-11
8.19 Base mat liner sub-model plastic strains.....	8-11

9.1	Thickness transition section.....	9-5
9.2	Cylinder with axial weld joining two different plate thicknesses.....	9-6
9.3	Cylinder with circumferential weld joining two different plate thicknesses .....	9-6
9.4	Cylinder with thickened insert plate .....	9-7
9.5	Cylinder with locally thinned area .....	9-7
9.6	Liner with thickened insert plate and nelson stud anchors.....	9-8

## LIST OF TABLES

2.1	Summary of results of experiments for steel containment models.....	2-3
2.2	Summary of experiments for reinforced concrete containment models and liner tearing and leakage .....	2-4
2.3	Summary of experiments for prestressed concrete steel containment models .....	2-5
2.4	Material properties of base metal and weld material .....	2-14
2.5	Strain hardening of base metal, weld material, and material in the HAZ .....	2-14
2.6	Coupon thickness of uncorroded specimens.....	2-17
2.7	Coupon thickness (t) of specimens corroded approximately 5%.....	2-18
2.8	Coupon thickness (t) of specimens corroded approximately 10%.....	2-18
2.9	Coupon thickness (t) of specimens corroded approximately 20%.....	2-19
2.10	Through-the-thickness “pitted” coupons .....	2-20
2.11	Stresses in “pitted” coupons .....	2-21
3.1	Occurrences of structural degradation at nuclear power plants .....	3-2
4.1	Knockdown factors used in failure criteria .....	4-8
5.1	Predicted failure pressures.....	5-9
6.1	Predicted failure pressures.....	6-12
7.1	Knockdown factors used in failure criteria .....	7-3
7.2	Failure pressures and strains.....	7-7
8.1	Concrete properties.....	8-2
8.2	Reinforcing bar and prestressing tendon stress-strain properties.....	8-3
8.3	Knockdown factors.....	8-4
8.4	Analysis results comparison .....	8-8
8.5	Failure pressures and strains.....	8-9
8.6	Controlling failure pressures and strains.....	8-12

# 1 INTRODUCTION

Corrosion damage has been found in approximately one-third of existing nuclear power plant containments, with the number increasing steadily [Johnson et al, 1990; Shah and McDonald, 1989; Shah et al, 1994]. Analytical efforts, scaled model containment tests, and tests on seals, gaskets, bellows, and electrical penetration assemblies have demonstrated that containment models without corrosion can resist static internal pressures that are about two to six times the containment's design pressure without significant leakage [Bridges, 1987; Brinson and Graves, 1988; Clauss, 1989; Fanous et al, 1993; Greimann et al, 1991; Horschel, 1988; Horschel, 1992a; Horschel 1992b; Julien and Peters, 1989; Jung, 1984; Koenig, 1986; Kulak et al, 1985; Lambert, 1993; Lambert and Parks, 1995; Miller, 1990; Parks, 1989; Reese and Horschel, 1985; Weatherby, 1990]. However, corrosion found in containments of operating nuclear power plants has prompted concerns regarding the capacity of the corroded containments to withstand accident loads.

Corrosion of containments can reduce the margin between the design and failure pressure and thus could increase the probability of containment failure under severe accident loads. In this report, failure is predicted when strains become large enough that a tear could initiate in the steel shell or the liner. The strain limits are discussed in detail in Section 4. Comparisons of the shell thickness after corrosion with the ASME Boiler and Pressure Vessel Code (ASME, 1992) minimum allowable thickness gives some indication of the reduction in containment capacity. However, the nature and the location of the corrosion must be considered to determine how much the affected areas degrade the ultimate capacity of the containment. For example, considerable corrosion in an area with excess thickness may not affect the ultimate capacity, while minor corrosion in a critical area would lower the ultimate capacity.

For uncorroded containments, previous analyses [Pilch et al, 1995, Appendix D] have shown that a few containments have a margin of safety about five or six times the design pressure, while many vessels have a margin of safety around three times the design pressure. Corrosion damage in a containment with a higher margin of safety would not be as significant as corrosion damage in a containment with a lower margin of safety. However, in this report, no attempt is made to determine a minimum required safety margin. Rather, the focus of this report is to show how pressure capacity is reduced as a result of corrosion damage.

Leak tests performed on operational containment vessels verify that they can withstand internal design

pressure, but these tests do not provide information about the safety margin. Leak rate tests don't provide any information about the affect of corrosion or other aging related degradation, unless a leak is detected. For containments with corrosion, the amount of reduction in the pressure capacity, and hence the safety margin, can not be determined from these leak tests.

The NRC needs to assess the operability of a containment when significant degradation, such as pits in a shell or liner, has been identified by a licensee. The staff has to determine whether the licensee can continue to operate the plant until the next refueling outage, or if repairs must be made immediately. Any reduction in margin needs to be quantified, and the containment must be able to withstand design basis accidents during operation. In a risk-informed decision making process, the staff need to evaluate the licensee's assessment, performed in accordance with Regulatory Guide 1.174.

The primary objectives of this research program are to:

- Develop a basis and rationale for using finite element methods to predict the ultimate capacity of pressure vessels that have become corroded, as well as understand the limitations and capabilities of the finite element method when applied to corroded structures. Obviously, any limitations that exist when analyzing an uncorroded containment would also be a limitation during the analysis of a corroded containment.
- Use finite element analyses to predict how corrosion found on a PWR Ice Condenser and a BWR Mark I steel containment degrade the pressure capacity,
- Use finite element analyses to predict how liner corrosion in a reinforced concrete and a prestressed concrete containment vessels degrade the pressure capacity, and
- Develop methodology to generate fragility curves for the PWR Ice Condenser and BWR Mark I steel containments, and the liner of a reinforced concrete containment, with varying amounts and locations of corrosion. Results of the fragility analyses are not included in this report. Fragility curves were generated for the PWR Ice Condenser containment, described in Chapter 5, by Ellingwood and Cherry (1999). Similarly, calculations were done to develop fragility curves for the BWR Mark I containment described in

Chapter 6 and the reinforced concrete containment in Chapter 7.

Three-dimensional finite element models have been developed for a few steel and concrete containments, and the pressure capacity has been calculated. Corrosion damage was accounted for by removing corroded material from the analysis model. Only quasi-static internal pressurization loads, such as could occur during a Loss of Cooling Accident (LOCA), have been analyzed. Although these methods could be used to investigate the response of aged containments with corrosion damage that are subjected to other loads, such as earthquakes or external missiles, those other loads have not been studied.

The finite element analyses were stopped when large strains indicated that a tear was likely to initiate in the steel shell or steel liner, or when a significant leak was expected from some other source. For example, some BWR Mark I containments have pressure relief vents that release pressure before a structural failure would be expected. In other cases, seals or other penetrations may leak and release the pressure. Leaks through seals, gaskets, airlocks, equipment hatches, electrical penetration assemblies, bellows, and drywell heads have been studied extensively in the past, and are not being analyzed in this program. However, the potential "non-structural" failure modes that previous studies have identified are considered when performing analyses in this program. If a significant "non-structural" leak is expected before a tear initiates, then the analysis is stopped at that pressure and it is assumed that no tear will initiate because the leak will relieve the pressure. The analysis is not stopped until the probability of the non-structural leak occurring is almost certain, such as is the case with pressure relief valves that are in the Mark I BWR containments.

Several studies of corrosion in containments were completed before this program began (Johnson et al,

1990; Shah et al, 1994; Shah and McDonald, 1989). Most of the focus of these earlier studies was to understand the corrosion issues that relate to nuclear power plant containments, to examine where corrosion had been found or might be expected to be found on a containment, and to propose ways to prevent future degradation. The NRC is continuing research to assess state-of-the-art techniques to estimate the extent and rate of progress of local degradation in containments. Lehner et al (1995) performed a probabilistic assessment to determine how corrosion affected the safety of containments during various accident scenarios. The work described in this report is an extension of these earlier efforts.

The primary objective is to evaluate how well finite element analyses can predict the pressure capacity of a containment with corrosion damage. Obviously, any uncertainty in the failure prediction of an uncorroded containment would also exist, generally with a higher degree of uncertainty, in the failure prediction of a corroded containment. The principle thrust of this report is to compare the relative capacity of corroded versus uncorroded containments, subject to the limitations inherent in predicting the capacity of an uncorroded containment. A few scaled model tests of uncorroded vessels, with accompanying analyses, have been used previously to benchmark how well finite element analyses codes can predict failure.

This report focuses on one type of containment degradation, that is, corrosion of the steel shell or the liner of a concrete containment. Other types of containment degradation, such as loss of prestressing due to corrosion induced failure of tendon elements or anchor-heads, or degradation of bellows were not included in the scope of this work. Issues related to loss of prestressing are being studied, and will be reported on in a future report. Likewise, bellows aging issues are also being investigated and the results will be reported in a future NUREG report.

## 2 BASIS FOR PREDICTING CAPACITY OF CORRODED CONTAINMENTS USING FINITE ELEMENT ANALYSIS

A principal objective in this report is to compare the relative capacity of corroded versus uncorroded containments. Obviously, the accuracy of predicting the response of a corroded containment is subject to the same limitations inherent in predicting the capacity of an uncorroded containment. The comparison of relative capacities (i.e., a percent reduction in capacity) of corroded versus uncorroded containments will be valid, even if the actual predicted failure levels are too high or too low. A summary of scaled model tests and analyses are presented in Section 2.1, however, to help the reader gauge how well previous analyses have been able to predict structural response.

Finite element analyses have been used extensively to model and predict the response of steel and concrete structures, such as automobiles, airplanes, bridges, and nuclear power plant containment vessels. A number of scaled models of containment buildings have been built and pressure tested to failure at Sandia and elsewhere over the last few decades (Hessheimer, et al, 1997a). As discussed in Section 2.1, finite element analysis methods have done a reasonable job of predicting the ultimate failure pressure for these scaled models (Clauss, 1985a; Luk, et al, 1998; Weatherby, 1990), although in many cases the structures failed in modes that were unexpected. In the cases where failure occurred in unexpected locations, the vessels were undergoing large inelastic strains, which were predicted by the analyses, and were close to their predicted failure levels. The actual failures occurred in areas where small details were left out of the analytical models, and those small details caused large strain concentrations to occur. Tests of scaled models and analyses have shown that there are many competing failure modes when the containment vessels are pressurized to several times their design pressure, and that small details in the geometry or condition of the vessel in local areas can effect the failure mode.

Analytical models have done a reasonable job of predicting the global response of scaled model containment structures, and if sufficient details are included in the analytical model, have also been able to predict the local behavior and ultimate failure. However, there are some disturbing discrepancies between scaled model tests and analyses, such as the analyses consistently overpredicting the pressure at which the steel shell yields, as discussed in Section 2.1. In spite of these difficulties, however, the failure predictions have generally been within 10% to 20% of failure pressures observed during the tests.

The oil and gas pipeline industry has been using finite element analyses to predict the leak and/or burst pressures of corroded pipelines for more than a decade. Localized damage, such as pitting corrosion, and a general loss-of-section damage, have been considered in their analyses. These analyses have been validated through pressure tests of corroded pipes. This industry has shown that the pressure capacity of a corroded pipe made with low-strength, low-carbon steel materials can be accurately predicted using finite element analyses and carefully modeling the geometry to reflect the reduced cross-section in the corroded area.

In low-carbon, low-strength steels that are used in containment buildings, the primary effect of corrosion is to reduce the cross-sectional thickness. In addition to this thinning effect, the rough and uneven corroded surface will cause stress and strain concentrations that may cause a tear to initiate in the concentration region. Other degrading mechanisms do not play a significant role for the low-carbon, low-strength steels because the material is resilient to the environment and/or the environment is low enough to not cause a problem. Corroded dog bone shaped coupons were tested to failure in uniaxial tension, and it was shown that the portion of the coupon that was not corroded maintained virgin material properties. In those tests, the corroded material was removed.

The basis for using finite element analyses to calculate the structural capacity of an aged/degraded containment is:

- Finite element analyses have successfully calculated the response of uncorroded containment structures,
- The primary affect of corrosion on low-carbon, low-strength steels is to reduce the cross-sectional thickness, and
- Finite element analyses can account for corrosion by reducing the material thickness in corroded areas. This will create stress/strain concentrations that are similar to concentrations caused by plate thickness changes in an uncorroded containment. Using reduced thickness in corroded areas, the gas and pipeline industry has been successful in using finite element analyses to predict the burst pressure of corroded pipelines.

## 2.1 Scaled Model Tests and Analyses of Uncorroded Containments and Pressure Vessels

Numerous tests and analyses have been conducted for uncorroded containments and other pressure vessels. Hessheimer, et al. (1997a) gives a summary of previous tests and test results in Tables 2.1, 2.2, and 2.3.

The results of the 1:32 scale tests (Table 2.1) indicated that simple shells, without significant perturbations such as stiffeners and penetrations could withstand pressures causing large strains up to the uniaxial material test limits. The presence of even "minor" perturbations or discontinuities resulted in a significant reduction of free field strains with some reduction in the failure capacity. Pretest analyses gave good comparisons with the global response and the observed failure pressures. The calculated failure pressures of SC0 and SC1 was 0.91 MPa with failure occurring at mid-height; for SC2 the calculated pressure was 0.95 MPa with failure of the stiffener rings; failure of SC3 was predicted to occur at 0.84 MPa at the sleeve of the equipment hatch (E/H). One interesting result of these tests was that the initial observed yield was below the calculated yield.

The 1:8 scale test was completed in 1984. Pretest analyses indicated failure would occur due to ovalization of the equipment hatch and leakage past the seals at 1.45 MPa (210 psi). During the test, the vessel failed catastrophically at 1.34 MPa (195 psi). Global behavior compared favorably with the predicted response, however, as with the 1:32-scale models, the analysis over-predicted the pressure at which generalized yielding of the shell occurred. Again, this discrepancy was dismissed since post-yield response approached the predicted behavior. Failure occurred before expected hatch leakage could occur when a tear, subsequently discovered as initiating at a stiffener detail adjacent to the equipment hatch, resulted in catastrophic rupture and fragmentation of the vessel.

The 1:10 scale test for NUPEC and the NRC was completed at the end of 1996. This test included the containment structure, as well as a "contact" structure, which was intended to behave similar to a shield building. Testing was terminated when a large tear developed adjacent to the equipment hatch insert plate weld seam at about six times the design pressure. At the time when the tear developed, there was significant contact between the containment model and the "contact" structure. If the gap between the containment and the "contact" structure had been somewhat smaller, then it is probable that complete contact would have occurred such that the "contact"

structure would have supported the containment shell and prevented the tear from occurring in the equipment hatch insert plate region. Separate blind analyses were performed by a variety of international agencies which were provided with identical design, fabrication, and material property data prior to the test. Pretest predictions of failure (although criteria for failure were not consistent) ranged from 5 to 15 times the design pressure. Most analysts predicted rapidly increasing plastic strains at the elevation of the equipment hatch; however, those with high failure predictions assumed that the vessel would contact the "contact" structure before a tear developed, and that the "contact" structure would prevent additional plastic strains from developing. If the contact structure had not been included in the analyses, the rapidly increasing strains near the equipment hatch would have caused failure in all of the models which included plasticity, and the largest predicted failure pressures would have been much less than 15 time design pressure. The lowest predicted failure pressures, which assumed a tear developed before contact with the "contact" structure, compared favorably with the test results.

One consistent problem with the analyses of steel containments has been that the test models began to yield below the predicted yield pressure. This is quite disturbing. However, the predicted failure pressures were a reasonable match with the test results, with the exception noted in the previous paragraph. Many of the analyses didn't predict the actual failure mode because the analytical models didn't contain sufficient details in local areas. However, during post test analyses, when sufficient details were included in the critical areas, the analyses were able to confirm both the failure pressure and the failure location.

The 1:6 scale reinforced concrete model (Table 2.2) was tested in July 1987, and failed by tearing of the liner plate at a row of studs adjacent to a thickened insert plate at 1.0 MPa. After the test, a number of smaller liner tears and incipient tears were also identified adjacent to thickened insert plates. Pretest predictions of global response by a number of independent analysts, compared favorably to the test results; however, as with the previous steel containment model tests, the mechanism which defined the limit state of the model was not recognized prior to the test by many of the analysts. Some analysts presented a list of candidate liner tearing locations and associated leakage pressure range and, in this way, were able to reasonably predict the test failure pressures. Posttest analysis confirmed the presence of large strain concentrations at these locations which are very similar to details used in prototypical plant construction.

Table 2.3 shows some test results of prestressed concrete model structures.

Table 2.1. Summary of Results of Experiments for Steel Containment Models

Test	Scale	Shape	R/t	Pressure Ratio	Global Strain at Failure	Material	Remarks
SNL SCO (12/2/82, 12/12/82)	1:32	Cylinder w/ hemispherical dome	450 (R=549, t=1.22)	0.93*	20%	AISI 1008	Catastrophic rupture and fragmentation initiating at vertical weld seam. [Horschel and Clauss, 1984; Horschel and Blejwas, 1983]
SNL SC1 (4/20- 21/83)	1:32	Cylinder w/ hemispherical dome	500 (R=546, t=1.09)	0.76*	6%	AISI 1008	Tearing and leakage next to vertical weld seam. [Horschel and Clauss, 1984; Horschel and Blejwas, 1983]
SNL SC2 (7/21/83)  (8/11/83)	1:32	Cylinder w/ hoop stiffeners and hemispherical dome	478 (R=546, t=1.17)	0.93*  0.97*	2.7%  2.5%	AISI 1008	Leakage and tears at cylinder-dome interface; repaired.  Retest; catastrophic rupture and fragmentation. [Horschel and Clauss, 1984; Horschel and Blejwas, 1983]
SNL SC3 (11/30/83)	1:32	Cylinder w/ penetrations and hemispherical dome	478 (R=546, t=1.17)	0.83*	14.5%	AISI 1008	Catastrophic rupture initiating at E/H. [Horschel and Clauss, 1984; Horschel and Blejwas, 1983]
SNL 1:8 (11/15- 17/84)	1:8	Cylinder w/ stiffening rings, penetrations and hemispherical dome	448 (R=2134, t=4.76)	4.9	3%	SA516, Gr. 70	Catastrophic rupture and fragmentation initiation at stiffener near E/H. [Reese and Horschel, 1985; Koenig, 1986; Clauss, 1985a]
NUPEC SCV (12/11/96)	1:10 geom.; 1:4 thick.	Improved BWR Mark II w/ contact structure	135-161 (R=2027 -2900, t=7.5- 9.0)	6.0	2.0%	SPV490, SGV 480	Tearing and leakage at vertical seam weld and at E/H insert plate weld. [Luk et al, 1997; Matsumoto, 1997; Luk and Klamerus, 1996; Porter et al, 1999]

\*Design pressure not specified, maximum pressure (MPa) given.

**Table 2.2. Summary of Experiments for Reinforced Concrete Containment Models and Liner Tearing and Leakage**

Test	Scale	Shape	R/t	Pressure Ratio	Global Strain at Failure	Liner Material	Remarks
SNL RCCV	1:6	PWR: cylindrical concrete shell w/ steel liner and hemispherical dome and penetrations	13.5 (R=3353 t=248)	3.2	1.7%	SA414 Gr. D, SA516 Gr. 60	Tearing and leakage at penetration insert plate. [Horschel, 1988; Horschel, 1992a; Weatherby, 1990; Clauss, 1987; Clauss, 1989b]
CTL Spec. 2.5	Full	prestressed concrete wall-base juncture	-	2.6*	0.2%	Steel	Several tears at wall-skirt juncture [Hanson, 1987]
CTL Spec. 2.4	Full	prestressed concrete wall with penetration	-	2.4*	2.2%	Steel	Large tear at penetration [Hanson, 1987; Dunham et al, 1985]
CTL Spec. 3.2	Full	Reinforced wall with penetration	-	2.9*	2.7%	Steel	Severe liner necking next to anchorage [Hanson, 1987; Dunham et al, 1985]
CTL Spec. 2.2	Full	prestressed concrete wall with initial liner flaw	-	-	-	Steel	Ductile extension of Pre-existing flaw [Hanson, 1987; Dunham et al, 1985]
CTL Spec. 3.3	Full	Reinforced	-	-	1.6%	Steel	Strain concentration measured near penetration (4.3% strain) [Hanson, 1987; Dunham et al, 1985]

\*best estimate based on global strains since models were not pressure vessels

**Table 2.3. Summary of Experiments for Prestressed Concrete Containment Models**

Test	Scale	Shape	R/t	Pressure Ratio	Global Strain at Failure	Liner Material	Remarks
<b>Pressure Vessel Tests</b>							
Fort St. Vrain G.A. Model 1, USA	1:4.5	Cylinder	5	3.5,2.5	0.22%	Steel	[Institute of Civil Engineers, 1967]
Wylfa Vessel, U.K.	1:12	Sphere	5	See remark	0.1%	Rubber	2.7 pressure ratio reached with no leakage [Institute of Civil Engineers, 1967]
Oldbury Vessel, U.K.	1:8	Cylinder		3	0.4%	Steel	[Institute of Civil Engineers, 1967]
"	1:12	Sphere	5	2 - 3	0.4%	Rubber	
"	1:8	Cylinder	3.5	2 - 3	-	Steel	Shear-type failure artificially induced [Institute of Civil Engineers, 1967]
1000 MWe HTGR G.A. Model 2, USA	1:4	Cylinder	2.4	2	0.06%	Steel	
<b>Containment Model Tests</b>							
Polish Model	1:10	(CANDU)	20	1.9	-	1mm steel liner	Liner tearing and leakage esp. around penetration [Donten et al, 1979]
Canadian Model	1:14	Gentilly-2: 4-buttress w/ ring buttress	12.6	8.6	-	none (hydrostatic)	Vertical and hoop tendon rupture. [MacGregor et al, 1979]
Sizewell-B	1:10	Sizewell-B	8.6	2.4	-	Rubber bladder (hydrostatic)	Basemat bending failure [Palfrey, 1990]
NUPEC PCCV	1:4	Large, dry PWR: 2-buttress cylinder w/ hemispherical dome	16.5	0.39*	--	SGV 410	[Hessheimer et al, 1997b]
EPR Model (Civaux Test)	?	Cylinder, inner containment	6.7	0.65*	-	unlined and partial composite liner	[Danisch, 1997]

\*Design pressure (MPa).

## 2.2 Lessons Learned from Corroded Pipeline Research

The National Bureau of Standards conducted corrosion tests on buried sections of pipe from 1910 to 1955 (Romanoff, 1957). More than 36,500 specimens, representing 333 varieties of ferrous, nonferrous, and protective coating materials, were buried in the soil at 128 test locations throughout the United States. Of that total, 300 specimens were made of carbon pipe steel and were buried at 15 different test locations. Half of the specimens were 14 inches long and 1 1/2 inches in diameter, and the other half were 10 inches long and 2 inches in diameter. Two specimens of each configuration and at each location were dug up and examined about every two and one-half years. The last specimens were removed fourteen years after burial. Weight loss data and information on the maximum penetration of pits, along with pictures of the specimens after 14 years exposure, help to quantify the damage to the pipe specimens. Some of the specimens were pressure tested before cleaning, and even though corrosion had completely penetrated the thickness of the wall, the pipes held design pressure. After cleaning, leaks occurred at pit locations. Note that pitting lead to leaks, and not to structural failure. However, the pipes were only pressurized to design pressures, and not to several times the design pressure.

Microbially Induced Corrosion (MIC) has caused significant pitting in a number of stainless steel pipes (Deardorff et al., 1989; Poole, 1989). The structural strength of the remaining pipe has been examined in a crude way to ensure that the pipes can withstand normal operating loads. These studies did not attempt to determine the margin between ultimate failure pressures and operating pressures. Although many "pin hole" leaks have developed from MIC, the pipes have not structurally failed due to the presence of the pitting damage. Leaks occurred through the pits, but the pits did not cause a tear to initiate, propagate, and cause the pipe to burst. As before, the pipes were only pressurized to design pressures, and not to "severe accident" pressures that are several times greater than the design pressure.

The oil and gas pipeline infrastructure is aging, and a great deal of research has been conducted to understand how to evaluate the remaining strength of corroded pipes. Two main areas of study have been growth of pits, which may cause a leak but probably not structural failure, and a loss of cross-sectional area, which may cause the vessel to tear and fail. Although pit growth and the resulting leak in the containment are of concern, a much more significant concern occurs if a larger section of the structure becomes thinner due to

corrosion, which can lead to reduced pressure capacity and catastrophic failures.

The current technique used to assess corroded pipelines is commonly referred to as the B31G criterion (ANSI/ASME, 1986; CAN CSA, 1986). This technique, which is based on fracture mechanics considerations of a longitudinal surface crack in a pressurized cylinder, has been effective in conservatively estimating the remaining strength of corroded pipes. This criterion is often conservative by a factor of two or more (Chouchaoui and Pick, 1994), which has lead the gas and petroleum industry to search for an alternate method that is less conservative. Much of the recent research for the pipeline industry has been devoted to showing that finite element analyses can accurately predict the burst pressures of corroded pipelines. Some of the conclusions from the pipeline research are:

- The 87 experiments on corroded pipe sections tested by Kiefner and Vieth (1989) exhibited ductile failure modes, and did not fail in a brittle manner.
- Corrosion defects in pipelines are typically blunt, having a radius of the same order of magnitude as the wall thickness (Stephens and Bubenik, 1993). Corrosion defects that are blunt have a stress concentration factor that is close to one. Failure occurs at these blunt defect locations in a ductile manner through uncontrolled plastic flow and material instability similar to necking in a tensile test specimen.
- The structural response of a corroded pipeline can be accurately predicted by finite element analyses. A detailed section of corrosion on a pipe was measured by Valenta, et al. (1996). The corrosion consisted of a very irregular shape and depth, with the length of corrosion about 629 mm long, and the depth varying between 1 and 6 mm. The deepest corrosion areas had a degraded thickness of about 50% of the original thickness. The corroded section was instrumented with strain gages, and then pressurized until it burst at 13.4 MPa. The theoretical burst pressure of a non-damaged section was about 16 MPa. The authors performed finite element analyses of the corroded section of pipe and compared their strain predictions with calculated strains. The finite element analyses were performed for pressures up to 10 Mpa, but were not continued until the pipe burst; therefore, failure predictions are not available. At 10 MPa, the strains in the thinned areas were about 5%, and up to these levels there was quite good agreement between the tests and

analyses. A fairly coarse mesh of twenty-node brick solid elements was adequate to capture the structural response of the corroded section.

- The burst pressure of a corroded pipeline can be accurately predicted by finite element analyses, using stress and/or strain based failure criteria. Chouchaoui and Pick (1992, 1993, and 1994) performed large displacement, elastic-plastic finite element analyses of single and multiple corrosion “pits”, where the pits were 25 to 50 mm in diameter, and the corrosion depth is up to 80% of the wall thickness. In the finite element analyses of these defects, high stresses and strains localized in the damaged area. In these areas, the maximum engineering stress from uniaxial tensile strain-to-failure tests was a reliable failure criteria, and the calculated burst pressures were in good agreement with the experimental results. The authors concluded that in the corroded area under the thinned area, a three by three grid of second order continuum elements (twenty node bricks) was adequate to predict the failure pressures with an accuracy of  $\pm 10\%$  or better. Similarly, an effective plastic strain criterion also gave reliable failure predictions.
- Stephens and Bubenik (1993) conclude that “corrosion defects fail after the membrane stress exceeds yielding and the defect strains sufficiently to allow uncontrolled plastic flow.” When this point is reached in a static finite element analysis, the code goes unstable because the structure is no longer stable. They explain that “bending stresses have limited influence on ultimate failure.” In local areas where high bending stresses are present, local plastic bending results in a redistribution of stress until the loads are carried predominantly as membrane forces.
- Popelar (1993) shows that stress in the pipe wall is almost the same for metal loss from the inside or the outside of a pipe.

## 2.3 Material Properties and Aging Issues

### 2.3.1 Types of Degradation.

Most corrosion engineers are seeking to control or prevent corrosion, and understanding the underlying cause of the corrosion is the first step in corrosion design. Therefore, corrosion and other types of degradation are usually categorized according to the mechanisms that cause the damage. For the low-carbon low-strength steels that containment structures

are built of, the categories of corrosion typically listed in textbooks, handbooks, and other reports are:

- *General (uniform) corrosion.* This type of damage results in a more or less uniform loss of metal over a large surface area. The net effect is that the metal cross section is reduced and the remaining surface is rough and uneven.
- *Pitting corrosion.* This type of corrosion produces small holes in the metal surface. The amount of metal that is actually corroded away by pitting is usually a very small percentage of the cross section.
- *Galvanic (two metal) corrosion.* Corrosion occurs where two dissimilar metals are in contact with water or an electrolyte. The resulting damage is a loss of metal over a local area that is near the dissimilar metal connection. The metal cross section is reduced near the connection, and the surface is rough and uneven, while material a short distance from the joint is not corroded.
- *Crevice corrosion.* This occurs in crevices or cracks where moisture can be trapped and become stagnant. The damage consists of small holes in the metal surface, and is a form of pitting corrosion.
- *Microbially influenced corrosion (MIC).* Some microorganisms feed on chemicals in the protective coatings on the metal shell and thus eventually expose the metal to harmful environments, allowing either pitting or general corrosion to occur. Other types of microorganisms accelerate corrosion by generating corrosive waste products. MIC is simply a “catalyst” that accelerates pitting and/or general corrosion.
- *Differential aeration.* This type of corrosion occurs on metal surface where two adjacent sites are exposed to two different concentrations of oxygen, such as at the water line in a BWR suppression pool. The result is damage from general and/or pitting corrosion.
- *Aggressive chemical attack.* Chemicals that come into contact with the metal surface and cause a marked increase in the local corrosion rates are termed chemical attack. This environmental condition causes pitting and/or general corrosion damage to occur.

Several categories of degradation do not affect the low-carbon steels used in containments. Except for the stainless steel bellows, the steels used in containment

structures are not adversely affected by the types of degradation discussed below. The important thing to note about the types of degradation discussed in the following paragraphs is that the strength and/or ductility of material can be degraded without visual warnings. These types of damage are difficult to see with the naked eye; they are difficult to detect, and extremely difficult to quantify. Fortunately, these types of degradation will not affect the low-carbon steel containment structure, except for the bellows. Degradation of the bellows has been addressed under a separate research project (Lambert, 1995), and research for the NRC is still underway. Bellows issues are not considered here.

- *Intergranular and transgranular stress corrosion cracking.* Low-carbon steels that are used in steel containment structures are not subject to intergranular or transgranular corrosion because of the chemical make-up of the metal. Typical environments that cause stress corrosion cracking include: a large number of cyclic loadings (fatigue issues), a long-term loading that causes significant stresses, or large residual stresses. However, containments see a small number of loading cycles, the resulting stresses are small, and the low-carbon steel is resistant to transgranular and intergranular stress corrosion cracking. These types of corrosion have not been found on the low-carbon, low-strength steel containments; carbon steels that are not subjected to long term tensile or cyclic loads and that have a yield strength less than 100 ksi are not very susceptible to stress corrosion cracking. Stainless steels, used in the bellows, are susceptible to intergranular and/or transgranular stress corrosion cracking. Bellows have large residual stresses and the stainless steel is susceptible to this type of damage; this type of damage has occurred in bellows of operational containments. Welds connecting stainless steel bellows or piping to the low-carbon steel of the containment structure are also susceptible to intergranular corrosion. Corrosion of stainless steel bellows have been studied previously (Lambert, 1995); corrosion of the bellows is not being considered in this study.
- *Hydrogen embrittlement.* Low-carbon steel is not sensitive to hydrogen embrittlement at the low temperatures containments are maintained at (Gangloff, 1986; Loginow and Phelps, 1975; Moody et al., 1990). When steel corrodes, hydrogen is a by-product. High strength steels become less ductile when subjected to hydrogen, but the relatively low strength carbon steels used in containment structures do not degrade. Tests on A516 pressure vessels (Loginow and Phelps, 1975) report that the vessels did not degrade with

respect to material ductility or strength after they were subjected to 10,000 psi internal pressure of hydrogen during long term storage tests. Therefore, this type of degradation is not a concern.

- *Radiation embrittlement.* Radiation embrittlement does not occur in low-carbon steel at the low neutron fluences that the containment structure is subjected to.

### 2.3.2 Damage Mechanisms for Low-Carbon Steel.

For the low-carbon, low-strength steels used in containment structures, the categories of corrosion listed in the preceding section can be condensed to two major types of damage. The degradation is caused by different methods of attack, but the resulting damage can be categorized as "loss of section" damage, "local pitting" damage, or a combination of the two. These mechanisms (Fig. 2.1) are:

- *Loss of section.* General (uniform) corrosion, galvanic action, differential aeration, and chemical attack all cause a reduction in the material cross-section. The section becomes thinner as the shell corrodes, and this results in a reduction in strength because of the reduced cross-section. Rough and uneven corrosion surfaces cause strain concentration regions, and failure can occur at lower-than-expected global strains because of tears that initiate in the strain concentration regions.
- *Local pits.* Local pits can be caused by pitting corrosion, crevice corrosion, or microbially influenced corrosion. This type of damage consists of small holes in the metal surface. The most likely result of this type of corrosion is a "leak" in the containment boundary if a pit becomes large enough to penetrate the wall. The amount of metal that is actually corroded away by pitting is usually a very small percentage of the cross-section, so there is no appreciable reduction in strength. Failure can occur at lower-than-expected global strains because of tears that initiate in the strain concentration regions at pit discontinuities. However, local pits can penetrate the steel shell and cause the vessel to leak.

If the density of pits becomes large enough, the pits can grow together and result in a loss of cross-sectional area. These two types of damage often occur simultaneously, so that damage is a combination of both categories.

Corroded material has virtually no strength and uncorroded material retains virgin material properties. As a structural member corrodes, the cross-sectional area of the undamaged portion decreases, and therefore the load-carrying capacity of the member is reduced. Also, a reduction in ductility is caused by stress and strain concentration regions at discontinuities such as pits or rough surfaces.

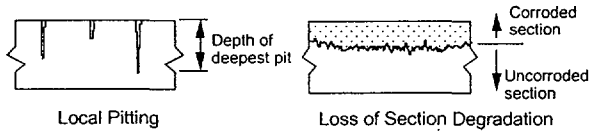


Figure 2.1. Corrosion damage modes.

### 2.3.3 Fracture toughness.

The low-carbon, low-strength materials used in containment structures have a high fracture toughness. These materials are not prone to crack initiation, crack growth, and brittle fracture. However, it is necessary to make sure that pits and the rough, uneven surfaces caused by corrosion don't serve as a "flaw" where a fracture crack can propagate.

General corrosion causes the surface of the steel to become rough and uneven. Corrosion damage that has been observed in pressure vessels made out of the low-carbon low-strength steels used in containment buildings has not resulted in sharp cracks. However, pitting has resulted in very local damage.

It is difficult to define a traditional fracture mechanics "flaw" (i.e., a sharp crack) that represents the rough uneven surface that has been observed in corroded areas of containment vessels. The pits that have been observed do not contain sharp cracks. Never the less, the fracture mechanics method, which assumes a sharp crack, can be used to make a conservative estimate of how large a flaw can be before it will cause a brittle fracture.

Fracture mechanics methods treat crack initiation, crack growth, and brittle fracture separately. There is a considerable amount of scatter in the amount of time it takes for a crack to initiate, which is the first phase. The second phase, after a crack has initiated, is to predict the stable crack growth rate. Finally, the third and last phase is to predict the crack size at which the crack becomes unstable, leading to brittle fracture.

In the following two sections, corrosion damage will be treated as a sharp crack, which is a worst case assumption. This will allow the crack growth rates to be estimated, and the critical crack size to be determined. Bear in mind, however, that sharp cracks have not been observed in the rough, uneven, and

pitted corrosion surfaces of steels used in containment buildings.

#### 2.3.3.1 Crack growth rate.

The ASME Code (1992) weld acceptance criteria in Section III, subsection NE-5300 allows flaws up to 0.635 cm (1/4 inch) in length for weld sections under 1.905 cm (3/4 inch) thick. In the simple analysis that follows, it has been assumed that a crack exists in a containment that is 0.635 cm deep and 1.27 cm long. These could be cracks that were undetected when the containment was constructed, or subsequent damage such as corrosion pits that developed after the plant was constructed. Assuming that the plate section is between 1.27 and 1.91 cm thick, and applying the fracture mechanics approach defined in Section XI, Appendix A of the ASME code (ASME, 1992), one can calculate how much the crack would grow under cyclic loading.

Most of the loads on steel containment buildings do not result in significant stresses, except in the discontinuity and thickness transition areas, where dead loads, sustained thermal strain effects, and residual stresses in heat affected zones could be significant. In reinforced concrete containments, the liner is meridionally strained to a significant level due to dead load, creep and shrinkage of concrete, thermal gradients, and residual stresses due to welding. In prestressed concrete containments, the liner is additionally strained due to prestressed, and additional concrete creep. These loads on the liner are principally compressive, except around the anchorage points. The major applied load which results in extensive, widespread tensile stresses in the steel is the pressure leak tests that are performed periodically throughout the life of the containment.

In this example, 24 cycles of stress have been applied to correspond to an assumed 24 pressure leak tests. The following crack growth rate curve is given as Eq. 1 in subsection A-4300

$$da/dN = C_0 (\Delta K_I)^n \quad (\text{Eq. 1})$$

with the constants defined in Equation 4 of subsection A-4300 of

$$n=1.95,$$

$$C_0 = 1.01 \times 10^{-7} S \quad (S=1 \text{ for } K_{\min}=0) \quad (\text{Eq. 2})$$

Be aware that these constants are for  $K_I$  in units of  $\text{ksi}\sqrt{\text{in}}$ . Also, the variable  $a$  in Equation 3 should be in units of inches,  $\sigma_m$  and  $\sigma_b$  should be in units of ksi, and the  $K_I$  calculated will be in units of  $\text{ksi}\sqrt{\text{in}}$ . The stress

intensity factor is given in Eq 1 of subsection A-3300 as

$$K_I = \sigma_m M_m \sqrt{\pi} \sqrt{(a/Q)} + \sigma_b M_b \sqrt{\pi} \sqrt{(a/Q)} \quad (\text{Eq.3})$$

Upon examining the tables associated with this equation, it becomes apparent that a surface flaw gives a higher stress intensity factor than an embedded flaw. It can also be seen that a membrane stress will have a higher stress intensity than the same magnitude bending stress. Therefore, the 0.625 cm deep by 1.27 cm long flaw will be assumed to be a surface flaw, and it will be assumed that the section is being stressed to its yield stress of about 345 MPa (50 ksi) in membrane tension. Using these assumptions, Figures A-3300-1 and A-3300-3 in the ASME code produce:

$$Q=2.4$$

$$M_m = 1.1$$

Using equation 3 with  $\sigma_m = 345$  MPa (50 ksi) gives

$$\begin{aligned} K_I &= (50 \text{ ksi}) * (1.1) * (\sqrt{\pi}) * (\sqrt{a}/2.4) \\ &= 63 \sqrt{a} \end{aligned} \quad (\text{Eq. 4})$$

Putting these values into equation 1 gives

$$\begin{aligned} da/dN &= 1.01 \times 10^{-7} * (63 \sqrt{a})^{1.95} \\ &= 0.0003258 * a^{0.975} \end{aligned}$$

Assuming that the vessel undergoes 24 pressure leak tests,  $N = 24$ . Using limits of integration of  $a_{\text{initial}} = 0.635$  cm (0.25 inch), and solving for  $a_{\text{final}}$  produces  $a_{\text{final}} = 0.6401$  cm (0.2520 inch). Remember that the variables in the above equation must be input in English units. Therefore, for a crack 0.635 cm deep by 1.27 cm long which is cyclically loaded between zero and yield stress 24 times, the predicted crack depth will increase from 0.6350 cm deep to 0.6401 cm deep.

### 2.3.3.2 Critical crack length.

The third phase of a fracture mechanics approach is to determine if a specified flaw size will fracture or be stable under a specified state of stress. Using Equation 4 with

$$a = 0.635 \text{ cm (0.25 inch)}$$

results in

$$K_I = 35 \text{ MPa}\sqrt{\text{m}} \text{ (32 ksi}\sqrt{\text{in}})$$

Tests performed on A516 steel that was 3.81 cm (1.5 inch) thick measured fracture toughness,  $K_{Ic}$ , values of 99 MPa $\sqrt{\text{m}}$  (90 ksi $\sqrt{\text{in}}$ ) for temperatures

below  $-65^\circ \text{C}$  ( $-150^\circ \text{F}$ ), and 495 MPa $\sqrt{\text{m}}$  (450 ksi $\sqrt{\text{in}}$ ) for temperatures above  $0^\circ \text{C}$  ( $32^\circ \text{F}$ ) (Wellman and Rolfe, 1984). Note that this material was not thick enough to be in a plane strain condition. *The Structural Alloys Handbook* (1994) shows A516 Grade 60 plane strain fracture toughness,  $K_{Ic}$ , values of 27 MPa $\sqrt{\text{m}}$  (25 ksi $\sqrt{\text{in}}$ ) at  $-149^\circ \text{C}$  ( $-300^\circ \text{F}$ ), 33 MPa $\sqrt{\text{m}}$  (30 ksi $\sqrt{\text{in}}$ ) at  $-107^\circ \text{C}$  ( $-225^\circ \text{F}$ ) and 46 MPa $\sqrt{\text{m}}$  (42 ksi $\sqrt{\text{in}}$ ) at  $-52^\circ \text{C}$  ( $-125^\circ \text{F}$ ). A516 Grade 70 critical stress intensity values range between 46 and 79 MPa $\sqrt{\text{m}}$  (42 to 72 ksi $\sqrt{\text{in}}$ ) at  $-52^\circ \text{C}$  ( $-125^\circ \text{F}$ ). Loginow and Phelps (1975) tested A516 steel specimens that were 2.54 cm (1 inch) thick. The thickness requirements weren't met to ensure that the specimen responded in a plane strain condition, but the thickness is fairly close to the thicknesses used in containments. In their tests, they measured a  $K_{Ic}$  of 84 MPa $\sqrt{\text{m}}$  (76 ksi $\sqrt{\text{in}}$ ). Vanderglas and Mukherjee (1981) report  $K_{Ic}$  values of 30 to 36 MPa $\sqrt{\text{m}}$  (27 to 33 ksi $\sqrt{\text{in}}$ ). Because of the crack sizes in the specimen they expected their predicted  $K_{Ic}$  values to be low. This data all appears to be fairly consistent at the very cold temperatures. The  $K_{Ic}$  values for material that was around 2.54 to 3.81 cm (1 to 1.5 inches) thick and not in plane strain was consistently higher than the  $K_{Ic}$  values for thicker specimens that were in plane strain.

Steel shells in containment structures are generally between 1.27 and 3.81 cm (0.5 and 1.5) inches thick, which is too thin to be in a plane strain condition. Also, containment structures operate at temperatures that are well above  $0^\circ \text{C}$  ( $32^\circ \text{F}$ ). For material in this condition, the  $K_{Ic}$  value measured by Wellman and Rolfe is much higher, as would be expected. The test data which most closely matches the condition of a containment shell is the Wellman and Rolfe testing, which found  $K_{Ic}$  values of about 495 MPa $\sqrt{\text{m}}$  (450 ksi $\sqrt{\text{in}}$ ) for temperatures above  $0^\circ \text{C}$  ( $32^\circ \text{F}$ ) and plates thinner than 3.81 cm (1.5 inches). The stress intensity for a crack that is 1.27 cm (0.5 inches) long is estimated to be 35 MPa $\sqrt{\text{m}}$  (32 ksi $\sqrt{\text{in}}$ ), and the capability to resist is around 495 MPa $\sqrt{\text{m}}$  (450 ksi $\sqrt{\text{in}}$ ). For this size of a crack, brittle fracture would not be expected.

### 2.3.3.3 Corrosion Pits and Fracture

It is unlikely that small pits will cause a pressure vessel to catastrophically fail. As the pit grows through the thickness, it will cause a leak to occur, but it won't initiate a tear that leads to total structural failure. It is conservative to evaluate the fracture potential of a pit by assuming that it is a sharp crack. For example, a 1.27 cm diameter pit that is 0.635 cm deep could be conservatively evaluated as a 1.27 cm long crack that is 0.635 cm deep. This was done in the previous section. If the pit has grown through the thickness, then the fracture potential can be estimated using appropriate

formulas. Assuming that a traditional sharp crack length,  $2a$ , is the diameter of the pit, and assuming the section is at yield stress under membrane loading, the following conservative estimation can be made.

For the case where the area of the pit is small compared to the total cross-sectional area (i.e.,  $\text{Area}_{\text{pit}}/\text{Area}_{\text{total}} < 0.1$ ), the stress concentration factor can be calculated as  $K_I = \sigma(\pi a)^{-0.5}$ . The largest  $a$  that can be tolerated can be estimated by selecting  $K_I = K_{Ic}$ , and  $\sigma = \sigma_{\text{yield}}$ . Using a conservative value of  $K_{Ic} = 35 \text{ MPa}\sqrt{\text{m}}$  (32 ksi  $\sqrt{\text{in}}$ ), and  $\sigma_{\text{yield}} = 345 \text{ MPa}$  (50 ksi), results in  $a = 0.33 \text{ cm}$  (0.13 inches). Therefore, a 0.66 cm (0.26 inch) diameter through-wall pit could be tolerated without initiating a tear that leads to catastrophic failure. (More information is given on  $K_{Ic}$  factors in the previous section.) This simple case is conservative.

#### 2.3.3.4 Fracture Summary.

Pits, cracks, or other flaws that are smaller than the postulated crack are stable, the crack growth rate is acceptably small, and the damage will not cause the section to fail in brittle fracture.

The parameters selected in the previous sections are conservative because:

- Fracture mechanics methods treat crack initiation, crack growth, and brittle fracture separately, and the simple analyses from the previous sections assumed that the first phase, crack initiation, had already occurred. In reality, a pit or the rough uneven surface in a corrosion area provide a high stress concentration region where crack initiation is more favorable, but it still takes time for a crack to initiate in those areas.
- Corrosion damage, such as a pit or a rough uneven surface in a corroded area generally have more rounded edges and not sharp edges. The analyses in the previous sections assumed the flaw was a sharp crack. The stress intensity will be lower in the vicinity of a pit or along a rough surface than the calculated stress intensity at a crack tip.
- The fracture toughness of the material is lowest when the material is in a plane-strain condition, which requires the plate thickness to be about 5 cm (2 inches) or more. Since actual containments have plate thicknesses that are smaller than 5 cm, the plate section is in a mixed state between plane stress and plane strain, and will be higher (by some unknown amount) than the test data for material that was in a plane strain condition. Also, the operating temperature of containments will be above  $0^\circ \text{ C}$  ( $32^\circ \text{ F}$ ), and at these warmer

temperatures the critical stress intensity factors increase significantly. Therefore, the critical stress intensity of the material ( $K_{Ic}$ ) will be much, much higher than the  $35 \text{ MPa}(\text{in})^{0.5}$  (32 ksi  $(\text{in})^{0.5}$ ) that would exist at the end of a 1.3 cm (0.5 inch) long by 0.6 cm (0.25 inch) deep crack.

- At design pressure, the stresses in the containment wall will be about one-half of the yield stress. The above examples assumed that the stress in the containment wall was at yield stress. Lower stresses in the containment wall will result in a smaller stress intensity factor.

Therefore, fracture mechanics show that small pits and the rough uneven surface in a corrosion area do not cause brittle failure. The very tiny holes caused by corrosion pits will have a negligible affect on the strength capacity of a containment structure.

The corroded pipeline industry has performed a number of tests on sections of pipes with holes that are 2.5 to 5.1 cm (1 to 2 inches) in diameter and up to 80% corroded through-the-thickness. Chouchaoui and Pick (1992) performed tests of single and multiple corrosion "pits", where the pit depth was up to 68% of the wall thickness. The ultimate pressure capacity of the pipe sections were reduced only a small amount. For example, the largest degradation in pressure capacity occurred for a 51 cm (2 inch) diameter pit that was 68% through the wall. In this case, the ultimate capacity was reduced from 18.7 to 14.7 MPa. The failure which occurred was to blow out the section that was only 32% of the original thickness. A leak developed, but the pipe section did not catastrophically rupture. Several other tests were also run, with similar results, except that the failure pressures were not degraded as much as described above.

Fracture mechanics methods should be used to evaluate the potential for a brittle failure if sharp cracks are detected during future inspections. However, fairly large "sharp" cracks will be required to initiate a brittle failure.

#### 2.3.4 Fatigue and Corrosion Fatigue.

Corrosion can significantly reduce the fatigue life of a structure. The rough corroded surface, pits, or other flaws cause stress concentrations that may cause crack initiation.

However, the number of cyclic loads on containment vessels is fairly small, and the associated stresses are well below yield for design conditions. Temperature transients during startup/shutdown, pipe reactions at penetrations, and crane loads, result in small stresses that are of little concern. Large stresses, but still well

below yield, result from pressurizing the vessel to perform leak tests. Several events, such as a large earthquake, could cause a few cycles with elastic or even plastic stresses in the containment structure. Other events that could cause plastic behavior are severe accidents that result in large internal pressure loads. These events could cause plastic deformation, but the number of cycles would be small (i.e., one cycle for an overpressure load, and less than 100 large strain cycles for an earthquake). The ductile carbon steels used in containment structures are not susceptible to low-cycle fatigue, and the few events which could cause large stresses occur a very limited number of times.

The fatigue curve in Appendix I (Figure I-9.1) of Section III of the ASME design code (ASME, 1992) shows that the ductile steels used in containment structures can be cycled up to yield stress about 5000 times without failure. They can be cycled past the yield stress to 1% strain about 40 times without failure, and they can be cycled to 2% strain about 10 times without causing a failure. These data are for uncorroded steel that has smooth surfaces; Shigley (1983) reports that corrosion reduces the fatigue life by as much as 40%.

Bruneau et al (1997) performed monotonic and cyclic tests on coupons that were cut from the web and flanges of a decommissioned bridge girder that had experienced up to 60% through-the-thickness corrosion. The limited testing results led Bruneau to conclude:

“Initial tests confirmed that the noncyclic ductility of the few corroded structural steel specimens considered here was not significantly affected by the presence of rust, in spite of severe area loss, when subjected to a monotonic tension loading condition. However, cyclic flexural tests on structural members revealed that, although stable hysteretic behavior comparable with that of unrudded specimens is possible, premature fracture under alternating plasticity (i.e., low-cycle fatigue) will typically develop. A considerable cumulative hysteretic energy can be dissipated prior to the development of fatal cracking, and it is sufficient to provide adequate seismic resistance in most applications. However, the observed reduced ductile behavior could be an issue in some specialty applications, such as with some types of passive energy dissipation devices in which steel plates can be subjected to very high local flexural ductility demands.”

If there were a significant number of higher-stress loading cycles, the presence of corrosion would cause a reduction in fatigue life. This would be especially true if the loading cycles caused alternating plasticity. However, under design loads, a containment should

remain essentially elastic so that it undergoes very few, if any, plastic cycles. If earthquake loads were significantly larger than the design values, the total number of cycles, especially cycles which cause alternating plasticity, would be small. In an accident scenario that caused internal pressure loads that were significantly larger than the design pressure, only a monotonically increasing load would be applied. According to the test data that is available, the small number of high tensile stress loading cycles in containment structures will not cause crack initiation, and therefore fatigue failure or fatigue-related damage is of little concern. In addition, if a small flaw did exist (i.e., smaller than the allowable flaw sizes allowed in the weld zones by the ASME code), the flaw would grow a negligible amount. Corrosion fatigue could be an important factor for other components that experience a larger number of high-stress loading cycles, however.

### 2.3.5 Welded Properties.

When subjected to severe loads, it is common for some materials to fail in the weld or in the heat-affected zone. However, for the low-carbon low-strength steels used in containment structures, testing has shown that failure occurs away from the weld area. Based on test data, the weld is not the “weak link” in structural failure of A516 or SA212 steels. During uniaxial tension tests, these materials failed in the base metal and not in the weld zone. Of course, a significant crack in the weld zone could cause brittle fracture, just as a large crack in the containment wall could cause brittle fracture. However, corrosion damage found in actual containments has not shown this kind of degradation along weld seams.

Welds have not become the “weak link” in containment structures because:

- the low-strength, low-carbon steels used in containment vessels are very weldable,
- the material is very tough and resistant to flaws propagating, and
- high quality welds are assured in containment vessels through tightly controlled weld procedures and 100% inspection of the welds for flaws.

The ASME Code (1992) weld acceptance criteria in Section III, subsection NE-5300, allows flaws up to 0.6 cm (¼ inch) in length for weld sections under 1.9 cm (¾ inch) thick. Flaws up to 1.9 cm in length are acceptable for weld sections over 5.7 cm (2¼ inches) thick. At the time of construction, welds in containment buildings are 100% inspected using radiography for butt welds and ultrasonic, liquid

penetrant, and/or magnetic particle examination for other welds. It was shown in sect 2.3.3 that a flaw that is 0.6 cm (¼ inch) long will not grow significantly, and will not lead to brittle failure.

### 2.3.5.1 Tests on welded specimens.

The *Structural Alloys Handbook* (1989) summarizes a number of tests on welded specimens. Following are excerpts from the Handbook:

“The crack-growth rate of A516-70 steel was determined by Ontario Hydro using thick compact-tension specimens. The orientation of the specimens was such that the plane of the fatigue crack was parallel to the rolling direction, the expected direction of weakest resistance. Tests conducted in parent material, weld metal, and heat affected zone showed the ASME Section XI reference curves as a good representation of fatigue-crack-growth properties (El Haddad et al, 1980).”

“The fracture characteristics of Delta specimens of A517-70 material were determined at Lafayette College. These specimens were produced by welding three segments into a triangular shaped specimen which was then supported at three points and loaded in the center. It was shown that the E-7018 electrode produced satisfactory welds in the one-inch thick material since all failures occurred in the plate with none in the weld metal or in the heat affected zone (McGeady, 1971).

“Wide-plate longitudinally-welded plates of one-inch thick ASTM A212-B steel were tested at the University of Illinois to determine the brittle fracture characteristics of the material. Specimens with a transverse notch thru the weld failed at less than 10 ksi for temperatures of from -40 to 40F. Unnotched specimens at -40F failed at from 10 to 22 ksi. Most cracks were arrested within a few inches, however, some traversed the entire test section. These latter specimens were seen to correspond to the catastrophic failures observed in some welded structures of A212-B steel. It was also shown that for unwelded plate, a cycle of hot-prestrain (400 to 600F) rendered material at the root of the notch susceptible to cracking for loads as low 87 percent of the yield strength for test temperatures of from -80 to 80F (Kiefner and Munse, 1967).

An earlier edition of the *Structural Alloys Handbook* (1973) contained test data that was not included in the later edition. Following are excerpts from the 1973 edition:

“Fusion welded specimens of 1/2, 3/4, and 1 inch thick ASTM A-201 Grade A steel plate were tested at Convair. It was shown that weld efficiencies of 100% were obtained for all thicknesses of plate. It was also shown that all weld joints, both free and guided bend, were capable of being bent thru 180 degrees without failure (Steir, 1959; Giutoli, 1960).”

Comments on the figures in the handbook show that all specimens failed in the parent material, 1.3 to 2.5 cm (1/2 to 1 inch) away from the weld joint.

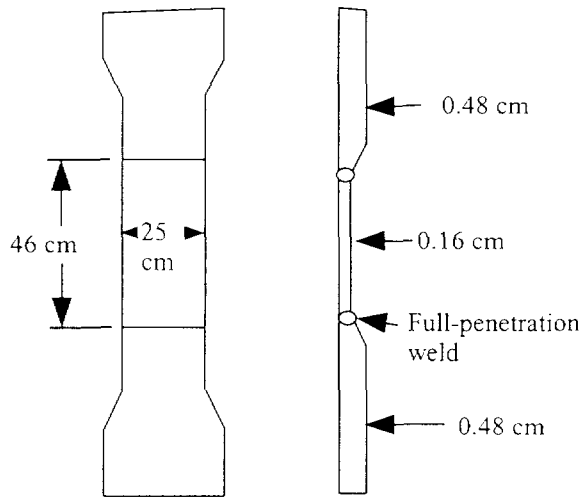
Data is shown in the *Structural Alloys Handbook* (1989) for tension tests of transversely butt-welded plates, 1.3 cm (½ inch) thick. A516-60 and A516-65 specimens welded using AWS E7018 electrodes were tested, and in all cases failure occurred in the base metal and the joint was 100% efficient (Melville, 1971).

During post-test evaluation of a 1:6 scale reinforced concrete containment vessel at Sandia (Weatherby, 1990), questions arose about transition regions where different thickness plates were welded together. To answer these questions, four specimens were made of A516 Grade 70 steel and tested to failure in uniaxial tension (Fig. 2.2). Following is an excerpt from the report (Spletzer et al., 1995).

“From this examination of the strain gage response of the weld and thickness transition specimens, it is apparent that the weld does not cause a strain increase. Further demonstration of this fact comes from the failure mode of the specimens. In total, four specimens were tested to failure. Owing to a machine malfunction, detailed data exist only for the three that have been reported. Of the four that were tested to failure, two of the specimens failed through tearing of the liner in the central region very far from the weld, and two specimens failed through a tear near the weld and a tear running across the width of the specimen. While this tear started near the weld, it was influenced by the strain concentration along the edge of the liner plate.”

A 1:8 Scale Steel Containment Vessel, made of A516 steel, was tested at Sandia in 1984 for the NRC. It underwent two pressure cycles before the final “severe accident” test. The vessel was subjected to 1.15 times its design pressure and the pressure was released. It was then subjected to 1.0 times its design pressure, and the pressure was released. Finally, it was subjected to 4.9 times its design pressure, which caused catastrophic failure. A failure investigation was conducted after the test, and the following summary is given in Appendix B of the report (Koenig, 1986):

“Fractographic and metallurgical evidence from this investigation indicate a failure sequence for the model which occurred as a series of ductile crack growth steps. Large displacements around the equipment hatches caused high local strains in the stiffeners, leading to ductile overload tear cracking at weld joint locations. The initial observed crack in the stiffener around EH1 was a ductile fracture generating a crack which the model structure was able to tolerate between 165 psi and 195 psi (4.1 to 4.9 times design pressure). At the upper pressure the crack propagated through the model wall, which for a short time sustained this additional flaw size. As indicated by increasing strain gauge readings and leaking for the last one-half minute, some slow ductile crack growth in the wall was likely. Final rapid failure of the structure occurred at some unknown critical flaw size, the high rate crack propagation was also ductile.”



**Not to Scale**

**Figure 2.2. Welded test specimens for 1:6 scale concrete containment liner**

As part of the failure investigation, tests were performed at Sandia on weld material and compared to properties on the base plate material that were measured by Chicago Bridge and Iron, who built the vessel. This data, included in Appendix B (Koenig, 1986) is presented here as Tables 2.4 and 2.5. This data shows how the strength and ultimate strain values vary between base metal and weld material. It also shows the effect of strain hardening on base metal, weld material, and material in the Heat Affected Zone (HAZ).

**Table 2.4. Material properties of base metal and weld material.**

	Base Material	Weld
Yield strength MPa (ksi)	400 (58)	430-490 (62-71)
Ultimate Strength MPa (ksi)	560 (81)	520-610 (76-88)
Uniform Strain	0.17	0.10-0.14
Fracture Strain	0.36	0.22-0.33

**Table 2.5. Strain hardening of base metal, weld material, and material in the HAZ.**

	Knoop hardness values (300G load)		
	Base	Fusion Zone	HAZ
Virgin material (material from “as built” structure -- no strain hardening)	185	200	195
Strained material (material cut from structure after test was completed -- considerable strain hardening)	227± 6	222 ± 6	223 ± 19

Also as part of the failure investigation, four test specimens were sectioned from an original equipment hatch cutout with the weld running transverse to the specimen tensile axis. This information is also included in Appendix B (Koenig, 1986):

“Two samples were tested as-welded, and two were tested with the weld bead ground flush to the plate thickness. All were at room temperature at a moderate strain rate. Each specimen broke in the base metal well away from the weld heat affected zone. . . . These tests show that the weld zone had higher strength than the base metal and did not exhibit regions of low ductility. In addition the

geometrical stress concentration at the weld bead fillet did not affect the fracture location.”

Sandia recently completed testing a 1/10 scale Steel Containment Vessel for NUPEC and the NRC. Tensile tests were performed on welded specimens. Excerpts from a memo summarizing these tests follow (Luk, 1997):

“Welded Plate No. 1 was composed of two 6 mm SGV 480 steel plates welded together to represent a section of the top head shell and Welded Plate No. 2 was made of a 8.5 mm SGV 480 steel plate welded to a 9.0 mm SPV 490 steel plate to represent a section of the material change interface. . . . Two test specimens were fabricated from each of the welded plates. . . . In all four tests, tensile specimens were failed by necking near the strain gage location and not at the weld seam. For the two specimens from welded plate number 2, necking occurred in the 8.5 mm SGV 480 steel plate. As can be seen in the test data plots . . . the engineering stress - engineering strain curves for these specimens from welded plates are very similar to those from the parent steel plate.”

The 1/10 scale SCV was tested pneumatically in Japan by NUPEC to 1.25 times design pressure before they shipped it to Sandia. At Sandia an initial instrumentation check was done at 1.5 times design pressure, and there were some indications that yielding occurred during this test. One month later the SCV was pressure tested to failure, which occurred at about 6 times the design pressure. The scaled model was pressurized and depressurized two times before being subjected to failure level pressures.

### 2.3.5.2 Welds in steel containments and liners.

Test data shows that for the low-carbon, low-strength steels used in containment structures the weld is stronger than the base material, although slightly less ductile. Numerous tests on simple coupons indicate that for a weld with no flaws or notches, the weld is not the “weak link”. However, the data also shows that a notch or significant flaw in the weld material can severely weaken the joint so that premature failure occurs in the weld region.

The ASME design intent is that a structure remain well below yield stress at the design pressure. However, it is possible that at design pressure small plastic strains occur in very local regions. This could be caused by stress concentrations, or by residual stresses in welds. Structural discontinuities, such as plate thickness changes and direction changes (i.e., where a stiffener meets a cylindrical shell at an angle of 90°), almost

always occur at weld lines. Very often these geometric changes cause a stress or strain that is larger than the free field stress, and the weld zone is in the region that is experiencing stresses that are larger than free field stresses. During a pressure test, the peak stresses are less than the yield stress, except for very local stress concentration regions. Residual stresses in the weld zone, which could help to contribute to these local stress concentrations, are self-limiting. Although high residual weld stresses could result in very local yielding during the first pressure test of a containment, subsequent pressure tests would not cause additional plastic yielding because of strain hardening which had already occurred.

Both the 1:8 scale steel vessel tested for the Nuclear Regulatory Commission in 1984 and the 1:10 scale steel vessel tested for Nuclear Power Engineering Corp of Japan and the U.S. Nuclear Regulatory Commission in 1996 were subjected to two larger-than-design-pressure cycles prior to the “severe accident” test that caused failure. The repeated testing did not appear to reduce the pressure carrying capacity of the vessels by degrading the weld material. Both structures failed considerably above their design pressures.

The work done by Ontario Hydro (El Haddad et al, 1980), indicates that the ASME Section XI reference curves for fatigue-crack-growth properties apply to the weld material and HAZ as well as the parent material. Based on this information and the reference curves in the ASME code, there is no reason to believe that Appendix J pressure leak tests or initial Structural Integrity Tests degrade the pressure capacity of a steel containment by weakening the weld.

Based on test data available in the literature, there is no reason to believe that pressurizing a containment vessel up to design pressure a few dozen times in its lifetime will degrade the pressure capacity by reducing the strength of the welds. This conclusion is based on:

- test data showing that the ASME fatigue-crack-growth curves are valid for base metal, weld material, and the HAZ,
- test data showing that in the absence of a significant flaw in a weld, failure occurs in the base metal and not in the weld,
- good weld procedures and inspection criteria that ensure that any initial flaws are small, and
- linear-elastic fracture mechanics (Section 2.3.3) that show the crack grows only 0.05 mm (0.0020 inches) under 24 cycles of loading and that there is a big margin between the applied stress intensity factor at the crack tip and the fracture toughness of

the material. Note, however, that fracture mechanics experts state that applying fracture mechanics techniques to weld areas is questionable, and indicate that further work is needed in this area (Barsom and Rolfe, 1987).

## 2.4 Corroded Coupon Tests

### 2.4.1 Uniform Corrosion.

In order to experimentally measure the structural degradation caused by corrosion, several 1.588 mm (1/16 inch) thick A516 Grade 70 steel plate samples were corroded and tested to failure in uniaxial tension. Three plate specimens were corroded by placing them in a  $\sim 93^\circ\text{C}$  ( $\sim 200^\circ\text{F}$ ) magnesium chloride solution; one plate was retained as a control sample and was not corroded. The three plates that were corroded were placed in a vertical position with about 63 mm (2.5 inches) of each plate submerged in the hot solution. Since the glass jar containing the plates and solution was covered and insulated, the 165 mm (6.5 inch) section of the plates that was above the waterline saw temperatures of  $\sim 93^\circ\text{C}$  ( $\sim 200^\circ\text{F}$ ) and humidity levels near 100%. One specimen was corroded for a period of one week, another for three weeks, and the last for six weeks. The corrosion products were removed from the plates by scraping, wire brushing, and using "Naval Jelly" rust remover, so that only the uncorroded steel remained.

After one week, the first specimen was removed from the solution. Damage to the specimen consisted of general corrosion and pitting, and these were a result of differential aeration, temperature, a corrosive environment, and so forth. Most of the corrosion occurred in the middle third of the plate, and the weight of the plate decreased by about 6 grams from its initial weight of 391.5 grams. Since most of the damage was in the middle third of the plate (portion just above the waterline), this plate experienced about 5% reduction in weight in the middle third, with minimal reduction to the rest of the specimen. Pits and pock marks that were in the corroded area were visibly deeper than the area that surrounds them. Although the average thickness decreased by about 5%, local areas experienced more degradation.

Damage to the second specimen was somewhat different. The portion of the plate that was submerged experienced less damage than the 2/3 of the plate that was above the waterline. The portion above the waterline experienced both general corrosion and pitting, as a result of differential aeration, temperature, corrosive environment, etc. Damage to the middle third of the plate was predominately general corrosion and was somewhat uniform. Damage to the top third of the plate was significant and had significant pitting.

Pits and pock marks that were in this area were considerably deeper than the areas that surrounded them. The weight of this plate decreased by 29 grams, from an initial weight of 380 grams. Since most of the damage occurred in the top 2/3 of the plate, the average weight loss in the damaged areas was about 10%.

The last plate that was removed from the solution looked much as the second plate, except more metal had corroded. The weight of this plate decreased by 56 grams from an initial weight of 383 grams. Once again, since most of the damage occurred in the top 2/3 of the plate, the average weight loss in the heavily damaged areas was about 20%.

After removing the corrosion products, the uncorroded control plate and each of the corroded plates were then cut into five dog bone shaped coupons, as shown in Figure 2.3. Therefore, five coupons had about 5% degradation, five coupons had about 10% corrosion, five coupons had about 20% corrosion, and five coupons were uncorroded. The coupons were all oriented in the same rolling direction in case material properties of the plate varied in the longitudinal and transverse directions. In the reduced section of the corroded coupons, thickness measurements were made on a 3 by 17 grid, as shown in Figure 2.4. Therefore, the thickness was measured at a total of 51 places for each of the corroded specimens. The grid shown was marked on the coupons, and photographs were taken of the corroded sections. Initially, the coupons were  $1.77 \pm 0.003$  mm thick. After corrosion, the coupons with about 5% corrosion were between 1.60 and 1.75 mm thick. The coupons with about 10% corrosion had thickness ranging from 1.50 to 1.70 mm and those with about 20% corrosion were between 1.22 and 1.60 mm thick. For each coupon, the average thickness was determined by averaging the 51 thickness measurements. The average cross-sectional area was estimated to be the average thickness multiplied by the width of the specimen.

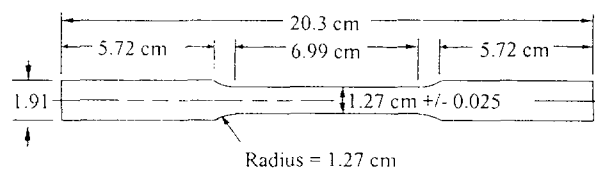


**Figure 2.3. ASTM dogbone shaped coupons used in tensile tests.**

The coupons were tested to failure in uniaxial tension in accordance with ASTM standards (1991). Data measured during the tests consisted of applied force and percent-elongation-in-a-2-inch-gage-length. Engineering stress was calculated by dividing the measured force by the average cross-sectional area of the coupon at the beginning of the test.

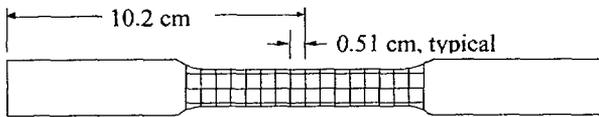


**Figure 2.4. Thickness measurement points.**

The uncorroded coupon specimens reached about 24% elongation before significant necking began, and about 28% total elongation before failure occurred. In Figures 2.6, 2.8, 2.10, and 2.11 stress was calculated by dividing the applied force by the original (unstrained) cross-sectional area. The thicknesses of the coupons for the uncorroded specimens are shown in Table 2.6. Three coupons were from taken from one plate, while the other 2 coupons were from a different plate section. The percent elongation is equivalent to engineering strain up to the point where necking began. After necking began and as the specimen continued to be stretched, additional plastic strain localized around the necking region. At this point, the strains in the necking region would be considerably higher than those shown in the figures.

**Table 2.6. Coupon Thicknesses of Uncorroded Specimens.**

	Min. Thick. (mm)	Max. Thick. (mm)	Ave. Thick. (mm)	Stand. Dev. (mm)
<b>Coupons</b>				
<b>4B,4C,4D</b>	1.76	1.78	1.770	0.003
<b>Coupons</b>				
<b>5A,5B</b>	1.74	1.76	1.750	0.003

Photographs of a typical section of the specimens that corroded approximately 5% through the thickness are shown in Figure 2.5. These reached the same stress levels as the uncorroded specimens, but necking of the specimen began at about 13% strains, and total strains at failure were around 16%, as shown in Figure 2.6. Stress was calculated as applied force divided by the average cross-sectional area, with the average of 51 thickness measurements being used on each coupon to calculate the average area. Three out of the five coupons with this amount of corrosion experienced necking that was outside the 2 inch extensometer. The stress-strain curves of the corroded coupons shown in Figure 2.6 are all comparable up to the point of

necking. The 3 specimens that necked outside the 2 inch extensometer region show an abrupt drop in load with no further elongation of the specimen. This is because the additional elongation that was occurring in the necking region was outside the extensometer region and was not measured. However, if necking had occurred inside the 2 inch extensometer length, then the stress strain curves would have rolled over gradually, as occurred in the uncorroded coupons and in two of the corroded coupons. The measured thicknesses of the corroded coupons are given in Table 2.7. Before the specimens were corroded, they had the same thicknesses as shown for coupons 4B, 4C, and 4D in Table 2.6.

Photographs of a typical section of the specimens that corroded approximately 10% through the thickness are shown in Figure 2.7. These specimens reached the same stress levels as the uncorroded specimens, but necking of the specimen began at about 12% strains, as shown in Figure 2.8. Stress was calculated as applied force divided by the average cross-sectional area, with the average of 51 thickness measurements being used on each coupon to calculate the average area. Four out of the five coupons with this amount of corrosion experienced necking that was outside the 2 inch extensometer. Although all five coupons were tested, the test data was lost on 3 of the specimens. Therefore, only two curves are available for these samples. The specimens that necked outside the 2 inch extensometer region show an abrupt drop in load with no further elongation of the specimen. This is because the additional elongation that was occurring in the necking region was outside the extensometer region and was not measured. However, if necking had occurred



**Figure 2.5. Photographs of Coupons 2A and 2E With 5% Corrosion.**

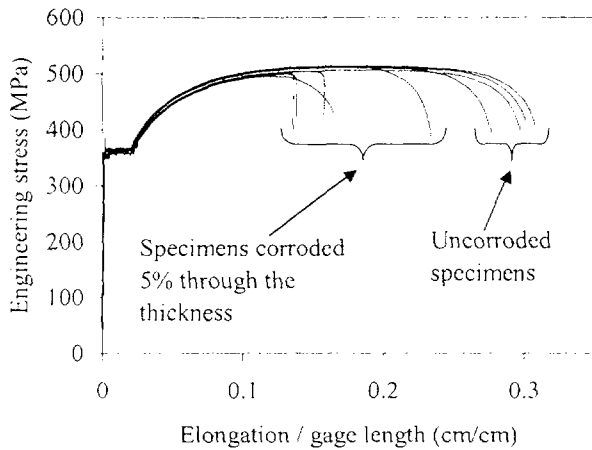


Figure 2.6. A516 Gr. 70 steel stress-strain curve - 5% corrosion.

inside the 2 inch extensometer length, then the stress-strain curves would have rolled over gradually, as occurred in the uncorroded coupons. The measured thicknesses of the corroded coupons are given in Table 2.8. Before the specimens were corroded, they had the same thicknesses as shown for coupons 4B, 4C, and 4D in Table 2.6.

Table 2.7. Coupon Thicknesses (t) of Specimens Corroded Approximately 5%.

	Min t (mm)	Max t (mm)	Ave t (mm)	Standard deviation (mm)
Coupon 2A	1.63	1.74	1.70	0.023
Coupon 2B	1.61	1.76	1.71	0.036
Coupon 2C	1.64	1.76	1.71	0.028
Coupon 2D	1.69	1.76	1.72	0.015
Coupon 2E	1.61	1.75	1.70	0.036

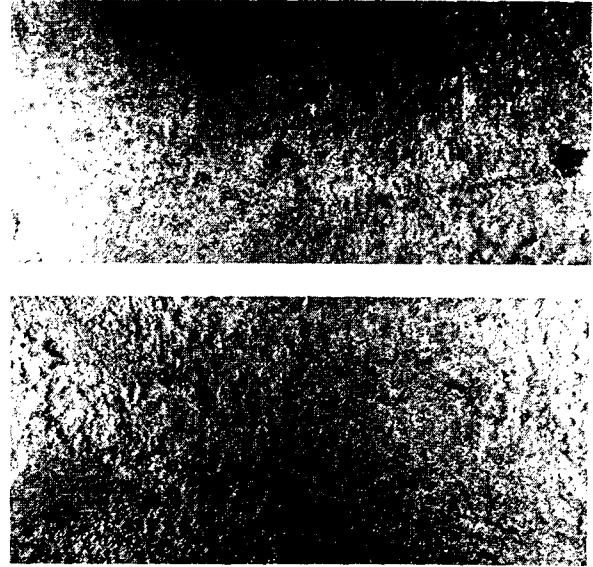


Figure 2.7. Photographs of Coupons 1C and 1D With 10% Corrosion.

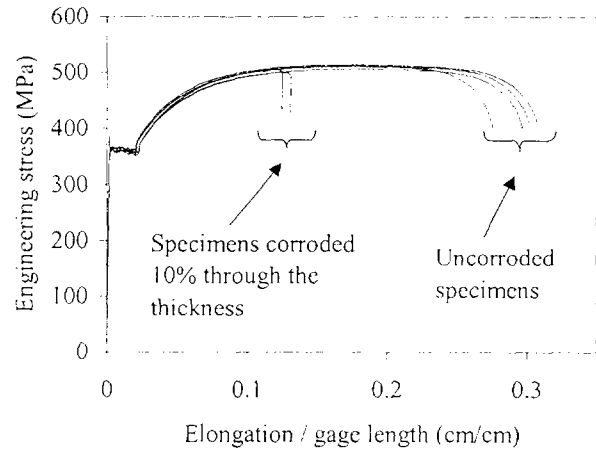


Figure 2.8. A516 Gr. 70 steel stress-strain curve - 10% corrosion.

Table 2.8. Coupon Thicknesses (t) of Specimens Corroded Approximately 10%.

	Min t (mm)	Max t (mm)	Ave t (mm)	Standard deviation (mm)
Coupon 1A	1.50	1.70	1.61	0.028
Coupon 1E	1.51	1.69	1.63	0.028

Photographs of a typical section of the specimens that corroded approximately 20% through the thickness are shown in Figure 2.9. Stresses were calculated by dividing applied force by the average cross-sectional area, with the average of 51 thickness measurements being used on each coupon to calculate the average area. These specimens reached stress levels that were about 4% less than the stress levels reached by the uncorroded specimens, as shown in Figure 2.10. This slight decrease in stress is a result of calculating stress using the average cross-sectional area, while the cross-sectional area varied along the length of the specimen; failure occurred in an area that had a lower cross-sectional area than the average. The limited number of thickness measurements, three across the width of the specimen, were not enough to determine what the minimum cross-sectional area really was. However, the three thickness measurements nearest the failure location averaged about 3% less than the overall average that was used to calculate the stresses. Necking of the specimens began at about 14% strains. All of the coupons with this amount of corrosion necked inside the 2 inch extensometer length. The measured thicknesses of the corroded coupons are given in Table 2.9. Before the specimens were corroded, they had the same thicknesses as shown for coupons 4B, 4C, and 4D in Table 2.6.

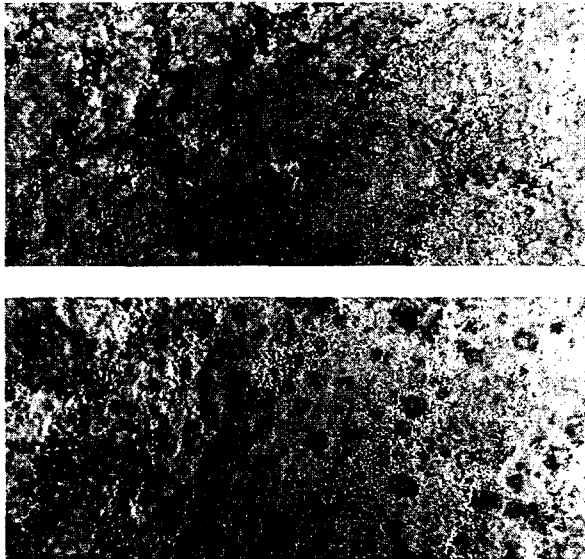


Figure 2.9. Photographs of Coupons 3A and 3C With 20% Corrosion.

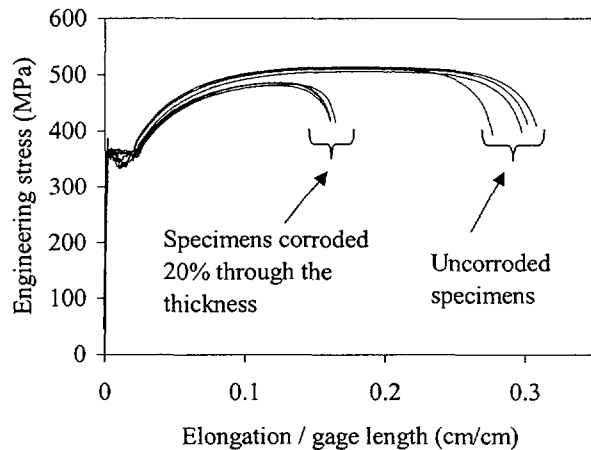


Figure 2.10. A516 Gr. 70 steel stress-strain curve - 20% corrosion.

Corroded coupons had a reduction in strength that was essentially proportional to the reduction in net cross sectional thickness. In elastic regions and at low plastic strains, the stress versus strain curve was the same for both the corroded and uncorroded coupons. In the plastic region, the stress versus strain curves for corroded and uncorroded material was about the same, except that the *percent elongation in a two inch gage length* decreased for the corroded coupons. When the plastic strains in the stress concentration region become large enough to initiate failure, the "net" or "effective" or "average" strain through the coupon cross section was about half of the strain-to-failure levels of uncorroded coupons.

Table 2.9. Coupon Thicknesses (t) of Specimens Corroded Approximately 20%.

	Min t (mm)	Max t (mm)	Ave t (mm)	Standard deviation (mm)
Coupon 3A	1.37	1.55	1.46	0.043
Coupon 3B	1.34	1.57	1.46	0.043
Coupon 3C	1.37	1.60	1.47	0.048
Coupon 3D	1.33	1.60	1.45	0.046

Up to about 12% strains, the stress versus strain curve was about the same for both the corroded and uncorroded coupons. However, plate sections that had corroded were able to carry less load because the cross-

sectional area had decreased. The corroded coupons failed at about 50% of the elongation that caused failure in the uncorroded specimens. This reduction was caused by very local stress and strain concentrations around pits and on the rough uneven surfaces. In these "micro" concentration regions, the plastic strains were larger than they were in areas outside of the concentration region. Failure was initiated as a result of these very local plastic strains. There is a large uncertainty associated with applying the results to containment structures. Corrosion is a random process and is heavily dependent on environmental conditions such as temperature, humidity, presence of chemicals such as chloride or boron, and so forth; it is possible to get an infinite combination of rough, pitted, uneven surfaces in a containment shell. Also, scaling effects could be important since the coupons tested were quite thin compared to the thicker sections that exist in containment structures. While the limited number of corroded coupons tested gave an indication of the change in ductility, there were not enough samples to get a good statistical picture of the potential extremes. The stress and *elongation in a two inch gage length* for the uncorroded coupons was quite uniform and repeatable from test to test. As expected, the stress and *elongation in a two inch gage length* for the corroded specimens exhibit a bigger range of answers. In other words, the uncertainty in when corroded material fails is significant.

Uncertainty in the failure strains of corroded A516 steel will lead to a similar uncertainty in finite element predictions of the ultimate capacity of corroded containment structures. However, variability can and will occur in containment structures because of reasons just discussed. There is a large combination of corrosion possibilities in existing containments. For example, the containments that have experienced corrosion have done so for very different reasons (sand pocket at Oyster Creek, torus at Nine Mile Point Unit 1, corrosion due to borated water at McGuire, etc.). If the corrosion products were removed from the steel, the remaining surface would be different for each of these installations. Therefore, the ductility degradation would also be different. The coupons that were tested may not represent as wide of a range of variability as exists in the real world examples just cited.

In section 4, the criteria that will be used to predict failure in containment structures will be discussed. The large uncertainty associated with the failure criteria is due in large part to the uncertainties associated with the variabilities just discussed.

## 2.4.2 "Pitted" Coupon Tests.

Eight uncorroded dog bone shaped coupons (Figure 2.3) had small through-the-thickness holes drilled in them to represent pits. Each coupon had one hole in the middle. Near the hole, the strain concentration regions were in a multi-axial stress state. These coupons were tested to failure in uniaxial tension in accordance with ASTM requirements. The size of the holes is shown in Table 2.10 and stresses in the coupons are shown in Table 2.11. The results from these tests are shown in Figure 2.11.

**Table 2.10. Through-the-thickness "Pitted" Coupons.**

Number of coupons	Diameter of hole in coupon (mm)	Reduction in Cross-sectional area
2	no hole	0.0%
2	0.15	1.2%
2	0.33	2.6%
2	0.48	3.8%
2	0.99	7.8%

As can be seen in Table 2.11, a 1.2% decrease in cross-sectional area does not affect the ultimate ductility or load capacity. (The slight increase in strength for specimens with a 0.15 mm hole is likely caused by scatter in the testing process, and would probably disappear if enough specimens were tested to be statistically significant.) When the "pitting" becomes significant enough to reduce the cross-sectional area by several percent, then the load capacity of the section does begin to decrease, but by an amount that is less than the percent reduction in cross-sectional area. For the case with a hole large enough to reduce the cross-sectional area by 7.8%, the reduction in strength of the section was only decreased by 4.1%. The multi-axial stress state around the hole causes the yield strength to increase slightly, and this increased yield strength tends to offset a portion of the reduction in area. This is consistent with the von Mises yield criteria, which stipulates that the yield stress of material under biaxial stress is about 15% larger than the yield stress of material under uniaxial stress.

**Table 2.11. Stresses in "Pitted" Coupons.**

Diameter of hole (Reduction in Area)	Peak Eng. Stress based on Gross Cross-Sectional Area (Reduction in Stress)	Peak Eng. Stress based on Net Cross-Sectional Area (Increase in Stress)
0.000 cm (0.0%)	513 ± 2 MPa (0.0%)	513 ± 2 MPa (0.0%)
0.015 (1.2%)	515 ± 3 (-0.4%)	521 ± 3 (1.6%)
0.033 (2.6%)	506 ± 1 (1.4%)	520 ± 1 (1.4%)
0.048 (3.8%)	505 ± 2 (1.6%)	525 ± 2 (2.3%)
0.099 (7.8%)	492 ± 2 (4.1%)	534 ± 2 (4.1%)

The important point to note is that if pits are small in diameter (relative to material thickness), and the net reduction in cross-sectional area is less than a few percent, the strength and ductility of the section is not significantly reduced. The material reaches high strains and stresses in very local regions around the hole, but because of the multi-axial stress state, the yield stress in the stress concentration region actually increases slightly. Any net reduction in strength or ductility is insignificant.

If the pits become larger so that the reduction in cross-sectional area is more than several percent, then the strength and ductility of the "net" cross section is

reduced. Pits that have been observed on containment structures have typically been small in diameter, and the net reduction in cross-sectional area has been much less than 1%. Therefore, these pits have no significant impact on the failure of containment vessels unless the pit completely penetrates the thickness and a leak results.

Necking of the specimens without holes began at about 24% strain. The coupons with a 0.15 mm diameter hole experienced very little decrease in elongation. However, as the hole size increased from 0.15 mm to 0.99 mm, the elongation decreased significantly. These specimens had the same thicknesses as shown for coupons 5A, and 5B in Table 2.6.

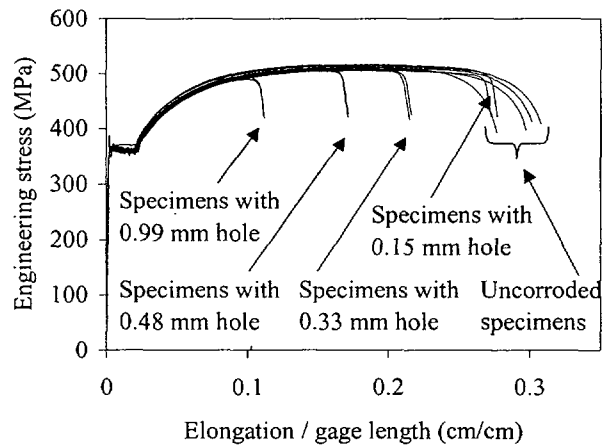


**Figure 2.11. Stress vs. Elongation for Coupons with "Pits".**

### 3 OBSERVED CORROSION DAMAGE

Corrosion degradation has been found in about one-third of the containment structures in operational nuclear power plants. The inside surface of the torus at Nine Mile Point has experienced general corrosion and pitting (MPR Associates, Inc., 1989; Jordan, 1988; USNRC, 1988). The Fitzpatrick plant experienced local corrosion caused by degradation of the coating on the inside wall of the torus (Jordan, 1988; USNRC, 1988). The Oyster Creek drywell had significant corrosion in local areas in the sand pocket region (Shah and McDonald, 1989). Significant coating damage and base metal corrosion on the outer surface at the base near the containment floor were observed at McGuire Unit 2 (USNRC Information Notice 89-79, 1989; McGuire Nuclear Station, Licensee Events Report 369/89-20; Catawba Nuclear Station, Docket No. 50-413, 1990). McGuire Unit 1 and two Catawba units experienced similar damage. Table 1 gives brief descriptions of damage, compiled by NRC personnel (Norris, 1994), that has been observed in operating plant steel containments.

Several NUREG publications (Shah et al, 1994; Shah and MacDonald, 1989; Johnson et al, 1990) give a thorough listing of BWR and PWR plants and typical design parameters, the materials used in the containment structures, environmental operating conditions, types of corrosion that can be expected for the materials involved, and the locations on the containment structures where the corrosion is likely to occur. They also provide detailed descriptions of corrosion degradation that has already occurred in containments of operational nuclear power plants. The information in these reports was used in selecting the location of corrosion in sections 5, 6, 7, and 8.

Although a number of containments have experienced corrosion, few analyses have been done to determine the ultimate capacity of corroded containments that are subjected to accidents that are beyond the design basis (Vora, 1993). Limited analyses have been done for corroded containments subjected to design basis accidents, such as in the case of Oyster Creek degradation (Miller, 1991) and the pitting that occurred

at Nine Mile Point. Both of these cases focused on the effects of corrosion on the design margins relative to the ASME code allowable values. In these studies, corrosion was characterized as a loss of metal thickness for structural considerations and there was no discussion of the effects of corrosion on ultimate behavior or failure modes.

For uncorroded containments, significant efforts have gone into performing scaled model tests and computer analyses to predict the ultimate capacity; no such tests or detailed three-dimensional and non-linear finite element analyses have been performed for corroded containments. For containments that have corroded, limited analyses using axisymmetric and linear-elastic models have been performed. In a few cases, axisymmetric and elastic-plastic analyses were done on corroded containments (Lehner et al., 1995; Tan and Bagchi, 1996). One obvious limitation of an axisymmetric analysis is that the corrosion damage must also be axisymmetric. Depending on the actual corroded geometry, an axisymmetric representation could be either conservative or non-conservative. The point is that analyses of corroded containments have not been performed with nearly the same level of detail that has been done for uncorroded containments. Corrosion damage to containments will generally not be axisymmetric, and large plastic strains will occur when the containment is subjected to beyond design basis accidents.

Similarly, work has been done in the shipping industry (Eric Green Associates, 1992) [54 -- bibliography listing hundreds of articles and abstracts], for off-shore structures, waste storage facilities, and for buildings and bridges (Kayser and Nowak, 1989). For these cases, significant efforts have been made to select corrosion resistant materials, estimate corrosion rates, allow excess material to account for the degradation, and take necessary steps to eliminate or reduce the effects of corrosion. However, efforts to calculate the degraded strength have been minimal and have consisted of thinning the cross section proportional to the amount of corrosion.

**Table 1. Occurrences of Structural Degradation at Nuclear Power Plants**

<b>Plant</b>	<b>Type</b>	<b>Degradation Damage</b>
Monticello	BWR - Mark I steel drywell & wetwell	Polysulfide seal at the floor to shell interface had become brittle allowing moisture to reach the steel shell
Oyster Creek	BWR - Mark I steel drywell & wetwell	Defective gasket at the refueling pool allowed water to eventually reach the sand cushion region which corroded the drywell shell
Nine Mile Point 1	BWR - Mark I steel drywell & wetwell	Corrosion of the torus
Fitzpatrick	BWR - Mark I steel drywell & wetwell	Degradation of the torus coating with associated pitting
Millstone 1 Pilgrim	BWR - Mark I steel drywell & wetwell	Degradation of the torus coating
Cooper	BWR - Mark I steel drywell & wetwell	Spot pitting corrosion on the inside of the torus
Dresden 2	BWR - Mark I steel drywell & wetwell	Peeling and discolored interior shell coatings; degraded electrical cables and valve operator components due to excessive operating temperature
Hatch 2	BWR - Mark I steel drywell & wetwell	Brittle fractures of 54-inch and 66-inch vent headers. Nitrogen inerting system line may have exposed material to below nil ductility temperature
Quad Cities 1 & 2 Dresden 3	BWR - Mark I steel drywell & wetwell	Two-ply containment penetration bellows leaked due to transgranular stress corrosion cracking (TGSCC)
McGuire 1 & 2 Catawba 1 & 2	PWR - Ice Condenser; steel cylinder	Corrosion on the outside of the steel cylinder in the annular region
McGuire 2	PWR - Ice Condenser; steel cylinder	Bare metal found in lower containment at various locations; general vessel corrosion and some pitting in lower annulus
Fort Calhoun Three Mile Island 1 Trojan	PWR Post-tensioned concrete	Grease leakage from tendon sheathings, at joints between conduit lengths, at tendon anchors, or through cracks in containment walls, as well as leaching
Ginna Turkey Point 3	PWR Post-tensioned concrete	Excessive tendon relaxation
Farley 1 Farley 2	PWR Post-tensioned concrete	Anchor head corrosion, free water in grease caps
Crystal River 3	PWR Post-tensioned concrete	Dome delamination due to low quality coarse aggregate
Salem 2	PWR Post-tensioned concrete	Minor corrosion on the liner
Beaver Valley 1	PWR - Subatmospheric	Rusted areas and peeling paint on the liner

## 4 FINITE ELEMENT MODELING

### 4.1 Modeling Considerations

Four steel and concrete containment buildings have been modeled and analyzed, assuming large internal pressure "severe" accident loading conditions. Finite element models were generated, and failure pressures were predicted for two typical steel vessels: a PWR Ice Condenser and a BWR Mark I containment. Two typical concrete vessels were also analyzed: a reinforced concrete sub-atmospheric containment, and a prestressed concrete containment. These containments were selected because of previous studies that have been performed for them (Miller, 1990; Mokhtarian, 1987; NUREG 1150; Sharma et al, 1985, Butler and Fugelso, 1982, IDCOR, 1983, Pananos et al, 1984). First, the capacity of the vessels with no age related degradation was calculated, and then the analyses were repeated with varying levels of corrosion in locations where corrosion has been observed, or in inaccessible regions that have a high potential for corrosion.

The primary objective of these analyses has been to show the relationship between the pressure capacity of a "new" containment, and the reduction in capacity that could result from corrosion. Internal pressure and thermal expansion are the primary loads that have been included in the finite element analyses, and they give a good indication of how the capacity is degraded with corrosion. However, for large areas of corrosion and significantly reduced cross-sectional thickness, it is possible to affect the stability of the structure (i.e., cause buckling) under seismic, dead, external pressure, and/or thermal loadings. These other loading cases have not been investigated.

The failure predictions for these typical containments should not be extrapolated to operational containments because of differences in important details. For example, the designs and geometry varies within each major class of containment. Also, the location and amount of corrosion that is observed in an operational plant is probably different than has been assumed in this study. Last of all, many load combinations must be evaluated to ensure that an operational containment meets its design requirements, while internal pressure was the primary loading investigated in this report. If significant corrosion is found in an operational containment, then each containment must be carefully evaluated on a case-by-case basis.

However, general trends can be identified, and these trends will apply to many types of containments. The method used to represent corroded material in the finite element analyses can be used for any containment.

Containment buildings include many potential leak paths, and only structural failures or leaks in the containment structure itself have been included in the analyses. Individual penetrations have not been included in the finite element models, with the exception of very large penetrations, such as vent lines and the upper head in BWR Mark I containments, or equipment hatches in the concrete containments. In addition, it has been assumed that weld material and material in the heat affected zone (HAZ) have identical properties to the base metal.

Although all potential failure modes have not been analyzed in this report, they have been considered when developing the models. For example, previous studies of steel PWR Ice Condenser containments have considered the possibility of anchorage failure at the basemat, seal leaks, and other failure mechanisms. Results from those reports indicate that the most likely failure mode is tearing of the shell wall. Therefore, that is the primary "failure" mode considered.

A previous study of a typical BWR Mark I concluded that one very likely leak mode is the seal at the upper head. In addition, operational plans call for venting when the pressure reaches a level that is considerably larger than the design pressure. In the unlikely event of a severe accident, the first expected pressure release would be venting through the hardened vent valve, followed by a seal leak in the upper head, and finally a tear in the containment vessel itself. Although not all of the potential leak paths have been evaluated in this report, those that have been identified in previous studies have been considered and the results from previous studies incorporated. A few of the potential leak paths that have been considered at great length in previous studies are discussed below.

Past analyses and tests on bellows (Greimann et al, 1991; Miller, 1990; Lambert and Parks, 1995) have shown that the bellows reach full compression at about the same pressure loading that failure is predicted to occur. Most of the "like-new" bellows that were tested did not fail even after being 100% compressed; however a few of the tests resulted in leaks in the bellows at slightly less than 100% of full compression. Therefore, it is expected that an uncorroded bellows will not develop leaks until the pressure loading gets large enough to cause the containment shell to fail due to large strains. Unfortunately, not enough corroded bellows have been tested to draw conclusions about what displacement level a corroded bellows will leak at. In any event, corrosion of bellows was not investigated as part of this research, and therefore is not accounted for in the finite element analyses.

Test results from electrical penetration assemblies, various seals, and a personnel airlock (Julien and Peters, 1989; Clauss, 1989a; Brinson and Graves, 1988; Parks, 1989) show that these components can withstand severe accident loads, and that failure is not likely at these penetrations. Based on previous tests of individual components, and the many scaled model tests discussed in section 2.1, it has been assumed that these penetrations and seals do not fail before a structural failure initiates. These details are not included in the finite element model.

Analyses of "typical" containments have not explicitly modeled the weld because it is assumed that weld material behaves the same as the parent material. Often, the highest stresses occur in areas where the plates of two thicknesses join. Generally, typical details taper the edges of the thicker plate, on a 4:12 slope, so that the transition from thick plate to thin plate is gradual. However, none of the governing subsections of Section III of the ASME Code require tapering at the transition. If a plate thickness change is abrupt, without a thickness transition region, then this could cause a stress concentration to occur in the weld zone, which may need to be considered in an analysis. As shown during the Separate Effects Tests described in the first section, a gradual transition did not cause a significant stress or strain concentration in the weld or transition region. Large stresses often result because of the specific geometry and discontinuities of the structure, but are not usually a result of welding. However, the peak stresses which occur in these transition regions are usually in the weld region joining the thick and thin plates.

Neither the weld nor effects of residual stresses in welds have been modeled. Under past programs, Sandia has coupled thermal and stress finite element codes so that the weld process can be calculated. This requires the capability to handle:

- phase changes of metal, since steel is liquid in the "fusion" melt zone and becomes solid as it cools,
- thermal heating and cooling with very high gradients in the weld region, including the phase change as the metal solidifies, and
- the buildup of residual stresses, including material creep and relaxation at high temperatures.

The material properties such as yield stress, ultimate stress, and elongation, vary throughout the fusion and HAZ. These past state-of-the-art calculations have been very intensive for simple "laboratory specimen" sized models. Because of the number of welds in a containment structure, and the amount of detail to

model even a small and simple weld, this level of detail in the analysis of a containment is not practical.

In a finite element model of a large structure, it is not practical to model the uneven surface of a corroded plate because of the large number of elements that would be required. Usually, this amount of detail about the condition of an existing structure is not available, and if it was, the amount of time to generate a finite element model that contained these details would be prohibitive. A model which contained this amount of detail would be far too large to solve using computers commonly available to industry. Because the exact location and number of pits or other "micro" discontinuities is not known, the effect of these is smeared across the entire element. For a number of reasons, it is not practical to model "pits" or other small discontinuities. Finite element analyses of a large containment structure will not be detailed enough to determine local strains caused by pits and other "micro" discontinuities. However, stress concentrations that result from geometry changes, such as a locally thinned area, plate thickness change, a penetration, or other "macro" discontinuities are calculated in a finite element analysis; the concentrations that occur in "micro" areas along the pitted and rough surface are accounted for by a knockdown factor. The knockdown factors are nothing more than simple observations about how omitted details typically reduce the calculated response.

Failure often initiates in regions of discontinuity because of large stresses and strains that exist in the local area. If a finite element mesh is modeled in sufficient detail, the finite element method is able to calculate many of the stress and strain concentrations that occur in the area of the discontinuities. However, pitted and rough surfaces consist of "micro" discontinuities that are much smaller than the elements in the mesh, and the method does not calculate stress and strain concentrations that form around these "micro" discontinuities. These "micro" discontinuities are accounted for by applying a knockdown factor to reduce the critical elongation for material in the affected area.

Damage can be grouped into the two categories discussed earlier. General corrosion damage degrades the surface of the metal containment structure somewhat uniformly, and can be handled in a finite element analysis by thinning the wall in the area(s) that have corroded. In order to model corrosion in a plate section, the shell thickness will be selected as the average thickness in the selected area, and the rough corroded surface will be approximated as a smooth surface. A knockdown factor is applied to account for the difference between a uniform thickness plate with smooth sides, and the degraded section that varies

somewhat in thickness and has a rough, uneven surface. The rough and uneven surface induces stress/strain concentrations that cause tears to initiate in the concentration regions.

The second category of damage is local pits that are scattered and cause stress concentrations. In areas where there is pitting, the thickness of the shell will not be reduced, but the ductility of the steel will be reduced to account for the strain concentrations around the discontinuities.

Obviously, each finite element analysis will be tailored to the specific plant geometry and corrosion area(s) that are being investigated. More detail is required in the corrosion area(s) to capture local effects, such as strains that result because the cross section is thinner than surrounding areas.

## 4.2 Failure Criteria of Steel

Several scaled model containments have been tested and analyzed over the last fifteen years (Horschel, 1992, Sammataro et al., 1992, Weatherby, 1990, Clauss, 1985). The finite element analyses of these uncorroded structures showed that failure is related to local strains, and that a critical strain failure criterion can be used to predict the onset of failure. As the material strains, voids coalesce into a flaw. At some critical strain level, the flaw reaches a critical size and a tear initiates. Most analyses that have been performed for containment structures have selected strain (or stress) based failure criteria, although fracture mechanics methods and failure criteria have been used in a few cases.

Linear elastic fracture mechanics (LEFM) have often been used to predict critical flaw sizes in piping, in pressure vessels, and in other situations where brittle fracture is expected. This method has been proven and is reliable for linear elastic problems. Similarly, elastic plastic fracture mechanics (EPFM) have also been proven for cases of moderate plasticity around the crack tip area. However, EPFM methods are not well proven in areas where the entire cross-section is experiencing high strains and gross plasticity. Furthermore, there is not a traditional fracture mechanics flaw or crack on the rough uneven surface that has been observed in corroded areas of containment vessels. Although cracks could be conservatively postulated, there is no basis for selecting the size or extent of cracks.

Finite element analyses, using strain based failure criteria, have been used successfully for uncorroded containments and for corroded pipelines. Fracture mechanics methods are difficult to apply to the corrosion damage. Therefore, finite element analyses

described in this report have relied on strain based failure criteria. Sharp cracks of significant size have not been observed in corroded areas of containment structures. However, fracture mechanics methods should be considered if sharp cracks are detected during future inspections.

Strain-based failure criteria, which have been successfully used in past containment analyses, have been modified to account for corrosion effects. In a corroded region, the metal loss region is typically very irregular in both depth and extent. Therefore, the shape of the metal loss region must be idealized. In the finite element model, a corroded area is modeled using the average thickness of the degraded section. Local stress and strain concentrations that are caused by the reduced thickness and the surrounding geometry are calculated by the analysis code. The stresses and strains increase in the degraded area. The stress-strain curve used in the reduced thickness region is identical to the curve for uncorroded material, except that the critical elongation of the corroded material is decreased, as described in the following section.

### 4.2.1 Failure criteria used in previous containment analyses.

In order to predict failure of a containment structure using finite element analyses, a failure model or other type of failure criteria must be established. A wide range of failure criteria have been used at Sandia and elsewhere for previous containment analyses. Failure criteria have consisted of selecting: maximum principal strains, maximum principal stresses, maximum effective plastic strains, maximum von mises stresses, fracture mechanics criteria ( $K_{Ic}$ ), maximum displacements, and so forth. Failure criteria have been based on global values, local values, membrane values, and/or bending stresses or strains. Following are a few cases and the methods that were used:

- *German risk study* (Hofler, 1985): In section 8.5 of the German Risk Study, a number of competing failure criteria were used. One criteria defined failure by comparing an equivalent plastic strain to a critical strain value; the critical strain was determined by multiplying a uniaxial failure strain by three knockdown factors. The three factors are similar in magnitude to the knockdown factors discussed in section 4.3 of this report. Another failure criteria used in this study was to compare the equivalent stress to an allowable stress. The allowable stress was selected by averaging the yield and ultimate stresses, and adjusting this value using a knockdown factor. A third criteria used in the report was to compare the maximum principal stress to an allowable value. The last method described in the report was a linear elastic fracture

mechanics approach which examined the possibility of brittle fracture.

- *Electric Boat Corp.* (Sammataro et al., 1992; Solonick, 1996): The recommendations in these papers were to use equivalent plastic strain-based criteria to predict failure. They recommended different critical failure strains for general plastic membrane strains, local plastic membrane strains, concentrated plastic membrane strains, general plastic surface strains, local plastic surface strains, and concentrated plastic surface strains. The recommended failure limits range from  $0.2\epsilon_u$  for a general membrane strain to  $0.5\epsilon_u$  for a concentrated membrane strain;  $\epsilon_u$  is the minimum ultimate strain for the metal.
- *Pretest predictions for 1:8 scale steel containment* (Clauss, 1985): Failure criteria used was 15% equivalent strain for global behavior that occurred over a large gage length (meaning several inches), and 20% strains for local strains or bending strains.
- *Analysis of Sequoyah, done in 1989* (Miller, 1990): Failure criteria used in this analysis was 15% equivalent strain, and then the 15% value was reduced using knockdown factors.
- *Post-test analysis of 1:6 scale RCCV liner* (Weatherby, 1990): Failure criteria in this report were obtained by adjusting uniaxial pull-to-failure data, which was 30% for the liner material, to account for multi-axial stress state. The equation used to modify the critical strain limits based on the multi-axial stress state was Mangoinés (1982). Using this model, no adjustment was made for material in a uniaxial stress state, while the critical strain limits were reduced by a factor of two for material in pure biaxial tension. Therefore, for material in a biaxial stress state, the critical failure level used in this study would have been 15%.
- *Mark I analysis by CBI* (Mokhtarian, 1987): This analysis used local membrane failure strain limits of 1%, surface (bending) failure strain limits of 2%, and local (concentrated) strain limits of 5%. The report states that these limits are conservative, and failure will probably occur at somewhat above the predicted values.
- *Containment analyses techniques report* (Greimann, 1984): This report summarizes analyses completed by a number of organizations and authors prior to 1983. Failure criteria used in these studies varied considerably, with the analysts using failure criteria such as  $\sigma_{yield}$ ,

$(\sigma_{yield} + \sigma_{ultimate})/2$ ,  $\sigma_{ultimate}$ , 2 times strain at first yield, 5 times strain at first yield, fracture mechanics criteria ( $K_{Ic}$ ), and so forth. Some of these reports intentionally selected conservative criteria, while others tried for a "best estimate" failure criteria. Much of the scatter in predicted results is because of: a) amount of detail in the analysis (i.e. hand calculations vs. axisymmetric analysis vs. 3D analysis), and b) the degree of conservatism in failure criteria.

- *NUREG-1150* (1989): For each containment considered, a number of failure modes not related to tearing of the steel were considered. For example, pullout of the anchor bolts from the concrete basemat was considered in Sequoyah. Leaks in seals at equipment hatches, leaks through electrical penetrations, and so forth have been considered. In Mark I BWR's, vents have been added which release pressure well below the critical values where structural failure is likely. Pressure unseating hatches or covers, such as the Mark I drywell head, can leak due to bolts stretching and opening a gap. Seismic failures, buckling concerns, and so forth have been considered in many of the studies.

A number of different empirical failure criteria have been used in previous analyses. Most of the criteria were based on a stress or strain criteria, such as a critical von mises stress, maximum principal stress, critical equivalent plastic strain, or maximum principal strain. The German Risk Study also included a fracture mechanics failure criteria. Because of the relationship between stress and strain (i.e., the stress – strain curve relationship) the stress or strain based criteria all provide similar predictions. However, stress based criteria tend to correspond to a "load control" result, while strain based criteria tend to relate to "displacement control". In some cases, one is more appropriate than the other. Generally speaking, however, there is not much difference if the failure limit is selected so that it corresponds to a value that is less than or equal to the maximum engineering stress for the material. For example, the predicted failure pressure would change very little for failure criteria of 1% effective plastic strain, 1% maximum principal strain, the von mises stress that corresponds to 1% effective plastic strain, or the maximum principal stress that corresponds to 1% maximum principal strain. The fracture mechanics failure criteria used in the German Risk Study, however, can yield results that are somewhat different from stress or strain based criteria.

For the static, monotonically increasing pressure loads considered in this report, relatively simple stress or strain based failure criteria do as good of a job at predicting failure of ductile steel as more complex

failure models. For cyclic behavior, large strain rates, or significant temperature changes, newer material models and failure models may perform considerably better. Also, concrete material models have significantly improved in the last 15 years, and it is essential to obtain a robust concrete material model in order to predict response and failure limits for concrete vessels. However, for steel vessels and the liners of concrete vessels that are loaded quasi-statically with a monotonically increasing loading, the simple stress or strain based failure models are as good as are available.

A failure criteria based on effective plastic strain gives very similar failure predictions to a criteria based on principal strains, principal stresses, von mises stresses, or similar criteria. Brittle fracture is not a concern for the low-carbon, low-strength steels used in containments at operating temperatures above 32° F. Reports in the literature that model ductile failure using fracture mechanics (J-integral methods) have not given any better results than the simple strain or stress based failure criteria. For static, monotonically increasing loads, and well-behaved materials, basing failure on effective plastic strains works as good as or better than other methods. Of the many analyses referenced throughout this paper, all of the analysts used either stress or strain based failure criteria. In addition to several different stress and strain based failure criteria, the German Risk Study (Hofler, 1985) also used a fracture mechanics criteria.

#### **4.2.2 Failure criteria in the literature.**

There are numerous failure theories that have been developed that can be used to predict structural failure in a finite element analysis (Mangoine, 1982; Hancock and Mackenzie, 1976; Mackenzie et al., 1977; Brownrigg et al., 1983; Oyane, 1972; Sammataro et al, 1992; Hofler, 1985). These models are empirical, and are based on fitting a curve through test data. Much of the failure data that is available has been obtained from uniaxial pull tests. Many of the models were calibrated using test data from one or two materials, such as 7075-T6 aluminum or 304L stainless steel, and the shape of the curve does not fit other materials very well. There is no consensus among experts about what failure model(s) are best, and in fact there is often strong disagreement. Some believe that a model should be based on micro-mechanics, while others argue for macro-mechanics. Despite the disagreement, several of the models appear adequate for thin shell pressure vessels that are subjected to a one-time only monotonically increasing load.

One of the simplest and most common methods that has been used to predict failure is to assume that failure occurs when the plastic strain exceeds some number. There is a large variation in the strain limits selected to

predict failure, based on the conservatism needed for each individual structure that is analyzed.

Failure models that are a little more complicated predict failure levels that vary with the multi-axial stress state. It is a well-known phenomenon that the failure strain, when subjected to biaxial or triaxial stresses, varies significantly from the failure strain of a uniaxial test (Mangoine, 1982; Hancock and Mackenzie, 1976; Mackenzie et al., 1977; Brownrigg et al., 1983; Oyane, 1972). These models relate failure in any stress/strain state to the stress/strain value from uniaxial strain-to-failure tests. This is generally done by calculating a ratio between the hydrostatic stress and the effective von mises stress, and then using the ratio to adjust the failure strains from uniaxial test data. This type of failure model handles static, monotonically increasing, non-cyclic loads reasonably well. However, when loads are cyclic, this type of model does not account for material damage which accumulates as the loads are repeated. As already mentioned, the small number of load cycles in a containment structure aren't enough to cause failure, so this type of a failure criteria is adequate. These relatively simple failure theories usually rely on data published in handbooks, such as yield stress, ultimate stress, and ultimate uniaxial strain.

More complex material and failure models have been developed that account for cyclic loading and damage accumulation, varying temperatures, strain rates, and so forth. Usually, they are concerned with following the correct stress/strain curve and maintaining cumulative damage criteria through hysteresis loadings (i.e. load reversals that cause yielding in tension, then yielding in compression, then yielding in tension, etc.). These models often require test series to empirically fit failure parameters. The containment structures are not cyclically loaded. They are pressurized and depressurized several times during leak testing, but the loadings are not large enough to cause plastic yielding, except perhaps in very local areas. Containment structures would only be loaded well into the plastic range one time, and then only if they are subjected to a severe accident in which the reactor vessel releases pressure into the containment building. Therefore, the extra bells and whistles in many of the complex failure models are not needed for our case.

#### **4.2.3 Fracture Mechanics Versus Effective Plastic Strain.**

In Section III of the ASME Boiler and Pressure Vessel Code (ASME, 1992), design criteria for containment structures consist of limiting the stresses to allowable levels. However, Section XI of the code, *Rules for Inservice Inspection of Nuclear Power Plant*

*Components.* is based on a fracture mechanics approach.

Both LEFM and EPFM approaches have often been used to predict critical flaw sizes in piping, in pressure vessels, and in other situations where repetitive loadings occur on a structure that is stressed below its yield point. Using the fracture mechanics approach, a flaw can develop and then grow in a stable pattern under long term static or fatigue loadings. If the flaw develops into a critical flaw, then failure can occur at nominal stresses that are well below the yield stress of the material.

LEFM is well established. If the stress intensity factor around a flaw is greater than the critical stress intensity factor ( $K_{Ic}$ ), then the crack can be unstable and propagate. The method is based on the assumption of an elastic stress field, and that there are no plastic strains except for the very small plastic strain region at a crack tip. The material dependent  $K_{Ic}$  factors are selected so that they are conservative, and failures are very unlikely to occur at stress intensity factors below the critical values. However, it is common for failure to occur at stress intensity factors that are well above the  $K_{Ic}$  factor.

EPFM is an established methodology for analyzing cracks with moderate plasticity around the crack tip. If the strain energy release rate, calculated using the *J Integral*, exceeds the critical value,  $J_{Ic}$ , which is determined according to the ASTM standard, then failure is predicted to initiate at the flaw location.

Large plasticity fracture mechanics, based on the assumption of significant plastic strains and yielding in the “gross” section, are not well established. Greimann et al (1993) states:

“No single parameter or combination of parameters have been found which satisfactorily characterize the growth of cracks through regions of high strain and with gross plasticity of highly ductile materials. Currently, the state-of-the-art in fracture mechanics permits the reliable prediction of small crack growths in regions of limited plasticity.”

LEFM and EPFM methods have been “proven” and are reliable, but large plasticity fracture mechanics are still being developed. There is not agreement between experts concerning the use of large plasticity fracture mechanics, and these evolving methods are not yet suitable for the analyses of containment structures.

A containment structure will not experience a large number of fatigue cycles, but will only see significant stresses during a few events, such as during leak testing

or after reactor failure during a severe accident. The steels used in containment structures are very ductile and resistant to fracturing at flaw locations. Even after corrosion degradation, the containment membrane would experience significant plastic strains before failure initiates. Therefore, the well-established LEFM and EPFM approaches do not apply. Because containment models that were tested experienced gross plasticity before failure, large plasticity fracture mechanics would be required to evaluate containments. As stated previously, large plasticity fracture mechanics methods are not well established. Furthermore, there isn't a crack or traditional fracture mechanics flaw in a corroded region. For all of these reasons, fracture mechanics methods and failure criteria were not used.

### 4.3 Steel failure criteria used in this project.

The criteria used in this report to predict potential containment failure differ significantly from criteria that would be acceptable for design. Containment structures are conservatively designed so that the probability of failure is very, very small under design loads. The design criteria are selected so that the vessel remains elastic, with a comfortable safety factor, under all design loads. However, when predicting failure, previous tests on scaled models have demonstrated that large plastic strains occur before the pressure boundary fails. The criteria used to predict failure are suitable for use in risk studies, but are clearly unacceptable for design. For example, in design, strains are typically limited to about 2/3 of the elastic limit. However, scaled model tests have failed when global free-field strains were 7 to 20 times larger than the elastic limit (i.e., free-field strains of about 1% to 3%). Near the failure regions, local strains in the models were typically 50 times, or more, than the elastic limit (i.e., local strains were 10% or more). A badly corroded containment can have plastic strains below limits where failure would be anticipated, but strains that are well above the elastic limit at design loads. Although the probability of failure may be low for this case, the level of conservatism necessary to ensure safety would be lacking. To ensure a conservative design, it is necessary to keep stresses and strains in corrosion areas from exceeding ASME code allowable limits.

However, the intent of the analyses discussed in Sections 5 – 8 is to predict when failure would actually occur. The analysis method that has been used to predict the ultimate capacity of corroded containments is to limit the effective plastic strains. Failure criteria that limit the effective plastic strain have been developed to simulate void growth in high stress intensity regions (Mangoine, 1982; Hancock and

Mackenzie, 1976; Mackenzie et al., 1977). As the material strains, voids coalesce into a flaw. At some critical strain level, the flaw reaches a critical size and a tear initiates. Therefore, the effective plastic strain analysis method will predict failure in high stress intensity regions caused by a critical flaw. In order to predict failure at a flaw location, the finite element mesh must be detailed enough to capture local strain concentrations. The strain-to-failure levels can vary considerably between material samples of different geometric configuration, different material lot numbers, and so forth. There will be a corresponding uncertainty in any analysis that predicts the ultimate capacity of a structure.

Because the objective of this report has been to understand how corrosion degrades the containment structure, non-structural failure modes have not been evaluated. If previous studies have concluded that a non-structural failure mode may occur before the structural failure mode, then that has been noted. In this report, it has been assumed that failure will occur at the lower pressure of the predicted structural failure (tearing of steel shell or liner) or at the non-structural failure pressure identified by previous studies.

For example, a prior analysis of the Sequoyah concrete basemat by Ames Laboratory showed that the anchor bolts could pull out and cause catastrophic failure at a pressure load of 0.54 MPa (79 psi). Analyses described in this report predict shell wall tearing between 0.43 MPa (62 psi) and 0.51 MPa (74 psi), with a "best estimate" at 0.47 MPa (68 psi). Therefore, it was concluded that the shell wall would tear before the anchorage failure could occur.

On the other hand, the BWR Mark I's have two failure modes that occur before the shell wall tears. One failure mechanism is a leak around the drywell head due to bolts stretching and relieving the load in the seal. The other mechanism is not an actual failure mode, but rather is intentional venting through the suppression pool when the pressure reaches a pre-determined limit that is well above design pressure. For the Peach Bottom containment, failure in the shell walls is not predicted to occur until the internal pressure exceeds 1.3 MPa (195 psi), while the pressure relief vents are set to vent at 0.69 MPa (100 psi). Therefore, it is assumed that an uncorroded structure will not fail, but that the vents will release pressure at 0.69 MPa. A significant amount of corrosion could cause the shell walls to rupture at pressures below 0.69 MPa, however. Failure modes other than tearing of the steel have been incorporated into these predictions, based on prior work. However, no effort has been made to degrade materials other than the steel shells. The seals, electrical penetrations, bellows, anchor

bolts, or other items have not been degraded in this study.

Another failure criterion that was considered, but has not been incorporated in this work, is a displacement based criteria. Many penetrations exist in the walls of the containment structure, and excessive displacements could cause either a failure in the penetration seals, or break pipes and other items that pass through the penetrations. Many items, such as overhead cranes, are supported by the containment walls. Excessive displacement could cause these items to fall onto critical items below. However, this additional displacement failure criterion was not used in this paper.

The failure criteria will be based on the effective plastic strain that the structure experiences. Failure is predicted to occur when calculated strains exceed a critical value. After a tear initiates, the failure criteria will not predict whether the tear will be unstable and propagate, resulting in catastrophic failure, or whether the crack will self-arrest and not propagate, resulting in a leak. Determining whether a crack will propagate has been tried in the past, and the results were not conclusive (Irvine and Gardner, 1983; Greimann et al., 1993). However, it appears likely that if the tear initiates in a region of high membrane strains, the tear will propagate rapidly and result in catastrophic failure. If the high strain is in a local region and the surrounding area is at a much lower strain, the failure may not be catastrophic.

The strain-based failure criterion that has been selected consists of applying knockdown factors to adjust uniaxial strain-to-failure test data. The first three factors are consistent with previous analyses (Miller, 1990, and Weatherby, 1990) and are not related to corrosion. These factors relate to the ability of the analysis model to correctly predict the structural response and to material property differences that exist in actual containments. The fourth factor has been added to account for the random effects of corrosion degradation.

The critical effective plastic strain at which failure is predicted to occur is determined as:

$$\epsilon_{failure} = \epsilon_{uniaxial} * f_1 * f_2 * f_3 * f_4 \quad (1)$$

where

$\epsilon_{failure}$  = effective plastic strain level at which failure is predicted to occur,

$\epsilon_{uniaxial}$  = elongation from uniaxial tensile strain-to-failure tests,

$f_1$  = knockdown factor to account for multi-axial stress state,  

$$= 1.648 * e^{-(\sigma_1 + \sigma_2 + \sigma_3) / 2 \sigma_{von}} \quad (2)$$

$f_2$  = knockdown factor to account for the sophistication of the analysis model.

$f_3$  = knockdown factor to account for variable material properties.

$f_4$  = knockdown factor to account for corrosion degradation.

$\sigma_{von}$  = von Mises effective stress.

$\sigma_{1,2,3}$  = principal stresses.

The  $f_3$  and  $f_4$  factors are selected before analyses are performed. The  $f_2$  factor is estimated after the analyses are completed. It is based on the amount of detail included in the finite element model in the critical failure region, and on analytical results such as strain gradients in the critical region. For each of the factors  $f_2$ ,  $f_3$ , and  $f_4$ , a best estimate has been selected, along with an upper and lower bound estimate. In the analyses in the following section, failure occurred in the cylindrical section of the containment. A few  $f_1$  factors for typical shapes are given in Table 1. However, the actual  $f_1$  factor is calculated at each point in the analyses, and so the value of this factor can vary from point to point as the stress field varies.

The factors (Table 1) are based on engineering judgment and the data already presented. Because the stress-strain curve is fairly flat at high plastic strain levels, a large change in strain only results in a small change in the stress. Therefore, predicted failure pressures are not very sensitive to changes in the plastic strain failure criteria, and hence to the knockdown factors.

#### 4.3.1 $f_1$ (stress triaxiality) factor.

Hancock et al. (1976), Mackenzie et al. (1977), Mangoine (1982), and others have shown that the critical failure strain varies as the stress state changes. The  $f_1$  knockdown factor used in this report is the Hancock and Mackenzie relationship between the triaxial stress state and the failure strain. This empirical relationship was based on test results, and the empirical curve and test data points are shown in figures in the papers just referenced.

Many similar empirical equations that account for multi-axial stress states are available in the literature (Ju et al, 1984, Wellman et al, 1992). These empirical equations have been utilized not only for steels, but

also for aluminum and beryllium (Priddy et al., 1979, Benzley et al, 1980, and Soo Hoo et al, 1980). There is some scatter between the various empirical equations, but most of them are within about 10% of the Hancock and Mackenzie relationship that has been used in this report.

**Table 1. Knockdown Factors Used in Failure Criteria.**

	Factor	Lower bound	Best estimate	Upper bound
Biaxial stress in a cylinder	$f_1$	0.69	0.69	0.69
Biaxial stress in a sphere	$f_1$	0.61	0.61	0.61
Analysis sophistication	$f_2$	0.40	0.50	0.60
Material properties	$f_3$	0.78	1.00	1.22
Corrosion	$f_4$	0.25	0.50	0.75

The sheet metal industry has used formability diagrams for many years. A formability diagram is made by stretching smooth sheets of material under biaxial strain until a tear develops. The strain in one of the directions at which a tear first developed is plotted versus the strain in the second direction. The test is repeated many times with different combinations of biaxial strain in the two orthogonal directions, and each test determines one point on the curve. A line is then drawn such that the strain components on one side of the line do not cause a tear, and the strain components on the other side of the line will cause a tear to initiate.

A formability curve was generated for one US containment steel (either A441 or A516, it wasn't clear from the report) based on test data (Eibl et al, 1988). The formability diagram shows that a plate that fails at 20% uniaxial strain will not fail under biaxial strain (two equal components of strain) until around 40-50% equivalent plastic strain. In contrast, the Hancock-McKenzie models show that a material that fails under 20% uniaxial strain should fail at about 12% biaxial strain (two equal strain components).

Both the formability diagrams and the Hancock-McKenzie type models are based on test data and appear to be valid. The primary difference is that the formability diagrams are based on smooth specimens with no geometric or discontinuous sections to cause

significant stress concentrations, while the Hancock-McKenzie model is based on a notch or other discontinuity causing a significant stress concentration. Since most tears initiate around holes, plate thickness changes, imperfections, or other discontinuities that lead to stress concentrations, the Hancock-McKenzie model has been chosen. However, in an area where a plate is smooth and there are no imperfections or other discontinuities to cause a stress concentration, the Hancock-McKenzie model will be fairly conservative.

Although there are many competing failure models that are presented in the literature, none of them seem to capture the effect of multi-axial stress states any better than the Hancock-McKenzie method (Eq. 2 in Section 4.3). There is considerable scatter in actual test data, but this model describes the general trend fairly well.

#### **4.3.2 f2 (model sophistication) factor.**

The second knockdown factor accounts for how detailed the finite element model is. For example, the element mesh size and details missing in the model affect the accuracy of the finite element prediction. This factor approaches 1.0 as the mesh size becomes small and includes all structural details.

Many details are left out of an analysis, such as welds, small holes, and so forth. Element size is also critical in the ability of a model to capture stress and strain gradients. A shell model generally does a good job of predicting failure at the maximum measured engineering stress or strain, but can miss strain or stress concentrations if the plate goes through an abrupt angle change, such as in an area where a rib stiffener is welded to a cylindrical section. In addition, many shell elements can give poor results if the element edge length becomes smaller than the thickness of the element. However, continuum elements can produce accurate analysis results in areas where there are abrupt angle changes, or around discontinuities that are too small to be modeled with shell elements. However, shell elements are used when possible because the resulting model is considerably smaller. It is not practical to build a complete model of a containment using finely meshed solid elements because the model would be too large to run on today's computers.

Based on types of elements used, size of elements, the amount of detail included in the model (i.e., does the model include all details of the actual structure, or has it been simplified), and the stress and strain gradients calculated, an appropriate failure criteria can be selected. For example, a very detailed mesh can calculate thinning and local necking around the failure region, with associated failure strains that are larger than the elongation value measured in a simple tensile test. As the element size increases, the failure strains

would decrease so that the strain in a 2 inch element would be equal to the measured engineering strain in a two inch test specimen. As the element size increased further, the failure strains would decrease so that the strain in a 8 inch element would be equal to the measured engineering strain in an eight inch test specimen. Therefore, element size has an important impact on selecting appropriate failure criteria.

In addition, if there is a large stress or strain gradient across the element (generally caused by a hole, or some other discontinuity), then the mesh may not be fine enough to completely capture the stress concentration. In that case, it is necessary to reduce the "failure" criteria to account for the concentrating effect of the discontinuity that is not calculated.

Determining appropriate failure criteria is subjective. However, it is very important to evaluate the amount of detail in the model, and select criteria that are consistent with the model. Miller (1990) discusses selecting appropriate failure criteria that is consistent with the amount of detail in the finite element model.

#### **4.3.3 f3 (material variability) factor.**

The third knockdown factor accounts for the fact that in an actual structure the material properties often vary from the mean by a significant margin. For example, test data from 489 specimens used in the Sequoyah containment had yield strengths that varied from the mean by  $\pm 12\%$ , ultimate strengths that varied from the mean by  $\pm 7\%$ , and elongations that varied from the mean by  $\pm 22\%$ . These variations are based on a normal distribution, with 90% of the test results falling within the specified deviations.

Material properties varied considerably even for plate sections of the same thickness. The scatter in the strength was large enough that it was not possible to identify a trend toward higher or lower strengths as the thickness changed. Therefore, the same material properties were used for all of the plates, even though they weren't the same thickness. Not enough data was found to account for material variability based on temperature. However, temperature curves from the Structural Alloys Handbook (1989) show there is certainly scatter associated with temperature as well. A516 Grade 70 specimens sent to Fatigue Technologies, Inc. of Seattle don't show much scatter, but this is probably because they were from the same lot of material.

#### **4.3.4 f4 (corrosion variability) factor.**

The last knockdown factor accounts for corrosion degradation, and is based on the limited set of corroded coupon tests. The pitted and rough surface "micro"

discontinuities are accounted for by this factor. When extrapolating corroded coupon test data to full scale containments, there is a considerable amount of uncertainty.

This reduction factor was based on the simple corroded coupon tests described in Section 2, and on the test data of Bruneau and Zahrai (1997). The test data showed a reduction in ductility because of the very local stress concentrations that occurred at the rough, uneven corroded surface. After removing the corroded material, the average stress of the uncorroded section was the same as for virgin material that had not been subjected to corrosion. The coupons tested in Section 2 of this report were fairly thin and were corroded artificially, while the test data of Bruneau and Zahrai were cut from the web and flange of a bridge girder. Those specimens were originally about 2.5 cm thick, and had been corroded about 50% through the thickness. Both sets of data gave similar reductions in elongation for corroded steel.

#### **4.3.5 Application.**

Minimum uniaxial strain-to-failure values for elongation in a 20.3 cm (8 in.) gage length are given in the ASME code as 21% for A516 Grade 60 and as 17% for A516 Grade 70 steel. For actual specimens, the elongation at failure is well above the 21% minimum; however. The average elongation used for A516 Grade 60 steel was 28%, while the average elongation used for A516 Grade 70 was 26%. Using these strain values, and the knockdown factors from Table 1, the "lower bound," "best estimate," and "upper bound" failure strain limits for a cylindrical

section for A516 Grade 70 steel would be about 5.6%, 9.0%, and 13.1% for uncorroded material. For corroded areas, the strain limits would be 1.4%, 4.5%, and 9.8%. Similarly, the strain limits for Grade 70 material were also estimated. The critical values allowed for bending strains were increased by 50%. In the analyses, the uncorroded failure strains were used to predict failure of the portions of the containment that were not corroded, and the corroded failure strains were used to predict failure of the corroded sections.

This damage/failure model will only predict the location(s) where the strains are high enough to cause a tear to initiate. It will not predict whether the tear will be unstable and propagate, resulting in catastrophic failure, or whether the crack will self-arrest and not propagate, resulting in a leak. This has been tried in the past, and the results have not been conclusive [Greimann et al, 1993, Irvine et al, 1983]. However, it appears likely that if the tear initiates in a region of high membrane strains, that the tear will propagate rapidly and result in catastrophic failure. If the strain is in a local region, the failure may not be catastrophic.

#### **4.4 Concrete Material Model.**

The material model used for the concrete was the ANATECH concrete material model (ANACAP, 1997), which is a modern version of the classic smeared cracking model (Rashid, 1968). A summary of the capabilities and details in this model are given in Appendix A of NUREG/CR-6639 (James et al. 1999).

## 5 ANALYSIS OF TYPICAL PWR ICE CONDENSER CONTAINMENT

The finite element model that has been developed is typical of PWR Ice Condenser containments in the United States. Although the analytical model was selected to be similar to the Sequoyah containment, there are several important differences. Therefore, throughout this report, the model is referred to as a PWR Ice Condenser containment, and not as the Sequoyah containment.

The dimensions, plate thicknesses, and vertical and horizontal stiffeners were modeled based on drawings of the Sequoyah containment. Although material properties of the Sequoyah containment were extensively reviewed, the material properties used in the analyses in this report are typical of A516 Grade 60 steel, and vary somewhat from the measured material properties in Sequoyah.

Furthermore, the postulated corrosion that is included in these analyses has not been observed in the Sequoyah containment. With the exception of postulated damage in the Ice Basket region, the location of the corrosion, but not the depth of corrosion, is representative of damage that has been observed in other PWR Ice Condenser containments, such as McGuire or Catawba.

To reduce the time required to complete an analysis, a section of the containment that is deemed to contain the largest stresses and strains has been modeled, and symmetry conditions have been assumed. The portion of the containment that is modeled, and the accompanying symmetry conditions, were carefully chosen so as to give realistic predictions of the stresses and strains in the selected area. However, it must be noted that these symmetry assumptions result in differences between the actual Sequoyah containment and the analysis model that has been developed.

Previous analyses of the Sequoyah containment indicate that largest stresses and strains occur at shell thickness discontinuities. The shell is 3.81 cm (1.5 in.) thick in areas where there are a large number of penetrations, and only 1.27 cm (0.50 in.) thick in adjacent areas that don't include penetrations. For this reason, and because the locations selected to place corrosion in the analyses were not by penetrations such as equipment hatches and personnel air locks, the penetrations were not modeled in the analyses. Penetrations such as equipment hatches, personnel air locks, and Electrical Penetration Assemblies were not modeled, but the varying plate thicknesses, and associated stress concentrations caused by the geometric discontinuities, were included.

Previous studies have examined possible failure modes for the Sequoyah containment. The failure mode deemed most likely has been tearing of the shell wall in the vicinity of a plate thickness change. Previous reports have dismissed other potential failure modes as less likely to cause failure.

One of the potential failure modes that was examined previously was the possibility of anchorage failure at the basemat. (The cylindrical steel shell is anchored to the basemat around the circumference.) This was examined extensively in previous studies, and it was concluded that tearing of the shell wall would occur before an anchorage failure. Therefore, the concrete basemat and associated anchorage details were not included in the finite element model generated for this report.

Containment vessels are designed to withstand many different loads, such as seismic or internal pressure. Although code requirements stipulate combinations of loads that a containment must be designed to resist, only internal pressure and loads caused by thermal expansion or contraction have been analyzed in this study. For free standing steel containments, buckling of the shell wall under load conditions such as seismic may be the worst case loading that dictates the wall thickness for the lower portion of the containment. The analytical results discussed in this chapter have not been evaluated during seismic or other load conditions that could cause buckling. When evaluating the effect of corrosion damage on an actual containment, it is important to remember that all code required load combinations must be evaluated to ensure that other failure modes, such as buckling, won't cause failure before the vessel fails due to internal pressure.

At pressures well above the design limit, the finite element model experiences large plastic strains; as the strains increase the shell wall becomes thinner. Eventually, the code fails to converge, indicating that a stability limit has been exceeded. However, in most cases, a tear will initiate before this stability limit is reached. After each analysis was completed, the calculated strains were examined to determine if local strain concentrations were large enough that a tear may have initiated. If high plastic stresses and strains are very local to the tear location, the tear may arrest itself such that the vessel will depressurize due to the tear in the wall. However, if the high stresses and strains cover a large enough area, then the tear is likely to propagate and result in total catastrophic failure.

## 5.1 Geometry

The typical PWR Ice Condenser containment (Fig. 5.1) is a circular cylinder capped with a hemispherical dome, and is constructed entirely from A516 Grade 60 steel. The cylindrical section has a diameter of 35 m (115 ft), and the height from its base to the top of the dome is about 53 m (174 ft). The shell thickness varies from 3.49 cm (1 3/8 in) at the bottom, to 1.11 cm (7/16 in) at the top of the cylinder, and then increases back to 2.38 cm (15/16 in) at the top of the dome. The shell is 3.81 cm (1 1/2 in) thick in the vicinity of pipe penetrations, airlocks, and other openings. Welded to the exterior of the shell is a web of vertical stringers, horizontal stiffeners, and other miscellaneous structures. The vertical stringers are spaced every four degrees circumferentially, and the horizontal stiffeners are about 2.9 m (9.5 ft) apart. The shell is embedded in and anchored to a reinforced concrete basemat.

For the PWR Ice Condenser (Figure 5.1), analyses were performed with corrosion in the following locations:

- The steel containment shell in the concrete basemat region, similar to the damage caused in McGuire and Catawba units by borated water (Figure 5.2).
- The steel containment shell in the vicinity of the upper floor and in the vicinity of the lower floor, similar to damage found in McGuire and Catawba (Figure 5.3).
- The steel containment shell around the area of the ice basket (susceptible area with a high potential for corrosion because of the presence of water, but in an area that is not accessible for inspection).

## 5.2 Finite Element Model

The ABAQUS finite element model (Fig. 5.4) consisted of 10125 four-node quadrilateral shell elements (S4R) and 10325 nodes. It included a 53° circumferential segment of the containment, and went from the concrete basemat to the top of the dome. This segment, which had symmetry boundary conditions applied to it, contained steel plates of several different thicknesses. In areas where the plate thickness transition occurred, the largest stresses and strains would be expected. This section was representative of a portion of an actual containment. Vertical stringers and the horizontal stiffeners were included in the model. The smallest elements had a side length of about 10 cm, while the average element had a length of about 30 cm (1° circumferentially). The concrete basemat was not modeled since it had been studied

previously (Fanous et al., 1993). The penetrations were not explicitly modeled either. In previous analyses (Miller, 1990; Greimann, et al., 1984) it was found that containment failure occurred where thin wall sections met the thicker plate sections that the penetrations passed through (Clauss, 1985; Greimann et al., 1987). In these studies, plastic yielding occurred in the thinner plate sections, and not in the thickened plates. Bellows were addressed under a previous program (Lambert, et al., 1995).

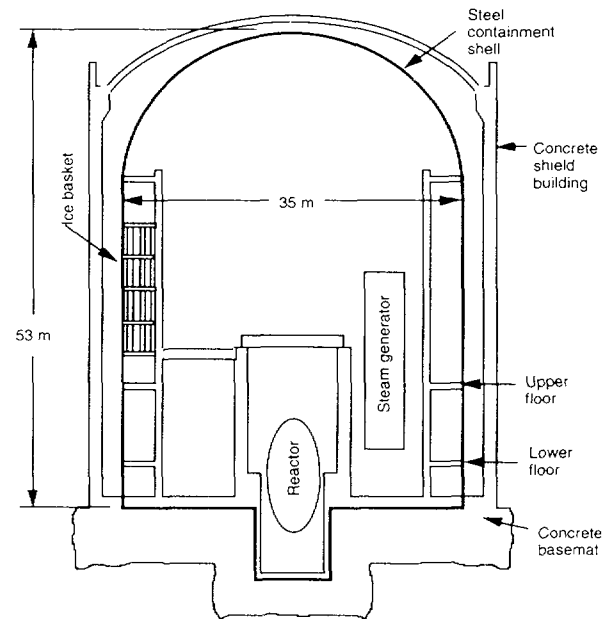


Figure 5.1 “Typical” PWR Ice Condenser containment.

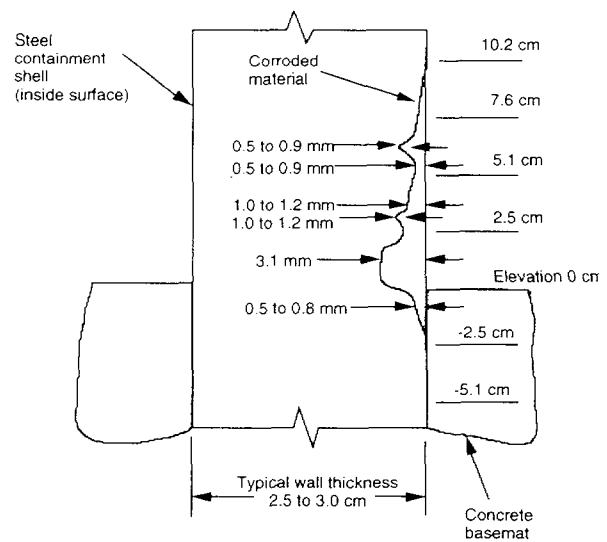
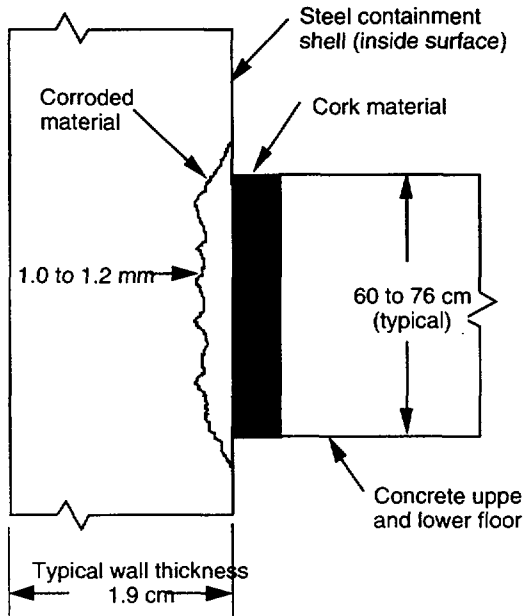


Figure 5.2 Observed damage to steel shell near basemat.



**Figure 5.3 Observed damage near upper and lower floor.**

Two submodels were generated to examine local response in more detail. A submodel of the upper floor corrosion is shown in Figure 5.5. Displacement boundary conditions from the global model were applied to the local models, as well as the temperature and pressure loadings used in the global model, and the submodel was analyzed. The predicted stresses and strains were up to a factor of two higher in very local stress concentration regions in the submodel. This increase in strain concentration was because of smaller elements used in the submodel. The stresses and strains near the edges of the local models were about the same as the corresponding stresses and strains in the global model. This indicates that the strain concentrations in the submodel were local to the submodel and did not affect the response in locations not adjacent to the local concentration.

The containment was modeled to determine failure level and location under several different degraded conditions. Three areas on the containment surface that were degraded (Fig. 5.4 and 5.6) correspond to the damaged or susceptible areas identified at nuclear power plants. In these areas corrosion was modeled by thinning shell elements and reducing the critical plastic failure strains. The depth of the corrosion was selected to ensure that failure occurred in the degraded area. Greater than 50% through the thickness damage was required at two locations to cause a failure in the degraded area. In the actual containment design, the wall section was thickened near the basemat to prevent buckling of the shell wall under compressive loads. This extra thickness was not needed to withstand the internal pressure loads. In the vicinity of the ice basket

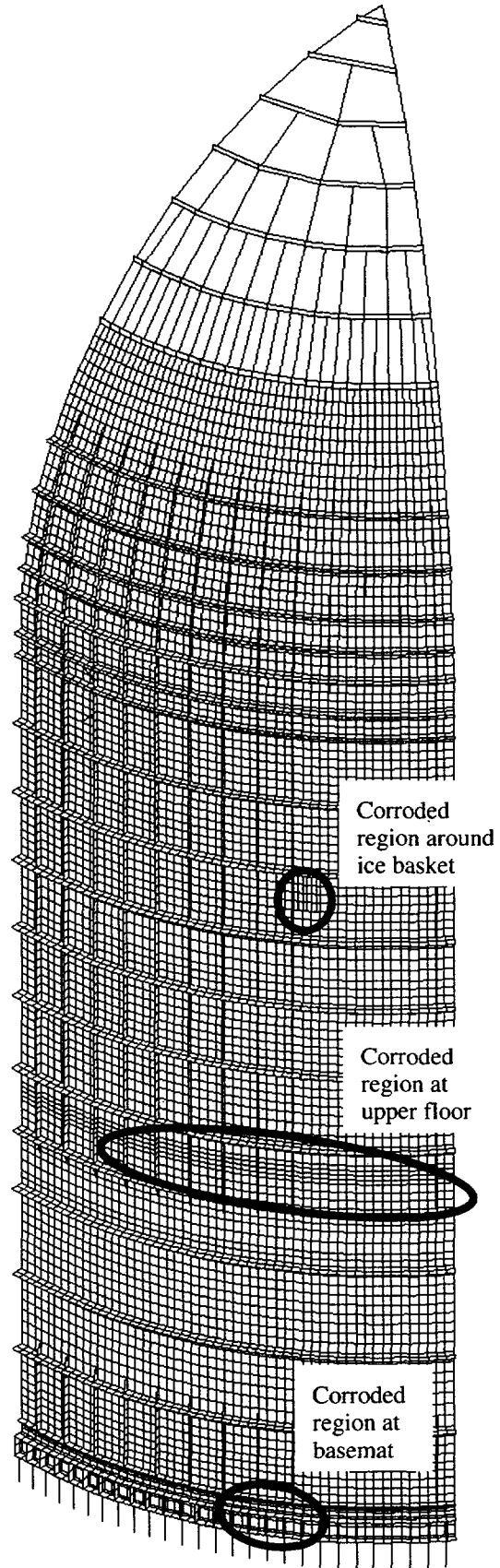


**Figure 5.4 Finite Element Model.**

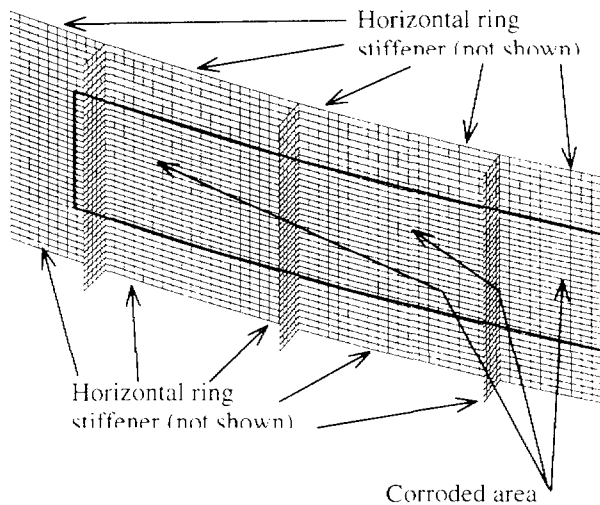


**Figure 5.5. Submodel of Upper floor region.**

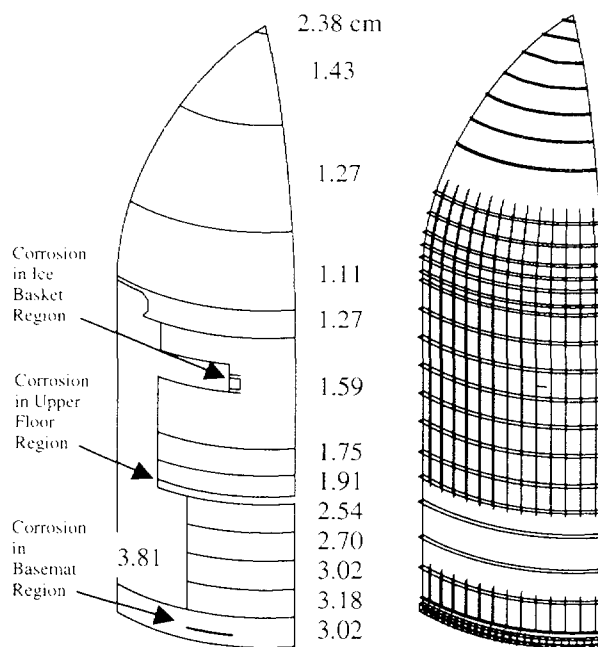


**Figure 5.6 Finite element model shell thickness and stringer and stiffener locations.**

region, the load that was worst for the vessel was internal pressure, and there was no excess thickness. Therefore, any reduction in thickness due to corrosion would be expected to reduce the pressure capacity of the vessel. However, in locations nearer the base where the wall thickness was increased to withstand buckle loads, the excess thickness could be corroded without substantially affecting the pressure capacity. If the area of corrosion is reasonably small, the buckling loads would not be adversely affected either. However, if the area of corrosion is significant, then

buckling should be evaluated to ensure that the degradation does not cause buckling failure.

The containment was analyzed in seven different configurations, with:

- No corrosion present.
- Corrosion near the top of the ice basket, with a 10% through the thickness corroded area of 1.09 m high by 0.91 m circumferentially. In operational containments, this area is susceptible to corrosion, but is inaccessible and does not get inspected. Analyses show this is the area of highest strains on an uncorroded containment, and the expected failure location.
- Corrosion near the top of the ice basket, as described above, except the damage is 25% through the thickness.
- Corrosion in the steel shell at the upper floor level, with a 50% through the thickness corroded area of 0.81 m high by 11.94 m around the circumference. Corrosion has been found in this location during inspections at the Catawba and McGuire plants.
- Corrosion at the upper floor level, as described above, except the damage is 65% through the thickness.
- Corrosion in the steel shell near the concrete basemat, with a 50% through the thickness corroded area of 0.102 m high by 3.99 m around the circumference. Corrosion has been observed here during inspections at the Catawba and McGuire plants.
- Corrosion in the concrete basemat region, as described above, except the damage is 65% through the thickness.

### 5.3 Material Properties

The material properties used in the analyses in this report are typical of A516 Grade 60 steel, and vary somewhat from the measured material properties in Sequoyah. Under ambient temperature conditions, A516 Grade 60 steel typically reaches yield at about 315 MPa, and the maximum engineering stress is about 460 MPa at 15% strain. ABAQUS requires that the material property stress-strain curves be true stress and true strain, and not engineering values. True stress and strain were estimated from engineering stress and strain values by the relationships

$$\sigma_{\text{true}} = (1 + \epsilon_{\text{engineering}}) \sigma_{\text{engineering}}$$

$$\epsilon_{\text{true}} = \log(1 + \epsilon_{\text{engineering}}).$$

Fatigue Technology Inc (1988) measured engineering stress-strain curves for A516 Grade 70 test coupons at temperatures of 22, 93, 149, and 204°C. The ambient temperature stress-strain curve used in the analyses in this report (Figure 5.7) is proportional to the Fatigue Technology data, but has been adjusted to pass through the true yield stress and true ultimate stress points for typical A516 Grade 60 material. The stress-strain curves at other temperatures is also proportional to the Fatigue Technology test data. ABAQUS linearly interpolates between the stress-strain curves shown in Figure 5.7 for other temperature values. The coefficient of thermal expansion of the steel was determined to be  $11.3 \times 10^{-6}/^{\circ}\text{C}$  over the range from 22 to 204°C.

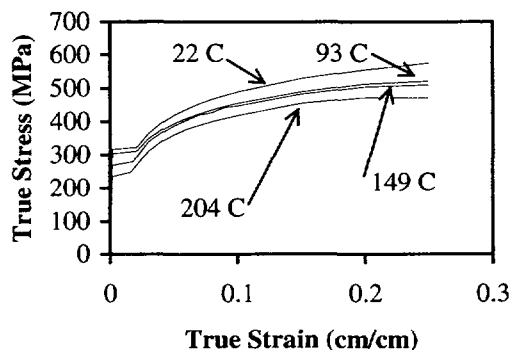


Figure 5.7 A516 Grade 60 temperature dependence.

## 5.4 Loads

Each model was loaded with quasi-static internal pressure that increased monotonically. During many postulated accidents, the pressure is caused by water turning into steam. Therefore, a thermal load was simultaneously applied to all steel parts above the concrete basemat; the temperature of the containment shell followed a saturated steam pressure vs. temperature relationship (Fig. 5.8). An initial stress-free state was assumed to exist at 22°C. As the pressure was increased, the temperature at every node in the model that was above the concrete basemat was increased to correspond to the saturated steam relationship.

## 5.5 Analysis Results

Analyses were performed using the ABAQUS/Standard finite element code. As the internal pressure load in the containment was increased beyond the design pressure, the finite element analyses first predicted local pockets of plastic strains developing. Then, as the pressure continued to increase, the code predicted global plastic strains. As the steel shell plastically

strained, it became thinner, and eventually the code failed to converge, indicating that a failure limit had been exceeded. This failure limit should be considered an upper bound on the solution, since local strain concentrations could cause a tear to initiate in the shell wall before this stability limit is reached.

Predicted results were examined after each analyses was completed to determine if local strain concentrations were large enough that a tear may have initiated. Elements in the model did not automatically fail when they reached the strain value where a tear could initiate. Instead, failure predictions were assessed during post processing. Failure was predicted when any element in the model reached the strain limits discussed in section 4. Although the analyses continued running until the code failed to converge, as discussed in the previous paragraph, experience has shown that containment vessels will fail in stress concentration regions at strains well below the levels at which the code fails to converge. No attempt has been made to predict the structural response after a tear is predicted to initiate at the strain limits discussed in Chapter 4.

In some cases, if the high plastic stresses and strains are very local to the tear location, it is likely that the tear will arrest itself and the vessel will depressurize due to the tear in the wall. However, if the high stresses and strains cover a large enough area, then the tear is likely to propagate and result in total catastrophic failure.

For each analysis, failure predictions consisted of a "lower bound", "best estimate", and "upper bound" failure pressure. Several different locations were

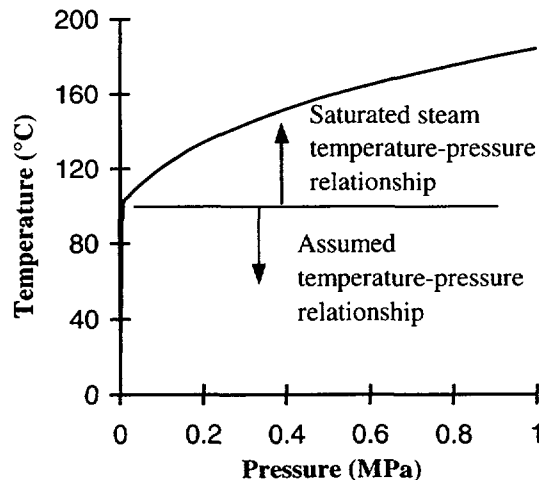


Figure 5.8. Saturated steam temperature-pressure relationship.

examined to determine where the likely failure locations were.

Three locations were chosen where there was a high potential for corrosion, and each of these locations was analyzed with two different amounts of assumed corrosion. For each of the corrosion areas, enough degradation was selected to cause the structure to fail in the corroded region at about the same pressure that would cause failure at the highest stress region of an uncorroded containment. The assumed degradation was then increased about 15% more, and the analyses were repeated.

The largest strains in an uncorroded containment occurred in the vicinity of the ice basket region, where a plate thickness change caused significant stress and strain concentrations. Figure 5.9 shows the largest plastic membrane strains that occurred in the ice basket region for an uncorroded vessel, a vessel with about 10% corrosion in the stress concentration region, and a vessel with about 25% corrosion in the stress concentration region. Although thermal gradients around the ice baskets (reduced by insulation around the ice baskets, but not eliminated) would cause large *elastic* strains, as internal pressure increased the vessel would plastically strain and the significant portion of the load would be carried through membrane action. Including thermal gradients in an *elastic* analysis would have a significant effect on the *elastic* strains, while including the same thermal gradients in a *plastic* analysis would only have a minimal impact on the *plastic* strains. Therefore, thermal gradients were not included in these analysis. At strain levels that were near the first yield strain, the surface strains (caused by bending) were slightly larger than the membrane strains. However, as the strains became plastic, the vessel carried the internal pressure almost entirely through membrane action, and the surface strains were nearly identical to the membrane strains. Therefore, only the membrane strains are shown for this location.

The largest strains that occurred in the corroded upper floor region are shown in Figure 5.10. As discussed previously, the predictions about the response in the upper floor region were based on a finite element submodel that had a much finer mesh; a finer mesh allowed the model to predict stress concentrations more accurately than could be achieved by the global model. The calculated strains in the stress concentration region were about two times bigger than they were in the global model. Once again, the largest stresses and strains occurred in a stress concentration region caused by a change in plate thickness. The surface strains were about the same as the membrane strains, again indicating that the pressure loads were resisted by the vessel through membrane action. When the upper floor region is

corroded to about 50%, the analyses predict that failure will occur at about the same pressure that would cause failure in the uncorroded containment in the vicinity of the stress concentration near the ice basket. The strains in the ice basket region of an uncorroded containment are shown in Figure 5.10 for comparison purposes.

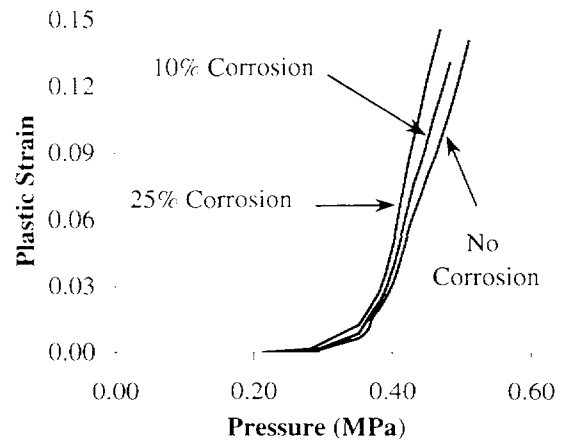


**Figure 5.9 Largest Equivalent Plastic Membrane Strains in Ice Basket Region.**

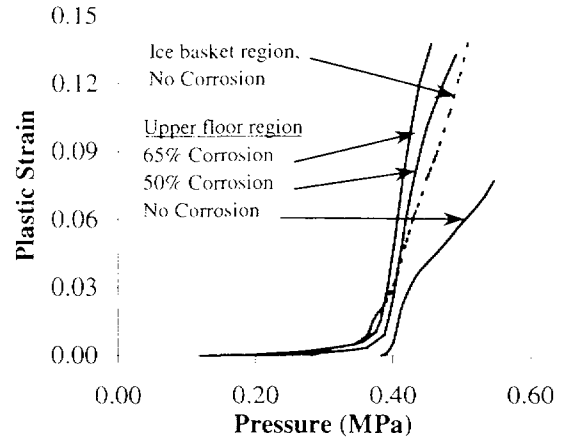


**Figure 5.10 Largest Equivalent Plastic Membrane Strains in Upper Floor Region.**

Figure 5.11 shows the equivalent plastic surface strain at one high-stress point in the corroded region near the basemat. At pressures above about 0.4 MPa, the plastic strains in Figure 5.11 are the largest in the basemat region. However, for pressures below 0.4 MPa, other nearby elements had larger plastic strains. The predictions about the response in the basemat region were based on a finite element submodel that had a much finer mesh. Local stress concentrations were calculated more accurately in the submodel because of the finer mesh. Calculated surface strains in

the stress concentration region were about 25% larger in the submodel than in the global model.

Because the shell wall is embedded in the concrete basemat, radial displacements of the shell wall are small, and membrane strains in the circumferential direction are also small. For this location, large surface strains are caused by bending. Since the surface strains are significantly larger than the membrane strains in this location, Figure 5.11 shows the largest surface strains in the corroded basemat region for several different corrosion levels. Once again, the membrane strains in the ice basket region of an uncorroded containment are shown for comparison. Figure 5.12 shows typical inner surface, membrane, and outer surface strains in the basemat region for a case with 50% corrosion in the basemat. The plastic strains shown in Figure 5.12 are the largest in the basemat region for pressures above about 0.4 MPa. However, at pressures below 0.4 MPa, other nearby elements have larger plastic strains than shown in the figure.

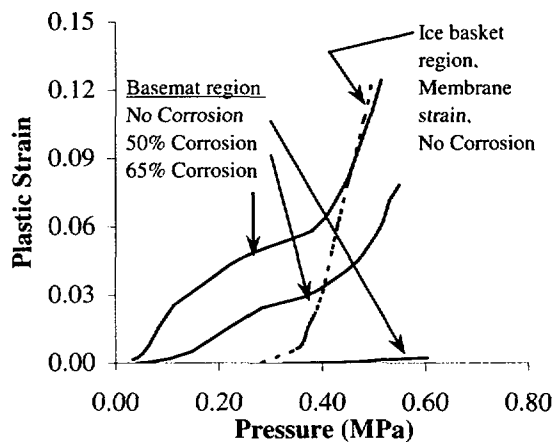


Figure 5.11 Typical Equivalent Plastic Surface (Bending) Strains in Basemat Region.

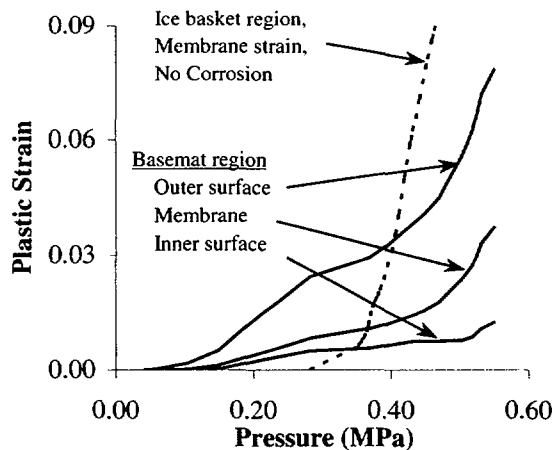


Figure 5.12 Typical Equivalent Plastic Strains in Basemat Region that has 50% corrosion.

Bending strains in the basemat region can be quite large if corrosion reduces the thickness around a significant portion of the circumference, and over a small height. This is the situation that was analyzed in the basemat region. High local bending does occur as the cylindrical wall transitions from its anchorage boundary condition to the free field condition, where loads are resisted primarily through membrane action. The bending stresses in the basemat region are limited, however, because when radial displacements become large enough, any additional pressure load will be resisted through membrane action. As can be seen in Figure 5.12, the bending strains are significantly higher than the membrane strains. As discussed in Chapter 4, the surface "failure" strain limit was 1.5 times larger than the membrane "failure" strain limit. However, because the bending strains in the basemat region are limited, a minimum surface "failure" limit of 5% strain was selected. No failure was deemed to occur unless the surface plastic strains exceeded 5%.

Predicted failure results (Table 5.1) show that corrosion in the area of highest strain will significantly reduce the pressure capacity of the vessel, while considerable corrosion in other areas can be tolerated without reducing the pressure capacity. The design pressure for the containment modeled was 0.074 MPa (10.8 psi).

The structural response of the first five cases (Table 5.1) was primarily membrane. Membrane forces in the cylindrical portion of the structure were twice as large in the circumferential direction as they were in the vertical direction. This is a known behavior of cylindrical sections. In the first three cases, internal pressure caused the structure to radially expand until failure occurred in the circumferential direction. Even while the structure was plastically flowing in the hoop direction, there was minimal plastic growth in the vertical direction. For these three cases, failure was predicted to occur near the top of the ice basket as a result of large hoop strains. In cases 2 and 3, the corrosion was located in the area of highest plastic strain. As expected, even small amounts of corrosion in high strain regions caused failure to occur at lower pressures. In cases 4 and 5, the thinned section was only 0.81 m high, but extended 11.9 m in the circumferential direction. The thicker sections above and below this degraded area were stiff enough that they did not undergo large hoop strains, and this support prevented the thinned section from experiencing large plastic hoop strains. It was not until the thickness of the corroded section was decreased by a factor of two that the vertical component of stress became large enough to cause large plastic membrane strains in the vertical direction, and failure was predicted at this location. For cases 6 and 7, the steel shell was relatively thick near the basemat and was

embedded in the concrete floor. Circumferential straining in the thinned section at the basemat was limited because of support from the basemat and the thick plate above the reduced area. It was not until the thickness of the corroded section was decreased by a factor of two that the vertical component of stress became large enough to cause large plastic strains in the vertical direction. In this case, however, the peak strains were a result of membrane and bending in the vertical direction.

Von mises stresses for the uncorroded containment are shown in Fig 5.13. The effective plastic strains (Fig 5.14) showed a few areas that experienced large plastic membrane strains. For the uncorroded containment, failure would be expected to occur at the high stress and strain location around the ice basket (Figs. 5.15 and 5.16). At this location a 3.81 cm thick plate protruded into a 1.59 cm thick area and caused large membrane strains in the thinner plate. A few other locations on the model with a thick section protruding into a thinner area also showed a region of large membrane strains in the thinner plate near the discontinuity. These strains were considerably larger than free field strains in the thin plate. However, many areas where thick plates transitioned to thin plates did not experience larger-than-free-field strains in the region near the weld joint. From Figs. 5.13 and 5.14 it can be seen that large stresses and plastic strains were only reached in a few regions, and that the global, free-field stresses and strains were considerably lower.

The analyses that included corrosion areas had higher strains in the locally thinned areas than corresponding strains in the undegraded case. Although the strains were higher in the locally thinned areas, the global responses were very similar to the response of a containment with no corrosion damage.

Von mises stresses and equivalent plastic strains for the submodel around the upper floor area are shown in Figs. 5.17 and 5.18. Once again, these figures are for the containment in an uncorroded state. When corrosion was modeled in the upper floor region, the calculated stresses became larger than shown in Figs 5.17 and 5.18, but the stress concentration points remain in the same location.

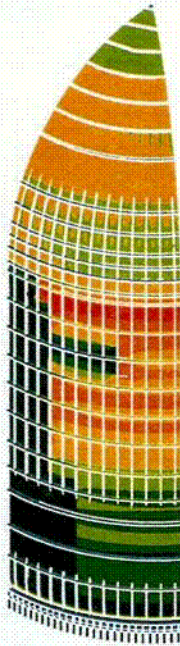
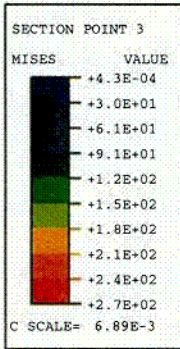
The criteria used in this report to predict potential containment failure differ significantly from criteria that would be acceptable for design. Containment structures are conservatively designed so that the probability of failure is very, very small under design loads. The design criteria are selected so that the vessel remains elastic, with a comfortable safety factor, under all design loads. However, when predicting failure, previous tests on scaled models have demonstrated that large plastic strains occur before the pressure boundary fails. The criteria used to predict failure are suitable for use in risk studies, but are clearly unacceptable for design. For example, in design, strains are typically limited to about 2/3 of the elastic limit. However, when predicting failure, strains that were 7 to 50 times larger than the elastic limit were selected. Some of the badly corroded containments that have been analyzed in this report had plastic strains below limits where failure would be anticipated, but strains that were well above the elastic limit at design loads. Although the probability of failure under design loads is low for some of the corroded containments that were analyzed, the level of conservatism necessary to ensure safety was lacking. To ensure a conservative design, it is necessary to keep stresses and strains in corrosion areas from exceeding ASME code allowable limits.

**Table 5.1. Predicted Failure Pressures**

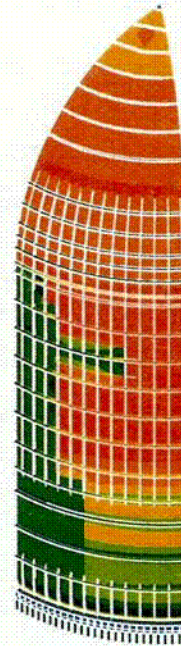
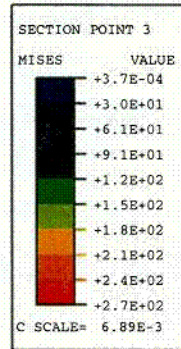
Case No.	Description	Failure Limit					
		Lower bound		Best estimate		Upper bound	
		Pressure	Membrane Strain	Pressure	Membrane Strain	Pressure	Membrane Strain
1	no corrosion	0.426 MPa (61.8 psi)	0.065	0.472 MPa (68.4 psi)	0.102	0.512 MPa (74.2 psi)	0.148
2	10% corrosion at ice basket	0.365 (52.9)	0.015	0.410 (59.5)	0.049	0.462 (67.0)	0.108
3	25% corrosion at ice basket	0.357 (51.8)	0.015	0.401 (58.1)	0.048	0.441 (63.9)	0.108
4	50% corrosion at upper floor	0.393 (57.0)	0.015	0.414 (60.0)	0.051	0.455 (66.0)	0.106
5	65% corrosion at upper floor	0.382 (55.4)	0.015	0.402 (58.3)	0.051	0.430 (62.4)	0.107
6	50% corrosion at basemat	0.407 (59.1)	0.015	*		*	
7	65% corrosion at basemat	0.168 (24.3)	0.015	0.398 ** (57.7)	0.074**	*	

\* Failure is not predicted to occur at the corroded location.

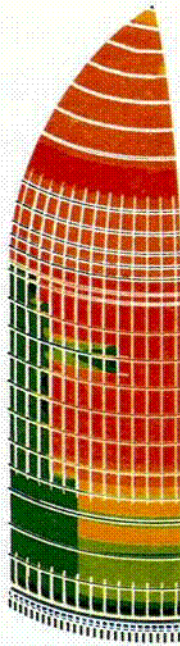
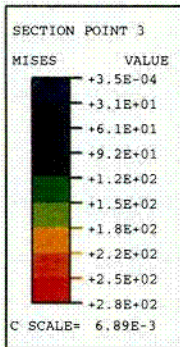
\*\* Surface strain (bending) was the "failure" limit at this point.



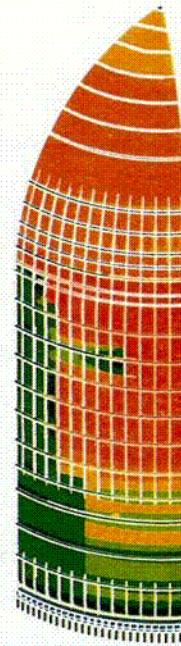
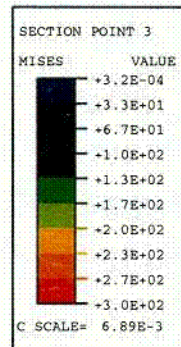
0.283 MPa (41 psi), 143° C



0.352 MPa (51psi), 148° C

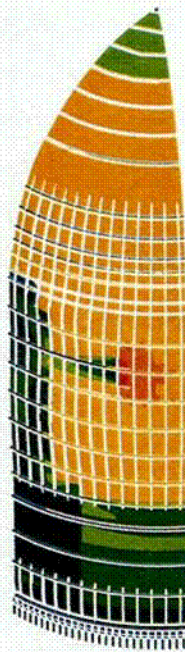
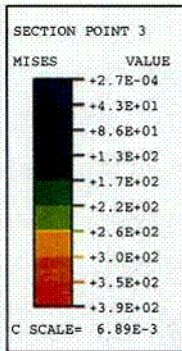


0.366 MPa (53psi), 149° C

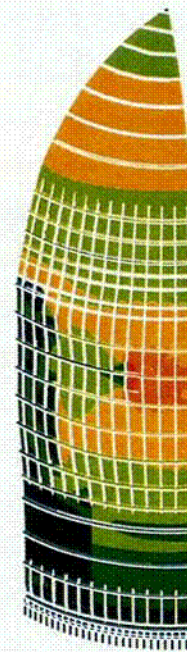
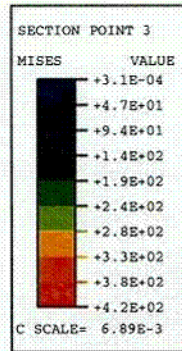


0.377 MPa (55 psi), 151° C

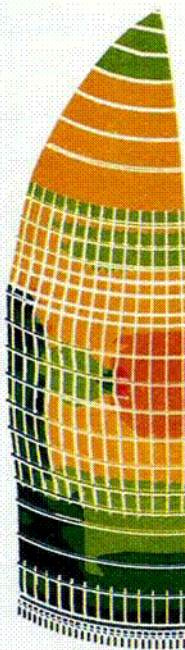
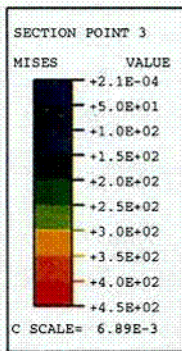
**Figure 5.13 Von mises membrane stress (MPa) in global model with no corrosion, displacements magnified by a factor of 5.**



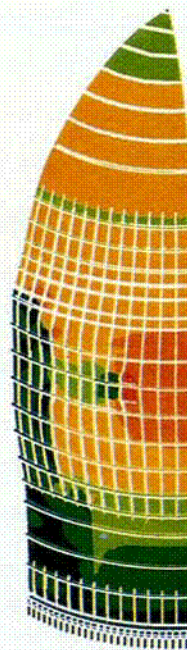
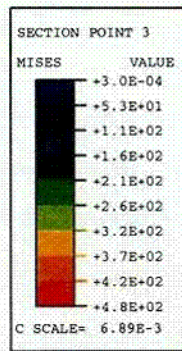
0.411 MPa (60 psi), 153° C



0.441 MPa (64 psi), 155° C

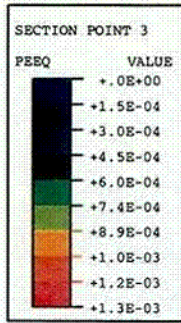


0.482 MPa (70 psi), 158° C

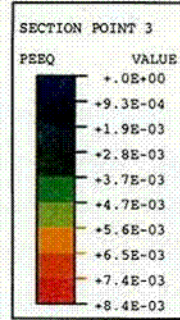


0.510 MPa (74 psi), 159° C

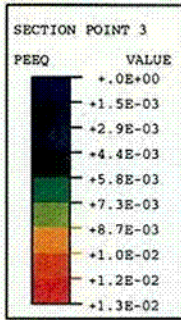
Figure 5.13 Von mises membrane stress (MPa) in global model with no corrosion, displacements magnified by a factor of 5. (continued).



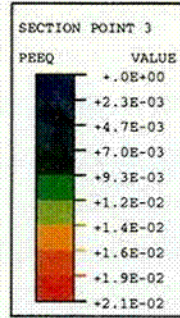
0.283 MPa (41 psi), 143° C



0.352 MPa (51 psi), 148° C

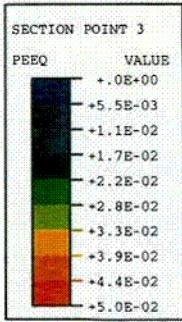


0.366 MPa (53 psi), 149° C

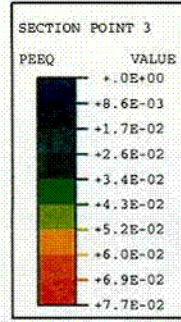


0.377 MPa (55 psi), 151° C

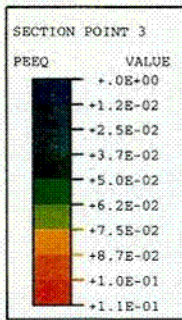
Figure 5.14 Equivalent plastic membrane strain in global model with no corrosion, displacements magnified by a factor of 5.



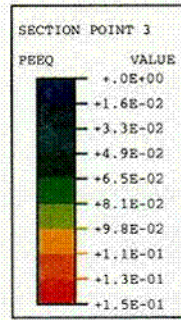
0.411 MPa (60 psi), 153° C



0.441 MPa (64 psi), 155° C

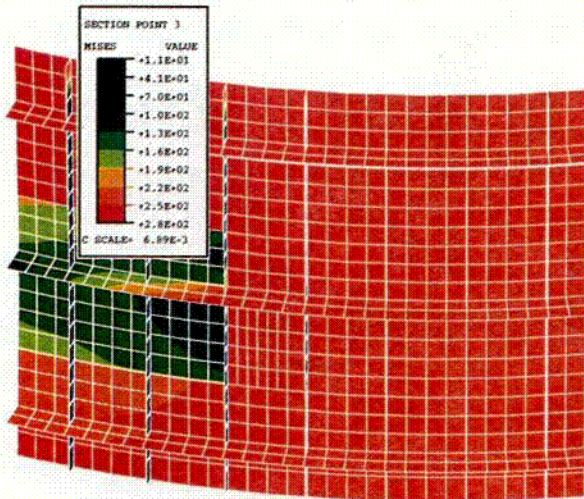


0.482 MPa (70 psi), 158° C

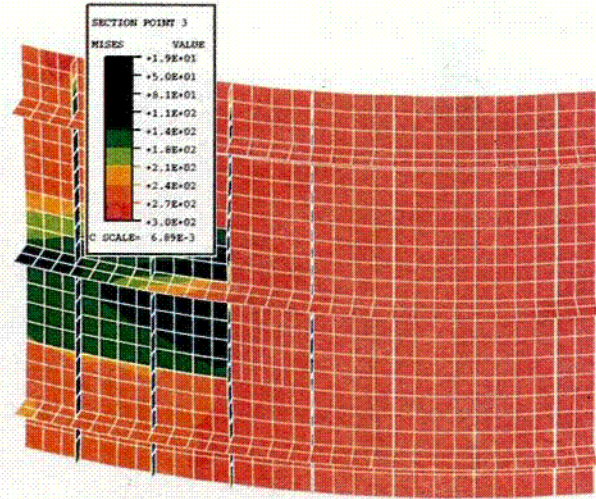


0.510 MPa (74 psi), 159° C

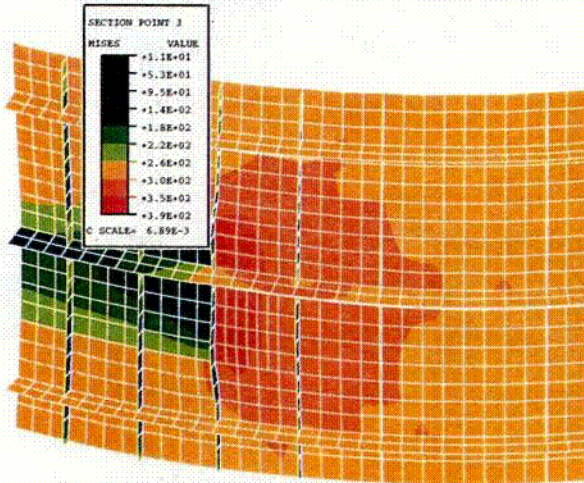
Figure 5.14 Equivalent plastic membrane strain in global model with no corrosion, displacements magnified by a factor of 5. (continued).



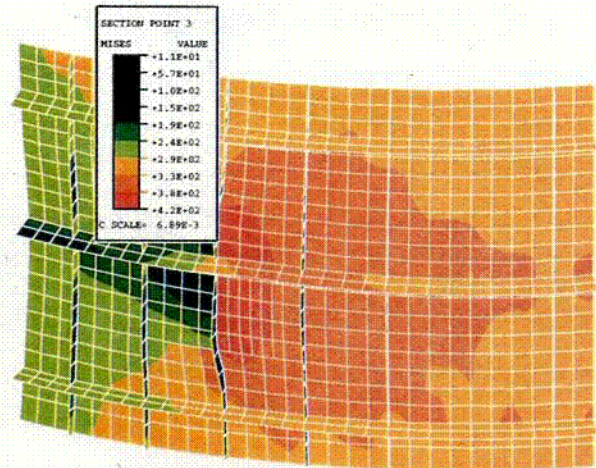
0.366 MPa (53 psi), 149° C



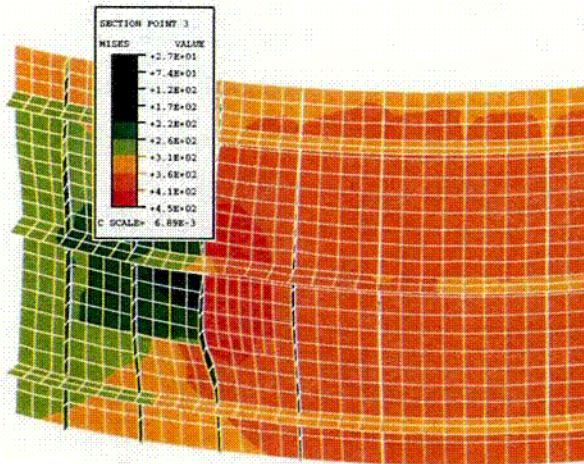
0.377 MPa (55 psi), 151° C



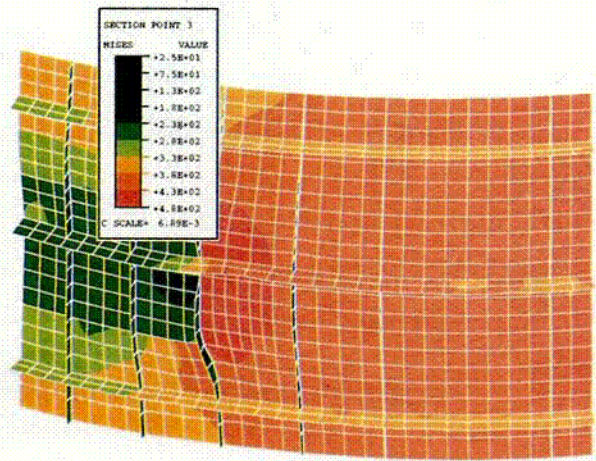
0.411 MPa (60 psi), 153° C



0.441 MPa (64 psi), 155° C

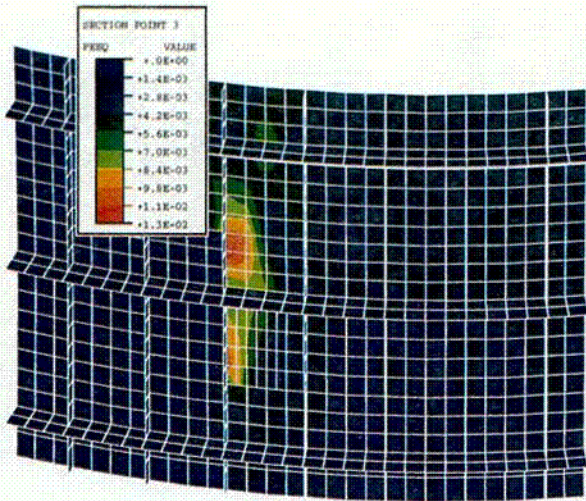


0.482 MPa (70 psi), 158° C

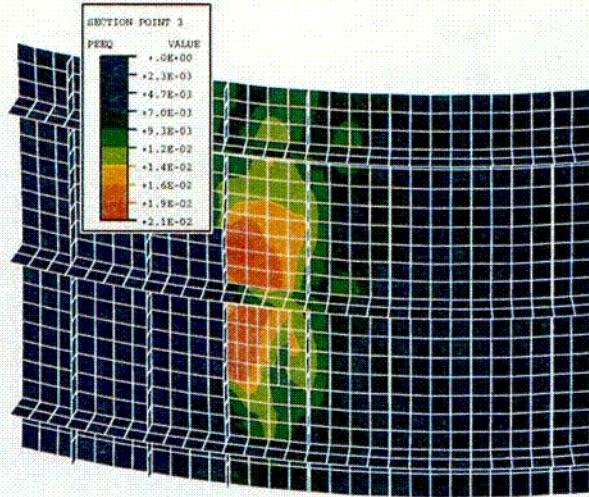


0.510 MPa (74 psi), 159° C

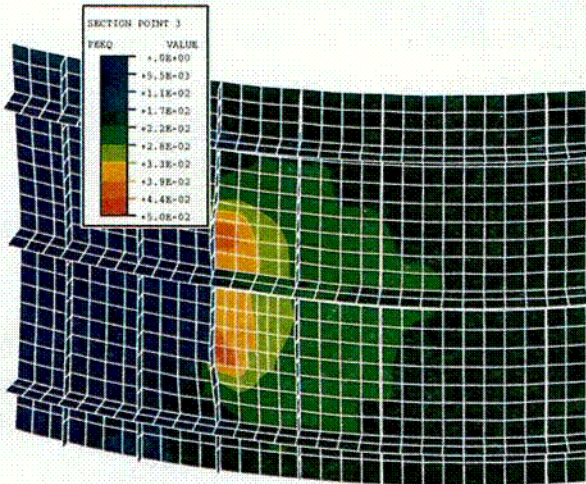
Figure 5.15 Von mises membrane stress (MPa) in ice basket region with no corrosion, displacements magnified by a factor of 5.



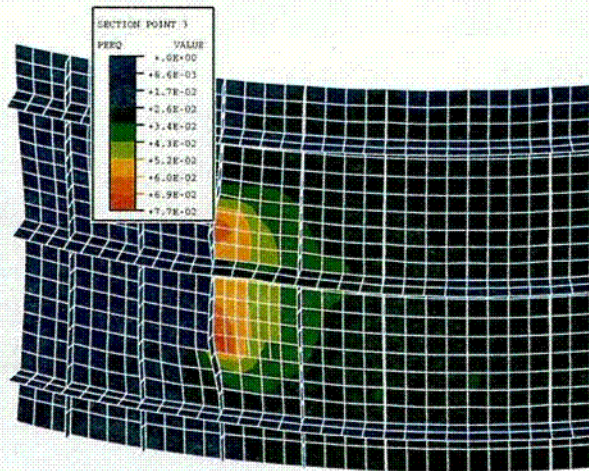
0.366 MPa (53 psi), 149° C



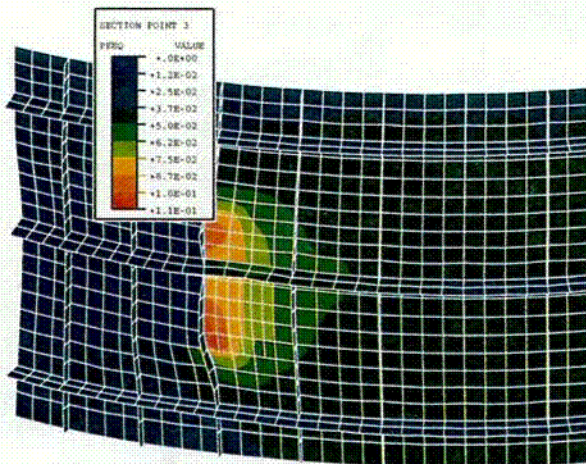
0.377 MPa (55 psi), 151° C



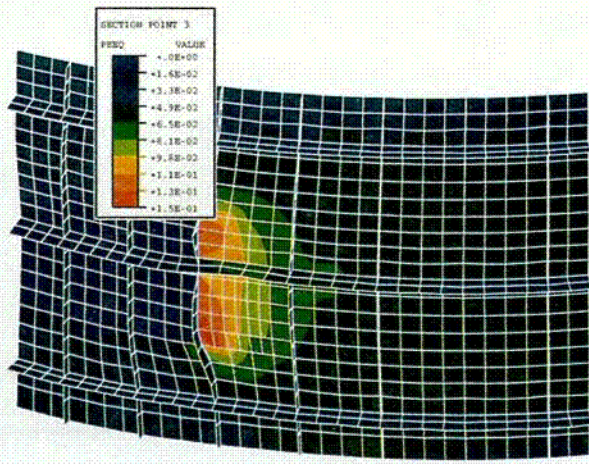
0.411 MPa (60 psi), 153° C



0.441 MPa (64 psi), 155° C

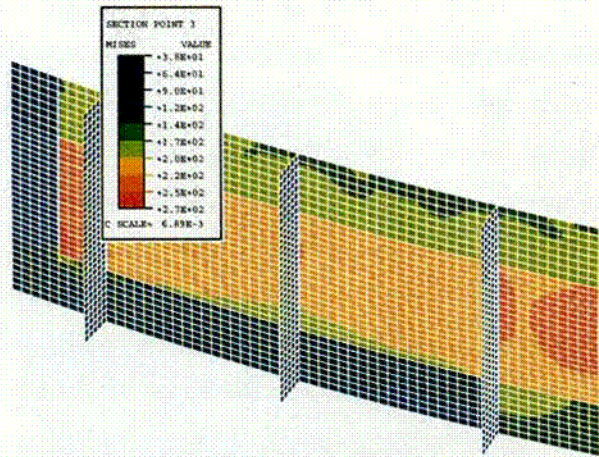


0.482 MPa (70 psi), 158° C

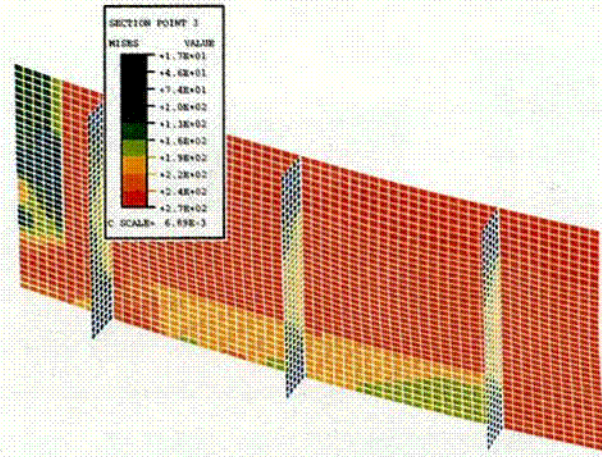


0.510 MPa (74 psi), 159° C

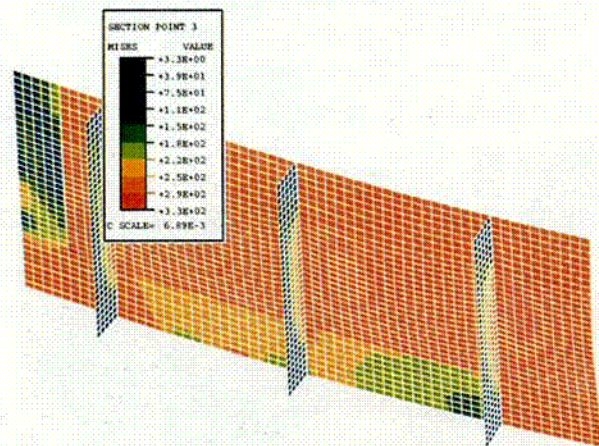
Figure 5.16 Equivalent plastic membrane strain in ice basket region with no corrosion, displacements magnified by a factor of 5.



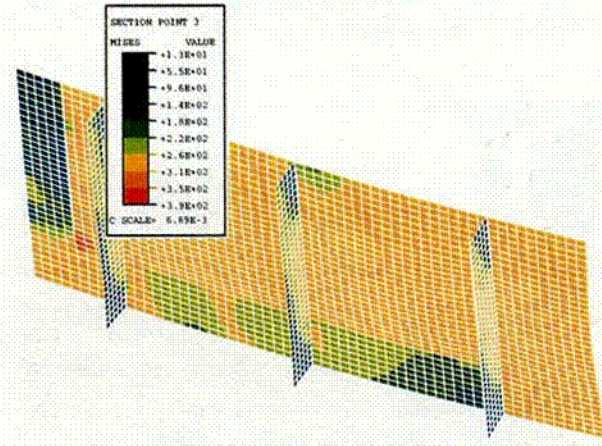
0.259 MPa (38 psi), 141° C



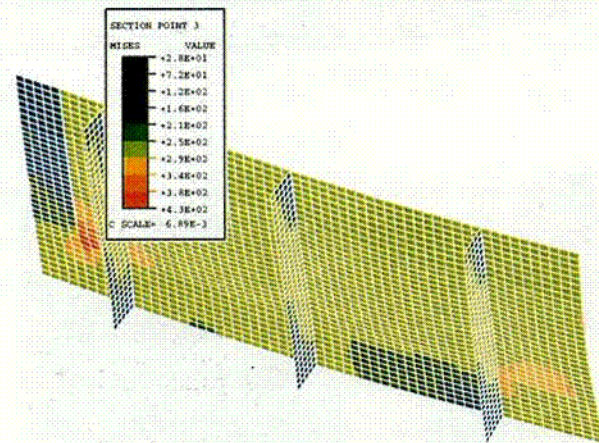
0.388 MPa (56 psi), 151° C



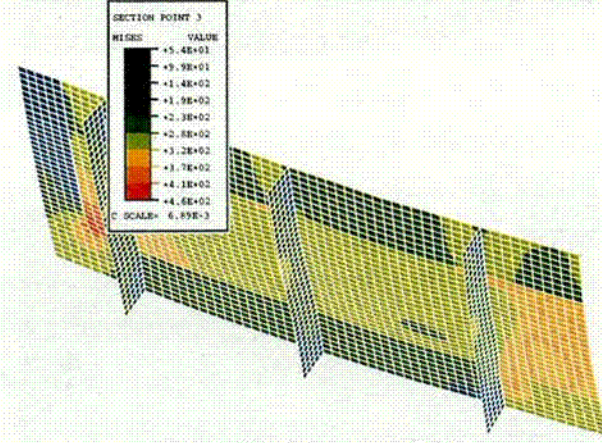
0.401 MPa (58 psi), 152° C



0.414 MPa (60 psi), 153° C

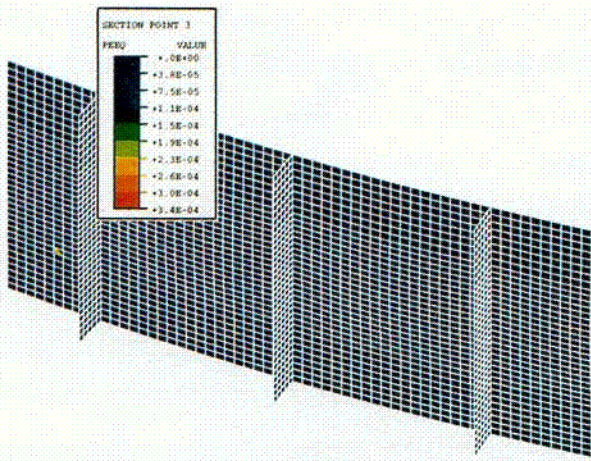


0.432 MPa (63 psi), 154° C

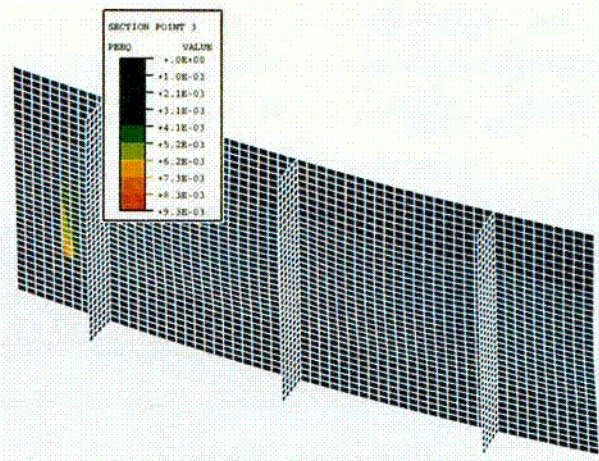


0.471 MPa (68 psi), 157° C

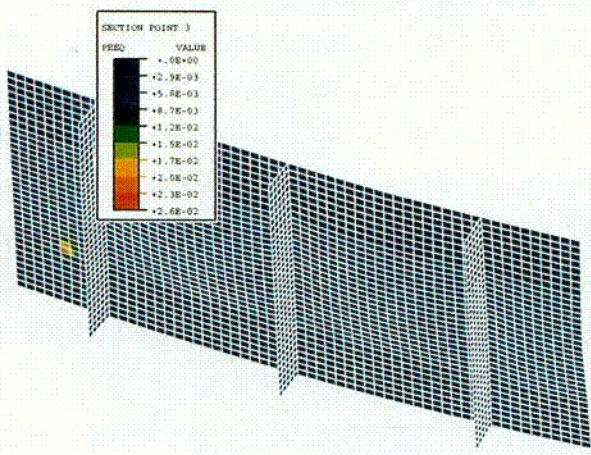
Figure 5.17 Von mises membrane stress (MPa) in local model of upper floor region with 50% corrosion, displacements magnified by a factor of 5.



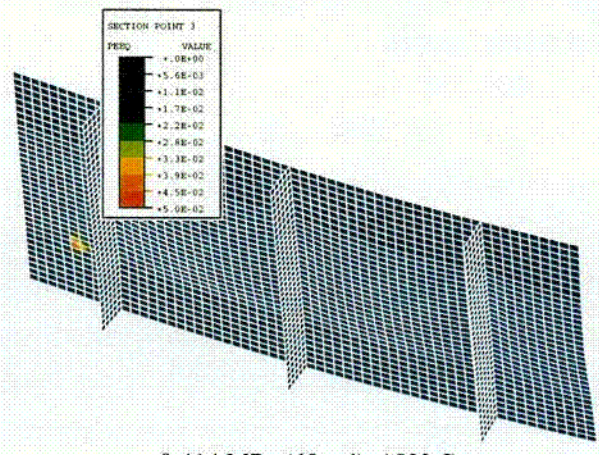
0.259 MPa (38 psi), 141° C



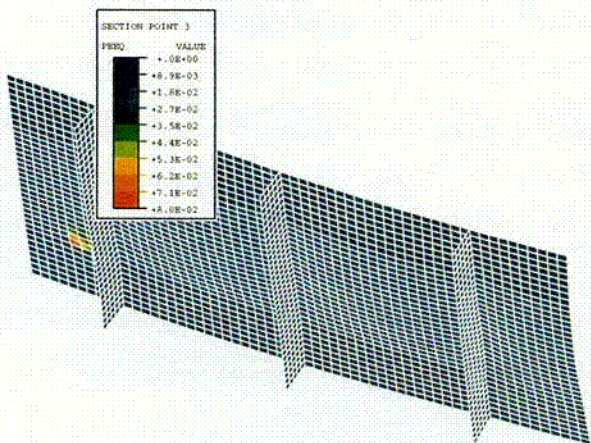
0.388 MPa (56 psi), 151° C



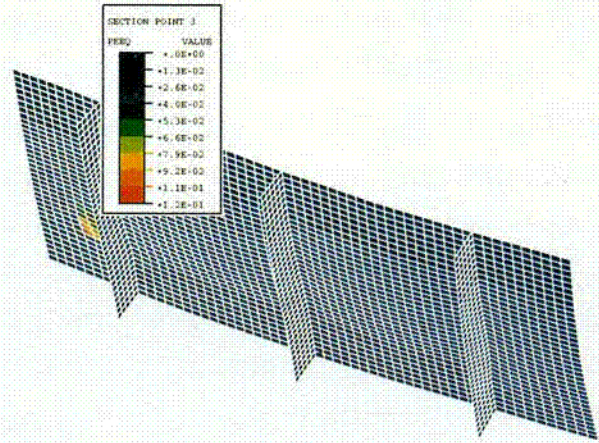
0.401 MPa (58 psi), 152° C



0.414 MPa (60 psi), 153° C



0.432 MPa (63 psi), 154° C



0.471 MPa (68 psi), 157° C

**Figure 5.18** Equivalent plastic membrane strain in local model of upper floor region with 50% corrosion, displacements magnified by a factor of 5.

## 6 ANALYSIS OF TYPICAL BWR MARK I CONTAINMENT

The finite element model that has been developed is typical of BWR Mark I containments in the United States. Although the analytical model was selected to be similar to the Peach Bottom containment, there are several important differences. Therefore, throughout this report, the model is referred to as a BWR Mark I containment, and not as the Peach Bottom containment.

The dimensions, plate thicknesses, and other details were modeled based on drawings of the Peach Bottom containment. However, the material properties used in the analyses in this report are typical of A516 Grade 60 steel, and vary somewhat from measured material properties of Peach Bottom.

Furthermore, the postulated corrosion that is included in these analyses has not been observed in the Peach Bottom containment. Symmetry assumptions, penetrations not modeled, and other simplifications to the model could result in differences between the calculated response of a "typical" BWR Mark I containment, and the actual response of the Peach Bottom containment.

In most accident sequences, an operator would intentionally vent the containment when it reached an internal pressure level that is well above the design level. Since the Peach Bottom containment would be vented at 0.69 MPa (100 psi), this is the value where venting is assumed to occur in this study. Unless the vessel is severely corroded, it is very unlikely that failure would occur below this pressure level.

Previous studies have examined other possible failure modes for BWR Mark I containments (Mokhtarian et al, 1987). One likely leak path is through the drywell top head gasket, between about 0.72 and 1.20 MPa of pressure. The exact pressure at which leakage would begin is difficult to determine because of uncertainty in the preload level in the top head bolts, and because of the uncertainty in the amount of springback in the gasket material. Based on hand calculations, a gap begins to open between the top head and the bottom portion of the drywell at about 0.72 MPa. The top head gasket, which was compressed when the top head was bolted on, will expand as the gap opens. The amount that the gasket will expand is dependent on the age of the top head gasket, the temperatures it has been exposed to, the amount of time it has been compressed, how rapidly the gap is opened, and numerous other factors. At 1.20 MPa, the gap between the top head and the drywell would be about 1 mm, and leakage would be quite likely. Further work was not performed to better understand when a leak through the top head gasket would begin because:

- Operational plan calls for venting at 0.69 MPa (100 psi) (design pressure is 0.39 MPa (56 psi)), and for a containment with no corrosion or other aging damage, venting is expected before any failure could occur.
- Venting is expected before leakage through the seal at the top head. However, if the containment was not vented for some reason, the next expected leak path would be through the seal at the top head. An entire test program could be devoted to better understanding gasket leakage issues. Indeed, many gasket and seals programs have been performed previously that have evaluated some aspects of this problem.
- The primary focus of this project was structural failure modes, specifically structural failure that relate to corrosion.

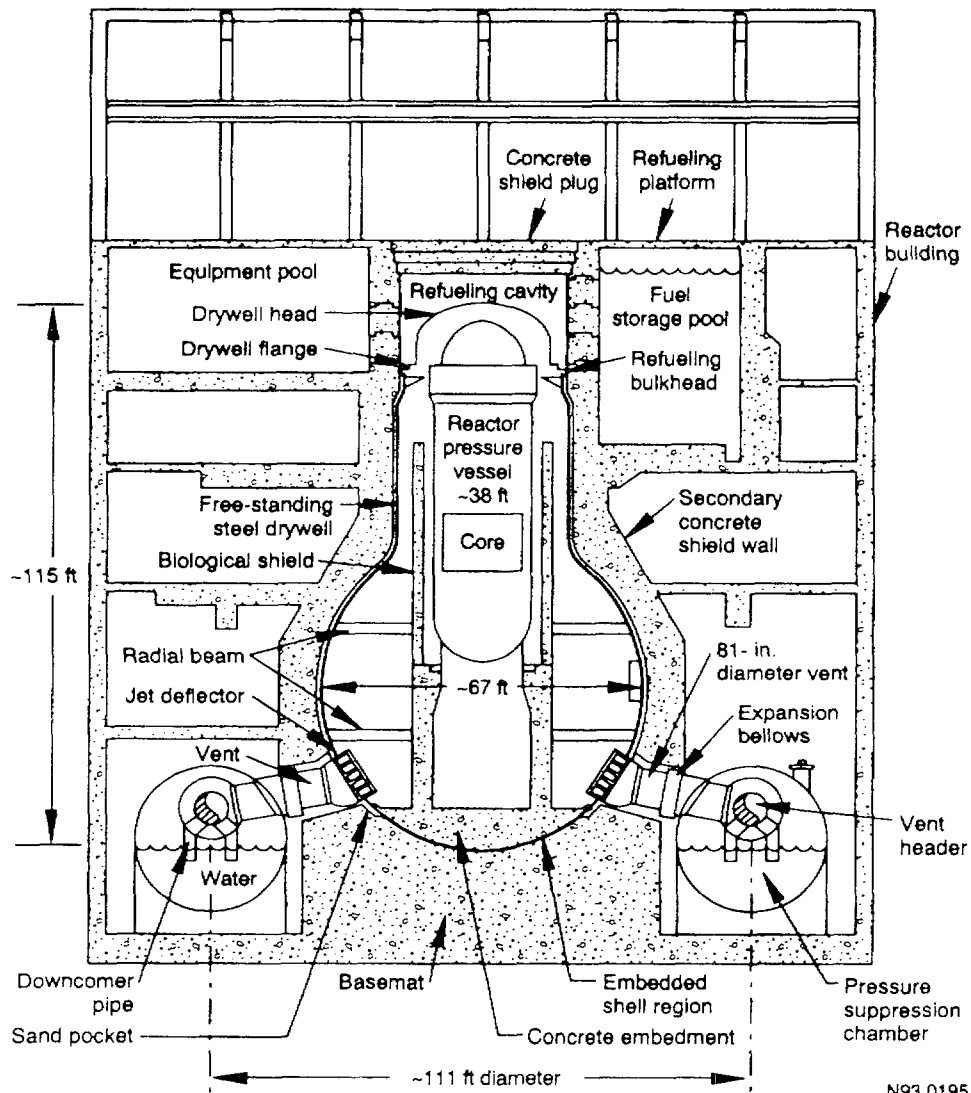
If the containment vents or leaks through the gasket at the top head, the internal pressure would be relieved, and therefore a structural failure would not occur. However, if sufficient corrosion occurs, a weakened shell wall could tear in the corroded location before the vent releases pressure, or pressure leaks through the top head seal, and a catastrophic failure could result.

Containment vessels are designed to withstand many different loads, such as seismic or internal pressure. Although code requirements stipulate combinations of loads that the vessel must be designed to resist, only internal pressure and loads caused by thermal expansion or contraction have been analyzed in this study. For free standing steel containments, buckling of the shell wall under load conditions such as seismic may be the worst case loading that dictates the wall thickness for some portions of the containment.

The analytical results discussed in this chapter have not been evaluated for seismic or other load conditions that could cause buckling. When evaluating the effect of corrosion damage on an actual containment, it is important to remember that all code required load combinations must be evaluated to ensure that other failure modes, such as buckling, won't cause failure before the vessel fails due to internal pressure.

### 6.1 Geometry

The typical BWR Mark I containment (Fig. 6.1) consists of a drywell and a suppression pool. The drywell has the shape of an inverted light bulb, and is connected to the torroidal-shaped suppression pool via vent lines. Bellows in the vent lines absorb differential



N93 0195

Figure 6.1 "Typical" BWR Mark I containment.

movement between the two vessels. Both the drywell and suppression pool are constructed from A516 Grade 70 steel.

The drywell is surrounded by a reinforced concrete shield wall, with a gap between the concrete shield wall and the freestanding steel containment of about 5 to 7.5 cm. Originally, the gap was filled with polyurethane foam, fiberglass, or other insulation-like materials. However, because of the fire hazard that exists if this material catches fire, it has been removed on some of the operational containments. The finite element model assumes this gap is air, and not an insulation material.

The spherical section of the drywell has a diameter of about 20 m, the cylindrical section has a diameter of about 12 m, and the height from its base to the top of the top head is about 34 m. The shell thickness varies from 3.18 cm in the lower portion of the spherical section to 1.91 cm in the upper portion of the spherical section. In the sphere-to-cylinder transition region, the shell wall is 7.30 cm thick. The cylindrical section varies from 1.91 to 3.18 cm thick. The elliptical-shaped top head is also 3.18 cm thick. The spherical shell is embedded in a concrete basemat.

The torus of the suppression pool is about 9 m in diameter. The bottom half of the torus is filled with

water. Below the waterline, the thickness of the shell is 1.71 cm. Above the waterline, the thickness is 1.53 cm, except for the section where the vent lines connect, which is 2.86 cm thick. Ring stiffeners are included between sections of the torus, and at these stiffener locations the torus is supported by saddle-shaped structures. The saddle support structures are pinned at the base to prevent uplift or twist, but holes are slotted so that they won't restrict radial movement. The base section is teflon coated to minimize friction forces and allow the torus to expand or contract radially.

Although underwater locations near the strainers where debris accumulates, as well as several other locations, could have been analyzed, for the BWR Mark I containment, (Figure 6.1), analyses were performed with corrosion in the following locations:

- The spherical section in the sand pocket region, similar to the damage found at Oyster Creek

(Figure 6.2). However, the depths of corrosion that were analyzed were postulated.

- At the water line, in one bay of the toroidal shaped suppression pool. Corrosion has been found over very large areas in the suppression pool of operational containments, such as the corrosion damage found at Nine Mile Point.
- In the sphere-to-cylinder knuckle region. This is a susceptible area with a high potential for corrosion, because water from leaks can be trapped by the insulation-like material between the containment shell and the concrete building. Since the outside of the shell is not accessible for inspection, it is not known if corrosion has actually occurred at this location in operational containments.

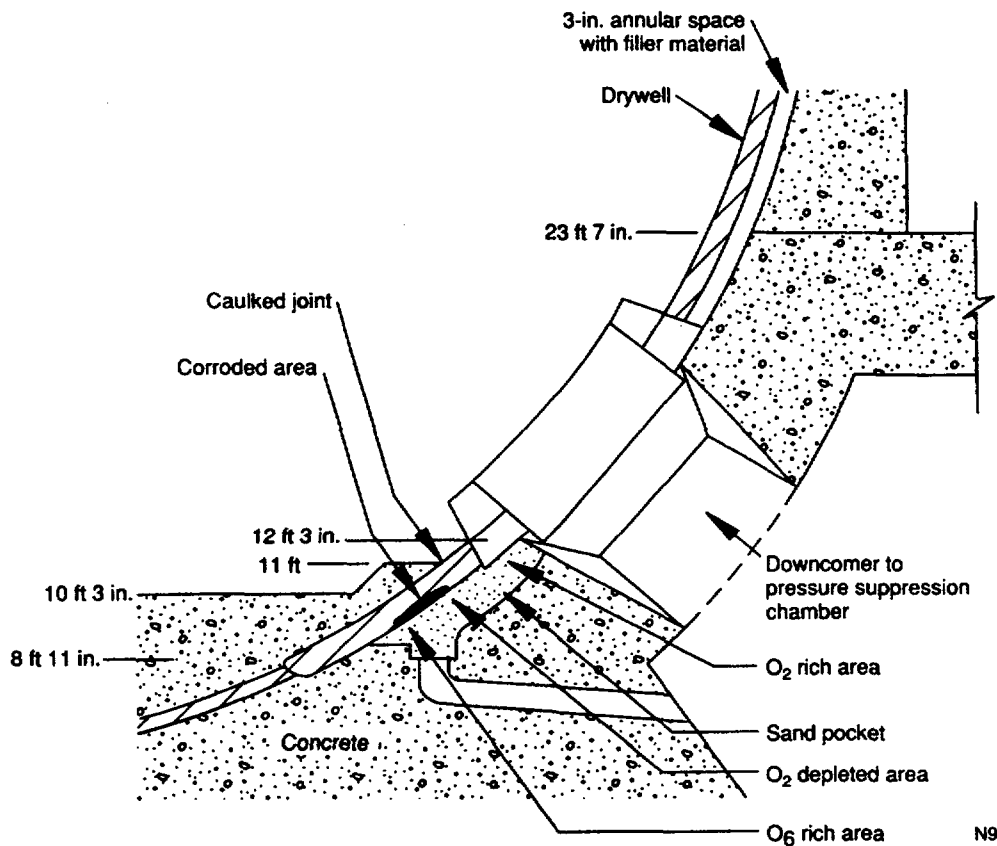


Figure 6.2 Observed damage in sand pocket region.

## 6.2 Finite Element Models

The analyses approach used in Chapter 5 was to analyze a global model to get the overall response, and then apply boundary conditions obtained from the global model to a finely meshed submodel. That approach was selected because of computer limitations, both in terms of memory, disk space, and the time required to complete the analysis. After the analyses in Chapter 5 were completed, a new and much faster computer was obtained. This made it possible to include a finely meshed region (i.e., the submodel) in the coarser-meshed global model. This is the approach that has been used for the analyses discussed in Chapter 6.

Two ABAQUS finite element models were constructed for the drywell, and one model was constructed of the suppression pool. The first drywell model contained an area with very fine meshing around the sphere-to-cylinder knuckle region (Fig. 6.3), and consisted of 5824 first order shell elements, with 5978 nodes. It included a 45° circumferential segment of the containment, and went from the concrete base to the top of the top head. Symmetry boundary conditions were applied along both vertical edges. A 22.5° segment of the drywell, with appropriate boundary conditions, could have represented an uncorroded containment, but the assumed corrosion area required analyzing a larger segment of the vessel. Corrosion was modeled in the knuckle region in the finely meshed area. The drywell shell was rigidly fixed at the bottom of the sand pocket, which is a good approximation for a containment that has had the sand removed from the pocket, such as occurred at Oyster Creek.

The second drywell model contained an area with very fine meshing around the sand pocket region (Fig. 6.4), and consisted of 4840 first order shell elements with 5050 nodes. It also included a 45° segment of the containment, with symmetry boundary conditions applied along both vertical edges. Corrosion was modeled in the finely meshed basemat region.

The model of the suppression pool (Fig 6.5) consisted of 3684 four-node quadrilateral shell elements, with 3788 nodes. This model included a 22.5° segment of the suppression pool. Symmetry boundary conditions were applied along both edges where the torus was discontinued. Because of the corrosion pattern that was selected, a 22.5° segment was adequate, and the larger 45° segment that was analyzed for the drywell wasn't needed. A model with a finely meshed region was generated, but the coarser model gave almost identical results. Therefore, the model with the area of

fine meshing wasn't used in subsequent analyses. Corrosion was modeled along the waterline in the bay that does not contain the vent line.

The drywell contained steel plates of several different thicknesses. In areas where the plate thickness transition occurred, the largest stresses and strains would be expected. The smallest elements had a side length of about 2.5 cm, while the average element had a length of about 30 cm.

The concrete basemat was not modeled. The vent line penetrations and the top head were the only penetrations that were explicitly modeled. Although the bellows themselves were not modeled, the penetration holes in the drywell and the suppression pool were included. Appropriate forces were applied along the edges of the vent line penetration holes to represent the force of deforming the bellows. This force was determined based on a linear spring constant and the calculated displacements. Bellows have been addressed under a previous program (Lambert, et al., 1995). In addition, the NRC has an on-going program to evaluate how corrosion degradation in bellows affects the containment capacity.

In previous analyses (Miller, 1990; Greimann, et al., 1984) it was found that containment failure occurred where thin wall sections met the thicker plate sections that the penetrations passed through (Clauss, 1985; Greimann et al., 1987). In those studies, plastic yielding occurred in the thinner plate sections, and not in the thickened plates.

Previous analyses of the PWR Ice Condenser containment, as well as analyses that were done by other people, indicate that large stresses and strains can occur at shell thickness discontinuities. The BWR Mark I drywell model includes a vent line hole, and a small section of the vent pipe. The suppression pool also includes a vent line hole, and a small section of the vent pipe. A previous analysis (CBI reference) showed that the drywell and wetwell were very loosely coupled. This is intuitively obvious since the bellows are designed to accommodate differential movement, so that movement in one of the structures does not have a significant effect on the structural response of the other. This loose coupling was achieved in the models by:

- analyzing the drywell with no attachment to the suppression pool,
- analyzing the suppression pool with no attachment to the drywell, and

- repeating both analyses with an applied force on both the drywell and suppression pool models (equal in magnitude, opposite in direction) based on the relative displacements between the two uncoupled responses.

This gives the same result as connecting the drywell and suppression pool in the analyses via a spring to represent the vent line and bellows. By splitting the model into two independent parts (drywell and suppression pool), it was possible to add considerably more detail into each of the models. The models could be split in this manner since they were only connected via the vent lines, and the vent line bellows absorbed the differential movement between the structures so that displacements in one vessel had a minimal affect on the other.

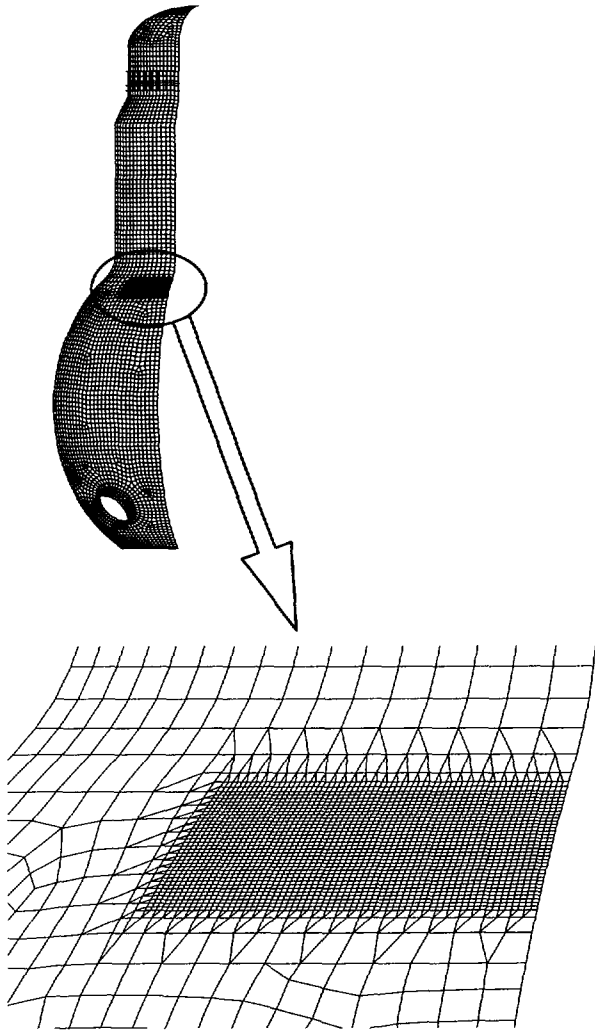


**Figure 6.3 Finite Element Model around Sphere-to-Cylinder Knuckle Region.**

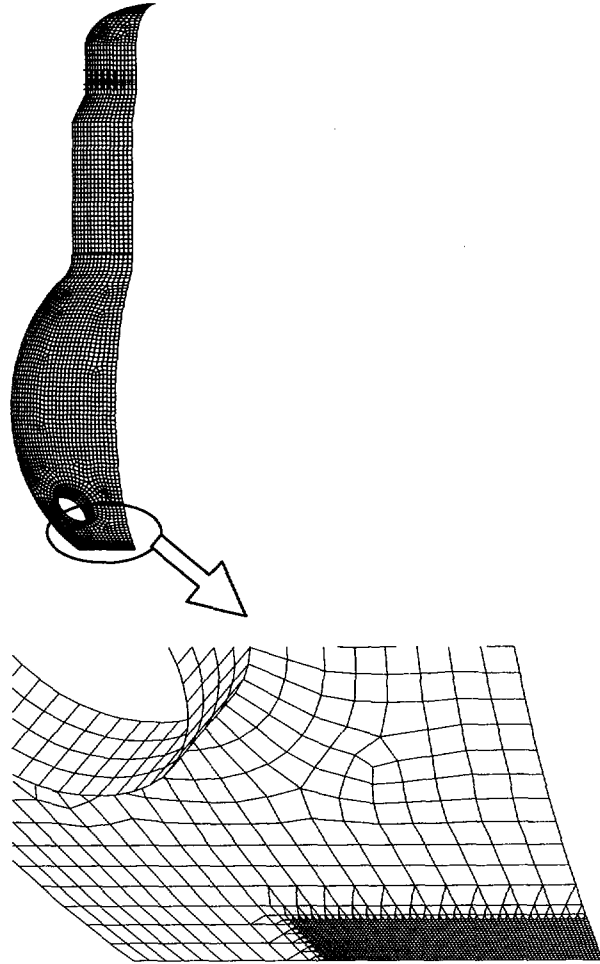


**Figure 6.4 Finite Element Model around Sand-Pocket Region.**

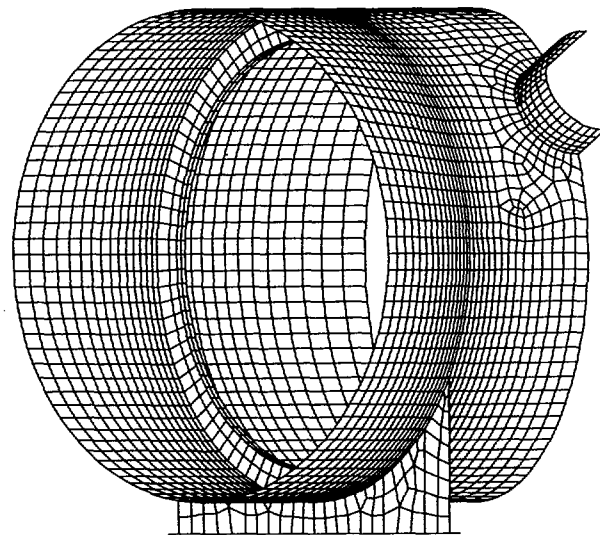


**Figure 6.5 Model of Suppression Pool.**

During the analyses performed in this report, the temperature of the wetwell shell and the temperature of the drywell shell increased as a function of pressure, and the pressure and temperature in the wetwell was assumed to be exactly the same pressure and temperature that was in the drywell. Under these temperature and pressure loading conditions, both the wetwell and drywell expand radially outward, so the relative displacement between them never becomes excessively large. Under many accident conditions, a differential pressure and temperature could exist. This could cause the bellows load to be larger than the assumed values in this analysis. The structural response to other postulated accidents must be evaluated on a case-by-case basis, however, so any effect of bellows loads could be accounted for during the specific evaluation.

The drywell head is modeled as a separate part, and is connected to the drywell via truss elements that represent the bolts. Other penetrations were not modeled, but varying plate thicknesses, and associated stress concentrations caused by geometric discontinuities, were included. Thickened plates around penetrations were not included except for the thickened section around the vent lines.

The stabilizers were not included in this model, based on previous analyses (CBI reference) that showed the stresses in the region of the stabilizer-to-drywell connection were not large enough to cause failure even when the vessel was at about three times the design pressure.

The shield building was also not modeled. The analyses predict that no contact would occur between an uncorroded containment and the shield building until pressures of around 0.9 MPa are reached. After contact is made, the shield building would begin to carry a portion of the load. Previous analyses (Mokhtarian et al, 1987) indicate that the shield building is capable of carrying the additional load from the expanding drywell until failure occurs in the suppression pool.

In corrosion areas, which were locally thinned in the analyses, failure is predicted in the locally thinned area either before contact would occur, or at about the same time that contact would occur. Modeling contact between the shield building and the containment would add a whole level of complexity that was not warranted in this case since:

- An *uncorroded* containment would reach 0.7 MPa and would be vented before contact between the structures would occur.

- If for some reason an operator was unable to vent the *uncorroded* containment at 0.7 MPa, the containment could contact the shield building, but the top head seal would probably begin to leak before a failure in the drywell or suppression pool occurred.
- If an operator was unable to vent the *uncorroded* containment, and the top head seal didn't leak, the predicted failure would be in the suppression pool, and not in the drywell.
- For a containment with severe *corrosion* in the knuckle region, the analyses performed predict that failure would occur either before contact is made in the locally corroded region, or very close to the time when contact would be expected.
- For a containment with lesser amounts of *corrosion*, the containment is predicted to vent or leak through the top head seal before or very near to the time when contact would occur in the corroded region.
- Ignoring contact is conservative, since any contact which occurs could delay or even prevent failure in the vicinity of the contact region.

The containment was modeled to determine failure level and location under several different degraded conditions. Three areas on the containment surface that were degraded (Figs. 6.6 and 6.7) correspond to the damaged or susceptible areas identified at nuclear power plants. In these areas corrosion was modeled by thinning shell elements and reducing the critical plastic failure strains. The depth of the corrosion was selected to ensure that failure occurred in the degraded area. A significant amount of damage was required to cause a failure in any of the degraded areas, and the primary reason is that leaks through the top head seal or intentional venting occur around 0.7 MPa, while the vessel is still primarily elastic. Failure of an uncorroded containment is not likely until the vessel is subjected to internal pressures that are about three times larger than design pressure. (Analyses indicate that 1% membrane strains occur in local stress concentration regions at about three times the design pressure.)

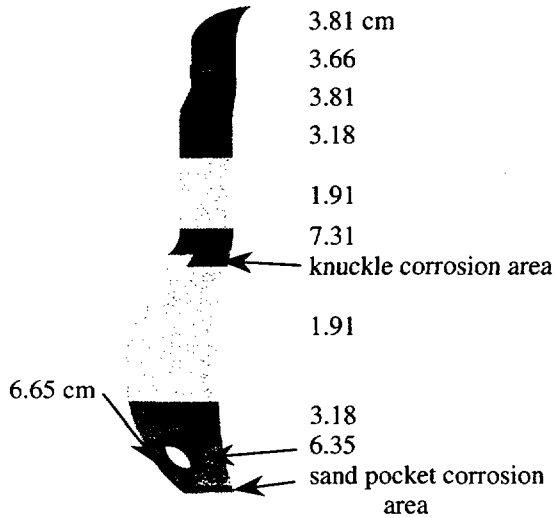


Figure 6.6 Drywell shell model thickness.

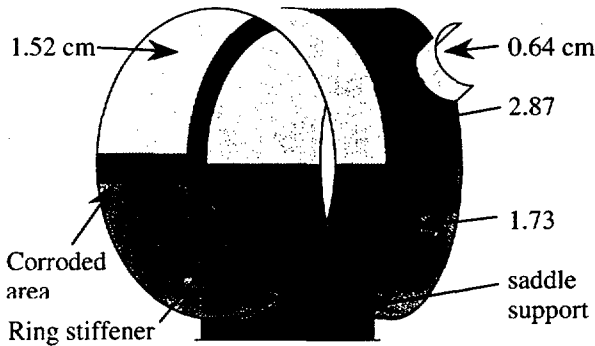


Figure 6.7 Suppression pool shell thickness.

The containment was analyzed in seven different configurations, with:

- No corrosion present.
- Corrosion near the sphere-to-cylinder knuckle region, with a 50% through the thickness corrod area of 0.91 m high by 22.5° circumferentially (~2.9 m). Because of the symmetry conditions used at the boundary, the corrod section is mirrored so that the actual degraded section is a 45° segment. In operational containments, this area is susceptible to corrosion, but the outer surface is inaccessible and does not get inspected.
- Corrosion near the sphere-to-cylinder knuckle region, as described above, except the damage is 65% through the thickness.
- Corrosion in the steel shell in the sand pocket region, with a 50% through the thickness corrod area of 0.25 m high by 22.5° around the circumference (~2.2 m). Because of the symmetry

conditions used at the boundary, the corrod section is mirrored so that the actual degraded section is a 45° segment. Corrosion has been found in this location during inspections at the Oyster Creek plant.

- Corrosion in the sand pocket region, as described above, except the damage is 65% through the thickness.
- Corrosion in the steel shell at the waterline in one bay of the suppression pool, with a 50% through the thickness corrod area of 1.03 m high by 11.25° around the circumference (~4.22 m). Corrosion has been observed in many areas of the suppression pool during inspections of the Nine Mile Point containment. Analyses show that the highest strains on an uncorrod containment are in the torus. This area of the torus is one of the expected failure locations.
- Corrosion in the suppression pool at the waterline, as described above, except the damage is 65% through the thickness.

### 6.3 Material Properties

The material properties used in the analyses in this report are typical of A516 Grade 70 steel, and vary somewhat from the measured material properties in Peach Bottom. Under ambient temperature conditions, A516 Grade 70 steel typically reaches yield at about 318 MPa, and the maximum engineering stress is about 483 MPa at 12-15% strain. ABAQUS requires that the material property stress-strain curves be true stress and true strain, and not engineering values. True stress and strain were estimated from engineering stress and strain values by the relationships

$$\sigma_{\text{true}} = (1 + \epsilon_{\text{engineering}}) \sigma_{\text{engineering}}$$

$$\epsilon_{\text{true}} = \log(1 + \epsilon_{\text{engineering}}).$$

Fatigue Technology Inc (1988) measured engineering stress-strain curves for A516 Grade 70 test coupons at temperatures of 22, 93, 149, and 204°C. The ambient temperature stress-strain curve used in the analyses in this report (Figure 6.8) is proportional to the Fatigue Technology data, but has been adjusted to pass through the true yield stress and true ultimate stress points for typical A516 Grade 70 material. The stress-strain curves at other temperatures are also proportional to the Fatigue Technology test data. ABAQUS linearly interpolates between the stress-strain curves shown in Figure 6.8 for other temperature values. The coefficient of thermal expansion of the steel was determined to be  $11.3 \times 10^{-6}/^{\circ}\text{C}$  over the range from 22 to 204°C.

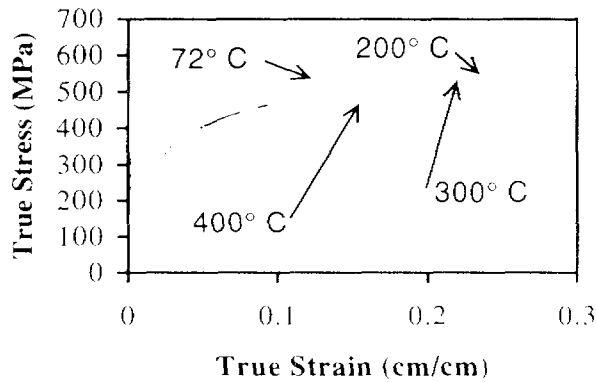


Figure 6.8 A516 Grade 70 temperature dependence.

## 6.4 Loads

Design pressure for the vessel is 0.386 MPa (56 psi). Quasi-static internal pressure was increased monotonically, with a thermal load simultaneously applied to all steel parts above the concrete basemat. The temperature of the containment shell followed a saturated steam pressure vs. temperature relationship (Fig. 5.8). An initial stress-free state was assumed to exist at 22°C. As the pressure was increased, the temperature at every node in the model that was above the concrete basemat was increased to correspond to the saturated steam relationship.

## 6.5 Analysis Results

Analyses were performed using the ABAQUS/Standard finite element code. As the internal pressure load in the containment was increased beyond the design pressure, the finite element analyses first predicted local pockets of plastic strains developing. Then, as the pressure continued to increase, the code predicted global plastic strains. As the steel shell plastically strained, it became thinner, and eventually the code failed to converge, indicating that a failure limit had been exceeded. This failure limit should be considered an upper bound on the solution, since local strain concentrations could cause a tear to initiate in the shell wall before this stability limit is reached.

Predicted results were examined after each analyses was completed to determine if local strain concentrations were large enough that a tear may have initiated. Elements in the model did not automatically fail when they reached the strain value where a tear could initiate. Instead, failure predictions were assessed during post processing. Failure was predicted when any element in the model reached the strain limits discussed in section 4. Although the analyses continued running until the code failed to converge, as discussed in the previous paragraph, experience has

shown that containment vessels will fail in stress concentration regions at strains well below the levels at which the code fails to converge. No attempt has been made to predict the structural response after a tear is predicted to initiate at the strain limits discussed in Chapter 4.

In some cases, if the high plastic stresses and strains are very local to the tear location, it is likely that the tear will arrest itself and the vessel will depressurize due to the tear in the wall. However, if the high stresses and strains cover a large enough area, then the tear is likely to propagate and result in total catastrophic failure.

For each analysis, failure predictions consisted of a "lower bound", "best estimate", and "upper bound" failure pressure. Several different locations were examined to determine where the likely failure locations were

Three locations were chosen where there was a high potential for corrosion, and each of these locations was analyzed with two different amounts of assumed corrosion. For each of the corrosion areas, 50% through-the-thickness corrosion degradation was selected, to cause the structure to fail in the corroded region at about the same pressure that would cause failure at the highest stress region of an uncorroded containment. The assumed degradation was then increased to 65% corrosion, and the analyses were repeated.

The largest strains in an uncorroded containment occurred in the suppression pool. The maximum calculated von Mises stress in the suppression pool was about 165 MPa (24 ksi), and was a result of bending at the ring stiffener location. The maximum calculated membrane stress was about 115 MPa (17 ksi).

Figure 6.9 shows the largest plastic membrane strains that would occur in the suppression pool if a section along the waterline was corroded to a depth of 50% or to a depth of 65%. For comparison, the strains that would be expected if no corrosion existed are also shown. As discussed in Chapter 5, *elastic* strains caused by thermal gradients could be significant for design, but at pressures above the design basis, the loads are carried by membrane action, and the *plastic* strains caused by thermal gradients become insignificant. At strain levels that were near the first yield strain, the surface strains (caused by bending) were slightly larger than the membrane strains. However, as the strains became plastic, the vessel carried the internal pressure almost entirely through membrane action, and the surface strains were nearly identical to the membrane strains. Therefore, only the membrane strains are shown for this location. Since

the design pressure is 0.386 MPa, Figure 6.9 shows that plastic strains won't occur in an uncorroded containment until about 2.5 times the design pressure. With 50% corrosion, plastic yielding begins shortly after design pressure, and at 65% corrosion, significant plastic yielding would occur before design pressure is reached.

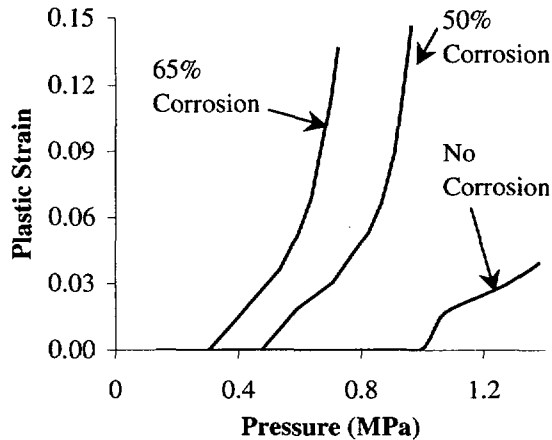


**Figure 6.9 Largest Equivalent Plastic Membrane Strains at Waterline in Suppression Pool.**

Figure 6.10 shows typical equivalent plastic surface strains that would occur in the knuckle region if it was corroded to a depth of 50% or to a depth of 65%. For comparison, the strains that would be expected if no corrosion existed are also shown. As in the suppression pool, surface stresses (i.e., bending stresses) were up to 50% larger than membrane stresses at pressures that caused the material to reach first yield. However, as the strains became plastic, the vessel carried the internal pressure almost entirely through membrane action, and the surface strains were within about 10% of the membrane strains. Therefore, only the membrane strains are shown for this location. As discussed in the previous paragraph, any thermal gradients would have minimal impact on plastic strains, although the effect on the elastic strains could be significant. For an uncorroded knuckle region, plastic yielding does not begin until the pressure reaches about 2.5 times design pressure. For the case where 65% corrosion is assumed in the knuckle region, significant plastic yielding begins at about design pressure. The peak calculated strains in a stress concentration region in the corroded region are about 50% larger than other strains that are in the corroded region, but outside the stress concentration region.

Figure 6.11 shows typical equivalent plastic surface strains at one high-stress point in the sand pocket region for cases with 50% and 65% corrosion. Note that Figures 6.9 and 6.10 showed membrane strains, while Figure 6.11 shows surface (bending) strains. The

surface strains shown in Figure 6.11 are the largest calculated values for portions of the analysis, but other nearby elements have slightly larger strains over the remaining portions of the analysis. The high bending stresses in the sand pocket region are almost entirely due to the fixed boundary condition at the base, as well as thermal expansion of the steel. Bending stresses generally don't cause failure unless the surface strains are considerably higher than the membrane strain failure limit. This is because the shell walls bend and deform until the structure reaches a shape where the loads are resisted almost entirely by membrane action. Considerable plastic strains occur on the surface before plastic membrane yielding begins. However, these surface strains are well below the limits where a tear would be expected to initiate, and no failure is expected before general membrane yielding and large plastic strains begin to accumulate.

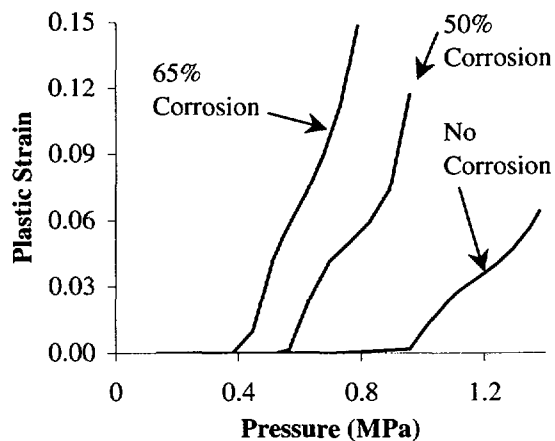


**Figure 6.10 Typical Equivalent Plastic Membrane Strains in Knuckle Region.**

Because the shell wall is embedded in the concrete below the sand pocket, radial displacements of the shell wall are small, and membrane strains in the circumferential direction are also small. For this location, large surface strains are caused by bending. For the case with 50% corrosion in the sand pocket region, the inner surface strain, membrane (mid-surface) strain, and outer surface strain for a highly stressed element are shown in Figure 6.12. As previously explained, the calculated strains for the element shown in Figure 6.12 are the largest over much of the pressure range, but other nearby elements have larger strains over some of the pressure range. As can be seen in the figure, plastic straining is occurring before the pressure even reaches the design level.

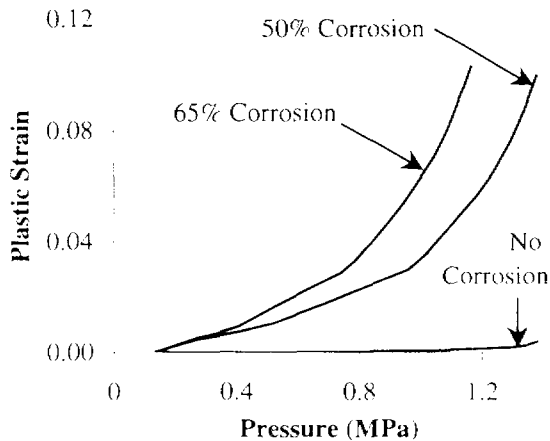


**Figure 6.11 Typical Equivalent Plastic Surface (Bending) Strains in Sand Pocket Region.**

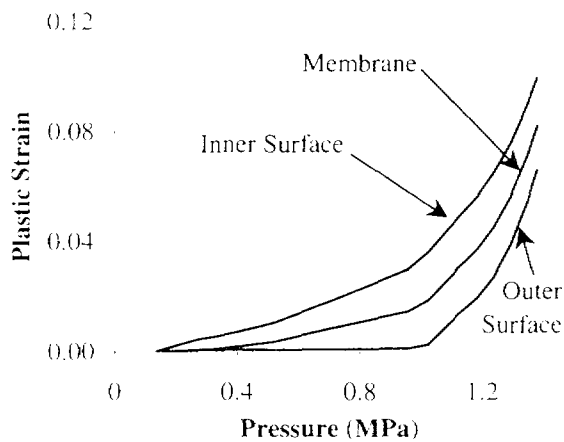


**Figure 6.12 Typical Equivalent Plastic Strains in Sand Pocket Region that has 50% corrosion.**

Bending strains in the basemat region can be quite large if corrosion reduces the thickness around a significant portion of the circumference, and over a small height. This is the situation that was analyzed in the basemat region. High local bending does occur as the cylindrical wall transitions from its anchorage boundary condition to the free field condition, where loads are resisted primarily through membrane action. The bending stresses in the basemat region are limited, however, because when radial displacements become large enough, any additional pressure load will be resisted through membrane action. As can be seen in Figure 6.12, the bending strains are significantly higher than the membrane strains. As discussed in Chapter 4, the surface "failure" strain limit was 1.5 times larger than the membrane "failure" strain limit. However, because the bending strains in the basemat region are limited, a minimum surface "failure" limit of 5% strain

was selected. No failure was deemed to occur unless the surface plastic strains exceeded 5%.

Predicted failure results (Table 6.1) show that corrosion in some areas will cause more of a reduction in capacity than corrosion in other areas would have caused. Because of the assumption that venting would occur at pressure levels of 0.69 MPa (100 psi), and calculations that show significant plastic yielding does not occur until about 2 to 2.5 times the design pressure, large amounts of corrosion were assumed in order to lower the calculated pressure capacity. The design pressure for the containment modeled was 0.386 MPa (56 psi).

The structural response of the region that was assumed to be corroded in the suppression pool (Table 6.1) was primarily membrane. For these analyses the peak surface strains were nearly identical to the peak membrane strains. For the drywell model that had assumed corrosion in the knuckle region, bending was more significant at stress levels near the elastic limit. At larger strain levels, in the range where failure would be expected, the surface strains were only about 10% larger than membrane values. Although significant bending occurred in the sand pocket region in the last two cases, failure was still predicted to result from the membrane deformations and not from the surface strain limits. At strain levels large enough to cause failure, the surface strains were a bit less than 50% bigger than the membrane strain values.

Membrane forces in the suppression pool were twice as large in the circumferential direction as they were along the length of the torus. For the suppression pool, internal pressure caused the structure to radially expand until failure occurred in the circumferential direction. Even while the structure was plastically flowing in the hoop direction, there was minimal plastic growth along the length of the torus.

Von mises stresses for the suppression pool, with 50% corrosion, are shown in Fig 6.13. The effective plastic strains (Fig 6.14) show that only the corroded region experienced large plastic membrane strains. For the suppression pool, with 50% corrosion, failure would be expected to occur at the high stress and strain location in the thinned area. The stresses and strains calculated for the drywell with 50% corrosion in the knuckle region are shown in Figures 6.15 and 6.16. As can be seen, the largest plastic strains all occur in the corroded region. Figures 6.17 and 6.18 show the stresses and strains in the finely meshed section of the drywell in the knuckle region. As can be seen from these figures, a stress and strain concentration region occurs in the corroded region, with the peak strains in the concentration region about 25 to 50% larger than the surrounding strains in the corroded region.

Figures 6.19 and 6.20 show local strains in the corroded region of the sand pocket for a case with 50% corrosion. As before, a strain concentration occurs in a corner, with the concentration about 25 to 50% larger than the remaining strains in the corroded region.

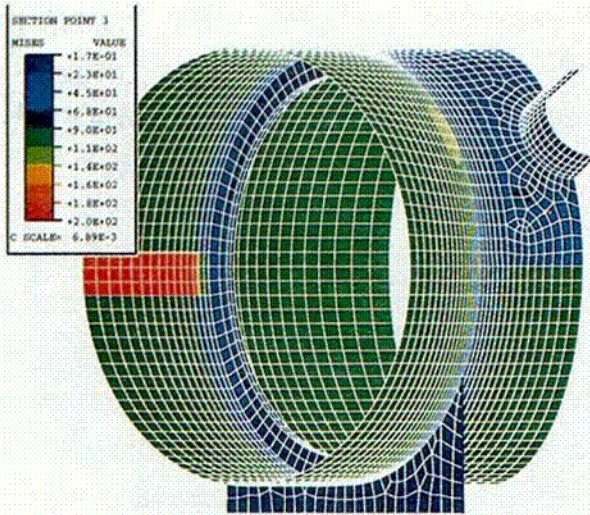
The criteria used in this report to predict potential containment failure differ significantly from criteria that would be acceptable for design. Containment structures are conservatively designed so that the probability of failure is very, very small under design loads. The design criteria are selected so that the vessel remains elastic, with a comfortable safety factor, under all design loads. However, when predicting failure, previous tests on scaled models have demonstrated that large plastic strains occur before the pressure boundary fails. The criteria used to predict

failure are suitable for use in risk studies, but are clearly unacceptable for design. For example, in design, strains are typically limited to about 2/3 of the elastic limit. However, when predicting failure, strains that were 7 to 50 times larger than the elastic limit were selected. Some of the badly corroded containments that have been analyzed in this report had plastic strains below limits where failure would be anticipated, but strains that were well above the elastic limit at design loads. Although the probability of failure under design loads is low for some of the corroded containments that were analyzed, the level of conservatism necessary to ensure safety was lacking. To ensure a conservative design, it is necessary to keep stresses and strains in corrosion areas from exceeding ASME code allowable limits.

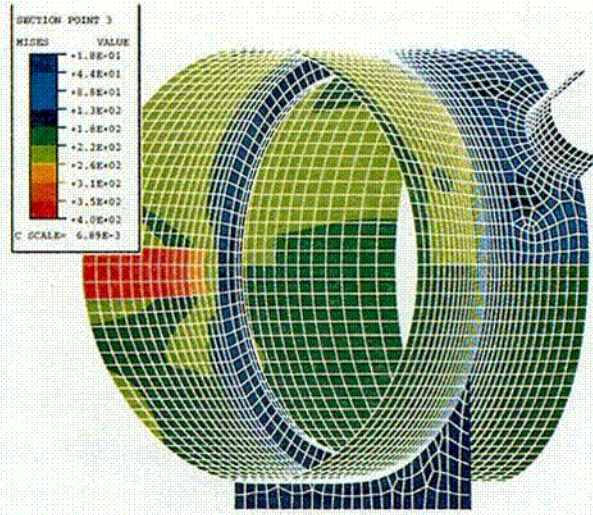
**Table 6.1. Predicted Failure Pressures**

Case No.	Description	Failure Limit					
		Lower bound		Best estimate		Upper bound	
		Pressure	Membrane Strain	Pressure	Membrane Strain	Pressure	Membrane Strain
1	no corrosion	1.34 MPa * (195 psi)	0.056	> 1.38 MPa * (> 200 psi)		> 1.38 MPa * (> 200 psi)	
2	50% corrosion at waterline in suppression pool	0.510 (74)	0.014	0.786 * (114)	0.046	0.924 * (134)	0.101
3	65% corrosion at waterline in suppression pool	0.331 (48)	0.014	0.545 (79)	0.046	0.683 (99)	0.101
4	50% corrosion at knuckle in drywell	0.600 (87)	0.014	0.731 * (106)	0.046	0.931 * (135)	0.101
5	65% corrosion at knuckle in drywell	0.455 (66)	0.014	0.531 (77)	0.048	0.696 * (101)	0.098
6	50% corrosion at sand pocket in drywell	0.876 * (127)	0.014	1.17 * (170)	0.044	1.36 * (197)	0.096
7	65% corrosion at sand pocket in drywell	0.676 (98)	0.014	0.855 * (124)	0.044	1.09 * (158)	0.096

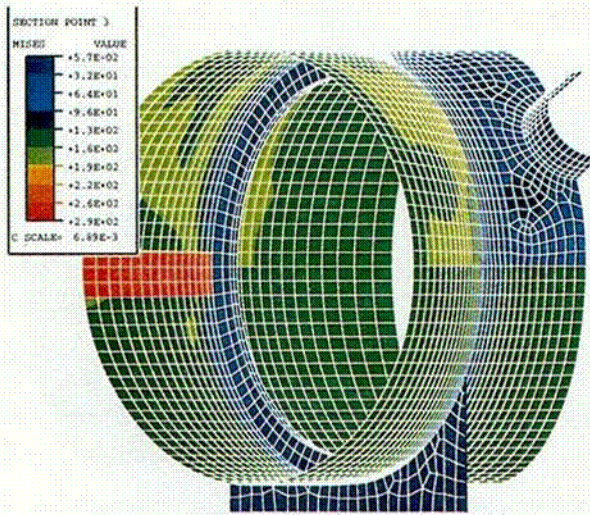
\* Failure is not predicted to occur at the corroded location. Venting is expected to occur at 0.69 MPa (100 psi) before the structural failure would occur.



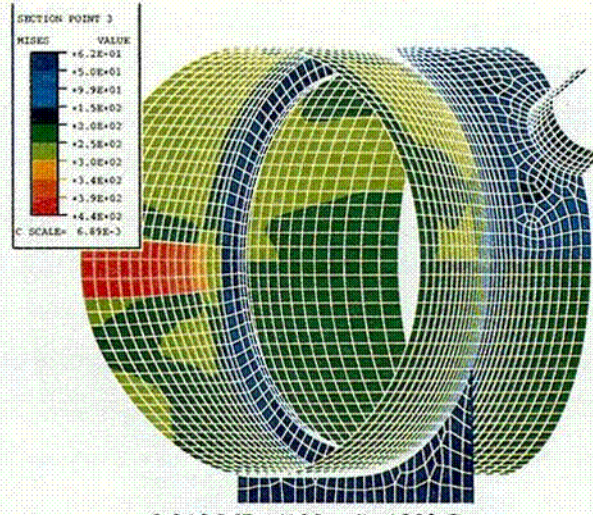
0.396 MPa (57 psi), 151° C



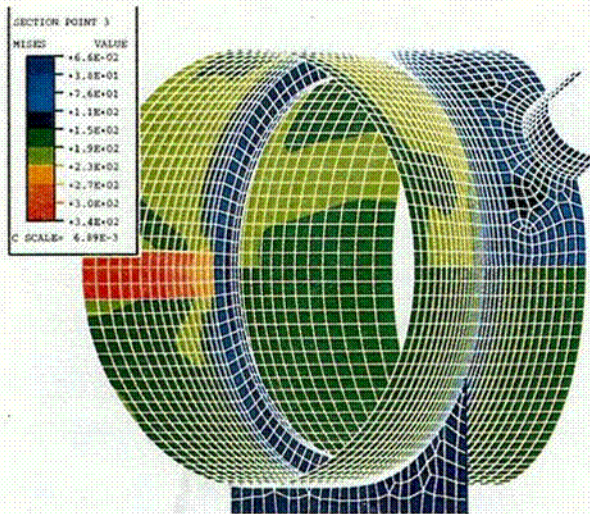
0.823 MPa (119 psi), 177° C



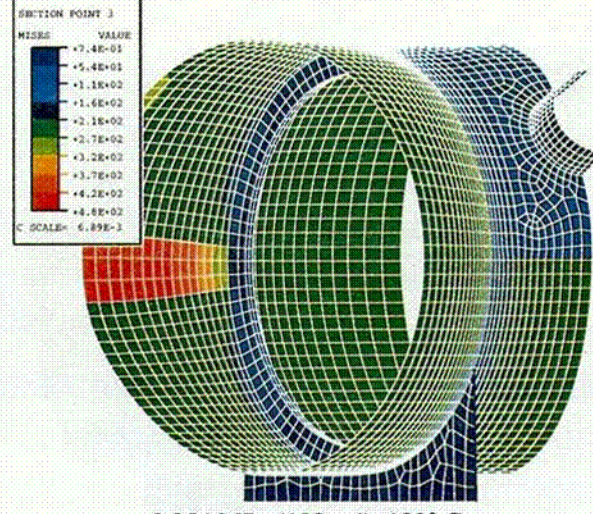
0.590 MPa (86psi), 164° C



0.910 MPa (132 psi), 180° C

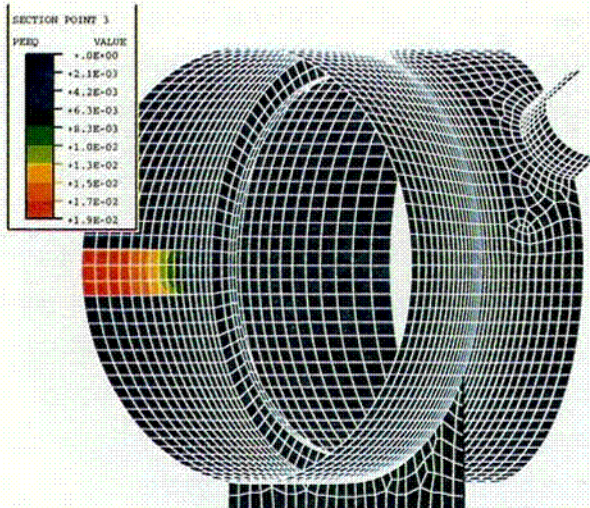


0.706 MPa (102 psi), 171° C

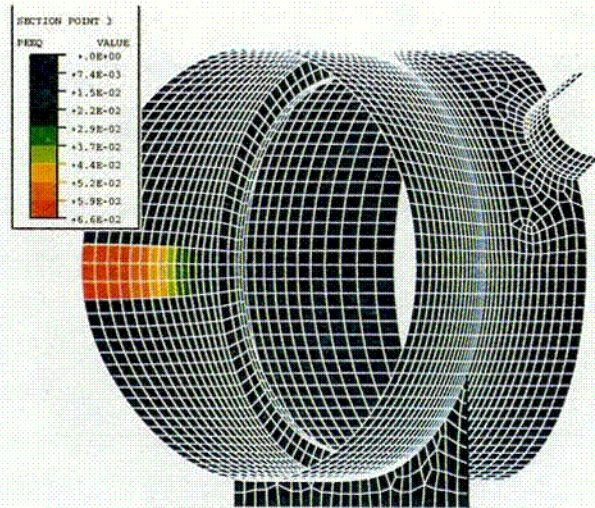


0.954 MPa (138 psi), 182° C

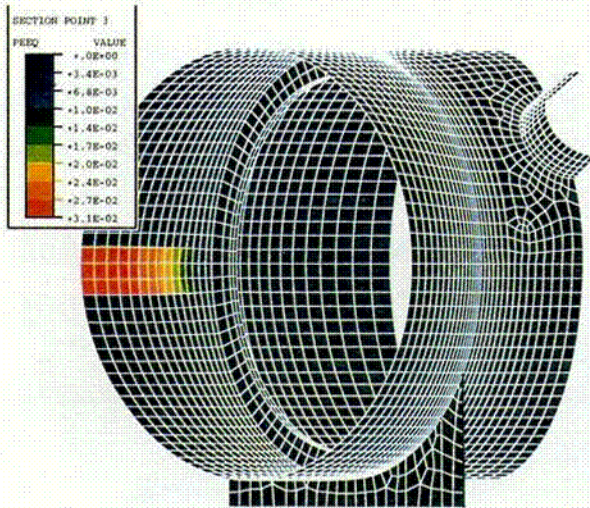
Figure 6.13 Von mises membrane stress (MPa) in suppression pool model with 50% corrosion, displacements magnified by a factor of 5.



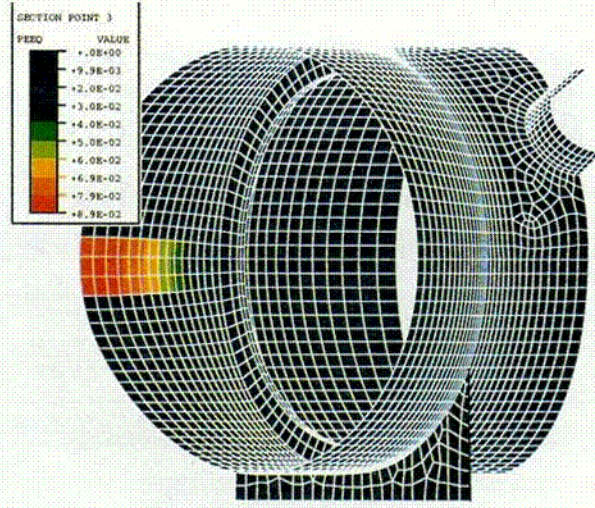
0.590 MPa (86psi), 164° C



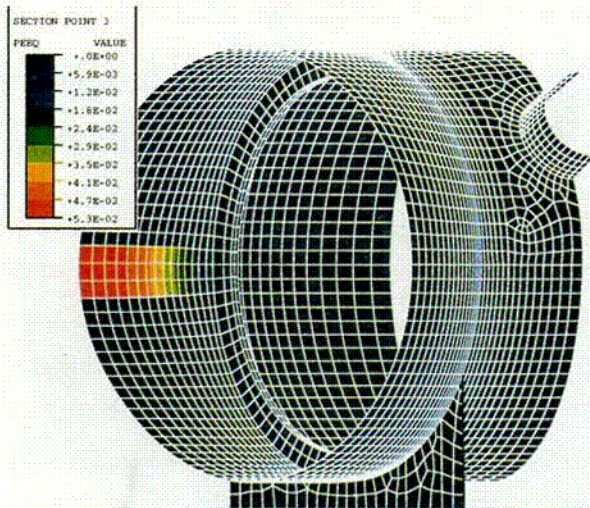
0.867 MPa (126 psi), 178° C



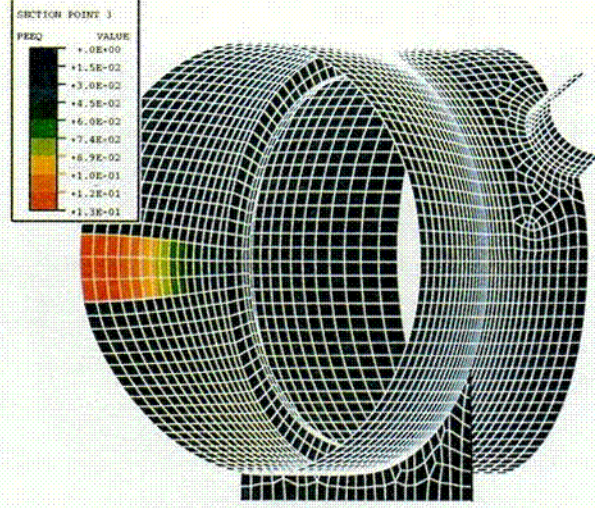
0.706 MPa (102 psi), 171° C



0.910 MPa (132 psi), 180° C

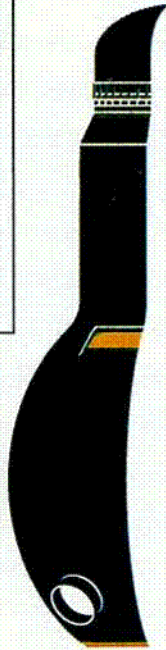
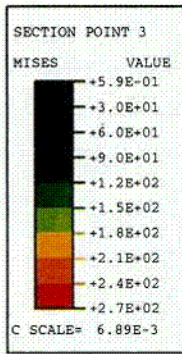


0.823 MPa (119 psi), 177° C

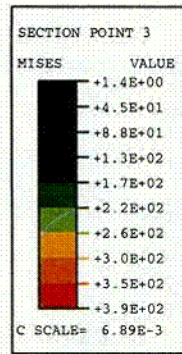


0.954 MPa (138 psi), 182° C

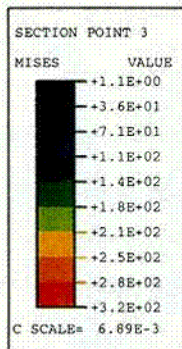
Figure 6.14 Equivalent plastic membrane strain in suppression pool model with 50% corrosion, displacements magnified by a factor of 5.



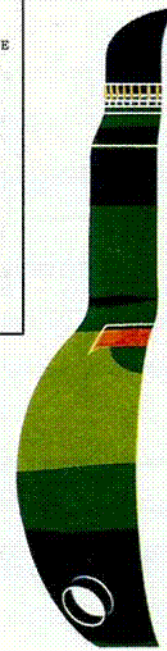
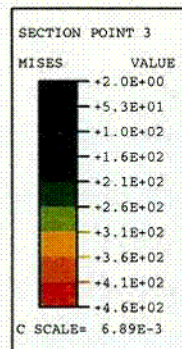
0.405 MPa (59 psi), 152° C



0.761 MPa (110 psi), 173° C

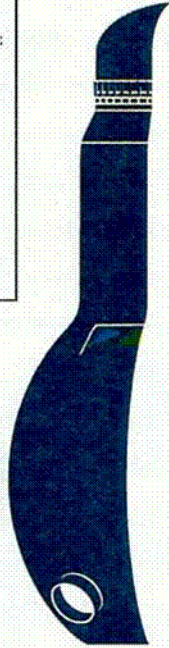
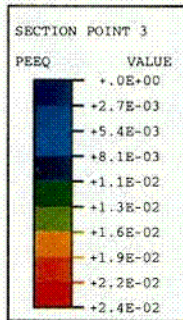


0.630 MPa (91 psi), 157° C

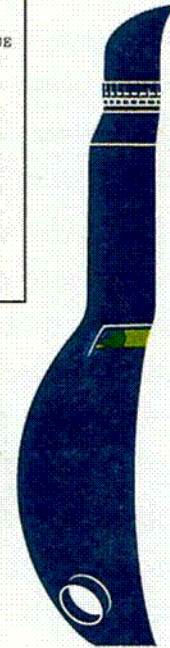
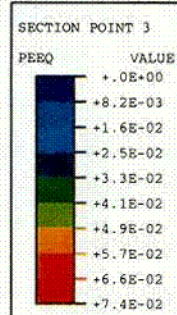


0.958 MPa (139 psi), 182° C

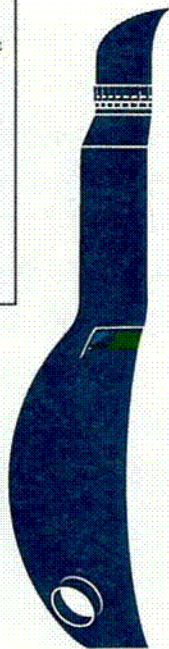
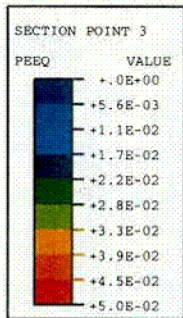
Figure 6.15 Von mises membrane stress (MPa) in drywell with 50% corrosion in knuckle region, displacements magnified by a factor of 5.



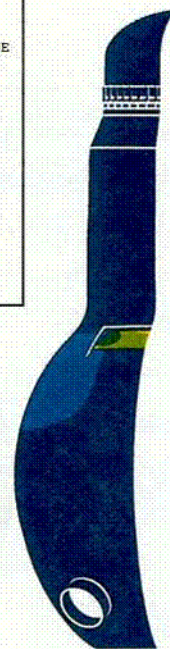
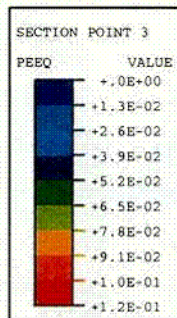
0.630 MPa (91 psi), 157° C



0.892 MPa (129 psi), 179° C

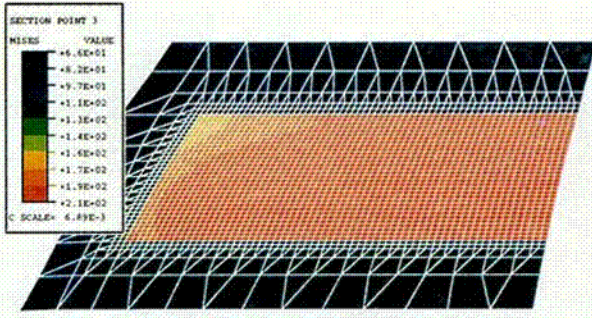


0.761 MPa (110 psi), 173° C

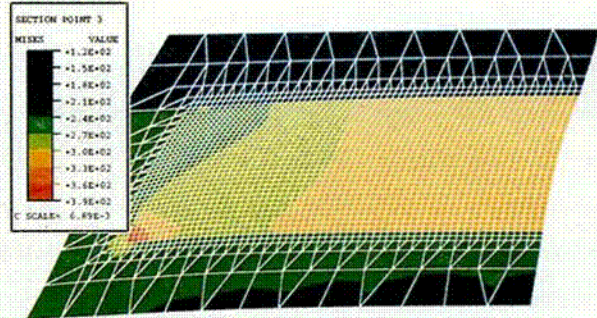


0.958 MPa (139 psi), 182° C

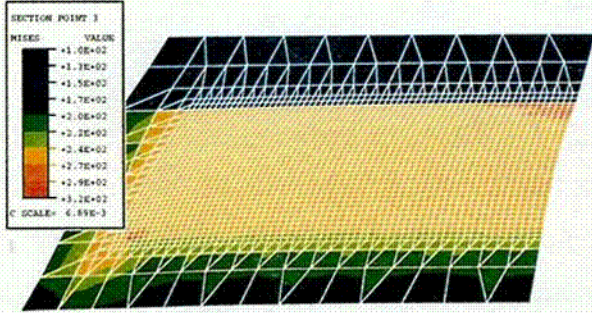
Figure 6.16 Equivalent plastic membrane strain (MPa) in drywell with 50% corrosion in knuckle region, displacements magnified by a factor of 5.



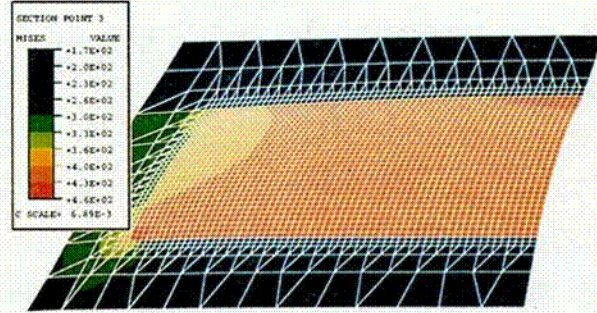
0.405 MPa (59 psi), 152° C



0.761 MPa (110 psi), 173° C

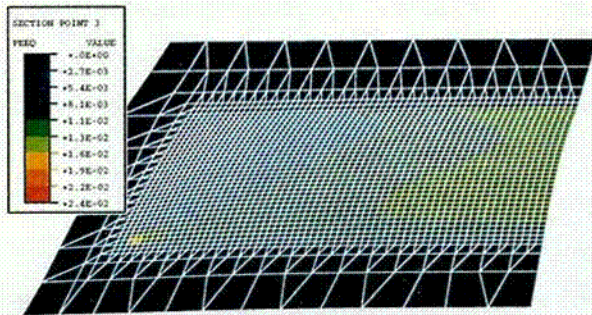


0.630 MPa (91 psi), 157° C

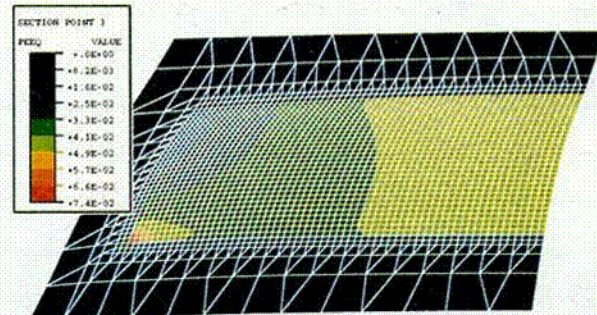


0.958 MPa (139 psi), 182° C

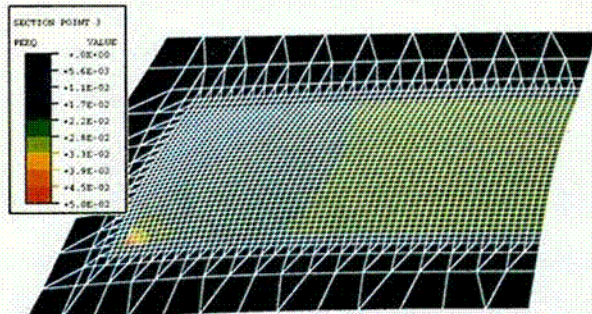
Figure 6.17 Von mises membrane stress (MPa) in knuckle region with 50% corrosion, displacements magnified by a factor of 5.



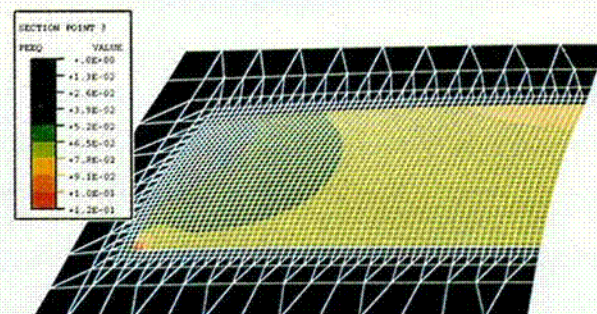
0.630 MPa (91 psi), 157° C



0.892 MPa (129 psi), 179° C

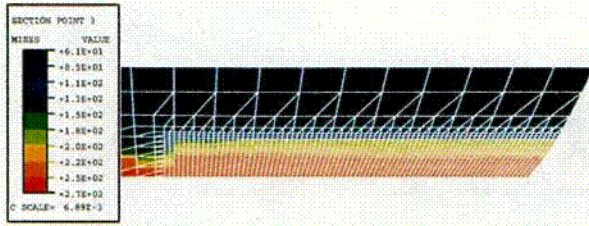


0.761 MPa (110 psi), 173° C

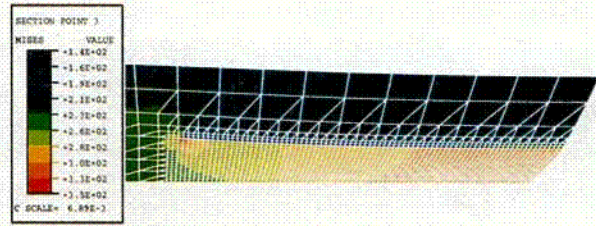


0.958 MPa (139 psi), 182° C

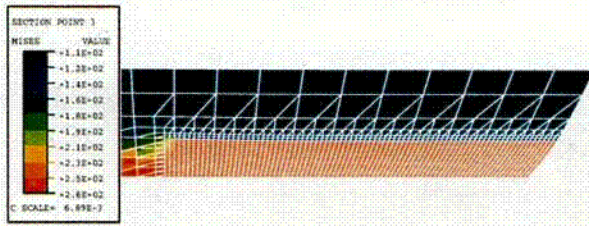
Figure 6.18 Equivalent plastic membrane strain (MPa) in knuckle region with 50% corrosion, displacements magnified by a factor of 5.



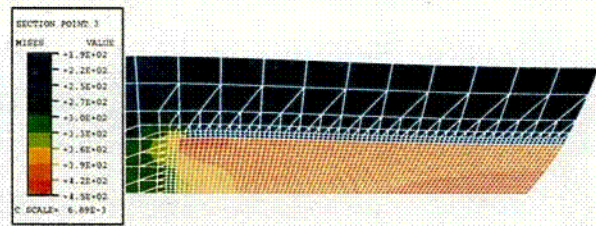
0.405 MPa (59 psi), 152° C



1.10 MPa (160 psi), 188° C

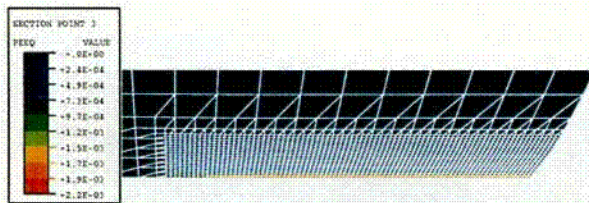


0.696 MPa (101 psi), 170° C

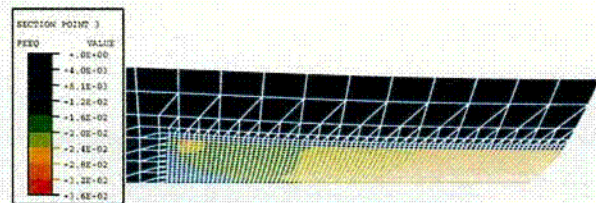


1.38 MPa (200 psi), 197° C

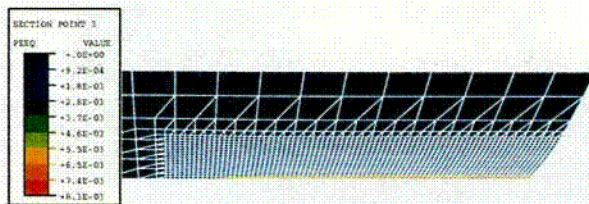
**Figure 6.19 Von mises membrane stress (MPa) in sand pocket region with 50% corrosion, displacements magnified by a factor of 5.**



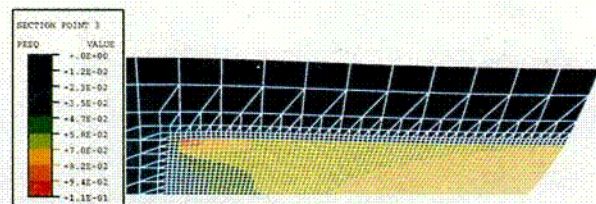
0.405 MPa (59 psi), 152° C



1.10 MPa (160 psi), 188° C



0.696 MPa (101 psi), 170° C



1.38 MPa (200 psi), 197° C

**Figure 6.20 Equivalent plastic membrane strain in sand pocket region with 50% corrosion, displacements magnified by a factor of 5.**

## 7 ANALYSES OF TYPICAL REINFORCED CONCRETE CONTAINMENT

Concrete containments have a host of potential degradation sites. The concrete can degrade, and the reinforcing bars and the liner can corrode. The following study examines a typical concrete containment with liner degradation during a loss of coolant accident (LOCA). Although concrete and reinforcing bar degradation could be a potentially serious condition, degradation at these locations were beyond the scope of this analysis.

A typical pressurized water reactor (PWR) reinforced concrete containment with a liner that is attached to the concrete with studs was examined with postulated liner corrosion degradation at three locations. The containment modeled is similar to the Surry containment. The dimensions, liner thickness, reinforcing bars spacing and size, and stud spacing were all taken from structural drawings of the containment at the Surry nuclear power station. However, the locations selected for the degradation are not locations of degradation of the liner in the containment at the Surry nuclear power station.

The degradation was located at the region of highest stress, where corrosion damage had been observed in existing containments, and in regions that are considered likely to experience corrosion. Specifically, the locations were at the basemat on the cylinder wall, at approximately midheight on the cylinder wall (location of highest liner stress), and near the equipment hatch. Finite element analysis (FEA) was used to examine the containment under accident conditions. Failure was predicted using a strain-based failure criterion. The effect of liner degradation was examined by varying the degree of corrosion at the selected locations and comparing the failure level with the uncorroded case.

To examine liner failure in the containment, sufficient detail must exist in the FEA model to detect strain concentrations at potential failure locations. However, due to the size and complexity of a containment building, a three dimensional model including sufficient detail of all penetrations and detail of the connections between the concrete and the liner for the whole containment building is unrealistic. In this study an axisymmetric model of the containment was analyzed to model the global behavior of the containment building. No penetrations were included in the axisymmetric model and the liner was continuously attached to the concrete at the nodes that were common between the concrete and the liner. The liner elements were sized to approximate the spacing of the studs that attach the liner to the concrete.

Results from the axisymmetric model were used to apply the loading to the more detailed sub-models of the areas of interest. A sub-model that models the concrete, reinforcing bars, and each stud explicitly requires a great number of degrees of freedom, is complex to construct, and the interaction of the studs with the concrete is difficult to model accurately. The liner is the primary area of interest in this study. Therefore, a FEA model that is refined enough to pick up strain concentrations in the liner was imperative. Since the region of the equipment hatch was considered a location of potential liner degradation a sub-model of this region was constructed. A three-dimensional sub-model including the concrete, reinforcing bars, and liner was developed. The studs were not included in the model. From this model, two-dimensional sub-models of only the liner were developed using spring elements to model the interaction of the liner and studs. Similarly, two-dimensional sub-models of the liner at the cylinder wall and basemat juncture and the liner at the midheight of the sidewall were constructed. The studs were modeled with spring elements in these models as well.

Containment vessels are designed to withstand many different loads, such as seismic or internal pressure. Although code requirements stipulate combinations of loads that a containment must be designed to resist, only internal pressure and loads caused by thermal expansion or contraction have been analyzed in this study. The analytical results discussed in this section have not been evaluated during seismic or other load conditions. When evaluating the effect of corrosion damage on an actual containment, it is important to remember that all code required load combinations must be evaluated to ensure that other loads won't cause failure before the vessel fails due to internal pressure.

### 7.1 Material Properties

The liner material properties used were for A516 Grade 60 steel. The true stress-strain curves are shown in Figure 7.1. These curves were developed by using a mean value of engineering yield and ultimate stress from test data obtained from the containment liner at the Sequoyah nuclear power station and developing curves proportional to the curves for A516 Grade 70 steel tested at 22, 93, 149 and 204 °C (Fatigue Technology, 1988). Engineering stress and strain values were converted to true stress and true strain, which are required by ABAQUS to define plastic material properties. The coefficient of thermal expansion used was  $11.3 \times 10^{-6}/^{\circ}\text{C}$ .

Material properties used for concrete were  $f'_c$  of 27.6 MPa (4000 psi), modulus of elasticity  $24.8 \times 10^9$  GPa ( $3.6 \times 10^6$  ksi), Poisson's ratio of 0.18, and a tensile cracking strain of the concrete was given a value of 0.0001. Reinforcing bar material was taken as grade 40 steel for number 11's and smaller, and grade 50 steel for number 14 and 18 bars. Typical curves for the reinforcing bars were developed from the stress strain curves for A615 grade 60 shown by Gamble (1973).

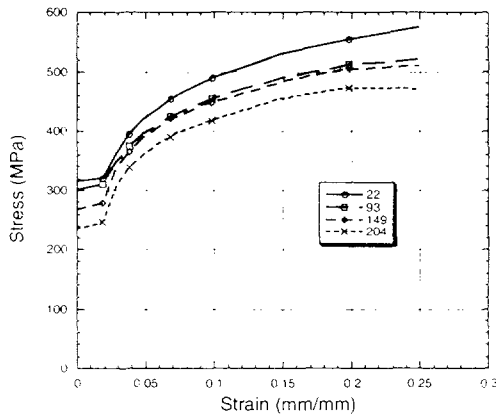


Figure 7.1. A516 Grade 60 true stress versus true strain.

## 7.2 Corrosion/Degradation

Degradation mechanisms were examined in Chapter 2 and it was determined that for low-carbon, low-strength steels used in containment structures, corrosion degradation can be simulated by using a loss of section. The corroded material does not have any strength and therefore the reduction of strength is due to the loss of section. In Chapter 2 it was also shown that there is a reduction in ductility caused by stress and strain concentration regions at discontinuities such as pits or rough surfaces. Bruneau and Zahrai (1997) found for a structural steel that the expected loss of strength for corroded specimens was directly proportional to the reduction of area and that the maximum elongation for tensile specimens was less than that for the uncorroded specimens. Therefore in this study, corrosion was modeled by investigating the effect of loss of section.

The locations chosen in this study for the degraded liner were at the junction of the basemat and cylinder wall (at the floorline of the containment), at approximately midheight of the cylinder wall (this is a region of high stress), and near the equipment hatch

opening. The floor to wall junction was chosen because corrosion damage has been observed in this location for steel containments, and it was considered to have a high likelihood for corrosion. The region at mid height of the cylinder wall was chosen because it is a region of high stress. The equipment hatch location was chosen as a likely area for corrosion and possible stress concentration at the opening.

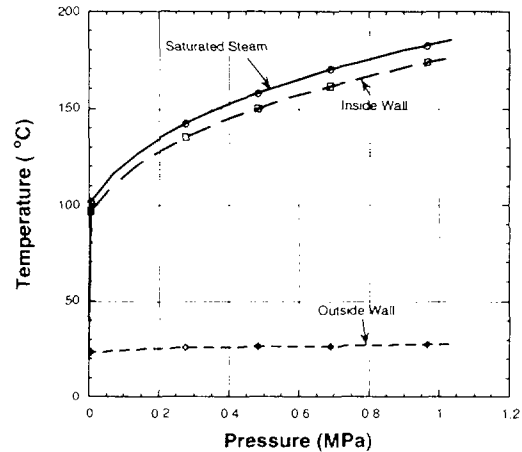


Figure 7.2. Temperature-pressure relationship.

## 7.3 Loading

The FEA models were loaded with a quasi-static internal pressure that increased monotonically. During many postulated accidents, the pressure is caused by water turning into steam. Therefore, a thermal load was applied to the models along with the pressure loading. A steady state thermal analysis was performed on the containment wall to determine the temperature distribution through its thickness. The temperature was applied in a linear distribution between the inside and outside surfaces (see Figure 7.2). The initial stress-free state was assumed to exist at 22 °C.

Although many possible accident scenarios exist and are important at near design pressures, for the calculation of ultimate containment capacity the thermal loads are not nearly as important. The effects of thermal loads on the liner strains are dissipated as the concrete cracks and reinforcing bars yield.

## 7.4 Failure Criteria

A strain-based failure criterion was selected for this study. Therefore, the failure is predicted to occur when the calculated strains exceed a critical value. Researchers such as Hancock and Mackenzie (1976), Mackenzie et al. (1977), and Mangoine (1982) have shown that the critical failure strain varies as the stress states change and that this strain can be related to the

stress states. The failure criteria discussed in Chapter 4 are used, except for some changes in the values of the knockdown factors. The knockdown factors adjust uniaxial failure strain data to a failure value. There are four knockdown factors that are applied. Three of these factors, which are not related to corrosion, are consistent with a previous study by Miller (1990). The fourth factor has been added to account for the corrosion degradation.

The relationship for the first knockdown factor, to account for the multiaxial stress state, is from Hancock and Mackenzie (1976). The factor is determined from the analyses and relates the triaxial state of stress to the failure strain. For the concrete containment discussed in this chapter, the approach taken by Miller (1990) and discussed in Chapter 4 has been applied. Lower bound, best estimate, and upper bound values were chosen for the remaining factors ( $f_2$ ,  $f_3$ , and  $f_4$ ).

The second factor accounts for how much detail is incorporated in the finite element model. For example, the element size in the mesh and missing structural details in the model affect the accuracy of the finite element prediction. This factor approaches 1.0 as the mesh size becomes small and includes all the structural details. The value chosen in this study was determined by reviewing the detail included in the finite element model in the critical failure region, and analytical results such as the strain gradient in the critical region. The details of the FEA will be discussed in a later section; however, since a detailed submodel of the containment liner was used, the  $f_2$  value chosen for these submodels was 0.9 for the lowest bound, best estimate, and upper bound values of the factor. Since the axisymmetric model did not include much detail (especially in the liner) a knockdown factor of 0.2 was chosen.

The third factor accounts for the fact that in an actual structure the material properties often vary from the mean by a significant margin. Since the liner material is the same as that used in Chapter 4, the same values for the  $f_3$  factor were used. These values were chosen from the variation in the material properties found for tensile tests of the liner material. It was found that the elongations for the material varied from the mean by 22 %.

Similarly, the same values chosen for the  $f_4$  factor in the analyses in Chapter 4 were used in this study. From tensile tests on corroded coupons it was found that the elongation of the specimens was reduced by approximately 50 percent. Therefore, the best estimate value for the  $f_4$  factor was chosen as 0.5. The values of the lowest and upper bound values are based on engineering judgment.

**Table 7.1. Knockdown Factors Used in Failure Criteria**

	Factor	Lower Bound	Best Estimate	Upper Bound
Analysis sophistication (axisymmetric)	$f_2$	0.2	0.2	0.2
Analysis sophistication (submodels)	$f_2$	0.9	0.9	0.9
Material properties	$f_3$	0.78	1.0	1.22
Corrosion	$f_4$	0.25	0.5	0.75

Table 7.1 shows the values chosen for the knockdown factors. It should be emphasized that these values are based on engineering judgment and therefore most likely would vary according to the analyst. The intent is that the analyst consider each of these areas and determines an overall failure limit that is reasonable. The best estimate failure strains that result from these factors are close to observed failure strains found during scaled model tests. The ASME code (ASME 1992) gives a minimum uniaxial failure strain for elongation in a 20.3 cm (8 in.) gage length as 21 percent for ASTM A516 Grade 60 steel. Therefore, a value of 0.21 was used for  $\epsilon_{uniaxial}$ .

## 7.5 FEA Models

A schematic of the typical reinforced concrete containment analyzed in this study is shown in Figure 7.3. The containment has an inside diameter of 38.4 m (126 ft) and inside height of 56.4 m (185.0 ft). The wall thickness in the cylinder is 1.37 m (4.5 ft) and in the dome 0.76 m (2.5 ft). The concrete basemat thickness is 3.1 m (10.0 ft). The steel liner is 6.35 cm (0.25 in) thick on the floor, 9.5 cm (0.375 in) thick in the wall, and 12.7 cm (0.5 in) thick in the dome. The studs which attach the liner to the concrete wall are 15.9 cm (0.625 in) diameter. The equipment hatch modeled has an inside radius of 2.21 m (7.25 ft) and is centered at a height of 7.42 m (24.33 ft) above the basemat. Typical wall reinforcing is shown in Figure 7.4.

The ABAQUS (Hibbit, Karlsson & Sorenson, 1997) finite element code was used in the analysis. ABAQUS is a general purpose finite element code that provides the option to use external material models. In this study the behavior of the concrete material was modeled using ANACAP\_U (ANATECH Corp, 1997). This material model uses the smeared crack approach (Rashid, 1968) to model the cracking concrete.

### 7.5.1 Axisymmetric

Initially a global axisymmetric model was analyzed and the results from this model were used to develop more detailed submodels of the areas where the degradation was located. The axisymmetric model consisted of 3598 nodes with 1312 elements (see Figure 7.6). Second order elements were used to model the liner (SAX2 in ABAQUS) and concrete (CAX8R in ABAQUS). The concrete elements used reduced integration. The basemat had spring elements (SPRING2 in ABAQUS) to model the soil under the basemat. The nonlinear spring modeled the soil pressure under the basemat but allowed unrestrained uplift of the basemat in areas where the pressure was zero. The dead load of the interior contents of the containment building was estimated and applied.

### 7.5.2 3-Dimensional Submodel

Since the equipment hatch was not included in the axisymmetric model a 3-dimensional (3D) submodel of the equipment hatch was developed. The model contains 4177 nodes and 3810 elements (see Figure 7.7). The liner elements are 4-node reduced integration quadrilaterals (S4R in ABAQUS) and the concrete elements are 8-node bricks (C3D8 in ABAQUS). Half of the hatch was modeled to take advantage of the vertical symmetry. Nodal displacements from this model were applied to the 2-dimensional (2D) submodels of the liner in the region of the hatch.

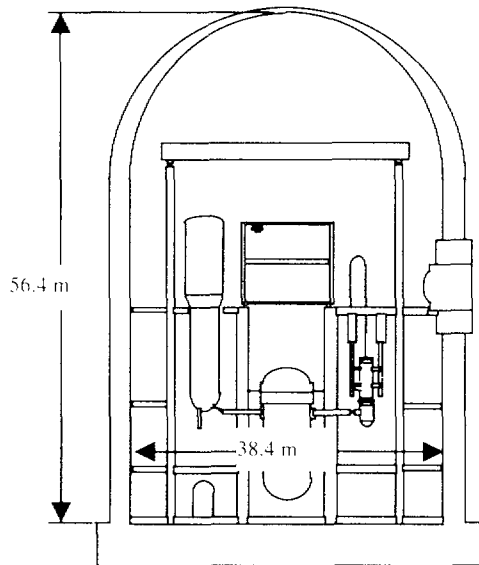


Figure 7.3. Schematic of typical reinforced concrete containment.

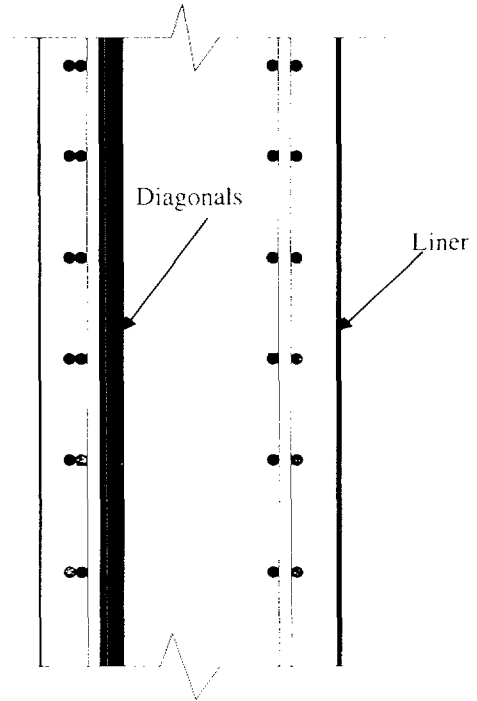


Figure 7.4. Typical reinforcing layout.

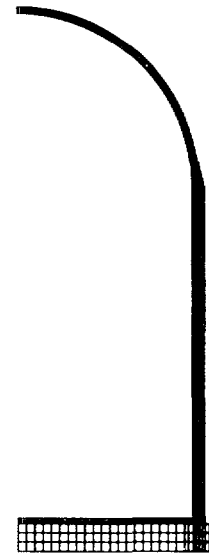


Figure 7.5. Axisymmetric finite element mesh.

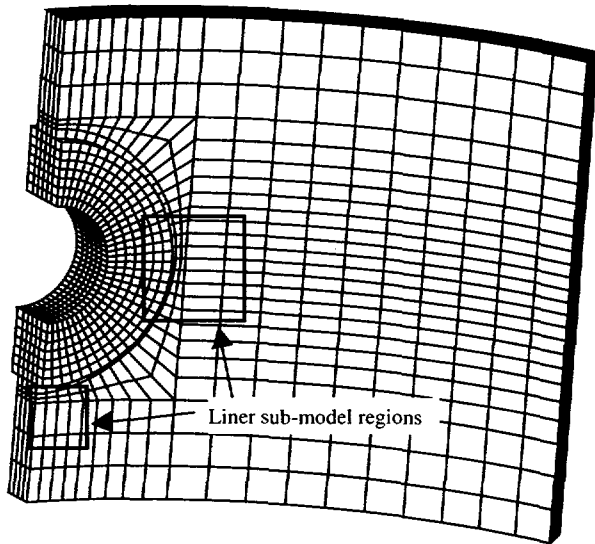


Figure 7.6. 3D hatch finite element model.

### 7.5.3 2-Dimensional Submodels

The actual degradation of the liner was modeled using 2D submodels of only the liner. The concrete was not modeled, but the displacements of the studs were applied consistent with the global axisymmetric model or the 3D hatch submodel. 2D quadrilateral elements were used to model the liner and spring elements were used to model the studs. The idealized load-slip relationship for a stud loaded in shear was obtained from a study by Doyle and Chu (1971) and is shown in Figure 7.7. These analyses were similar to those conducted by Weatherby (1990). A parametric study was conducted by Weatherby comparing the equivalent plastic strain near the edge of the studs for 2D analyses using 4-node bilinear quadrilateral elements (CPS4 in ABAQUS) and discrete spring elements (SPRINGA in ABAQUS) with detailed 3D models of the liner and stud. The element sizes in the 2D liner analyses were varied. It was found that when the 2D liner element size was equivalent to the radius of the stud (using square elements) the liner equivalent plastic strain near the edge of the stud gave nearly the same results as the detailed 3D FEA.

The curvature of the liner was neglected since only a small portion was modeled. Friction and bonding between the concrete and the liner were also neglected. In addition to the displacements applied to the end of the springs, displacements were applied to the edges of the liner. Vertical displacements were applied to the top and bottom edges and horizontal displacements were applied to the side edge that was not the line of symmetry.

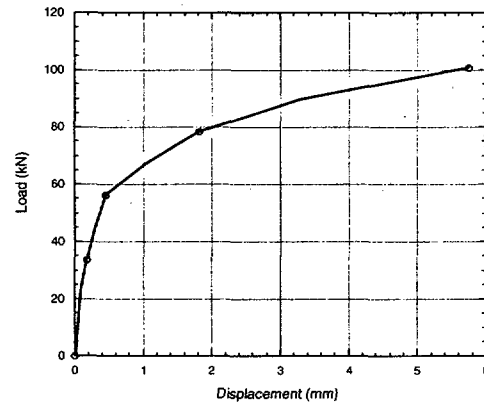


Figure 7.7. Load displacement relationship for studs.

Four of these 2D submodels were analyzed: one model near the basemat, one at midheight of the containment, and two near the equipment hatch opening (one at the bottom of the hatch and one at the side, as shown in Figure 7.6). The area of corrosion was chosen as typical of what could be found in an actual containment. Figure 7.8 shows the 2D model of the liner at the mid-height location. The area of degradation modeled is 1.0 m (3.2 ft) by 0.1 m (3.8 in). The base mat liner region model is shown in Figure 7.9. The area of degradation for this model is 1.8 m (6.0 ft) wide by 0.16 m (6.32 in) tall. This case would be similar to a continuous ring of corrosion around the containment. Various regions of degradation were chosen for the two sub-models of the hatch region. However, as will be discussed in the next section, none were found to control the failure pressures of the containment.

The corrosion was placed so a stud was at or near the edge of the corroded section (a variety of corrosion dimensions and locations relative to the studs were examined and the cases shown in Figures 7.8 and 7.9 were the ones that resulted in the highest strains). No corrosion was accounted for in the studs. Any corrosion damage that weakened the shear resistance of the stud would reduce the stresses in the liner around the degraded stud. Therefore, the assumption of no degradation of the stud is a "worst case" analysis. Further discussion of stud location and corrosion area will be given later.

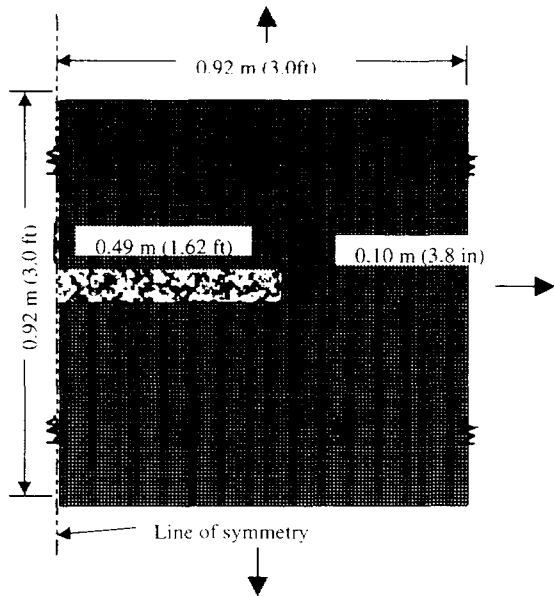


Figure 7.8. Liner mid-height 2D sub-model.

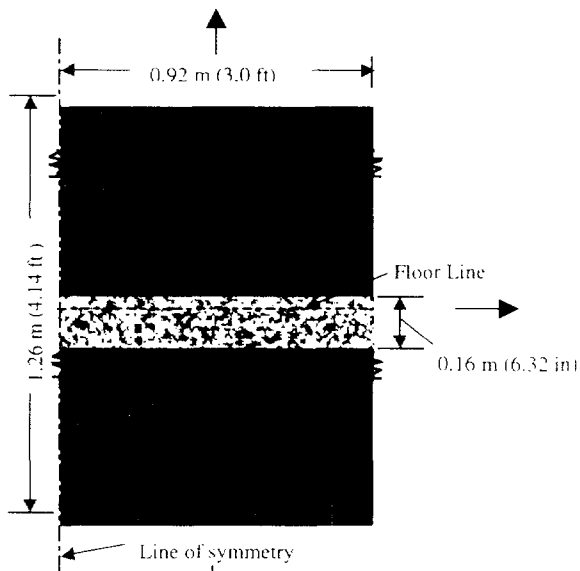


Figure 7.9. Liner base mat 2D sub-model.

## 7.6 Finite Element Results

The axisymmetric model provided displacements to be applied to the submodels and an initial estimate of the failure loading. Although no degradation of the liner was applied to the axisymmetric model the failure criterion was applied (with the knockdown factor for corrosion set to 1.0) and an estimate of the failure pressure was found. In each case of the FEA the models were run and during the post processing a failure pressure was estimated. The models were run until the FEA code stopped for the axisymmetric models and the respective submodels were run until convergence could not be reached or the maximum pressure from the axisymmetric models was reached. The final pressure reached for the axisymmetric models should be considered the upper bounds on the failure

pressure for the containment. However, with the ANATECH material model the ABAQUS code was run with the option to continue despite not reaching convergence. Therefore, the computer code analyzed the structure beyond what could be considered reasonably possible.

Since the containment modeled is similar to the Surry containment, the results of the axisymmetric analysis were compared with the results from previous studies (Weatherby 1988, Pananos and Reeves 1984, Rashid 1985). None of these studies used FEA, their results were based on limit-load analyses that determined the yield limit of the reinforcing bar and liner. It should be emphasized that this study is not an analysis of the Surry containment and that the similarities are only with the geometric dimensions and some of the material properties. The containment is considered representative of a reinforced concrete containment with the liner attached to the concrete with studs.

A plot of the reinforcing bar and liner stresses versus pressure is shown in Figure 7.10. In this study, the exterior hoop reinforcing was the first to yield at a pressure of 0.52 MPa (75 psi). Following this, the interior hoop reinforcing bars yielding at approximately 0.76 MPa (110 psi). The liner was the last component to yield. Of the previous studies, only the study by Pananos and Reeves (1984) included the effects of temperature. That study also found that the liner was the last component to yield. However, that study assumed a constant temperature gradient through the wall thickness. Therefore, the interior and exterior hoop reinforcing bars yielded at the same pressure of 0.82 MPa (119 psi). In this study the interior reinforcing bars and the liner were subjected to higher temperatures and kept the inside of the containment wall in compression longer than the exterior. Therefore, the exterior concrete cracked first and the exterior reinforcing bars carried more load initially.

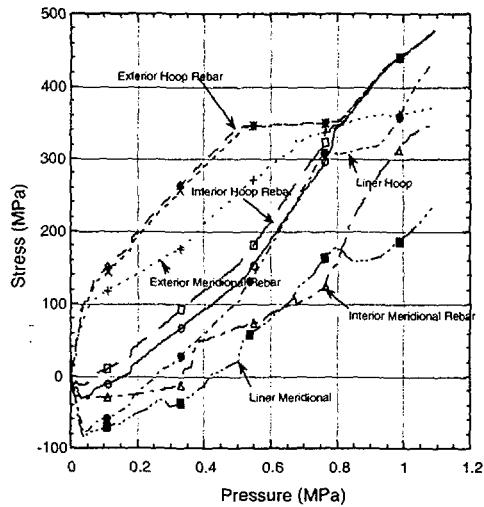


**Figure 7.10. Reinforcing and liner stresses for axisymmetric model.**

In all the studies, except for WASH-1400 (Rashid 1985), all of the hoop reinforcing bars eventually yielded between 0.69 MPa (100 psi) and 0.83 MPa (120 psi). The WASH-1400 study was extremely conservative and gave a failure pressure (first yield of the hoop reinforcing bars) of 0.59 MPa (85 psi). The global axisymmetric FEA model ran until the pressure reached approximately 1.09 MPa (158 psi). At this point the concrete on the floor of the containment began to experience large displacements and failure was considered imminent.

The failure predictions for the axisymmetric analysis with no degradation and the submodels with 10%, 25%, and 50% degradation are shown in Table 7.2. Values for the lowest bound, best estimate, and upper bound estimate (as discussed in the previous section and Chapter 2) were calculated. The different values for each case should emphasize that the predictions cannot be expected to be precise and provide some indication of the variability of the values. Despite a reduction of section by more than 50 %, the strains in the hatch area did not reduce the failure pressure below the upper bound prediction for the uncorroded axisymmetric model. In each of the cases when the capacity of the containment was reduced, the failure strain was located at a stud. The strains within the degraded section of the liner were increased but not near failure levels.

The results for the axisymmetric model with no degradation show that under a lowest bound case the failure would be predicted at 0.99 MPa (143 psi). The best estimate shows that the liner would fail at 1.03 MPa (150 psi). The upper bound failure pressure was found to be 1.08 Mpa (156 Psi). In terms of strain values, the lowest bound failure strain is 2.2 %, the best estimate value is 2.9 %, and the upper bound case is 3.5%.

A plot of the displaced shape of the axisymmetric model is shown in Figure 7.11. The plastic strains in the liner at a pressure of 1.11 Mpa (150 Psi) are shown in Figure 7.12. As can be seen in the figure, the highest plastic strains are in the region of the mid-height of the containment cylinder wall.

**Table 7.2 Failure Pressures and Strains**

	Lowest Bound		Best Estimate		Upper Bound	
	Pressure Mpa (Psi)	Strain (%)	Pressure Mpa (Psi)	Strain (%)	Pressure Mpa (psi)	Strain (%)
Axisym. -(0%)	0.99 (143)	2.2	1.03 (150)	2.9	1.08 (156)	3.5
Base mat -(10%)	0.98 (142)	2.7	***	***	***	***
-(25%)	0.96 (139)	2.8	0.99 (143)	7.2	1.05 (152)	10.8
-(50%)	0.94 (137)	2.0	0.97 (141)	7.3	1.00 (145)	13.2
Mid height(10%)	0.96 (139)	2.5	***	***	***	***
-(25%)	0.82 (119)	2.7	1.05 (152)	6.6	***	***
-(50%)	0.79 (115)	2.6	0.88 (127)	7.0	1.01 (147)	12.1
Hatch	***	***	***	***	***	***

\*\*\* indicates the analysis did not reach a failure strain prior to stopping

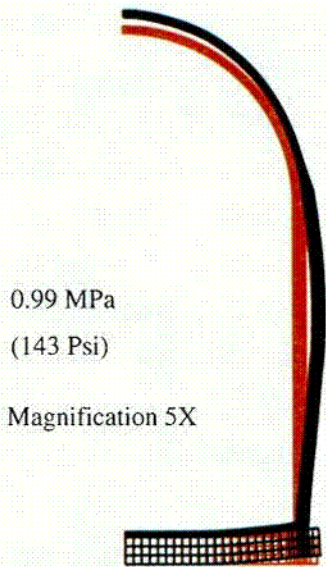


Figure 7.11. Displaced mesh of axisymmetric model.

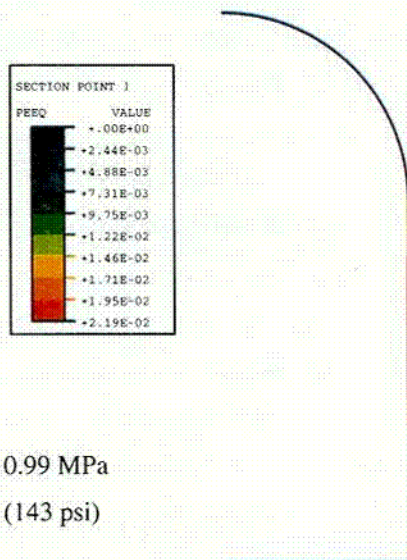


Figure 7.12. Plastic strains in liner of axisymmetric model.

The hatch model degradation was varied in dimension and location to attempt to find a combination of degradation depth and area that would make the failure pressure for this model control. However, despite degrading the section by greater than 50%, the hatch models failure pressures did not control. Therefore, no results from the hatch models are shown. The hatch region appears to be stiffer than other areas in the containment, resulting in lower strains in the liner. The degradation in this region appears to be less critical than in other areas of the containment.

Figures 7.13 and 7.14 show plots of plastic strain versus pressure for the base mat and mid-height submodels.

The 10%, 25%, and 50% data are shown for comparison. For the case of the base mat, the plastic strains begin to increase rapidly at approximately 0.9 MPa (130 Psi). As expected, once the plastic strains begin to rise they are highest for the 50% degradation case, followed by the 25% and 10% cases. The mid-height sub-model values follow a similar trend except they begin to increase at a lower pressure of approximately 0.75 MPa (109 Psi). For the case of the base mat, the 50%, 25% and 10% data all follow a similar trend of increasing very rapidly once the plastic strains begin to develop. The mid-height case shows a more gradual increase in plastic strains as the pressure increase.

As a comparison of the base mat and mid-height cases, the plastic strains for the 50% degradation case for each of these models is shown in Figure 7.15. The 25% and 10% degradation values show similar trends. As can be seen in the figure, plastic strains for the mid-height model begin to rise at a lower pressure. It is not until the strains are greater than 10% that the base mat model overtakes the mid-height model.

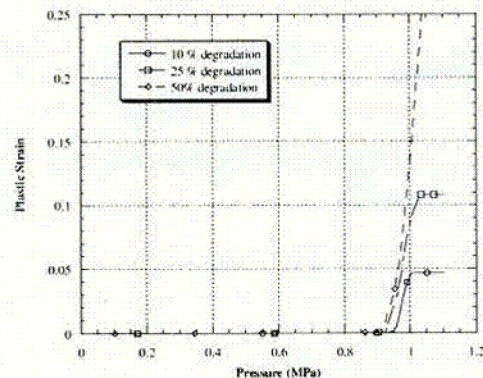


Figure 7.13. Plastic strains versus pressure for the base mat sub-model.

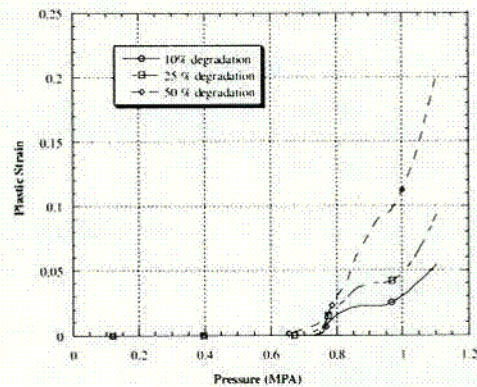


Figure 7.14. Plastic strains versus pressure for the mid-height liner sub-model.

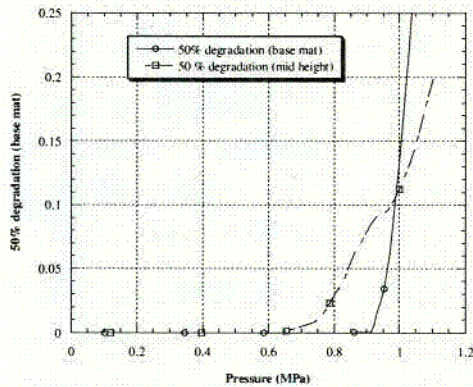


Figure 7.15. Plastic strain versus pressure for the 50% degradation cases.

The base mat model with 10% degradation only resulted in a failure pressure for the lowest bound estimate (0.98 MPa at 2.7% strain). For the best estimate and upper bound cases, the strains did not reach a failure strain level prior to the analysis completing. For the 25% degradation case the failure pressures varied from 0.96 MPa (139 Psi) to 1.05 MPa (152 Psi) and for the 50% degradation case the failure strains varied from 0.94 MPa (137 Psi) to 1.00 MPa (145 Psi). A contour plot of the plastic strains near the best estimate case is shown in Figure 7.16 and the failure pressures and strains for all the cases are listed in Table 7.2.

Figure 7.17 shows a contour of the plastic strain in the liner near the mid-height of the cylinder wall with 50% degradation. Just as was the case for the other sub-models, the highest strains are in the liner near a stud. In this case, the highest strain values are at the stud nearest the edge of the degraded section. The global hoop strains are the highest at the mid-height of the containment. The strain concentration occurs between the stud and the liner that is not degraded. The failure pressure for the best estimate case with 50% degradation is 0.88 MPa (127 Psi) at a failure strain of 7.0%. The case run with 10% degradation only reached a value of failure strain for the lowest bound estimate and the 25% degradation never reached a failure strain prior to completion for the upper bound case. The complete list of failure pressures and stains are listed in Table 7.2.

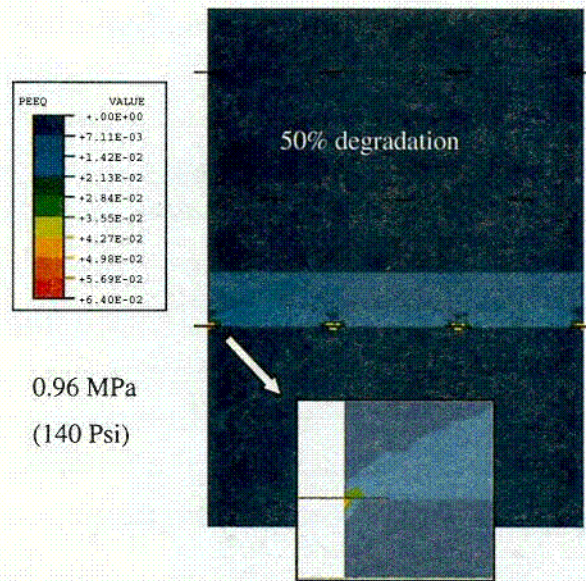


Figure 7.16. Plastic strain in liner near the base mat of the containment.

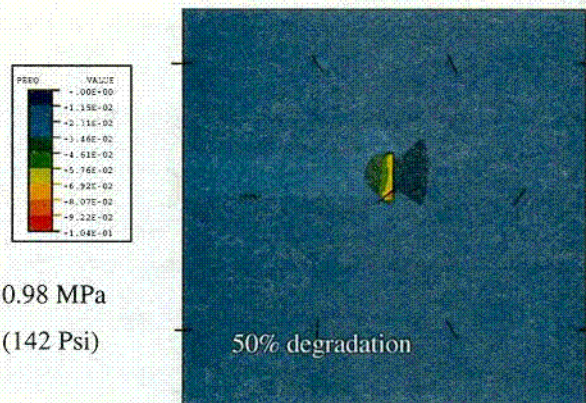


Figure 7.17. Plastic strain in liner at mid-height of the containment.

## 7.7 Discussion

The resulting failure pressures and strains shown in Table 7.2 show how degradation can influence the capacity of the containment. In this study, the degradation at the mid-height location controls in almost every case. The one exception is the upper bound value for the 50% degradation. As can be seen in Figure 7.15, the plastic strains for the mid-height models are generally larger than for the model in the base mat area. The variation in plastic strains in the degraded section for the base mat model does not vary significantly (as can be seen in Figure 7.13). For example, there is only a 3.5% variation between the

failure pressures for the 10% and 50% degradation cases for the base mat location model. However, degradation in the mid-height area has a significant impact on the values of failure pressures. There is a 27.8% variation in failure pressures between the lowest bound and upper bound values for the 50% degradation case. The best estimate failure pressure is 15.5% lower than the base line value calculated from the axisymmetric analysis. As these results suggest, degradation in the region of the base does not have a significant impact on the failure pressure. The liner at this location is not as highly stressed as the liner at the mid-height and therefore is not as critical of a section of the liner; although, this is a likely region of degradation.

As discussed in Chapter 4, changes and discontinuities of the liner are areas of strain concentrations and the locations of ultimate failure. However, in this study the liner had a uniform thickness in each of the basemat, sidewall, and dome. Therefore, the only locations of discontinuities are at the corroded areas and stud locations. For the analysis of an actual containment any known discontinuities should be an area of concern and analyzed. As was found in the 1/6<sup>th</sup> scale model analyzed by Weatherby (1990), stud location in relation to a change of liner thickness can develop strain concentrations at these discontinuities. However, in this study it was found that if the studs shear off prior to the liner tearing the strain concentrations in the degraded areas examined are considerably lower. The loads in the studs for these analyses were examined and determined not to be near failure. The loads in the studs, modeled as spring elements, were well below the ultimate stud load found experimentally by Goble (1968). In that study, the specimens with 15.9 cm (0.625 in) diameter studs that failed by stud shear had ultimate stud loads ranging from 101.8 kN (22.9 kip) to 109.0 kN (24.5 kip). A typical plot of stud load versus pressure for the sidewall submodel with 50% degradation is shown in Figure 7.18.

Goble (1968) found that when the ratio of the diameter of the stud to the plate thickness was approximately 2.7 the failure mode of studs changed from shear to the stud pulling out from the plate (pullout). This study was done using typical commercially available studs and A36 steel. The studs are typical of what would be in a typical containment. For the 1/6<sup>th</sup> scale model analyzed by Weatherby (1990), which liner material more closely matches the material in this study, the ratio of stud diameter to plate thickness was 2.4. If these studs followed a trend similar to those studied by Goble (1968), then the studs would have been expected to shear off prior to the studs failing by pullout. However, a strain concentration was forced between two stud lines due to a change in plate thickness

Consequently, the liner tore at this discontinuity prior to the studs shearing or failing by pullout.

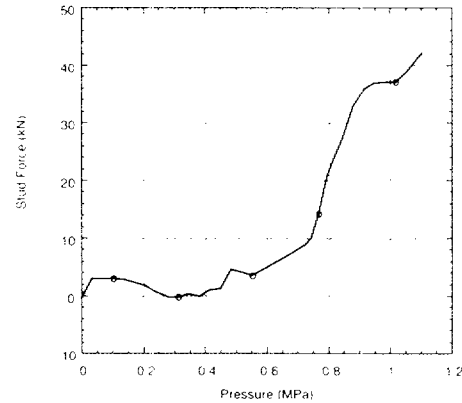


**Figure 7.18. Stud force for typical stud in 50 % corrosion liner model.**

In this study, the ratio of stud diameter to liner thickness in the wall was 2.0. Again, if the trend in the Goble (1968) study held, the studs would shear off prior to stud pullout (or the strains reaching a critical value at the stud locations). However, the Goble (1968) study was conducted using different materials than those used in this study and the stud spacing was different. Since the loads in the studs for this study are below the ultimate shear loads found by Goble (1968), the studs were assumed to not shear off and a critical strain at the stud location was considered the initiation of a tear and subsequent failure of the liner. Stud shear would make a liner tear under the degraded conditions examined unlikely since strain concentrations would not build up at the stud locations.

The equipment hatch was modeled because it seemed a likely location for corrosion around the opening and a likely location for stress concentrations. However, large deformations do not occur due to the large amount of reinforcing in the hatch area. Therefore, the liner stresses in this location were very low. The submodels analyzed in this area, despite substantial degradation, did not reveal a likely failure in this area.

The criteria used in this report to predict potential liner failure differ significantly from criteria that would be acceptable for design. Containment structures are conservatively designed so that the probability of failure is very small under design loads. When predicting liner tearing, previous tests on scaled models have demonstrated that large plastic strains occur before a liner tear develops. The criteria used to predict failure are suitable for use in risk studies, but are

clearly unacceptable for design. For example, in design, strains are typically limited to about 2/3 of the elastic limit (ASME Code does allow for higher liner strains under service conditions). However, when predicting failure, strains that were 7 to 50 times larger than the elastic limit were selected (and 3 to 25 times larger than those allowed in the ASME code). For a badly corroded liner, it is possible to have plastic strains that are below limits where failure would be anticipated, but the strains may still be well above the elastic limit at design loads. To ensure a conservative design, it is necessary to keep stresses and strains in corroded liner areas from exceeding ASME code allowable limits.

## 7.8 Conclusions

Degradation of the liner in a typical reinforced concrete containment with the liner attached to the concrete with studs can degrade the ultimate capacity of the containment. The most critical location of degradation examined in this study was at the region of highest liner stresses (at approximately mid-height of the containment). In this case, the ultimate pressure capacity of the containment was reduced by more than 20 % when the liner was corroded by 50 %. These results are dependent on the studs not shearing off. In addition, details in an actual containment may differ from the typical containment modeled in this study. This might cause the capacity of the actual degraded containment to differ from the typical model discussed in this paper. Since liner corrosion has been found in existing containments the liner was the emphasis of this study. However, reinforcing bar corrosion, or concrete degradation, could also have an affect on containment capacity.

## 8 ANALYSES OF TYPICAL PRESTRESSED CONCRETE CONTAINMENT

Prestressed concrete containments have numerous potential degradation sites. The concrete can degrade, prestressing, reinforcing bars, and the liner can corrode. The following study examines a typical prestressed concrete containment with liner degradation during a loss of coolant accident (LOCA). Although concrete, prestressing tendon and reinforcing bar degradation could be a potentially serious condition, degradation at these locations were beyond the scope of this analysis.

A typical pressurized water reactor (PWR) prestressed concrete containment with a liner that is continuously attached to the concrete with channel and angle iron was examined with postulated liner corrosion degradation at three locations. The containment modeled is similar to the Zion containment. The dimensions, liner thickness, reinforcing bars spacing and size, prestressing spacing and liner anchors were all taken from structural drawings of the containment at the Zion nuclear power station. However, the locations selected for the degradation are not locations of degradation of the liner in the containment at the Zion nuclear power station.

The degradation was located at the region of highest global stress, where corrosion damage had been observed in existing containments, and in regions that are considered likely to experience corrosion. Specifically, the locations were near base mat on the cylinder wall, at approximately mid-height on the cylinder wall (location of highest global liner stress), and near the equipment hatch. Finite element analysis (FEA) was used to examine the containment under accident conditions. Failure was predicted using a strain-based failure criterion. The effect of liner degradation was examined by varying the degree of corrosion at the selected locations and comparing the failure level with the uncorroded case.

To examine liner failure in the containment, sufficient detail must exist in the FEA model to detect strain concentrations at potential failure locations. However, due to the size and complexity of a containment building, a three dimensional model including sufficient detail of all penetrations and detail of the connections between the concrete and the liner for the whole containment building is unrealistic. In this study an axisymmetric model of the containment was analyzed to model the global behavior of the containment building. No penetrations were included in the axisymmetric model and the liner was continuously attached to the concrete at the nodes that were common between the concrete and the liner. The liner elements

were sized to approximate the spacing of the continuous liner anchorage that attaches the liner to the concrete.

Results from the axisymmetric model were used to apply the loading to the more detailed sub-models of the areas of interest. A sub-model that models the concrete, prestressing tendons, reinforcing bars, and continuous liner anchorage explicitly requires a large number of degrees of freedom, is complex to construct, and the interaction of the liner anchorage with the concrete is difficult to model accurately. Therefore, a method to simplify the analyses was required. Since the goal of these analyses was to examine degradation in the liner, a FEA model that is refined enough to pick up strain concentrations in the liner was imperative. Consequently, a method similar to that discussed in Chapter 7 was used to develop the liner sub-models with shell and spring elements.

Since the region of the equipment hatch was considered a location of potential liner degradation a sub-model of this region was constructed. A three-dimensional sub-model including the concrete, prestressing tendons, reinforcing bars, and liner was developed. The liner anchorage was not included in the model. From this model, a two-dimensional sub-model of only the liner was developed using spring elements to model the interaction of the liner and anchorage. Similarly, two-dimensional sub-models of the liner near the cylinder wall and base mat juncture and the liner at the mid-height of the sidewall were constructed. The anchorage was modeled with spring elements in these models as well. These models will be discussed in detail in section 8.5 of this chapter.

Containment vessels are designed to withstand many different loads, such as seismic or internal pressure. Although code requirements stipulate combinations of loads that a containment must be designed to resist, only internal pressure and loads caused by thermal expansion or contraction have been analyzed in this study. The analytical results discussed in this section have not been evaluated during seismic or other load conditions. When evaluating the effect of corrosion damage on an actual containment, it is important to remember that all code required load combinations must be evaluated to ensure that other loads won't cause failure before the vessel fails due to internal pressure.

## 8.1 Material Properties

The liner material properties used were for A516 Grade 60 steel. The true stress-strain curves are shown in Figure 8.1. These curves were developed by using a mean value of engineering yield and ultimate stress from test data obtained from the containment liner at the Sequoyah nuclear power station. The curves were developed to be proportional to curves for A516 Grade 70 steel tested at 22, 93, 149 and 204 °C (Fatigue Technology, 1988). Engineering stress and strain values were converted to true stress and true strain, which are required by ABAQUS to define plastic material properties. The coefficient of thermal expansion used was  $11.3 \times 10^{-6}/^{\circ}\text{C}$ .

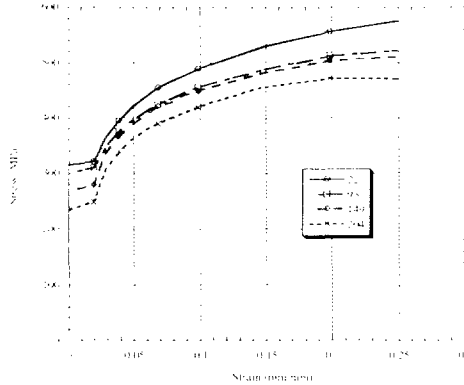


Figure 8.1. Liner Material Stress-Strain Curves.

Material properties used for the concrete are shown in Table 8.1. These values are the as-built material properties of the concrete in the base slab and above the base slab from Butler and Fugelso (1982). The material properties for reinforcing bars and prestressing tendons were taken from Weatherby (1988) and are shown in Table 8.2.

## 8.2 CORROSION/DEGRADATION

Degradation mechanisms were examined in Chapter 2 and it was determined that for low-carbon, low-strength steels used in containment structures, corrosion degradation can be simulated by using a loss of section. The corroded material does not have any strength and therefore the reduction of strength is due to the loss of section. In Chapter 2 it was also shown that there is a reduction in ductility caused by stress and strain concentration regions at discontinuities such as pits or rough surfaces. Bruneau and Zahrai (1997) found for a structural steel that the expected loss of strength for corroded specimens was directly proportional to the reduction of area and that the maximum elongation for tensile specimens was less than that for the uncorroded specimens. Therefore in this study, corrosion was modeled by investigating the effect of loss of section.

Table 8.1 Concrete Properties

	Above Base Slab	Base Slab
Uniaxial Maximum Compressive Stress ( $f'_c$ )	45.5 MPa (6,600 psi)	40.7 MPa (5,900 psi)
Poisson's Ratio	0.19	0.19
Modulus of Elasticity	39.3 GPa ( $5.7 \times 10^6$ psi)	34.5 GPa ( $5.0 \times 10^6$ psi)

**Table 8.2 Reinforcing Bar and Prestressing Tendon Stress-Strain Properties**

Reinforcing Bars		Prestressing Tendons	
Stress MPa (psi)	Strain %	Stress MPa (psi)	Strain %
459.2 (66.6)	0.23	1448.0 (210.0)	0.78
505.4 (73.3)	1.18	1516.9 (220.0)	1.0
590.2 (85.6)	2.27	1654.8 (240.0)	5.0
682.6 (99.0)	4.01		
724.0 (105.0)	10.0		

The locations chosen in this study for the degraded liner were near the junction of the base mat and cylinder wall (approximately 3 meters above the floor-line of the containment), at approximately mid-height of the cylinder wall (this is a region of high stress), and near the equipment hatch opening. The location near the junction of the base mat was chosen because the axisymmetric FEA of the containment revealed a strain concentration in this location and the structural details of the liner anchorage in this location suggests it is a likely location for a strain concentration due to these details. The region at mid height of the cylinder wall was chosen because it is a region of high stress. The equipment hatch location was chosen as a likely area for corrosion and possible stress concentration at the opening.

### 8.3 Loading

The FEA models were loaded with a quasi-static internal pressure that increased monotonically. During many postulated accidents, the pressure is caused by water turning into steam. Therefore, a thermal load was applied to the models along with the pressure loading. The temperature gradient through the wall thickness was approximated from information given in the Zion FSAR (1971) and following a saturated steam temperature-pressure relationship. The temperature decreases very rapidly through the wall thickness. The highest temperature was applied to the innermost nodes of the finite element (FE) models. Then, the next nodes within the model have a degraded temperature profile. All other nodes in the model maintain the initial temperature during the postulated accident. The saturated steam temperature-pressure relationship and the temperature profiles applied to the FE model are shown in Figure 8.2. The initial stress-free state was assumed to exist at 22 °C.

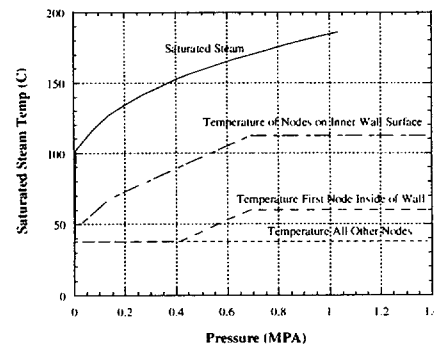


**Figure 8.2. Temperature Pressure Relationship.**

Although many possible accident scenarios exist and are important near design pressures, for the calculation of ultimate capacity of the containment under internal pressure the thermal loads do not have a significant affect. The effects of thermal loads on the liner strains are dissipated as the concrete cracks and reinforcing bars yield. The effects of temperature on the material properties of the liner have been accounted for in the stress-strain curves shown in Figure 8.1.

### 8.4 Failure Criteria

As discussed in Chapter 2 and Chapter 7, a strain-based failure criterion was used for this analysis. The same relationship discussed in the previous chapters is used for the analysis of this prestressed concrete containment. The only variations from the previous applications are the values of knockdown factors shown in Table 8.3.

**Table 8.3 Knockdown Factors**

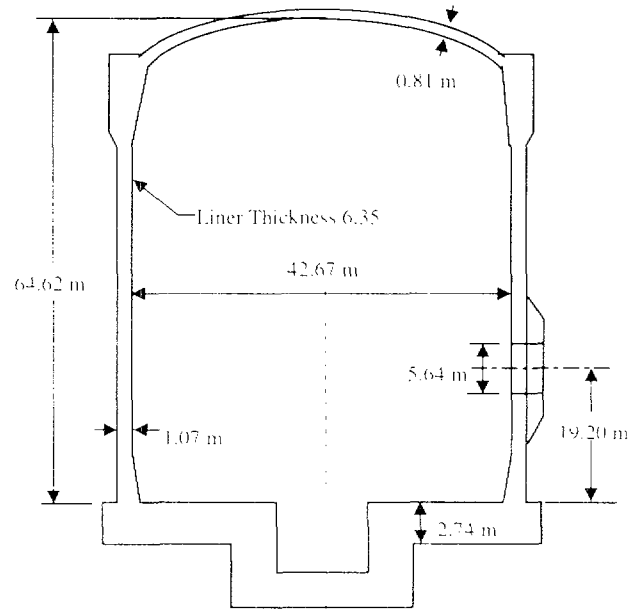
Analysis Sophistication Factor ( $F_2$ )			
	Lowest Bound	Best Estimate	Upper Bound
Axisymmetric	0.2	0.2	0.2
Mid-Height	0.75	0.75	0.75
Base Mat	0.75	0.75	0.75
Hatch	0.75	0.75	0.75

Material Property Factor ( $F_3$ )			
	Lowest Bound	Best Estimate	Upper Bound
All Models	0.78	1.0	1.22

Corrosion Factor ( $F_4$ )			
	Lowest Bound	Best Estimate	Upper Bound
All Models	0.25	0.5	0.75



**Figure 8.3. Schematic of Prestressed Containment.**

### 8.5 FEA Models

A schematic of the typical prestressed containment modeled in the FEA is shown in Figure 8.3. The containment's inside diameter is 42.67 m (140 ft) and inside height is 64.62 m (212 ft). The wall thickness in the cylinder is 1.07 m (3.5 ft), 0.81 m (2.67 ft) in the dome, and the steel liner is 6.35 mm (0.25 in) thick. The concrete base mat thickness is typically 2.74 m (9 ft) thick. The equipment hatch modeled has an inside diameter of 5.64 m (18.5 ft) and is located 19.20 m (63.0 ft) above the base mat. The typical wall layout of the reinforcing bars and prestressing tendons is shown in Figure 8.4.

The prestressed containment modeled uses continuous anchors to secure the liner to the concrete. The continuous anchors consist of channel and angle sections welded to the liner and embedded in the concrete. A schematic showing the typical details of the continuous anchorage is shown in Figure 8.5.

The ABAQUS (Hibbit, Karlsson & Sorenson, 1997) finite element code was used in the analysis. ABAQUS is a general purpose finite element code that provides the option to use external material models. In this study the behavior of the concrete material was modeled using ANACAP\_U (ANATECH Corp, 1997). This material model uses the smeared crack approach (Rashid, 1968) to model the cracking concrete.

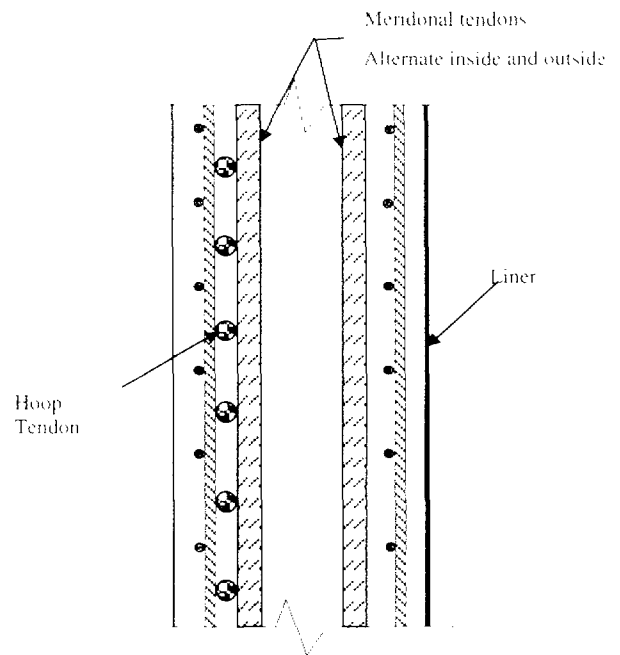


**Figure 8.4. Schematic of typical prestressing tendon and reinforcing bar layout.**

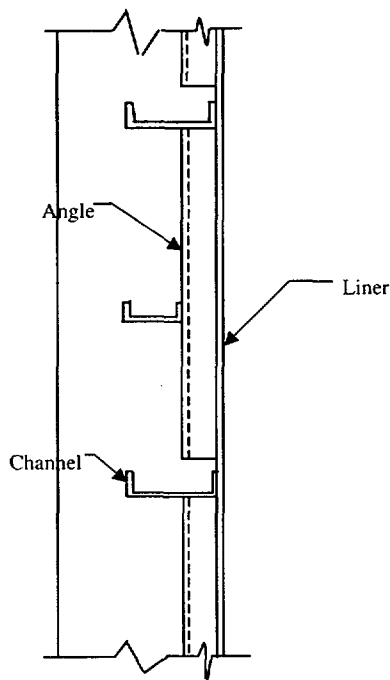


Figure 8.5. Continuous liner anchorage layout.

### 8.5.1 Axisymmetric

Initially a global axisymmetric model was analyzed and the results from this model were used to develop more detailed sub-models of the areas where the degradation was located. The axisymmetric model consisted of 4344 nodes with 1580 elements (see Figure 8.6). Second order elements were used to model the liner (SAX2 in ABAQUS) and concrete (CAX8R in ABAQUS). The concrete elements used reduced integration. The base mat included spring elements (SPRING2 in ABAQUS) to model the soil under the base mat. The nonlinear spring modeled the soil pressure under the base mat but allowed unrestrained uplift of the base mat in areas where the pressure was zero. The dead load of the interior contents of the containment building was estimated and applied.

The hoop prestressing tendons were modeled as reinforcing bars. This results in tendons that are fully bonded to the concrete continuously along their length. The meridional tendons were modeled using truss elements. Therefore, they are not bonded to the concrete except at their respective node points. No friction was included for the meridional tendons. The average prestress values were taken from the FSAR (1971). They included prestressing losses from friction, elastic loss, stress relaxation, and creep and shrinkage of the concrete. The prestress values were 981.2 MPa (142.3 ksi), 970.1 MPa (140.7 ksi), and 1014.2 MPa (147.1 ksi) in the dome, hoop, and meridional tendons

respectively. The INITIAL CONDITION and PRESTRESS HOLD options in ABAQUS were used to apply the prestress loads. The first step of the analysis applied the prestress and dead loads to the containment. A second step applied the pressure and temperature loading.

In actual containments the liners can be subjected to strains beyond the elastic limit due to creep, shrinkage, thermal effects and prestressing. However, in these analyses the dead load and prestressing are applied to the axisymmetric models where the connection between the liner and the concrete are not modeled explicitly. Therefore, the liner loads due to prestressing are not transferred to the liner anchors until they are modeled in the 2D sub-models. In these sub-models, the displacements applied to the anchors are the same as the displacement of the concrete at the same location. Thus, there is no differential displacement and therefore no strain concentrations applied to the liner at the anchors until the liner is degraded.

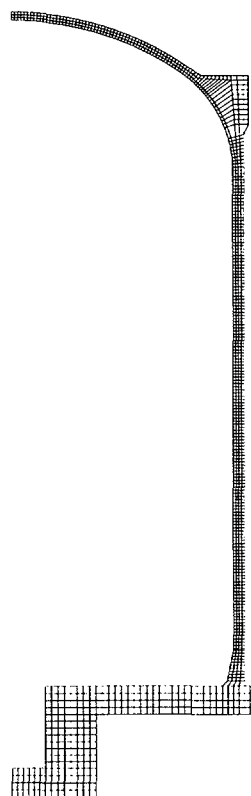


Figure 8.6. Axisymmetric Finite Element Mesh.

### 8.5.2 3-Dimensional Sub-model

Since the equipment hatch was not included in the axisymmetric model a 3-dimensional (3D) sub-model of the equipment hatch was developed. The model contains 1994 nodes and 1816 elements (see Figure 8.7). The liner elements are 4-node reduced integration quadrilaterals (S4R in ABAQUS) and the concrete elements are 8-node bricks (C3D8 in ABAQUS). Meridional tendons were modeled using truss elements while hoop tendons were modeled as reinforcing bars. Half of the hatch was modeled to take advantage of the vertical symmetry. Nodal displacements from this model were applied to the 2-dimensional (2D) sub-model of the liner in the region of the hatch.

### 8.5.3 2-Dimensional Sub-models

The actual degradation of the liner was modeled using 2D sub-models of only the liner. The concrete was not modeled, but the displacement of the liner was applied consistent with the global axisymmetric model or the 3D hatch sub-model. 2D quadrilateral elements were used to model the liner and beam elements were used to model the liner anchorage. Spring elements were used between the beam elements and the liner elements to represent the load-slip relationship of the interaction of the continuous liner anchorage with the liner. The idealized load-slip relationship for the continuous anchorage loaded in shear was obtained from a study by Burdette and Rogers (1975) and is shown in Figure 8.8.

The curvature of the liner was neglected since only a small portion was modeled. Friction and bonding between the concrete and the liner were also neglected. In addition to the displacements applied to the end of the beam elements (representing the angle and channel members), displacements were applied to the edges of the liner. Vertical displacements were applied to the top and bottom edges and horizontal displacements were applied to the side edge that was not the symmetry boundary.

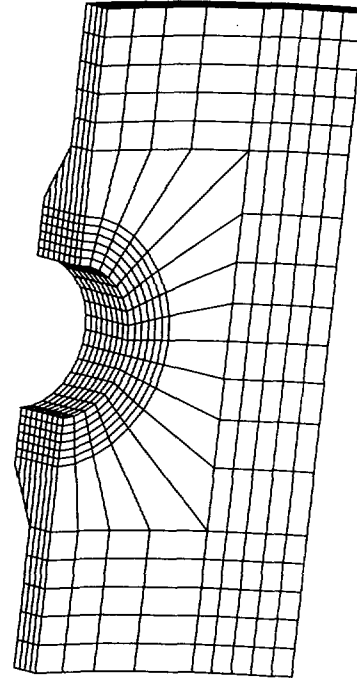


Figure 8.7. Hatch three dimensional model.

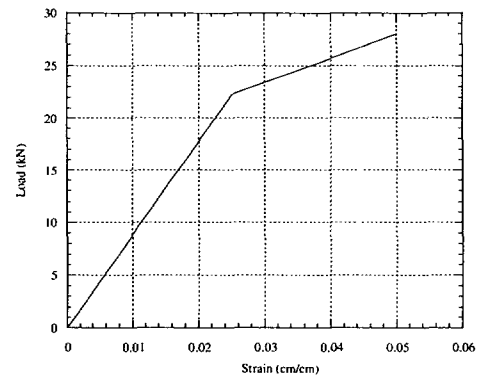


Figure 8.8. Load displacement relationship for continuous anchors.

Three of these 2D sub-models were analyzed: one at mid-height of the containment (Figure 8.9), one model near the base mat (Figure 8.10), and one near the equipment hatch (Figure 8.11). The size of the area of corrosion was chosen as typical of what could be found in an actual containment. The corrosion (thinning of the liner) was located relative to liner plate thickness changes and the continuous anchorage for the worst case scenarios. As shown in Chapters 5 and 6, degradation located near regions of increased stiffness (i.e. plate thickening), are areas where strain concentrations occur. In the sub-models, the areas of degradation were varied to determine the worst case prior to determining the final cases to be run. The resulting worst cases for the location of the degradation

are shown in Figures 8.9, 8.10, and 8.11. These are schematics of the sub-model meshes for the liner at the mid-height location, the base mat region, and near the equipment hatch.

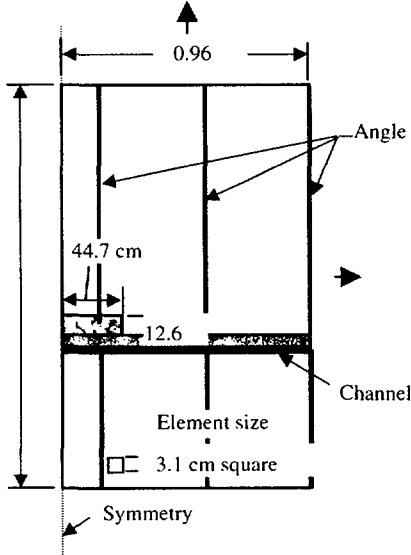


Figure 8.9. Schematic of the liner mid-height model.

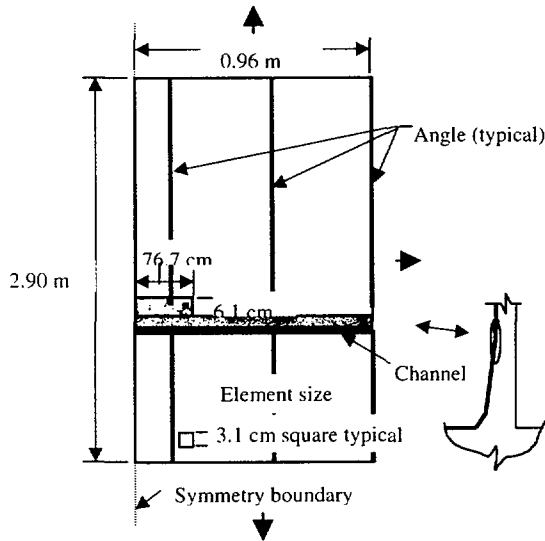


Figure 8.10. Schematic of liner mid-height model.

The sub-model of the liner in the region of the mid-height of the containment is shown in Figure 8.9. The model consisted of 3200 elements and 3028 nodes. The meridional angles and hoop channels were modeled using beam elements. The liner elements were modeled using quadrilateral elements. Where the channel flange is located the elements thickness was increased to represent the flange of the channel and the liner. The

area of corrosion was located adjacent to the channel flange and incorporated the end of one of the meridional angles. The dimension of the degraded area is 44.7 cm by 12.6 cm.

The schematic in Figure 8.10 shows the sub-model of the liner near the base mat region of the containment. The location on this model considered the most critical was at the intersection of the hoop channel and the meridional angle that is 3.5 m from the floor of the containment. The model used in this case was the same as that used for the mid-height case. The only aspect that varied was the applied displacements and the area of degradation was changed. In this case the area of degradation is 76.7 cm by 6.1 cm.

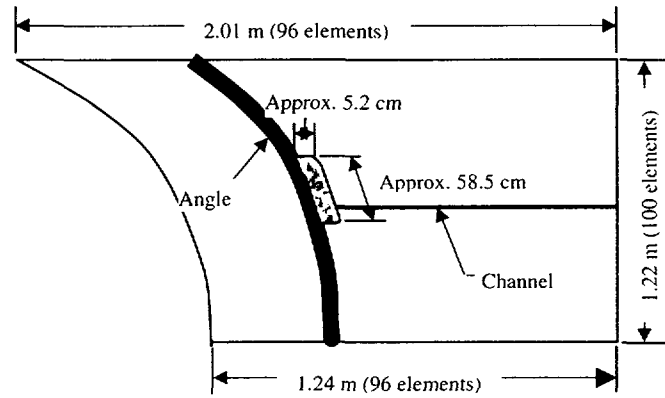


Figure 8.11. Schematic of the hatch liner sub-model.

The sub-model of the liner near the equipment hatch was modeled in a similar manner to the other liner sub-models. The model consisted of 9852 elements and 9898 nodes. Once again, quadrilateral elements were used for the liner and beam elements were used to model the channel and angles. In this case, the critical area is where a hoop channel stops near the angle that is welded to the liner plate. The liner elements were thickened to represent the flange of the angle. The size of the degraded section of liner is approximately 5.2 cm by 58.5 cm.

## 8.6 Finite Element Results

The axisymmetric model provided displacements to be applied to the sub-models and an initial estimate of the failure loading. Although no degradation of the liner was applied to the axisymmetric model the failure criterion was applied (with the knockdown factor for corrosion set to 1.0) and an estimate of the failure pressure was found. In each case of the FEA the models were run and during the post processing a failure pressure was estimated. The models were run until the FEA code stopped for the axisymmetric

models and the respective sub-models were run until convergence could not be reached or the maximum pressure from the axisymmetric models was reached. The final pressure reached for the axisymmetric models should be considered the upper bounds on the failure pressure for the containment. However, with the ANATECH material model the ABAQUS code was run with the option to continue despite not reaching convergence. Therefore, the computer code analyzed the structure beyond what could be considered reasonably possible.

The results of the current FEA of the axisymmetric model were compared to previous analyses of the Zion containment to verify the results. Although there was some variation in the material properties and the prestressing levels, the current analysis was considered reasonable upon comparison. In this analysis the pressure that the hoop prestress was overcome (no concrete hoop stress) is 0.45 MPa (65 Psi), concrete cracking in the hoop direction occurred at 0.57 MPa (83 Psi), and liner yielding occurred at 0.77 MPa (112 Psi). In the analysis by Weatherby (1988) the respective values were 0.44 MPa (64 Psi), 0.59 MPa (85 Psi), and 0.79 MPa (114 Psi). These and other results are shown in Table 8.4. It should be emphasized once again the current analysis is not an examination of

the Zion containment. However, verification that the current results are reasonable was considered prudent.

In previous analyses of the Zion containment (wash1400, etc) the consideration of a shear failure on the cylinder wall near the base mat was discussed. The resulting failure pressures for this mode of failure varied from as low as 0.76 MPa (110 Psi) to being listed as not likely. Although the purpose of this analysis was to investigate degradation due to corrosion of the liner (and the respective failure pressures) shear failure of the prestressed containment cannot be ignored. Shear failure of concrete is a complex concept and different FEA codes handle it in different ways. The standard ANACAP material model used in these analyses does account for shear retention across a crack. The results of this analysis did not indicate a shear failure. However, near the end of the analysis there was considerable cracking in the cylinder wall near the base mat. Shear reinforcement was not included in the axisymmetric analysis and likely would have helped to prevent some of this cracking. When the pressures in the containment are very high there are several possible competing failure modes (such as liner tearing, tendon failure, reinforcing bar failure, and shear failure near the base mat). Although the FEA did not end with a shear failure near the base mat in this case, at internal pressures this high it is a possibility.

**Table 8.4 Analysis Results Comparison**

This Analysis Pressure Mpa (Psi)	Weatherby (1988) Pressure Mpa (Psi)	Event
0.45 (65)	0.44 (64)	Hoop Stress in Concrete=0.0
0.57 (83)	0.59 (85)	Concrete cracking in hoop direction
0.77 (112)	0.79 (114)	Liner yielding
0.88 (127)	0.83 (120)	Hoop bars yield
0.88 (127)	0.88 (127)	Hoop tendons yield
0.92 (133)	0.91 (132)	Strain in hoop tendons reach 1%
1.05 (152)	1.03 (149)	Strain in hoop tendons reach 5%

The results from the sub-models were used to predict the failure pressures of the degraded containment with no corrosion degradation, 30 percent degradation, and 50 percent degradation. Table 8.5 shows the resulting failure pressures and strains for the lowest bound, best estimate, and upper bound estimates (as discussed in the previous section and Chapter 2).

The axisymmetric model was also used to predict a failure pressures with no liner corrosion. Figure 8.12

shows the displaced mesh of the model (with a 5X magnification factor) and Figure 8.13 shows the plastic strains in the liner at a pressure of 1.0 MPa (145 Psi). As can be seen in Fig. 8.13, the highest liner strains are in the cylinder wall approximately at the mid-height of the containment, and there is a strain concentration in the sidewall near the base mat. The best estimate failure pressure from the axisymmetric model with no corrosion degradation is 0.99 MPa (143 Psi) and a plastic strain of 1.5 percent.

Figures 8.14, 8.15, and 8.16 show plots of plastic strain versus pressure for the hatch, mid-height, and base-mat liner sub-models. Each figure includes results for the 0%, 30%, and 50% degradation cases. In each case, the strains begin to increase rapidly in the range of 0.90 MPa (130 Psi) to 0.93 MPa (135 Psi). The results for the hatch sub-model shown in Figure 8.14 demonstrates that degradation does not significantly affect the failure pressure in the hatch region. However, as expected, the more degradation there is the lower the failure pressure. The liner mid-height and base mat cases show a greater influence of the degradation. The base mat area shows the greatest influence of the degradation.

Figure 8.17 shows a contour plot of the plastic strain in the hatch sub-model (with 50 % degradation) at a pressure of 0.96 MPa (139 Psi). The highest plastic strains are located in the degraded liner that is between the end of the continuous liner anchorage and the angle around the hatch. Although there is a strain concentration in this region, when the failure criterion

was applied this region resulted in higher failure pressures than in the mid-height and base mat regions.

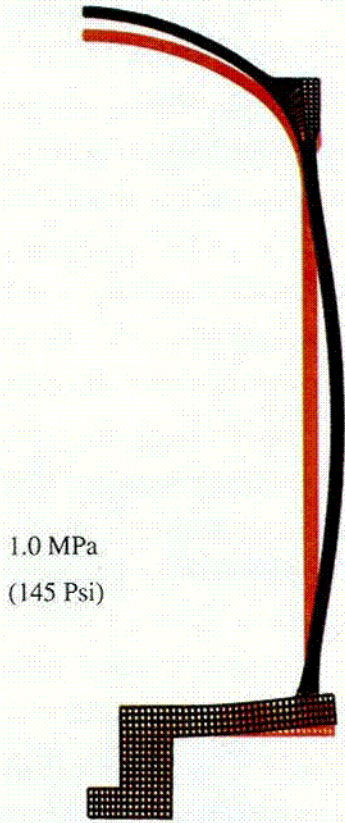
As shown in Figure 8.13, the liner in the cylinder mid-height region is an area of high liner strains. Figure 8.18 shows the plastic strains for the 30% degradation case of the liner mid-height sub-model. The highest plastic strains can be seen in the degraded area between the continuous anchorage and the flange of the channel iron. The figure shows the plastic strains at a pressure of 0.96 MPa (140 Psi).

The liner near the base mat is also another region of high strains. As shown in Figure 8.13, the area where there is a slight geometric discontinuity in the liner near the base mat has a strain concentration. The plastic strain at a pressure of 0.93 MPa (135 Psi) and 30% degradation is shown in Figure 8.19. Once again, the highest plastic strains are in the region between the end of the continuous anchorage and the flange of the channel of the hoop continuous anchorage.

**Table 8.5 Failure Pressures and Strains**

	Lowest Bound		Best Estimate		Upper Bound	
	Pressure Mpa (Psi)	Strain (%)	Pressure Mpa (Psi)	Strain (%)	Pressure Mpa (psi)	Strain (%)
Axisym. -(0%)	0.96 (140)	0.6	0.99 (143)	1.5	1.01 (146)	2.7
Hatch -(0%)	1.08 (157)	5.4	1.10 (159)	6.7	1.10 (160)	8.6
-(30%)	0.96 (139)	3.1	0.99 (144)	7.9	1.03 (149)	14.4
-(50%)	0.95 (138)	3.1	0.99 (143)	7.9	1.01 (147)	16.5
Mid height -(0%)	1.06 (154)	8.5	***	***	***	***
-(30%)	0.90 (131)	2.2	0.99 (143)	5.8	1.03 (150)	10.2
-(50%)	0.87 (127)	2.2	0.93 (135)	5.5	1.01 (147)	11.2
Base Mat -(0%)	1.12 (162)	8.4	1.12 (162)	10.8	1.12 (162)	13.2
-(30%)	0.91 (132)	2.1	0.94 (137)	6.6	1.06 (153)	10.0
-(50%)	0.90 (131)	2.1	0.92 (134)	6.6	0.94 (136)	10.0

\*\*\* indicates the analysis did not reach a failure strain prior to stopping



1.0 MPa  
(145 Psi)

Figure 8.12. Displaced shape of axisymmetric model (5X).

SECTION POINT 1	
PEEQ	VALUE
0	+ .00E+00
1	+3.05E-03
2	+6.09E-03
3	+9.14E-03
4	+1.22E-02
5	+1.52E-02
6	+1.83E-02
7	+2.13E-02
8	+2.44E-02
9	+2.74E-02

1.0 MPa  
(145 Psi)

Figure 8.13. Plastic strain in axisymmetric model.

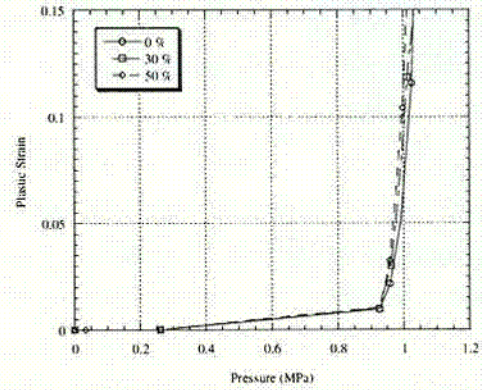


Figure 8.14. Plastic strain versus pressure for hatch liner sub-model.

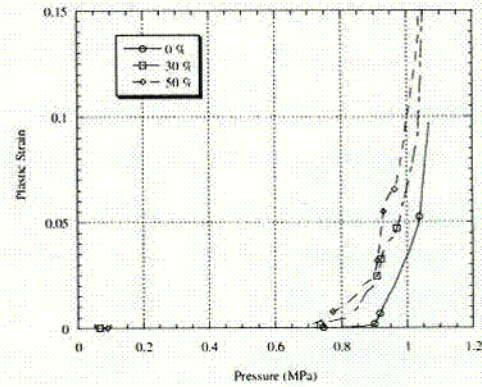


Figure 8.15. Plastic strain versus pressure for the liner mid-height sub-model.

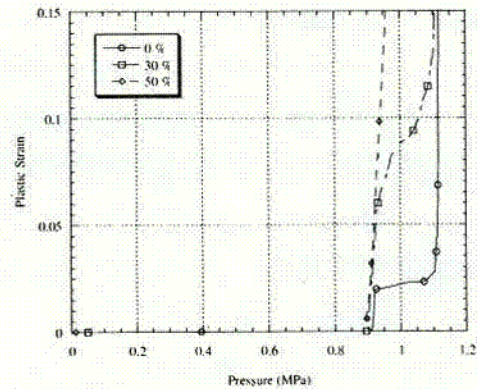


Figure 8.16. Plastic strain versus pressure for the liner mid-height sub-model.

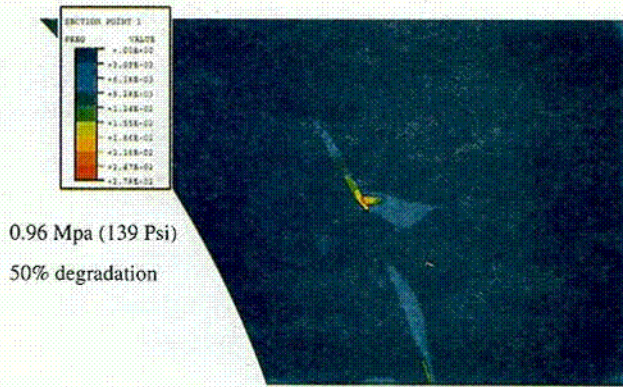


Figure 8.17. Hatch liner sub-model plastic strains.

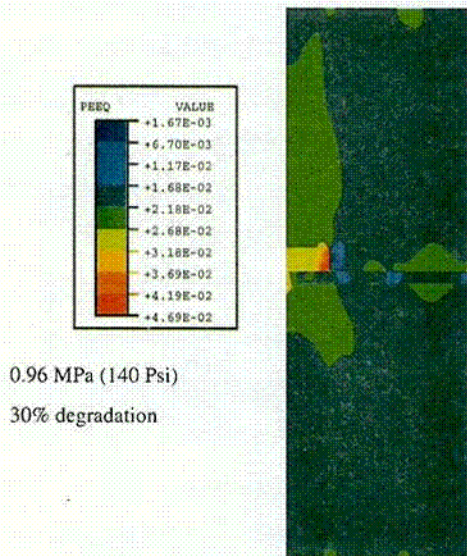


Figure 8.18. Liner mid-height sub-model plastic strains.

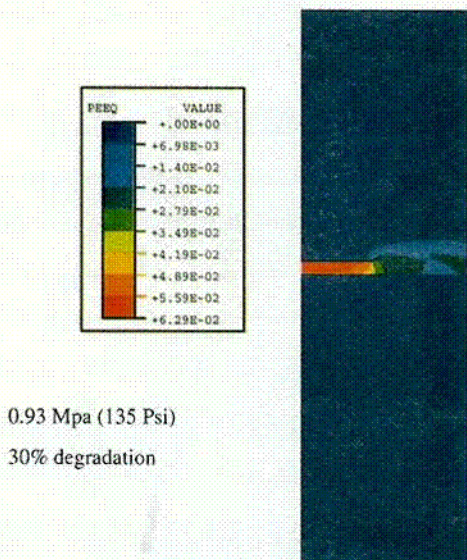


Figure 8.19. Base mat liner sub-model plastic strains.

The three figures of the plastic strains for the liner sub-models are typical of what was found at different degradation levels and pressures. The controlling cases for each degradation level is shown in Table 8.6. With no degradation, the axisymmetric models provided the controlling failure pressures. This could be expected since the models contain little detail and have the most conservative knockdown factors to account for the lack of detail. For the 30% and 50% degradation levels, the controlling location varied for the lowest bound, best estimate, and upper bound estimates. The hatch location was never the controlling case. The base mat model provided the controlling case for the best estimate failure pressure for the 30% and 50% cases.

The criteria used in this report to predict potential liner failure differ significantly from criteria that would be acceptable for design. Containment structures are conservatively designed so that the probability of failure is very, very small under design loads. The design criteria are selected so that the vessel remains elastic, with a comfortable safety factor, under all design loads. However, when predicting liner tearing, previous tests on scaled models have demonstrated that large plastic strains occur before a liner tear develops. The criteria used to predict failure are suitable for use in risk studies, but are clearly unacceptable for design. For example, in design, strains are typically limited to about 2/3 of the elastic limit. However, when predicting failure, strains that were 7 to 50 times larger than the elastic limit were selected. For a badly corroded liner, it is possible to have plastic strains that are below limits where failure would be anticipated, but the strains may still be well above the elastic limit at design loads. To ensure a conservative design, it is necessary to keep stresses and strains in corroded liner areas from exceeding ASME code allowable limits.

## 8.7 Discussion

The calculated failure pressures for the degraded cases shown in Tables 8.5 and 8.6 are all within 10% and the best estimate values are within 6% for all cases. This indicates that all the locations of the degradation are competing closely and that the failure could likely occur and any one of these locations. Calculating the lowest bound, best estimate, and upper bound failure pressures emphasizes that these are estimates of failure pressures and that actual failure could vary. Since the failure pressures for the 30% and 50% degradation are within 10% it shows that the reduction in ultimate capacity does not directly correlate to the degradation of the liner. However, the ultimate capacity is reduced. There is a 0 to 10% reduction in ultimate capacity from the capacity calculated from the axisymmetric analysis and there is a 10 to 25% reduction in capacity compared to the ultimate capacity calculated at the specific locations of the degradation.

Tensile loads in prestressed concrete containments are carried by the reinforcing bars, prestressing tendons, and the liner. The liner does not carry a major portion of the tensile loads. Therefore, when examining the ultimate capacity of a prestressed concrete containment with a degraded liner, there will not be a direct correlation between degradation of the liner and the decrease in ultimate capacity.

For the prestressed containment with the continuous anchorage examined in this study the interaction of the concrete, the continuous anchorage and the degraded liner are critical to the estimation of ultimate capacity. The locations of the degradation in this study were estimated and placed in areas that appeared to be likely to have corrosion and placed with respect to the details that were deemed critical. In a case of actual degradation in an existing containment, the actual detail should be modeled as realistically as possible. Although it is possible to have as much as 50% degradation of the liner in certain areas and not

significantly reduced the ultimate capacity of the containment, small amounts of degradation in certain locations can be significant. Therefore, any degradation found in the liner of the containment must be analyzed to quantify the impact on the capacity of the containment and to examine possible repair solutions.

## 8.8 Conclusions

As has been shown, degradation of the liner for a typical prestressed concrete containment with the liner continuously attached to the concrete can degrade the ultimate capacity of the containment. The most critical location examined in this study was at the mid-height of the containment cylinder wall. However, the cases examined in this study were only potential areas of degradation. In an actual containment, anywhere degradation is found, would have to be examined using a similar methodology to determine the degradation's influence on the containment capacity.

**Table 8.6 Controlling Failure Pressures and Strains**

	Lowest Bound			Best Estimate			Upper Bound		
	Pressure MPa (Psi)	% Strain	Case	Pressure MPa (Psi)	% Strain	Case	Pressure MPa (Psi)	% Strain	Case
0%	0.96 (140)	2.3	Axi	0.99 (143)	2.9	Axi	1.01 (146)	3.6	Axi
30%	0.9 (131)	2.2	Mid Height	0.94 (137)	6.6	Base Mat	1.03 (150)	10.2	Mid Height
50%	0.87 (127)	2.2	Mid Height	0.92 (134)	6.6	Base Mat	0.94 (136)	10.0	Base Mat

## 9 SUMMARY AND CONCLUSIONS

### 9.1 Basis For Predicting Capacity of Corroded Containments Using Finite Element Analyses

The basis for using finite element analyses to calculate the pressure capacity of steel containments that have corrosion damage, or concrete containments with corrosion damage to the liner, is:

- Finite element analyses have successfully calculated the response of uncorroded containment scaled models, and predicted failure pressures were within about 10% to 20% of test results.
- Finite element analyses can predict the structural response and the ultimate failure pressure of an actual containment, although the uncertainty in the predicted results may be somewhat larger than was observed from the scaled model tests and analyses. This is because actual containments may have local details that were neglected in the containment models.
- The primary affect of corrosion on low-carbon, low-strength steels is to reduce the cross-sectional thickness.
- Finite element analyses can account for corrosion by reducing the material thickness in corroded areas. This will create stress/strain concentrations that are similar to concentrations caused by plate thickness changes in an uncorroded containment.

#### 9.1.1 Scaled Model Tests and Analyses of Uncorroded Containments.

A number of scaled model tests and analyses have been conducted for uncorroded containments and other pressure vessels. Analyses have been able to do a reasonable job of predicting the response of steel, reinforced concrete, and prestressed concrete structures. Often there are several competing modes of failure, and analysts have predicted that the model would fail in one mode while the structure actually failed in a different mode. However, in most cases the predicted failure pressure was within about 10 to 20% of the actual failure pressure. In a few cases, many independent analyses were performed before a test was done, and the global responses predicted by the different analysts were similar. The biggest difference between the analysts was in how they interpreted their results to select a failure pressure.

### 9.1.2 Material Properties and Aging Issues.

For the low-carbon, low-strength steels used in containment structures, corrosion damage can be categorized as "loss of section" damage, "local pitting" damage, or a combination of the two. As a shell section becomes thinner in a corroded area, the strength is reduced because of the reduced cross-section. Corroded material has virtually no strength and uncorroded material retains virgin material properties. In addition, the rough and uneven corrosion surface causes strain concentration regions, and failure can occur at lower-than-expected global strains because of tears that initiate in the strain concentration regions. The most likely result of local pitting is a "leak" in the containment boundary if a pit becomes large enough to penetrate the wall. The amount of metal that is actually corroded away by pitting is usually a very small percentage of the cross-section, so there is no appreciable reduction in strength.

Corrosion can significantly reduce the fatigue life of a structure. The rough corroded surface, pits, or other flaws cause stress concentrations that may cause a crack to initiate and grow. The total number of cycles of large stress that a containment could be subjected to are small (less than 100). Therefore, fatigue is not likely to cause failure. However, if any portion of a structure is found that has corrosion and a large number of high-stress cycles, then fatigue could be a serious concern in that local area.

When subjected to loads that cause steel to exceed its elastic limit, it is common for welds to fail in the weld or in the heat-affected zone. However, for the low-carbon low-strength steels used in containment structures, testing has shown that failure occurs away from the weld area. Based on test data, the weld is not the "weak link" in structural failure of A516 or SA212 steels. During uniaxial tension tests, these materials failed in the base metal and not in the weld zone. Of course, a significant crack or flaw (i.e., incomplete penetration of the weld) in the weld zone could cause brittle fracture, just as a large crack in the containment wall could cause brittle fracture. However, corrosion damage found in actual containments has not shown corrosion damage to be preferentially attracted along weld seams.

Welds have not become the "weak link" in containment structures because:

- the low-strength, low-carbon steels used in containment vessels are very weldable,
- the material is very tough and resistant to flaws propagating, and
- high quality welds are assured in containment vessels through tightly controlled weld procedures and 100% inspection of the welds for flaws. However, attachment welds, which could become stress risers, are not 100% inspected.

### 9.1.3 Lessons Learned From Corroded Pipeline Research.

Using reduced thicknesses in corroded areas, the gas and pipeline industry has been successful in using finite element analyses to predict the burst pressure of corroded pipelines. The industry has performed tests and analyses on pipes with a significant loss of cross-sectional area, which could cause the pipe to tear and fail catastrophically, as well as for pipes with pits, which may cause a leak but probably wouldn't tear. Some of the conclusions from the pipeline research are:

- Corroded pipe sections exhibit ductile failure modes, and do not fail in a brittle manner. Corrosion defects in pipelines are typically blunt, having a radius of the same order of magnitude as the wall thickness, with a stress concentration factor that is close to one. Failure in a corrosion area occurs through uncontrolled plastic flow and material instability, similar to necking in a tensile test specimen.
- The structural response of a corroded pipeline can be accurately predicted (about  $\pm 10\%$ ) by finite element analyses using a fairly coarse mesh (3 or 4 second order elements across the corroded section) and stress based failure criteria. Similarly, an effective plastic strain criterion can also give reliable failure predictions.
- Bending stresses have limited influence on ultimate failure of pipe sections. In local areas where high bending stresses are present, local plastic bending results in a redistribution of stress until the loads are carried predominantly as membrane forces. Stress in the pipe wall is almost the same for metal loss from the inside or the outside of a pipe.

### 9.1.4 Corroded Coupon Tests.

Corroded coupons that were tested had a reduction in strength that was essentially proportional to the reduction in net cross sectional thickness. In elastic

regions and at low plastic strains, the stress versus strain curve was the same for both the corroded and uncorroded coupons. In the plastic region, the stress versus strain curves for coupons without any corrosion, and for coupons that had corrosion by-products (i.e., rust) removed, was about the same, except that the *percent elongation in a two inch gage length* decreased for the coupons that had been corroded. When the plastic strains in the stress concentration region become large enough to initiate failure, the "net" or "effective" or "average" strain through the coupon cross section was about half of the strain-to-failure levels of uncorroded coupons. There is not a real reduction in the material's ductility, but rather the change in the cross-section causes stress risers which cause failure at about the same stress level, but at a reduced elongation.

## 9.2 Finite Element Modeling

### 9.2.1 Modeling Corrosion.

Failure often initiates in regions of discontinuity because of large stresses and strains that exist in the local area. If a finite element mesh is modeled in sufficient detail, the finite element method is able to calculate stress and strain concentrations that occur in the area of the discontinuities. However, pitted and rough surfaces consist of "micro" discontinuities that are much smaller than the elements in the mesh.

In a finite element model of a large structure, it is not practical to model the rough, uneven surface of a corroded plate because of the large number of elements that would be required. Usually, this amount of detail about the condition of an existing structure is not available, and if it was, a model containing this amount of detail would be prohibitively large.

The information that can be readily measured on a corroded plate section is the cross-sectional thickness at a number of specified points. For example, if a grid is drawn on the corroded surface, thickness measurements could be made at each grid point. In a finite element model with elements that have edge lengths that are about the distance between grid points, all that is known about the cross-sectional thickness is the measurement of the nearest point(s). However, the surface of a corroded section is generally rough and uneven, often with some pitting. Since the finite element model assumes an element with constant thickness, local strain concentrations caused by pits or the rough, uneven surface are not calculated.

However, stress concentrations that result from geometry changes that are larger than the element size, such as a locally thinned area, plate thickness change, a penetration, or other "macro" discontinuities are calculated in a finite element analysis.

The "micro" discontinuities are accounted for by applying a knockdown factor to reduce the critical elongation for material in the affected area. The knockdown factors are nothing more than simple observations about how omitted local corrosion details typically cause a tear to initiate at a lower element strain level.

Damage can be grouped into the two categories discussed in Section 2. General corrosion damage degrades the surface of the metal containment structure somewhat uniformly, and can be handled in a finite element analysis by thinning the wall in the area(s) that have corroded. In order to model corrosion in a plate section, the shell thickness was selected as the average thickness in the selected area, and the rough corroded surface was approximated as a smooth surface. A knockdown factor was applied to account for the difference between a uniform thickness plate with smooth sides, and the degraded section that varies somewhat in thickness and has a rough, uneven surface. The rough and uneven surface induces stress/strain concentrations that cause tears to initiate in the concentration regions.

The second category of damage is local pits that are scattered and cause stress concentrations. In areas where there is pitting, the thickness of the shell was not reduced, but the ductility of the steel was reduced to account for the strain concentrations around the discontinuities.

### **9.2.2 Failure Criteria for Steel Shell and Liner of Concrete Containments.**

The analysis method that was used to predict the ultimate capacity of corroded containments was to limit the effective plastic strains. Failure criteria that limit the effective plastic strain have been developed to simulate void growth in high stress intensity regions. As the material strains, voids coalesce into a flaw. At some critical strain level, the flaw reaches a critical size and a tear initiates. Therefore, the effective plastic strain analysis method will predict failure in high stress intensity regions caused by a critical flaw. In order to predict failure at a flaw location, the finite element mesh must be detailed enough to capture local strain concentrations.

Because the objective of this report has been to understand how corrosion degrades the containment structure, non-structural failure modes have not been evaluated. If previous studies have concluded that a non-structural failure mode may occur before the structural failure mode, then that has been noted. In this report, it has been assumed that failure will occur at the lower pressure of the predicted structural failure

(tearing of steel shell or liner) or at the non-structural failure pressure identified by previous studies.

Either a strain or stress based failure criteria could be successfully used to predict when the structure reaches a state where a tear could initiate. The effects of the multi-axial stress state, the amount of detail that is included in the model, and the potential variation in material properties should be considered when selecting a failure criteria. In addition, a corroded section may tear at a lower strain than an uncorroded section would.

No consensus has been reached in the analysis community about what failure limits are most appropriate. Therefore, the failure criteria used in this report is somewhat subjective, and other similar criteria could have been used instead. The selection of failure criteria could shift the predicted failure pressures either up or down.

Fortunately, after the material exceeds its elastic limit and begins to plastically flow, a large change in strain value is associated with a small change in stress. Therefore, the predicted failure limits are not overly sensitive to the analysts selection of strain-based failure limits.

### **9.2.3 Actual Containment Behavior versus Analytical Predictions.**

Material properties vary from one lot of steel to the next. The material properties used in the analyses in this report are typical values, but vary somewhat from the measured material properties for any specific containment. Even when a specific containment is selected, there is variation in material properties for the steel in that vessel. Properties such as yield stress and ultimate stress often vary by  $\pm 10\%$  or more about the mean, while the ductility measured often varies by  $\pm 25\%$  or more.

The strain-to-failure levels vary between material samples of different geometric configuration, different material lot numbers, and so forth. There will be a corresponding uncertainty in any analysis that predicts the ultimate capacity of a structure.

In the analyses that have been performed during this study, many details such as penetrations or local weld conditions have been neglected. Other details have been simplified, but are included in the model. For example, in an actual containment a thick plate is tapered near the edge where it is welded to a thinner plate to reduce the stress concentration that would be caused by an abrupt change. In the finite element model, this thickness change occurs abruptly if the tapered transition zone is smaller than the element size.

Other details, such as symmetry boundary conditions, can greatly reduce the size of the model and decrease the amount of time required to complete the analysis. However, the symmetry assumptions can have an impact on the predicted results.

In the extremely unlikely event that a severe accident caused pressures that were significantly larger than the design pressure, non-structural failure modes could occur before a structural failure model. Examples of non-structural failure modes are failure of an electrical penetration assembly, valve failure, the seal of a hatch, or a crane rail falling because of excessive displacements. Only structural failure modes are predicted by the analyses discussed in Chapters 5 to 8.

Containment vessels are designed to withstand many different loads, such as seismic or internal pressure. Although code requirements stipulate combinations of loads that a containment must be designed to resist, only internal pressure and loads caused by thermal expansion or contraction have been analyzed in this study. Under other loading conditions, such as an earthquake, combinations of loads not considered in this study could be more severe and control. When evaluating the effect of corrosion damage on an actual containment, it is important to remember that all code required load combinations must be evaluated to ensure that other failure modes, such as buckling, won't cause failure before the vessel fails due to internal pressure.

Last of all, the criteria used in this report to predict potential containment failure differ significantly from criteria that would be acceptable for design. Containment structures are conservatively designed so that the probability of failure is very, very small under design loads. The design criteria are selected so that the vessel remains elastic, with a comfortable safety factor, under all design loads. However, when predicting failure, previous tests on scaled models have demonstrated that large plastic strains occur before the pressure boundary fails. The criteria used to predict failure are suitable for use in risk studies, but are clearly unacceptable for design. For example, in design, strains are typically limited to about 2/3 of the elastic limit. However, when predicting failure, strains that were 7 to 50 times larger than the elastic limit were selected. Some of the badly corroded containments that have been analyzed in this report had plastic strains below limits where failure would be anticipated, but strains that were well above the elastic limit at design loads. Although the probability of failure under design loads is low for some of the corroded containments that were analyzed, the level of conservatism necessary to ensure safety was lacking. To ensure a conservative design, it is necessary to keep

stresses and strains in corrosion areas from exceeding ASME code allowable limits.

## 9.2.4 Analyses of Typical Steel Containments.

The primary failure mode that has been analyzed during this study is tearing of the shell wall. However, failure modes, and the associated failure pressure, identified during previous studies have been used in this study. For example, previous studies have concluded that the first expected failure mode is shell wall tearing for the typical PWR Ice Condenser containment. Other failure modes, such as leakage through a seal, or anchorage failure, were deemed to not occur until after the shell wall tore. Therefore, the calculated failure limit was deemed to be the controlling case.

On the other hand, the BWR Mark I containment would be expected to vent before any structural failure would occur. If for some reason the vessel wasn't vented, then the next expected failure limit would be leakage through the top head seal. Therefore, structural failure was not the expected failure mode.

Code requirements stipulate combinations of loads that a containment must be designed to resist. Only internal pressure and loads caused by thermal expansion or contraction have been analyzed in this study. Many other load combinations must be evaluated, such as buckling of the shell wall under earthquake loads. When evaluating the effect of corrosion damage on an actual containment, it is important to remember that all code required load combinations must be evaluated to ensure that other failure modes, such as buckling, won't cause failure before the vessel fails due to internal pressure.

No attempt has been made to predict the structural response after a tear is predicted to initiate. In some cases, if the high plastic stresses and strains are very local to the tear location, it is likely that the tear will arrest itself and the vessel will depressurize due to the tear in the wall. However, if the high stresses and strains cover a large enough area, then the tear is likely to propagate and result in total catastrophic failure.

Results show that even small amounts of corrosion in the area of highest strain can significantly reduce the pressure capacity of the vessel, while considerable corrosion in other areas can be tolerated without reducing the pressure capacity.

The structural response of most of the containment shell was primarily membrane. Membrane forces in the cylindrical portions of the structure were twice as large in the circumferential direction as they were in

the vertical direction. This is a known behavior of cylindrical sections. Therefore, in sections of the containment that were cylindrical, the shell wall became inelastic and began gross plastic flow in the hoop direction while the response in the meridional direction was still elastic. In spherical sections, the hoop and meridional membrane forces were about the same, and hence there was no preferred failure direction.

### 9.2.5 Analyses of Typical Concrete Containments.

In reinforced concrete containments, the concrete cracks when internal pressure is applied, and the reinforcing bars carry about 80 to 90% of the pressure load. The remaining 10 to 20% of the load is carried by the liner. In prestressed concrete containments, both the reinforcing bars and the prestressing tendons carry the significant majority of the load, with the liner the remaining portion. The shell wall must resist 100% of the loads in a steel containment.

When a section of the shell wall in a steel containment is reduced in thickness due to corrosion, pressure loads can cause yielding in the reduced cross section area. Eventually, the loads cause the section to become unstable and a tear initiates. In contrast, if the liner in a reinforced or prestressed concrete containment is locally thinned, the change in load carrying capacity is minimal because the rebars and tendons carry a majority of the loads.

If two coupons are pulled to failure in uniaxial tension, one under force control and the other under displacement control, there will be some fundamental differences in the failure. Both coupons will behave the same until the peak engineering stress is reached. In a test under force control, the coupon will go unstable as soon as the peak engineering stress is reached, and the coupon will fail immediately. In a test under displacement control, the coupon will not fail immediately, but will continue to support load and plastically strain. The strain at which the coupon will become unstable in a force control experiment is about half of the strain at which failure eventually occurs during a displacement control experiment.

The steel containment vessel, when placed under increasing pressure load, can be compared to the coupon under force control. When the peak engineering stress is reached over a significant area (i.e., global plastic membrane stresses), the vessel wall will fail catastrophically. A locally thinned section of the liner in a concrete containment, on the other hand, will respond similar to the coupon under displacement control. Since the reinforcing bars and tendons resist

most of the load, the liner is going to follow the displacements of the concrete wall.

The liner in a concrete containment is attached at points (Nelson stud anchors) or along lines (T anchors embedded in the concrete). This causes stress concentration regions around the anchors where failure is expected to initiate. In addition, thickened insert plates will increase the strains at nearby anchorage points.

It is possible that a stud may shear off before the liner tears, and thus allow loads to redistribute themselves. This would postpone liner tearing for a while. On the other hand, it is quite clear that embedded T anchors will not shear off, so concentrated forces can occur in the liner at the anchorage point.

## 9.3 Simplified Analogy

All of the analyses that have been discussed in this report, both corroded and uncorroded, can be explained and are consistent with the following simplified analogies. In real life and in the analyses, failures would be expected to occur at stress concentration points. The following cases explain the basic stress concentration points that occurred in the analyses, and that would be expected to cause failure.

### 9.3.1 Steel Containments.

A previous test program has shown that a thick plate welded to a thin plate, with an appropriate thickness transition zone, does not cause an appreciable stress concentration region. Therefore, the section shown in Figure 9.1 would be expected to fail very near the force  $F$  that would cause failure in a plate of constant thickness  $t$ . Obviously, the thinner plate section begins to yield while the thick plate remains elastic.

Consider the cylinder shown in Figure 9.2, with one-half of the cylinder of thickness  $2t$ , and the other half of thickness  $t$ . Assuming the thickness transition is tapered as in Figure 9.1, the cylindrical section shown in Figure 9.2 would have about the same pressure

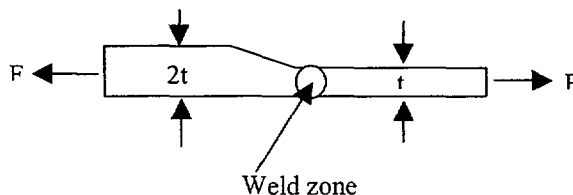
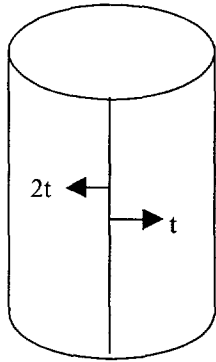


Figure 9.1. Thickness transition section.

capacity as a cylinder of uniform thickness  $t$ . This case is similar to the portion of the typical PWR Ice Condenser containment model that transitions from the thickened section where penetrations occur to the much thinner sections outside the penetration region. For a cylinder with end caps, the hoop stresses will be twice as large as the axial stresses. Therefore, under increasing internal pressure, the section of thickness  $t$  would reach its elastic limit and begin to plastically yield in the hoop direction, while the stresses in the axial direction were still elastic. The section of cylinder of thickness  $2t$  would also remain elastic at these pressure levels. Failure would occur because of unconstrained plastic flow in the thinner section in the hoop direction. The failure pressure would be very near the failure pressure of a cylinder of constant thickness,  $t$ .



**Figure 9.2. Cylinder with axial weld joining two different plate thicknesses.**

The cylindrical section shown in Figure 9.3 is also similar to some of the plate thickness changes in the steel models. At some distance from the weld joint, the thinner cylindrical section would begin to yield and plastically flow in the hoop direction, while the thicker section would remain elastic. The thicker plate section would serve as a stiffener, and reduce the stresses and strains in the thin section near the connection point. For a very long cylinder, the response of the cylinder to internal pressure would transition from the response for a cylinder of constant thickness  $2t$ , to the response for a cylinder of constant thickness  $t$ . For the case of a long cylinder, the failure pressure would be nearly the same as for a cylinder of constant thickness,  $t$ . For a cylinder where the thin section is relatively short, the failure pressure of the cylinder shown in Figure 9.3 will be greater than a cylinder of constant thickness,  $t$ , but less than the capacity of a cylinder of constant thickness,  $2t$ . Actual containments have transition regions that are similar to this case. There is no significant stress concentration caused by this thickness transition, and

hence no significant reduction in capacity results from this type of transition.

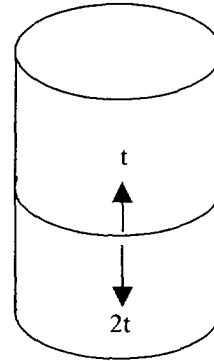


**Figure 9.3. Cylinder with circumferential weld joining two different plate thicknesses.**

The case shown in Figure 9.2 will not cause a stress concentration, and will fail at about the same pressure as a cylinder of constant thickness  $t$ . The case shown in Figure 9.3 will not cause a stress concentration either, and depending on the geometry the failure pressure could range from the failure pressure for a cylinder of thickness  $t$ , to an upper limit of the failure pressure of a cylinder of thickness  $2t$ .

Now assume that a cylinder of constant thickness  $t$  has a section that has been thickened, as shown in Figure 9.4. In contrast to the previous two examples, this configuration will cause a stress concentration, and the failure pressure will be lower than for a cylinder of constant thickness  $t$ . As internal pressure is increased, the cylinder section that is of thickness  $t$  will begin to yield and plastically flow in the hoop direction. However, the thickened insert plate of thickness  $2t$  will remain elastic. Therefore, at both ends of the thickened insert plate, a section of the thinner plate will have plastic strains that are larger than the free-field strains in the cylinder. These stress concentrations can be very significant, depending on the size of the thickened plate, the ratio between the thick and thin plates, and any differences in yield and ultimate strength between the two plate sections. The previous two cases did not cause a stress concentration that significantly reduced the pressure capacity from what would be expected for a cylinder of constant thickness  $t$ , but a thickened insert plate will reduce the pressure capacity.

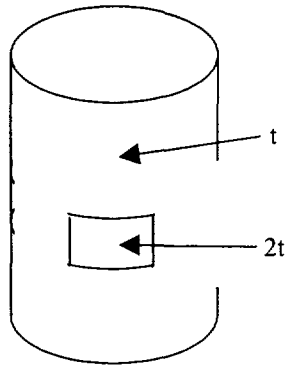


**Figure 9.4. Cylinder with thickened insert plate.**

A very similar case, shown in Figure 9.5, is for a locally thinned area, rather than for a thickened insert plate. For this case, as pressures increase, the locally thinned area will begin to plastically yield in the hoop direction before the rest of the cylinder. If the locally thinned area is reasonably small, then the stresses would be carried by the surrounding material. Typically, the stress concentration factor for stresses in the elastic range would be considerable, but as the material immediately adjacent to the thinned area began to yield and redistribute the load, the surrounding material would prevent excessive strains from accumulating in the locally thinned area. If the distance across the locally thinned section is on the order of a few times the shell thickness, the small locally thinned area would not cause a significant reduction to the capacity of the cylinder. On the other hand, if the locally thinned area is large, then a significant reduction in pressure capacity could result.

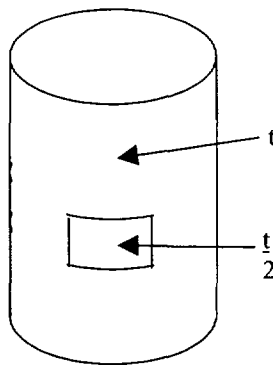


**Figure 9.5. Cylinder with locally thinned area.**

Of course, in an actual containment, there are shapes other than the cylindrical sections used in these examples. One other very common shape is spherical or elliptical for a dome section. The primary difference between the cylindrical examples used, and the

expected response if the thickness change occurred in a spherical section, is the stress field. For a cylindrical section, the stress in the hoop direction is twice as large as the stress in the axial direction, and so plastic straining would begin in the hoop direction, and little if any plastic deformation would occur in the axial direction. For a spherical section, the stress in two orthogonal directions on the shell would be expected to be about equal, and so biaxial plastic flow would result when the stresses reached the yield limit.

In transition regions that connect spherical shapes to cylindrical or conical sections, the stress field is more complex. Nevertheless, the basic explanation of how the stress/strain concentration develops is valid for these transition sections as well. In the transition regions, it is common to have surface stresses and strains that are somewhat larger than the membrane values because of bending. Therefore, one needs to be careful that failure doesn't initiate at the surface from these larger values.

Last of all, at the base, the containments are essentially "fixed" to the concrete basemat. This results in a case that is similar to Figure 9.3, except that the bottom portion of the cylinder is infinitely stiffer than the top portion. This results in substantial bending and high surface strains. Therefore, it is critical that both surface stresses and strains, as well as membrane values, be examined to determine if failure could initiate from the surface strain levels.

### 9.3.2 Liners in Concrete Containments.

The primary difference between the liner in a concrete containment, and the shell wall in a steel containment, is the Nelson stud anchors, or T anchors, that cause concentrated loads in the liner. The anchor points move to follow the concrete wall.

If there are no thickness changes in the liner and no geometric discontinuities to the concrete wall, then the liner will want to stretch uniformly when internal pressure is applied to a vessel. Generally, changes in the liner (i.e., a thickened insert plate) occur in areas where there is some geometry change in the concrete wall (i.e., a penetration hole). These are the areas where a stress concentration would be expected to develop, and eventually a tear initiate. If both the liner and the concrete wall are uniform in thickness, reinforcing, and other geometric details, then no significant stiffness changes exist. Since the concrete and liner both want to stretch uniformly, no significant stress concentration points develop at liner anchorage point for this case.

Now consider what happens at a thickened insert plate. This case, shown in Figure 9.6, is similar to the case

shown in Figure 9.4, except that liner anchors are added. Thickened insert plates are generally used around penetration holes. Most penetration holes through the concrete wall have heavier reinforcement around the hole, and so the stiffness change in the concrete wall section is minimized. As the pressure is increased, the liner anchors move to follow the concrete. The portion of the liner that is regular thickness begins to plastically yield, but the thickened insert plate remains elastic. This causes large plastic stresses to occur in the thinner plate section between the line of anchor studs and the thick plate. In particular, the points directly under the first row of studs in the thinner plate will experience significant local stress concentrations.

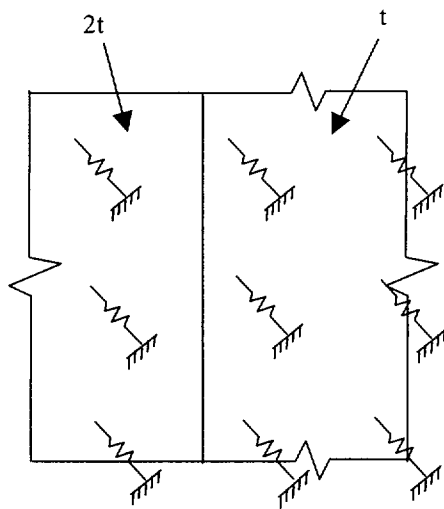


**Figure 9.6. Liner with thickened insert plate and Nelson Stud Anchors.**

The thicker plate in Figure 9.6 could be replaced with a section that is thinner, due to corrosion. The effect is identical. The thinner plate section can experience significant stress concentration, depending on the location of the anchors.

If liner anchors are welded to the thickened insert plate, as close to the thick/thin plate weld line as possible, the stress concentration problems will be minimized. This is because stress concentrations will not be forced to occur in the thinner plate section. In addition, if T anchors are welded to the thicker plate very near the thick-to-thin plate weld line, then they will not shear

off, and any stress concentration in the thinner plate will be minimal. However, if Nelson studs are welded to the thicker plate very near the thick-to-thin plate weld line, then the studs could shear off and cause stress concentrations in the thinner plate. If rows of studs in the thinner plate also sheared off before the thin plate tore, then the stress concentrations in the thinner plate would be further reduced. However, it can be difficult to determine whether the studs will shear off or the liner will tear.

The location and type of liner anchors can be selected during design to minimize stress concentrations around thickened insert plates. However, corrosion damage could locally thin a section of liner so as to cause the maximum stress concentrations. Therefore, when evaluating corrosion damage to a liner, one of the most critical things that must be determined is the location of the anchors with respect to the damaged area. Each case must be evaluated individually.

#### **9.4 Repairs of Steel Containments or Liners of Concrete Containments.**

As discussed in the previous sections, one of the primary factors that can cause stress concentrations that can lead to a tear initiating, is a difference in plate or liner thickness. Therefore, any repair to a containment should seek to minimize the differences in plate thickness. For example, welding a plate section over an area that has experienced corrosion would in effect be a thickened insert plate, and depending on the thickness of the repair plate, a stress concentration could result. In some cases, a locally thickened plate can cause failure in the resulting stress concentration region at a lower pressure than the vessel would have failed at without the repair.

There are many ways to make a repair to a locally thinned area without increasing the thickness beyond the original thickness. For example, the thickness could be built up with weld material and ground smooth. Alternately, an entire section could be cut out and replaced with a new section. Last of all, the thickness can be ground thinner, and a new plate welded to the ground section such that the new total thickness is equivalent to the original thickness.

## 10 REFERENCES

- ANATECH Corp., 1997, ANACAP-U User's Manual, Version 2.5, ANA-QA,118, ANATECH Corp., San Diego, CA.
- ANSI/ASME, 1986, "Guide for Gas Transmission and Distribution Piping Systems, B31G, Manual for Determining the Remaining Strength of Corroded Pipelines," American Society of Mechanical Engineers, New York.
- ASME Boiler & Pressure Vessel Code, 1992, Section II, Part A, pp. 655-656.
- ASME Boiler & Pressure Vessel Code, 1992, Section III, Division 1, Appendix I, Figure I-9.1.
- ASME, 1992, American Society of Mechanical Engineers Boiler & Pressure Vessel Code, 1992, Section III, Division 1.
- ASME, 1992, American Society of Mechanical Engineers Boiler and Pressure Vessel Code, 1992 Edition, Section III, subsection NE, NE-5300.
- ASTM, 1991, "Standard Test Methods of Tension Testing of Metallic Materials," Designation E8 - 91.
- Barsom, J. M., and Rolfe, S. T., 1987, *Fracture & Fatigue Control in Structures, Application of Fracture Mechanics*, Second Edition, pp 437
- Benzley, S. E., Soo Hoo, M. S., and Priddy, T. G., 1980, "A Numerical and Experimental Study of the Ductile Failure of 7075-T651 Aluminum," SAND80-1891, Sandia National Laboratories, Albuquerque, NM.
- Bridges, T. L., 1987, "Containment Penetration Elastomer Seal Leak Rate Tests," NUREG/CR-4944, SAND87-7118, Idaho National Engineering Laboratory, Pocatello, ID.
- Brinson, D. A., and Graves, G. H., 1988, "Evaluation of Seals for Mechanical Penetrations of Containment Buildings," NUREG/CR-5096, SAND88-7016, ERC International.
- Brownrigg, A., Spitzig, W. A., Richmond, O., Teirlinck, D., and Embury, J. D., 1983, "The Influence of Hydrostatic Pressure on the Flow Stress and Ductility of a Spheroidized 1045 Steel," *Acta Metallurgica*, Vol. 31, No. 8, 1983
- Brozzo, P., Deluca, B., and Rendina, R., 1972, "A New Method for the Prediction of the Formability Limits of Metal Sheets," Proceedings of the 7th Biennial Congress of International Deep Drawing Research Group, 1972.
- Bruneau, M., and Zahrai, S. M., 1997, "Effect of Severe Corrosion on Cyclic Ductility of Steel," ASCE, *Journal of Structural Engineering*, Vol. 123, No. 11, pp. 1478-1486.
- Burdette, E.G. and Rogers, L.W., 1975, "Liner Anchorage Tests," *Journal of Structural Engineering*, ASCE, Vol. 101, No. 7, pp. 1455-1468.
- Butler, T. A., and Fugelso, L. E., 1982, "Response of the Zion and Indian Point Containment Building to Severe Accident Pressures, NUREG/CR-2569, LA-9301-MS, Los Alamos National Laboratory.
- CAN/CSA-Z184-M86, 1986, "Gas Pipeline Systems," Canadian Standards Association, 178 Rexdale Blvd, Rexdale, Ontario.
- Catawba Nuclear Station Unit 1, "Abnormal Degradation of Steel Containment Vessels due to Corrosion by Standing Water in the Annulus Area," Docket No. 50-413, January 8, 1990.
- Chouchaoui, B. A., and Pick, R. J., 1992, "Burst Pressure Predictions of Line Pipe Containing Single Corrosion Pits Using the Finite Element Method," ASME, Proceedings of the 11th International Conference on Offshore Mechanics and Arctic Engineering, Volume V, Pipeline Technology.
- Chouchaoui, B. A., and Pick, R. J., 1993, "Interaction of Closely Spaced Corrosion Pits in Line Pipe," ASME, Proceedings of the 12th International Conference on Offshore Mechanics and Arctic Engineering, Volume V, Pipeline Technology.
- Chouchaoui, B. A., and Pick, R. J., 1994, "A Three Level Assessment of the Residual Strength of Corroded Line Pipe," ASME, Proceedings of the 13th International Conference on Offshore Mechanics and Arctic Engineering, Volume V, Pipeline Technology.
- Clauss, D. B., 1985a, "Comparison of Analytical Predictions and Experimental Results for a 1:8-Scale Steel Containment Model Pressurized to Failure," NUREG/CR-4209, SAND85-0679, Sandia National Laboratories, Albuquerque, NM.

Clauss, D. B., 1985b, "Pretest Predictions for the Response of a 1:8-Scale Steel LWR Containment Building Model to Static Overpressurization," NUREG/CR-4137, SAND85-0175, Sandia National Laboratories, Albuquerque, NM.

Clauss, D. B., 1987, "Round Robin Pretest Analyses of a 1:6-Scale Reinforced Concrete Containment Model Subject to Static Internal Overpressurization," NUREG/CR-4913, SAND87-0891, Sandia National Laboratories, Albuquerque, NM.

Clauss, D. B., 1989a, "Severe Accident Testing of Electrical Penetration Assemblies," NUREG/CR-5334, SAND89-0327, Sandia National Laboratories, Albuquerque, NM.

Clauss, D. B., 1989b, "Round Robin Analysis of the Behavior of a 1:6-Scale Reinforced Concrete Containment Model Pressurized to Failure: Posttest Evaluations," NUREG/CR-5341, SAND89-0349, Sandia National Laboratories, Albuquerque, NM.

Deardorff, A. F., Copeland, J. F., Poole, A. B., and Rinaca, L. C., 1989, "Evaluation of Structural Stability and Leakage from Pits Produced by MIC in Stainless Steel Service Water Lines," presented at Corrosion Symposia April 17-21, 1989 in New Orleans, Louisiana, Paper Number 514.

Danisch, R., L'Huby, Y., 1997, "Containment Design of the European Pressurized Water Reactor (EPR)," *Advanced Reactor Safety (ARS '97)*, American Nuclear Society Annual Meeting, Orlando, Florida, June 1-5, 1997.

Donten, K., M. Knauff, A. Sadowski, and W. Scibak, 1979, "Tests on a Model of Prestressed Reactor Containment," *Archiwum Inzynierii Ladowej*, vol. XXVI, no. 1/1980, pp. 231-245 (also *Proceedings of the 5th International Conference on Structural Mechanics in Reactor Technology*, Scibac, Berlin, Germany, August 13-17, 1979, Paper J 4/8).

Doyle, J.M. and Chu, S.L., 1971, "Some Structural Considerations in the Design of Nuclear Containment Liners," *Nuclear Engineering and Design*, No. 16, pp. 294-300.

Dunham, R. S., Rashid, Y. R., Yuan, K. A. and Lu, Y. M., 1985, "Methods for Ultimate Load Analysis of Concrete Containments," EPRI NP-4046, Electric Power Research Institute, Palo Alto, CA.

Eibl, J., Schluter, F. H., and Terbeck, G., 1988, "Ultimate Strains of Liner Sheets under Biaxial Tension," *Massivbau Baustofftechnologie Karlsruhe*, Germany.

El Haddad, M. H., Vanderglas, M. L., and Mukherjee, B., 1980, "Development and Application of Material Properties for Fracture Control in Engineering Structure", *Canadian Metallurgical Quarterly*, Vol. 19, 1980.

Ellingwood, B. R., and Cherry, J. L., 1999, "Fragility Modeling of Aging Containment Metallic Pressure Boundaries," NUREG/CR-6631, ORNL/SUB/99-SP638V, Oak Ridge National Laboratory, Oak Ridge, TN.

Eric Green Associates, Inc., "Ship Structure Committee Publications, A Special Bibliography," Ship Structure Committee 1992, Available from NTIS.

Fanous, F., Greimann, L., Wassef, W., and Bluhm, D., 1993, "Performance of Sequoyah Containment Anchorage System," SAND92-7308, IS-5012, Ames Laboratory, Institute for Physical Research and Technology, Ames, IA.

Fatigue Technology Inc., 1988, "Sandia High Temperature Tensile Test Report," FTI Test Report 8057-1, Fatigue Technology Inc., Seattle, Washington.

Fisher, J. W., Yen, B. T., and Wang, D., 1991, "Corrosion and Its Influence on Strength of Steel Bridge Members," *Transportation Research Record 1290*, Transportation Research Board, Washington DC., pp. 21-219.

Gamble, W.L., 1973, "Some Observations of the Strengths of Large Reinforcing Bars," *ACI Journal*, Proceedings V. 70, No. 1, pp. 31-35.

Gangloff, R. P., 1986, "A Review and Analysis of the Threshold for Hydrogen Environment Embrittlement of Steel," *Corrosion Prevention and Control*, Proc. 33rd Sagamore Army Materials Research Conference, S. Isserow, ed. 1986.

Giutoli, A., 1960, "Fusion Welded ASTM A-201 Steel Plate", Convair Report No. MP-58-440 Addendum 1, March 1960, AD 838225.

Goble, G.G., 1968, "Shear Strength of Thin Flange Composite Specimens," *AISC Engineering Journal*, pp. 62-65.

Greimann, L., Fanous, F., and Bluhm, D., 1984, "Final Report, Containment Analysis Techniques, A State-of-the-Art Summary," NUREG/CR-3653, Ames Laboratory, IA.

Greimann, L., Fanous, F., Rogers, J., and Bluhm, D., 1987, "An Evaluation of the Effects of Design Details

on the Capacity of LWR Steel Containment Buildings," NUREG/CR-4870, SAND87-7066.

Greimann, L., Wassef, W., Fanous, F., and Bluhm, D., 1991, "Analysis of Bellows Expansion Joints in the Sequoyah Containment," NUREG/CR-5561, SAND90-7020, Institute for Physical Research and Technology, Iowa State University, Ames, IA.

Greimann, L., Fanous, F., and Bluhm, D., 1993, "Crack Propagation in High Strain Regions of Sequoyah Containment," NUREG/CR-4273, Ames Laboratory, Iowa State University, Ames, IA.

Hancock, J. W., and Mackenzie, A. C., 1976, "On the Mechanisms of Ductile Failure in High-Strength Steels Subjected to Multi-Axial Stress States," *Journal of Mechanics and Physics of Solids*, Vol. 24, pp. 147-169, 1976.

Hanson, N., 1987, "Concrete Containment Tests, Phase 2: Structural Elements with Liner Plates-Final Report," EPRI NP-4867-M, Electric Power Research Institute, Palo Alto.

Hessheimer, M. F., Dameron, R. A., and von Riesemann, W. A., 1997a, "A Summary of Containment Integrity Research," Proceedings of the seminar on Containment of Nuclear Reactors held in conjunction with 14th International Conference on Structural Mechanics in Reactor Technology, August 25-26, 1997, Saclay, France.

Hessheimer, M. F., et. al., 1997b "Instrumentation and Testing of a Prestressed Concrete Containment Vessel Model." Proceedings of the 14th International Conference on Structural Mechanics in Reactor Technology, Lyon, France, August 18-22, 1997..

Hibbit, Karlsson & Sorenson, 1997, "ABAQUS/Standard User's Manual, Version 5.7," Hibbit, Karlsson & Sorenson, Inc, Pawtucket, RI.

Horschel, D. S., and Blejwas, T. E., 1983, "An Analytical Investigation of the Response of Steel Containment Models to Internal Pressurization," *Proceedings of the 7th International Conference on Structural Mechanics in Reactor Technology*, Volume J, Chicago, August 1983, Paper J 6/4, pp. 297-304.

Horschel, D. S., and Clauss, D. B., 1984, "The Response of Steel Containment Models to Internal Pressurization," *Structural Engineering in Nuclear Facilities*, J. J. Ucciferro: Editor, Raleigh, North Carolina, September 1984, Vol. 1, pp. 534-553.

Horschel, D. S., 1988, "Design, Construction, and Instrumentation of a 1/6-Scale Reinforced Concrete

Containment Building," NUREG/CR-5083, SAND88-0030, Sandia National Laboratories, Albuquerque, NM.

Horschel, D. S., 1992a, "Experimental Results From Pressure Testing A 1:6-Scale Nuclear Power Plant Containment," NUREG/CR-5121, SAND88-0906, Sandia National Laboratories, Albuquerque, NM.

Horschel, D. S., 1992b, "The Design, Fabrication, Testing, and Analyses of Four 1:32-Scale Steel Containments Models," SAND84-2153, Sandia National Laboratories, Albuquerque, NM.

Hofler, A, and Eisert, P., 1985, "Untersuchungen zum Versagensverhalten des DWR-Sicherheitsbehalters im Rahmen der Risikostudie", Beitrag 9.1, Jahresbericht 1984, Gesellschaft fur Reaktorsicherheit (GRS) mbH, Koln, Mai, 1985.

IDCOR Program Report, 1983, "Technical Report 10.1: Containment Structural Capability of Light Water Nuclear Power Plants," Atomic Industrial Forum, 7101 Wisconsin Avenue, Bethesda, MD.

The Institute of Civil Engineers, 1967, *Conference on Prestressed Concrete Pressure Vessels*, at Church House, Westminster, SW1, March 1967.

Irvine, W. H., and Gardner, C. J., 1983, "Pneumatic Burst Test Under 'Upper Shelf Conditions' of a Pressure Vessel Containing an Axial Defect," United Kingdom Atomic Energy Authority Safety and Reliability Directorate, Warrington, September 1983.

James, R. J., Zhang, L., Rashid, Y. R., and Cherry, J. L., 1999, "Seismic Analysis of a Prestressed Concrete Containment Vessel Model," NUREG/CR-6639, ANATECH Corp., San Diego, CA

Johnson, A. B. Jr., Jarrell, D. B., Sinha, U. P., and Shah, V. N., 1990, "Understanding and Managing Corrosion in Nuclear Power Plants," PNL-SA-18407, August 1990, Pacific Northwest Laboratory.

Jordan, B., 1988, "Nine Mile Point Torus Corrosion Reopens Mark I Containment Issue," *Nucleonics Week*, October 1988.

Ju, F. D., and Butler, T. A., 1984, "Review of Proposed Failure Criteria for Ductile Materials," NUREG/CR-3644, LA-10007-MS, Los Alamos National Laboratory, Los Alamos, NM

Jung, J., 1984, "Ultimate Strength Analyses of the Watts Bar, Maine Yankee, and Bellefonte Containments," NUREG/CR-3724, SAND84-0660, Sandia National Laboratories, Albuquerque, NM.

- Julien, J. T., and Peters, S. W., 1989, "Leak and Structural Test of Personnel Airlock for LWR Containments Subjected to Pressures and Temperatures Beyond Design Limits," NUREG/CR-5118, SAND88-7155, CBI Research Corporation.
- Kayser, J. R., and Nowak, A. S., 1989, "Reliability of Corroded Steel Girder Bridges," *Structural Safety*, 6(1):53-63.
- Kiefner, F. F., and Munse, W. H., 1967, "Influence of Thermal and Strain Cycling on Fracture Susceptibility of Mild Steel," University of Illinois, Ship Structure Committee, Feb. 1967, AD 647906.
- Kiefner, J. F., and Vieth, P. H., 1989, "A modified criterion for Evaluating the Remaining Strength of Corroded Pipe," Final Report on Project PR 3-805, Battelle Memorial Institute, Columbus, OH.
- Koenig, L. N., 1986, "Experimental Results for a 1:8-Scale Steel Model Nuclear Power Plant Containment Pressurized to Failure," NUREG/CR-4216, SAND85-0790, Sandia National Laboratories, Albuquerque, NM.
- Kulak, R. F., Hsieh, B. J., Ash, J. E., Kennedy, J. M., McLennan, G. A., and Pan, Y. C., 1985, "Structural Response of Large Penetrations and Closures for Containment Vessels Subjected to Loadings Beyond Design Basis," NUREG/CR-4064, SAND84-7177, Argonne National Laboratory.
- Lambert, L. D., 1993, "Posttest Destructive Examination of the Steel Liner in a 1:6-Scale Reactor Containment Model," NUREG/CR-5961, SAND92-1721, Sandia National Laboratories, Albuquerque, NM.
- Lambert, L. D., and Parks, M. B., 1995, "Experimental Results From Containment Piping Bellows Subjected to Severe Accident Conditions," Vol. 1 and 2, NUREG/CR-6154, SAND94-1711, Sandia National Laboratories, Albuquerque, NM.
- Lehner, J. R., Morante, R., Lin, C., and Nimnual, S., 1995, "Inservice Containment Degradation Report," SRED-36, Brookhaven National Laboratory.
- Loginow, A. W., and Phelps, E. H., 1975, "Steels for Seamless Hydrogen Pressure Vessels", Corrosion, Vol. 31, No. 11, pp. 404-412, November 1975.
- Luk, V. K., and Klamerus, E. W., 1996, "Round Robin Pretest Analyses of a Steel Containment Vessel Model and Contact Structure Assembly subject to Static Internal Pressurization," NUREG/CR-6517, SAND96-2899, Sandia National Laboratories, Albuquerque, NM.
- Luk, V., 1997, memo to Mr. Tomoyuki Matsumoto, dated February 6, 1997, Message No. SN-97-015, Sandia National Laboratories, International Nuclear Safety Department 6403, Albuquerque, NM.
- Luk, V. K., Hessheimer, M. F., Matsumoto, T., Komine, K., and Costello, J. F., 1997, "Testing of a Steel Containment Vessel Model," *Proceedings of the 14th International Conference on Structural Mechanics in Reactor Technology*, Lyon, France, August 18-22, 1997.
- Luk, V., Ludwigsen, J., Hessheimer, M., Komine, K., Iriyama, M., Matsumoto, T., and Costello, J., "Steel Containment Vessel Model Test: Results and Post-Test Analysis," Transactions of the Twenty-Sixth Water Reactor Safety Information Meeting, Bethesda, Maryland, October 26-28, 1998, NUREG/CP-0165.
- MacGregor, J. G., S. H. Simmonds, and S. H. Rizkalla, 1979, "Test of a Prestressed Concrete Secondary Containment Structure," University of Alberta, Dept. of Civil Engineering Structural Engineering Report No. 85, 1980 (also *Proceedings of the 5th International Conference on Structural Mechanics in Reactor Technology*, Scibac, Berlin, Germany, August 13-17, 1979, Papers J3/2, J3/5 and J 4/2).
- Mackenzie, A. C., Hancock, J. W., and Brown, D. K., 1977, "On the Influence of State of Stress on Ductile Failure Initiation in High Strength Steels," *Engineering Fracture Mechanics*, Vol. 9, pp. 167-188, 1977.
- Mangoine, M. J., 1982, "Creep-Rupture Behavior of Weldments," *Welding Journal Research Supplement*, Vol. 61, No. 2, American Welding Society, February 1982.
- Matsumoto, T., 1997, "Preliminary Results of Steel Containment Vessel Model Test," *Proceedings of the 14th International Conference on Structural Mechanics in Reactor Technology*, Lyon, France, August 18-22, 1997.
- McGeady, L. J., 1971, "Response of the Delta Test to Specimen Variables," Ship Structures Committee Report SSL-221, Sept. 1971, AD733086.
- McGuire Nuclear Station Unit 1 and 2, Licensee Events Report 369/89-20, Docket No. 50-369, September 25, 1989.
- Melville, A. G. et al, 1971, "Quality Strand-Cast Slabs for Plate Applications", *Metals Engineering Quarterly*, Vol. 11, No 4, Nov. 1971.

- Miller, J. D., 1990, "Analysis of Shell-Rupture Failure Due to Hypothetical Elevated-Temperature Pressurization of the Sequoyah Unit 1 Steel Containment Building," NUREG/CR-5405, SAND89-1650, Sandia National Laboratories, Albuquerque, NM.
- Miller, C. D., 1991, "Evaluation of Stability Analysis Methods Used for the Oyster Creek Drywell," Docket No. 50-219, September 12, 1991, CBI Technical Services Company, Report prepared for GPU Nuclear Corporation.
- Mokhtarian, K., Horacek, D. R., Endicott, J. S., and Waldman, M. A., 1987, "Mark I Containment Severe Accident Analysis" by CBI Na-Con, Inc., April 1987.
- Moody, N. R., Robinson, S. L., and Garrison, W. M. Jr., 1990, "Hydrogen Effects on the Properties and Fracture Modes of Iron-Based Alloys," *Res Mechanica* 30 (1990) 143-206.
- MPR Associates, Inc., 1989, "Nine Mile Point Unit 1 Assessment of Torus Wall Thickness," prepared for Niagara Mohawk Power Corporation, MPR-1152.
- National Cooperative Highway Research Program Report 333, 1990, "Guidelines for Evaluating Corrosion Effects in Existing Steel Bridges," Transportation Research Board, Washington DC.
- Nine Mile Point Nuclear Station Inspection Summary, Units 1 and 2, US Nuclear Regulatory Commission, Region I, Docket Nos. 50-220 and 50-410, Section 5-3 Torus Shell, Report 50-220/88-09 and 50-410/88-09 Inspection Dates March 7-11, 1988 and April 4-8, 1988.
- Norris, W. E., U. S. Nuclear Regulatory Commission, Table provided in April 1994.
- Nuclear Regulatory Commission (U.S.), Washington, D.C., NUREG 1150 "Severe Accident Risks: An Assessment for Five US Nuclear Power Plants," 1990.
- Oyane, M., 1972, "Criteria of Ductile Fracture Strain," Bulletin of the Japanese Society of Mechanical Engineers, Vol. 15, No. 90, 1972.
- Palfrey, J., 1990, "A Comparison of the Results of a 1/10th Scale Containment Model Test with Non-linear Axisymmetric Analyses," vols. I and II, Nuclear Design Associates, Knutsford, England.
- Panos, W. J., and Reeves, C. F., 1984, "Containment Integrity at Surry Nuclear Power Station," TP 84-13, Stone and Webster Engineering Corp., Boston, Massachusetts.
- Parks, M. B., 1989, "Evaluation of the Leakage Behavior of Inflatable Seals Subject to Severe Accident Conditions," NUREG/CR-5394, SAND89-1454, Sandia National Laboratories, Albuquerque, NM.
- Pilch, M. M., Allen, M. D., and Klamerus, E. W., 1995, "Resolution of the Direct Containment Heating Issue for all Westinghouse Plants with Large Dry Containments or Subatmospheric Containments," NUREG/CR-6338, Sandia National Laboratories, Albuquerque, NM.
- Poolé, A. B., 1989, "Trending of the Extent of Damage to Stainless Steel Pipe Welds Affected by Microbiologically Induced Corrosion (MIC) Related to Strength Reserve Factor," presented at Corrosion Symposia April 17-21, 1989 in New Orleans, Louisiana, Paper Number 515.
- Popelar, C. H., 1993, "A Plane Strain Analysis Model for Corroded Pipelines," ASME, Proceedings of the 12th International Conference on Offshore Mechanics and Arctic Engineering, Volume V, Pipeline Technology.
- Porter, V. L., Carter, P. A., and Key, S. W., 1999, "Pretest Analyses of the Steel Containment Vessel Model," NUREG/CR-6516, SAND96-2877, Sandia National Laboratories, Albuquerque, NM.
- Priddy, T. G., Benzley, S. E., and Ford, L. M., 1979, "A Consistent Stress-Strain Ductile Fracture Model as Applied to Two Grades of Beryllium," SAND79-2126, Sandia National Laboratories, Albuquerque, NM.
- Rashid, Y. R., 1968, "Ultimate Strength Analysis of Prestressed Concrete Pressure Vessels," Nuclear Engineering and Design, 7, pp. 334-344.
- Rashid, Y.R., 1985, "Review of the WASH-1400 Surry Containment Capability Assessment," in Appendix B of *Surry Source Term and Consequence Analysis*, EPRI NP-4096, Electric Power Research Institute, Palo Alto, CA.
- Reese, R. T., and Horschel, D. S., 1985, "Design and Fabrication of a 1/8-Scale Steel Containment Model," NUREG/CR-3647, SAND84-0048, Sandia National Laboratories, Albuquerque, NM.
- Romanoff, M., 1957, "Underground Corrosion," National Bureau of Standards Circular 579.
- Sammataro, R. F., Solonick, W. R., and Edwards, N. W., 1992, "A Generic Approach for Containment Success Criteria Under Severe Accident Loads,"

Proceedings of the Fifth Workshop on Containment Integrity, NUREG/CP-0120.

Shah, V. N., and MacDonald, P. E., 1989, "Residual Life Assessment of Major Light Water Reactor Components -- Overview," Volumes 1 and 2, NUREG/CR 4731, EGG-2469, Idaho National Engineering Laboratory, Pocatello, ID.

Shah, V. N., Sinha, U. P., and Smith, S. K., 1994, "Insights for Aging Management of Light Water Reactor Components, Metal Containments," NUREG/CR-5314, EGG-2562, Vol. 5, Idaho National Engineering Laboratory, Pocatello, ID.

Sharma, S., Wang, Y. K., and Reich, M., 1985, "Ultimate Pressure Capacity of Reinforced and Prestressed Concrete Containments," NUREG/CR-4149, BNL-NUREG-51857, Brookhaven National Laboratory.

Shigley, J. E., 1983, *Mechanical Engineering Design*, 2nd edition, McGraw-Hill, New York.

Solonick, W. R., 1996, "Elastic-Plastic Strain Acceptance Criterion for Structures Subject to Rapidly Applied Transient Dynamic Loading," 1996 ASME International Mechanical Engineering Congress and Exposition, Pressure Vessels and Piping Division, PVP-Vol 343, pp. 3-14.

Soo Hoo, M. S., Benzley, S. E., and Priddy, T. G., 1980, "Experimental Aspects of an Investigation of Macroscopic Ductile Failure Criteria," SAND80-1917, Sandia National Laboratories, Albuquerque, NM.

Spletzer, B. L., Lambert, L. D., Bergman, V. L., and Weatherby, J. R., 1995, "Separate Effects Testing and Analyses to Investigate Liner Tearing of the 1:6-Scale Reinforced Concrete Containment Building," NUREG/CR-6184, Sandia National Laboratories, Albuquerque, NM.

Steir, H., 1959, "Mechanical Tests of Welded Joints in USS-T-1 and A-201 Steels," Convair Report MP-58-440, Oct. 1959, AD 834061.

Stephens, D. R. and Bubenik, T. A., 1993, "Development of Guidelines for Acceptance of Corroded Pipe," Proceedings Eighth Symposium on Line Pipe Research, Paper Number 25, sponsored by the Pipeline Research Committee, American Gas Association.

*Structural Alloys Handbook*, Vol. 3, 1989, Metals and Ceramics Information Center, Battelle, Columbus, OH.

*Structural Alloys Handbook*, R. L. Brockenbrough, 1994 revision, Purdue Research Foundation, West Lafayette, Indiana.

Tan, C. P., and Bagchi, G., 1996, "BWR Steel Containment Corrosion," NUREG-1540, Nuclear Regulatory Commission, Washington, DC.

Thomason, P. F., 1990, *Ductile Fracture of Metals*, Pergamon Press, Oxford, England.

US Nuclear Regulatory Commission, Information Notice No. 89-79, "Degraded Coatings and Corrosion of Steel Containment Vessels," December 1, 1989.

Valenta, F., Sochor, M., Spaniel, M., Michalec, J., Ruzicka, M., and Halamka, V., 1996, "Theoretical and Experimental Evaluation of the Limit State of Transit Gas Pipelines Having Corrosion Defects," *International Journal of Pressure Vessels and Piping*, Vol. 66, pp187-198.

Vanderglas, M. L., and Mukherjee, B., 1981, "Growth of Surface Cracks in A516 Gr 70 Pressure Vessel Steel", presented at 6<sup>th</sup> SMiRT held in Paris, France, Ontario Hydro Research Division, Toronto, Ontario, Canada

Vora, J. P., 1993, "NRC Research Program on Plant Aging: Listing and Summaries of Reports Issued Through September 1993," NUREG-1377, Rev 4, U. S. Nuclear Regulatory Commission.

Weatherby, J.R., 1988, "Structural Assessments of the Surry and Zion Reactor Containment Buildings for NUREG-1150," memorandum to R.J. Breeding, Sandia National Laboratories, Albuquerque, NM.

Weatherby, J. R., 1990, "Posttest Analysis of a 1:6-Scale Reinforced Concrete Reactor Containment Building," NUREG/CR-5476, SAND89-2603, Sandia National Laboratories, Albuquerque, NM.

Wellman, G. W., and Salzbrenner, R., 1992, "Quasistatic Modeling and Testing of Exclusion Region Barrier Mock-Ups," SAND92-0024, Sandia National Laboratories, Albuquerque, NM.

Wellman, G. W., and Rolfe, S. T., 1984, "Engineering Aspects of CTOD Fracture Toughness Testing", *Welding Research Council Bulletin*, Bulletin 299, November 1984, ISSN 0043-2326).

Zion FSAR, 1971, "Zion Final Safety Analysis Report," Vol. VIII, Figures 5.22-1 to 5.22-3, Commonwealth Edison Company, Chicago, Illinois.

Zion FSAR, 1971, "Zion Final Safety Analysis Report," Vol. VIII, Figures 5.22-1 to 5.22-3, Commonwealth Edison Company, Chicago, Illinois.

<b>NRC FORM 335</b> (2-89) NRCM 1102, 3201, 3202	<b>U.S. NUCLEAR REGULATORY COMMISSION</b>  <b>BIBLIOGRAPHIC DATA SHEET</b>  <i>(See instructions on the reverse)</i>	<b>1. REPORT NUMBER</b> <i>(Assigned by NRC, Add Vol., Supp., Rev., and Addendum Numbers, if any.)</i>  NUREG/CR-6706 SAND2000-1735											
<b>2. TITLE AND SUBTITLE</b>  Capacity of Steel and Concrete Containment Vessels With Corrosion Damage	<b>3. DATE REPORT PUBLISHED</b> <table border="1" style="width: 100%;"> <tr> <td style="width: 50%; text-align: center;">MONTH</td> <td style="width: 50%; text-align: center;">YEAR</td> </tr> <tr> <td style="text-align: center;">February</td> <td style="text-align: center;">2001</td> </tr> </table>	MONTH	YEAR	February	2001								
MONTH	YEAR												
February	2001												
<b>5. AUTHOR(S)</b>  J.L. Cherry, J.A. Smith	<b>4. FIN OR GRANT NUMBER</b>  J6042												
<b>8. PERFORMING ORGANIZATION - NAME AND ADDRESS</b> <i>(If NRC, provide Division, Office or Region, U.S. Nuclear Regulatory Commission, and mailing address; if contractor, provide name and mailing address.)</i>  Sandia National Laboratories Albuquerque, NM 87185-0744	<b>6. TYPE OF REPORT</b>  Technical												
<b>9. SPONSORING ORGANIZATION - NAME AND ADDRESS</b> <i>(If NRC, type "Same as above"; if contractor, provide NRC Division, Office or Region, U.S. Nuclear Regulatory Commission, and mailing address.)</i>  Division of Engineering Technology Office of Nuclear Regulatory Research U.S. Nuclear Regulatory Commission Washington, DC 20555-0001	<b>7. PERIOD COVERED</b> <i>(Inclusive Dates)</i>												
<b>10. SUPPLEMENTARY NOTES</b>  H.L. Graves III, NRC Project Manager													
<b>11. ABSTRACT</b> <i>(200 words or less)</i>  <p>Corrosion damage has been found in a number of nuclear power plant containment structures, and this could degrade the pressure capacity of the vessel. This has prompted concerns regarding the capacity of corroded containments to withstand accident loadings. For the low-carbon, low-strength steels used in containments, the effect of corrosion on material properties is discussed in this report, and a basis for using finite element analyses to calculate the capacity of a vessel with corrosion damage is developed. The pressure capacity was calculated for two typical steel containment vessels with no corrosion damage: a PWR Ice Condenser containment and a BWR Mark I containment. The pressure capacity was also calculated for two typical concrete containment vessels with no corrosion damage: a PWR reinforcement concrete sub-atmospheric containment and a PWR prestressed concrete containment vessel. Multiple analyses were then performed with the location of corrosion and the amount of corrosion varied in each analysis. A "lower bound", "best estimate", and "upper bound" failure level was predicted for each case. These limits were established by: determining the amount of variability that exists in material properties of typical containments, estimating the amount of uncertainty associated with the level of modeling detail and modeling assumptions, and estimating the stress concentration effect caused by a rough, uneven, corroded surface.</p>													
<b>12. KEY WORDS/DESCRIPTORS</b> <i>(List words or phrases that will assist researchers in locating the report.)</i>  Corrosion, containment, degradation	<table border="1" style="width: 100%;"> <tr> <td><b>13. AVAILABILITY STATEMENT</b></td> <td style="text-align: center;">unlimited</td> </tr> <tr> <td><b>14. SECURITY CLASSIFICATION</b></td> <td style="text-align: center;">unclassified</td> </tr> <tr> <td><i>(This Page)</i></td> <td></td> </tr> <tr> <td><i>(This Report)</i></td> <td style="text-align: center;">unclassified</td> </tr> <tr> <td><b>15. NUMBER OF PAGES</b></td> <td></td> </tr> <tr> <td><b>16. PRICE</b></td> <td></td> </tr> </table>	<b>13. AVAILABILITY STATEMENT</b>	unlimited	<b>14. SECURITY CLASSIFICATION</b>	unclassified	<i>(This Page)</i>		<i>(This Report)</i>	unclassified	<b>15. NUMBER OF PAGES</b>		<b>16. PRICE</b>	
<b>13. AVAILABILITY STATEMENT</b>	unlimited												
<b>14. SECURITY CLASSIFICATION</b>	unclassified												
<i>(This Page)</i>													
<i>(This Report)</i>	unclassified												
<b>15. NUMBER OF PAGES</b>													
<b>16. PRICE</b>													



Federal Recycling Program

ISBN 0-16-050738-3

90000



9 780160 507380

**UNITED STATES**  
**NUCLEAR REGULATORY COMMISSION**  
WASHINGTON, DC 20555-0001

---

OFFICIAL BUSINESS  
PENALTY FOR PRIVATE USE, \$300